Universitat Autònoma de Barcelona

Sources and distribution of artificial radionuclides in the oceans: from Fukushima to the Mediterranean Sea

Maxi Castrillejo Iridoy

UNIVERSITAT AUTÒNOMA DE BARCELONA

INSTITUT DE CIÈNCIA I TECNOLOGIA AMBIENTALS

TESI DOCTORAL

Doctorat en Ciència i Tecnologia Ambientals

2017

Sources and distribution of artificial radionuclides in the oceans: from Fukushima to the Mediterranean Sea

Maxi Castrillejo Iridoy

Directors:

Dr. Pere Masqué Barri

Dr. Jordi Garcia Orellana

Dra. Núria Casacuberta Arola

Sources and distribution of artificial radionuclides in the oceans: from Fukushima to the Mediterranean Sea

PhD candidate: Maxi Castrillejo Iridoy

PhD Supervisors:

Dr. Pere Masqué Barri Dr. Jordi Garcia Orellana Dr. Núria Casacuberta Arola

Doctorat en Ciència i Tecnologia Ambientals

Institut de Ciència i Tecnologia Ambientals

Universitat Autònoma de Barcelona

This PhD thesis has been funded by the Ministerio de Educación, Cultura y Deporte de España with a fellowship of the Programa de Formación de Personal Universitario (FPU, reference number: AP2012-2901) from May 2013 to December 2016, and with the 'Beca Predoc' (referece number: BFI-2012-138) from the Government of the Basque Country from January to April 2013.

Funding was also provided from the following research projects, as well as from own funds of the Laboratory de Radioactivitat Ambiental and the Consolidated Research group MERS (2014 SGR-1356, Generalitat de Catalunya):

- Impacto de las fugas de radioactividad artificial de la central nuclear de Fukushima-Daiichi en el medio marino. Ministerio de Ciencia e Innovación (CTM2011-15152-E).
- COordination and iMplementation of a pan-European instrumenT for radioecology (FRAME-COMET). The European Commission 7th Framework (Grant Agreement Number 604974).
- Gordon and Betty Moore Foundation (Grant #3007).
- The Deerbrook Charitable Trust.
- Mediterranean Sea Acidicication (MedSeA) project. The European Commission 7th Framework (Grant grant no. 265103).
- The ETH-Zurich Laboratory of Ion Beam Physics was partially funded by its consortium partners EAWAG, EMPA, and PSI.
- The Swiss National Science Foundation (AMBIZIONE PZ00P2_154805).
- Vici project in the Black Sea. Netherlands Organisation for Scientific Research (NWO Vici grant no. 865.13.005).

Euskara/Basque

‘Gizonen lana jakintza dugu, ezagutuz aldatzea,
naturarekin bat izan eta harremanetan sartzea.
Eta indarrak ongi errotuz, gure sustraiak lurrari lotuz,
bertatikan irautea: ezaren gudaz baietza sortuz,
ukazioa legetzat hartuz beti aurrera joatea…
Eta ametsa bilakaturik egiaren antziduri,
herri zahar batek bide berritik ekingo dio urduri’

Català/Catalan

‘El coneixement és l'objectiu de l'ésser humà,
comprendre i transformar, relacionar-se i ser part de la natura.
Lligarem fortament les nostres arrels a la terra, resistirem i progressarem,
crearem oportunitats prenent la negació com a llei...
I farem els nostres somnis realitat,
il·lusionats, triarem i farem el nostre propi camí’

English

‘Knowledge is human’s goal, change based on the understanding,
interact and be part of nature.
We will privail by joining our roots to the Earth,
progress by creating opportunities against widespread denial,
make dreams happen, chose our own path’

Izarren Hautsa – Xabier Lete (Xabier, I apologize for the mediocre translations)

ACKNOWLEDGEMENTS

ESKER ONAK / AGRADECIMIENTOS / AGRAÏMENTS / REMERCIEMENTS

Vaig arribar al Laboratori de Radioactivitat Ambiental el 2013 i des de llavors sembla que el temps 'hagi volat' de manera exponencial com la radiació. Han estat uns anys viscuts molt intensament, travessant mars, visitant diversos països, i sobretot, coneixent i interaccionant amb gent meravellosa.

Abans de tot volia agrair haver viscut aquesta experiència al meus directors, o 'advisors', com els agrada que els diguin. Pere, Jordi i Núria, m'he sentit molt valorat i recolzat durant la tesi, tant a nivell professional com personal. Heu estat exemplars transmetent l'esforç, el 'buen hacer' i l'esperit crític. No us ha faltat paciència per aguantar el 'cabezón' dels bolis BIC. M'atreviria a dir fins i tot, que heu aconseguit que un basc adquireixi una mica de diplomàcia. Totes les persones que vaig a anomenar a continuació les he conegut per la vostra culpa. Per això i per tot l'anterior, moltíssimes gràcies!

I would like to acknowledge Catalina Gascó Leonarte, Elena Chamizo Calvo, Sabine Charmasson, José Luis Mas Malbuena, Olivier Radakovitch and John N. Smith for kindly agreeing to review and evaluate this thesis dissertation. Thanks to Sabine Charmasson also for facilitating the information on radionuclide releases from nuclear industry to the Rhône River. Part of this thesis has already been published thanks to, aside my supervisors, the following co-authors: Ken O. Buesseler, Steven M. Pike, Crystaline F. Breier, Marcus Christl, Christof Vockenhuber and Hans-Arno Synal. *Chapters 2 and 3* that have already been published were greatly improved with the constructive comments from 5 anonymous reviewers and Dr. Daniel Giammar.

During these years I processed more than 7 tons of seawater that were collected thanks to the effort of uncountable scientists and crew members. A big thank to all of you. More in particular, I would like to say 'arigato gozaimas' (thank you) to the captain and crew from *R/V Daisan Kaiyo Maru* for their work in the coast off Japan and our japanese collegues on board including Chief Scientists Jun Nishikawa and Hiroaki Saito. Thanks to

the laboratory of M. Charette for assistance with groundwater sampling. Muchas gracias a los investigadores principales Patricia Ziveri y Jordi Garcia Orellana de la campaña *MedSeA-GA04S* en el Mar Mediterráneo. Fue un placer trabajar a bordo del *B/O Ángeles Alvariño*. No hubo 'albariño' pero sí una comida riquísima y buena compañía que amenizó el intenso muestreo. Moitas gracinhas a los marineros por toda su ayuda durante el muestreo y en particular, a Miguel por ayudarnos con las bombas. Un abrazo a los de máquinas y a Kikil-handi por el paseo que nos disteis por la sala de máquinas y por las lecciones de vida: sempre avanti! Seawater samples from the Black Sea were collected during the *Black Sea-Fe-Vici* cruise on board dutch *R/V Pelagia* with the help of the captain, crew and scientist that were lead by the Chief Scientist Caroline Slomp. Pendant les années de thèse j'ai aussi participé à l'expédition océanographique *GEOVIDE* le printemps 2014. Merci beaucoup au capitan et aux marins du *N/O Pourquoi pas?* ainsi que aux investigateurs principales Géraldine Sarthou et Pascale Lherminier. Sans votre aide, on n'aurait pas pu avoir des si beaux échantillons. GEOVIDE was a truly 'french' experience surrounded by great people that helped keeping with the good vibes during almost 50 days of cloudy and foggy landscapes in the North Atlantic. Mes salutations à Marie, Manon, Julia, Virginie, Hélène, Catherine, Leonardo, los gallegos, Jan Lukaaaaaaaas, Arnout, Debany, Fabien-insitu pumps… et surtout, la pêtit bretonne. Yi, I think we did a great job sampling together, it was a pleasure meeting you and I promiss to come back to your data soon.

The determination of multiple radionuclides studied in this PhD project sometimes required the resources, facilities and expertise from foreign institutions such as the Woods Hole Oceanographic Institution (WHOI) and the Lamont Doherty Earth Observatory (LDEO) in the USA, and the ETH-Zürich in Switzerland. Special thanks go to Ken, Spike and Crystal for making my stay so productive and friendly at the Café Thorium lab in WHOI. I learnt a lot from you. Even if I fell asleep when I should not…. I have very good memories, including the delicious dinners at Ken and Wendy's place, the pizza at Spike's and that 5 km run with Crystal and her family. Tim and Marty, you tried to teach me the reasoning and theory behind each step in the radiochemistry of plutonium and neptunium. I am thankful for that, but also for making me feel like at home. Marty, gracias por las

conversaciones en el shuttle de Manhattan a LDEO y por presentarme a tu familia. Espero que estéis muy bien. My warmest regards and acknowledgements for the hardworking colleagues at the Laboratory of Ion Beam Physics in ETH-Zürich. I would like to thank Hans-Arno Synal for providing the laboratory space and the AMS facilities during my stay in Switzerland. Núria Casacuberta, Marcus Christl and Christof Vockenhuber, I much appreciated your advise, guidance and discussions. Here is also a reminder for watering the plant in the office at least once a month! Anita Schlatter, you excelled in your work always with a big smile and willing to help, keep working motivated by Ska-P! In addition to the above ones, I met many more people in ETH that I would like to acknowledge for their friendship. Chrisi, Laura, Adam, Daniele, Sascha, Ewelina, Olivia, Marieta, Mantana, Carooo, David, Giulia, Anne-Marieeeeee and others…. Vielen Dank! Lots of power! Please go to Letten after work. Be sure that I will do my best to come back. Iodine samples from the Mediterranean Sea, as well as the sequential extraction of radionuclides in some samples from the North Atlantic was carried out at EAWAG thanks to the laboratory space provided by Nathalie Dubois and Mattias Brennwald. I regret not having more time and dedicating it to socializing with two great laboratory technicians: Alfred Lück and Silvia Bollhalder. In particular, Alfred, I much appreciated your patience and the always, positive attitude. During my stay in Switzerland I also had the support from Nora Schaffner. Nora, you kindly provided your place and you were truly, a great flatmate. I never met someone so easy going. I hope one day I can give you back at least a small part of what you gave me. Catanyoles, thank you so much for…. now I would need a whole chapter to write a long list, but briefly: for your friendship.

Los agradecimientos van ‘in crescendo’ así que ahora me toca agradecer en un miserable párrafo vuestra ayuda incondicional y amistad ‘de la bona’. Después de haber dado más vueltas que una peonza durante el master y el doctorado, os puedo decir que sois unos mega-currantes, muy profesionales y que el ambiente en el laboratorio ha sido simplemente, genial. Joan Manuel, tú fuiste mi guía al principio en el LRA y tuviste la desgracia te compartir despacho conmigo con lo que ello conlleva: aguantar mis momentos de ira, estrés y alegría, incluyendo unos bailes tropicales. Otra que sufrió mis idas y venidas en el despacho fue Giada jejeje. Una ‘champion’ que me atrevería a decir, sustenta

el récord de haber finalizado la tesis en el menor tiempo posible en el LRA. Avanti Giada!!!! Muntsa, lo que unió Sangonera la Seca y el cortar corers en el Mar Mediterráneo a altas horas no lo separará nada, ni nadie. Has sido un gran apoyo moral y me he reído mucho contigo! Incluso te agradezco haberme dado esas 'chapas' a partir de la 'hora 20' de la jornada laboral jajaja. Ets fantàstica! Si algún día te casas con el Narciset, os regalaré una noche en Sangonera La Seca con entrada al palco de la plaza de Toros. Vienaaaaa, la verdad es que no hemos coincidido demasiado. Pero tengo muy buenos recuerdos y casi te tengo a ti en versión de cartón y tamaño real en casa… per cert, saluda a la teva mare. Gracias por llevarme a aquel roof-top al lado de tu casa y por enseñarme que una hamburguesa vegetariana puede ser realmente buena. Espero que sigas alegrando al personal por Australia y que tus compañeros no tengan mucha tortícolis por mirar al techo. ¡Ai, me estoy riendo mucho mientras que escribo estas líneas! Valentines!!! Te agradezco, entre otras muchas cosas, haber traído a casi todo el LRA al Basque Country en tu furgo y sin carnet. Eres un máquina, pero sigues sangrando al romper nueces con la frente como un beginner. Tendrás que volver a perfeccionar la técnica. Otra compañera lusa, la Teresa, también lo dio todo por Hernani echando unos buenos bailes a ritmo de ska y rock radical vasco. Teresa, ya eres casi una persona libre, ¡parabéns! Ester, te admiro por haber sobrevivido en Hernani con un disfraz de sumo. Veo que te tomaste la revancha y por tu culpa, me poseyó la camomilla de Linyolas. El txurrut es un tema complicado, pero a algunas personas no les hace falta para estar alegres y traer un poco de marcha al LRA. Joya, hablo de ti, ya lo sabes. La sal y la pimienta del día a día, que ha tenido que sobrevivir en terrenos 'hostiles' en el Baskenland y Catalunya. Qué suerte tienes que podrás gozar de los calçots unos años más. Ari, aquella chica que se sentaba y no paraba de trabajar, creo que es una de las pocas personas que conseguía no distraerse conmigo ¡qué poderío! Me vienen a la cabeza todos esos 'dancing skills' que nos has enseñado. Ei, muchas gracias por acogerme en tu casa y la del Rocky Balboa. Sigue 'tamissando, tamissando…' que llegarás muy lejos. Paradissss, gracias por cuidarme tan bien, trayendo bocatas mientras que finalizaba esta tesis, gracias por la pantalla y por meter los cesios en los GM3 y GM4 (estos agradecimientos también van dirigidos a Joan Manuel, Giada y demás personas que tuvisteis que meter los interminables 'MS' y 'GV'). Xènia, me alegro de que estés de vuelta por tu tierra. Ahora tienes la oportunidad de seguir haciendo

estiramientos entre muestra y muestra, y a la vez, aprovechar para nadar e ir a la montaña. Aprofita-ho! Marc, otro que es inmune a mis cánticos como la Ari y el Aaron que no lo es tanto… sois la nueva savia, sempre endavant! Jordi, Pere y Núria, os nombro en esta sección en la que la línea entre trabajo y la parte humana se juntan. Un abrazo a tod@s.

La feinada que s'ha fet en aquesta tesi ha estat en gran part possible gràcies a la feina de formiguetes de Sara Cobo, Cristina Durán, Contxi Saumell i la resta del personal d'administració de l'ICTA i la UAB. També m'agradaria anomenar al Manel, per construir el sistema UV i solucionar tants marrons relacionats amb el material de mostreig i laboratori. Agraeixo molt la feina que has fet sempre amb rigor i afecte.

Badira 13 urte Euskal Herria atzean utzi nuela itsasoa aztertzeko. Beraz, bada garaia ingurukoak agurtu eta zuen babesa eskertzeko. Zuen hutsunea ez da erraza izan gainditzen, nahiz eta nire alboan izan zareten Ameriketan, Suitzan, Japonian, baita Atlantikoaren erdian nengoenean ere. Hok ez pattuk eta izandakoak ere (Beñat eta Axur!), eskerrikasko zuen animoak aurrera in ta itxeki-iten lagundu didatelako. Txirton, Mitxel, Manex, Haitz (nik baino gehio daki itsasoaz), Julen eta gainontzeko lehengusu, lehengusu-ttikiak, bizipoza eman didazue etxeratu naizen bakoitzean, zuentzat besarkada bero bat! Elenius, Anuxki, Laura, Nagoriuz eta Olatz, laister ospatuko dugu urte hauen amaiera, milaesker denagatik! Gertukoei heltzeko garaia da. Izeba-osabak, amona ta aitonak, zinetelako ta zaztelako gera, ta txol lasai egozte ongi ikasiak gera ta. Guk jarraituko dugu gazte ta ez horren gazte, aurrera. Als companys de batalla: Malako, el Guillem, Uxi… també una forta abraçada. Lastly, especial acknowledgements for always being supportive to the women that i loved the most. Nolwenn, surtout merci à toi. Merci d'avoir fait les dernières années de la thèse étaient plus heureux (je pense la traduction n'est pas top ;)).

Azkenik, aita eta ama, ama eta aita, zuentzat paragrafo hau. Eman didazuen guztiaren aldean tesi hau ekarpen xume bat besterik ez da. Egindako ibilibidearen mugarri bat. Hala ere, ez diogu erez merito guzia kenduko egindako lanari. Zuengandik ikasi ditut gauza pila, baina azpimarratuko nituzke bereziki bi: xumetasunetik lan egiteko kemena eta ingurukoei begirunea. Tesi hau, noski, zuena ere bada.

Eskerrikasko, moltes gràcies, gracias, thanks, merci beaucoup.

Table of contents

List of figures

List of tables

CHAPTER 1

Introduction

In this *Chapter 1* we provide with a brief introduction on the main concepts regarding the sources and distributions of artificial radionuclides in the oceans.

In order to contextualize it, general concepts on the sources and distributions of artificial radionuclides in the oceans are introduced. Main sources of artificial radioactivity are known and described elsewhere, but their inputs for some of the targeted radionuclides (^{90}Sr, ^{129}I, ^{134}Cs, ^{137}Cs, ^{236}U, ^{237}Np, ^{239}Pu and ^{240}Pu) are not well constrained. This is especially true for the long-lived radionuclides that in the last years to decades have become available thanks to improvements on their measuring techniques, and hence, more relevant as potential tracers of ocean circulation (e.g. ^{129}I, ^{236}U, ^{237}Np). This PhD was firstly motivated by the nuclear accident at the Fukushima Dai-ichi Nuclear Power Plant (FDNPP) in 2011 that caused the largest accidental release of artificial radioactivity into the oceans (Buesseler et al., 2011). Our efforts focused on quantifying the impact of ongoing releases of ^{90}Sr (*Chapter 2*), a radionuclide that was largely overlooked despite its importance from the radiological point of view and its potential for tracing Fukushima derived contamination in the Pacific Ocean. Secondly, the GEOTRACES program (www.geotraces.org) and the MedSeA project provided the opportunity to carry out an unprecedented large-scale sampling of artificial radionuclides in Mediterranean waters. The Mediterranean Sea was particularly interesting for this PhD project because this semi-enclosed sea accumulates the radionuclide inputs from several intentional and accidental releases (Delfanti and Papucci, 2010). The main focus of the two studies carried out in the Mediterranean Sea (*Chapters 3 and 4*) was studying the global distribution and sources of artificial radionuclides that are, or may ultimately become, tracers of ocean water circulation and of particle cycling (e.g. ^{129}I, ^{236}U, ^{237}Np and Pu isotopes).

More detailed background information is provided for both the coast off Fukushima and the Mediterranean Sea in their respective *Chapters 2, 3 and 4*.

1.1. Sources of artificial radionuclides

Artificial radionuclides have been introduced to the environment through multiple sources since the 1940s. According to UNSCEAR (2000), **atmospheric nuclear weapon tests**

were carried out from 1945 to 1980 accounting for more than 80% of the total yield (530 Mt) released by atmospheric and underground tests (Figure 1.1). The largest radionuclide release from this source occurred during the time period (1950s-1960s) when most of the nuclear tests took place (Figure 1.1 A), combined with detonations with the highest yields (Figure 1.1 B). The main input from atmospheric nuclear weapon tests, termed *global fallout*, was distributed along latitudinal bands (Figure 1.1 C), especially between 30 and 60 ºN (~43% of the input), because of the location of tests and the global atmospheric circulation and precipitation patterns. Most radionuclides produced during atmospheric nuclear weapon tests and deposited as global fallout were gone due to radioactive decay by 2017 (Table 1.1).

Nuclear reprocessing plants are used to recover recyclable fissile material (~96% uranium and 1% plutonium) and separate them from fission products (~3%) and non-fissile actinides produced during burn up of fuel in nuclear power plants. Liquid and gaseous releases from reprocessing plants comply with regulatory limits set for those radionuclides posing major radiological risk to the environment and humans (Table 1.2). Yet, historical discharges from European reprocessing plants show that significant amounts of artificial radionuclides have been introduced from these facilities to the ocean (e.g. Sellafield and Marcoule, Figure 1.2; and La Hague, not shown in the Figure). Radionuclide releases from Sellafield (Figure 1.2 A), one of the largest reprocessing plants in the world, were larger than for Marcoule (Figure 1.2 B). However, Marcoule deserves special mention because its operation resulted in the input of artificial radionuclides to sediments and water column in the Mediterranean Sea (*Chapters 3 and 4*) between 1958 and 1997 (e.g. Charmasson, 1998; Eyrolle et al., 2004). By the 1990s, Marcoule releases nearly doubled the sediment inventory of ^{137}Cs in the Rhône river mouth (Charmasson, 2003) and increased the concentrations of ^{129}I (Yiou et al., 1997) up to 5 orders of magnitude above the expected from global fallout (~10^6 at·kg^{-1}, e.g. Snyder et al., 2010) in surface seawater off the Rhône estuary.

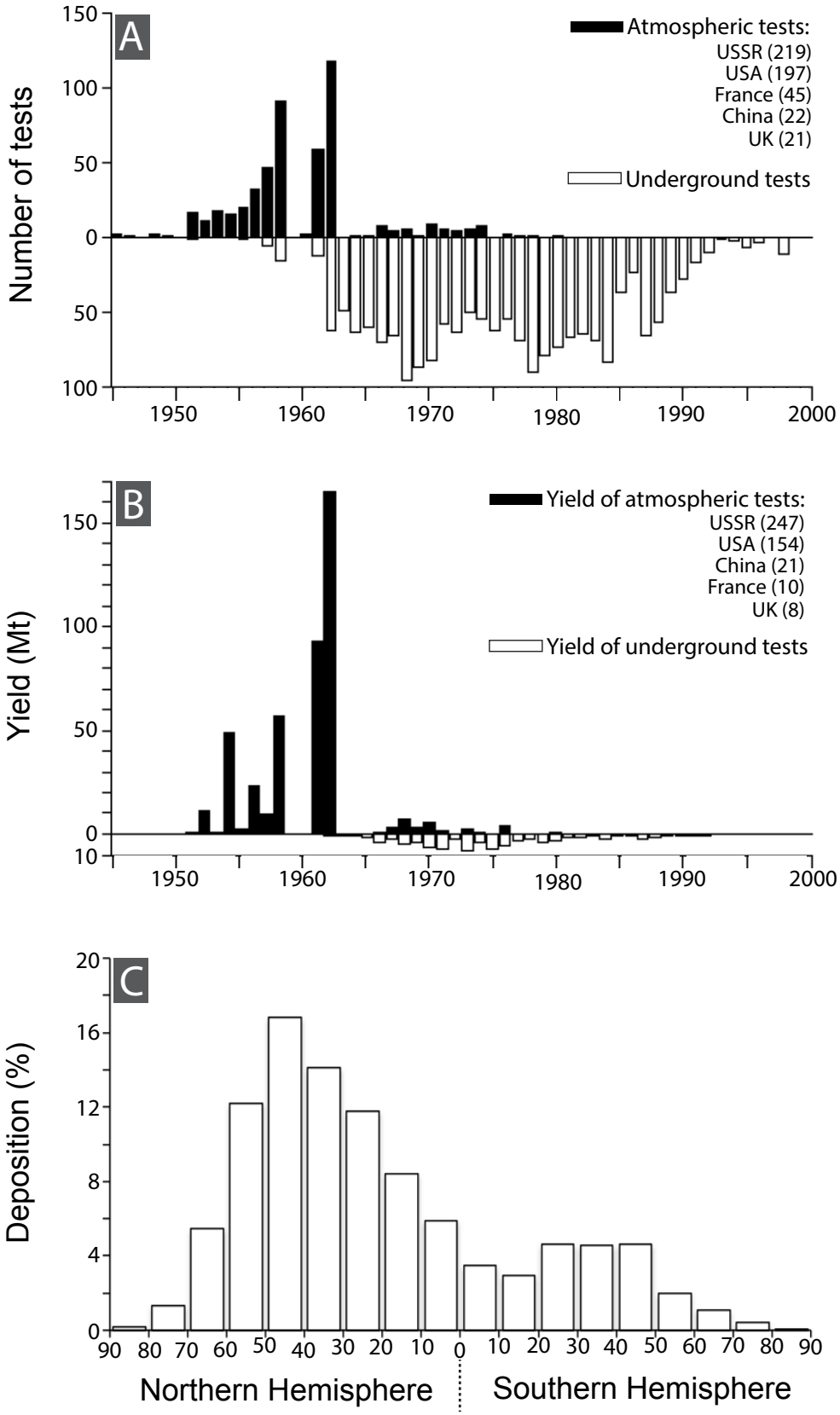

Figure 1.1. Number of atmospheric and underground nuclear weapon tests (A). Total yield of atmospheric and underground tests (B). Global fallout deposition in the Northern and Southern hemispheres (C). Data for this figure was taken from UNSCEAR (2000).

Table 1.1. Radionuclides released during atmospheric nuclear weapon tests. Data are taken from UNSCEAR (2000) unless indicated otherwise.

Radionuclide	Half-life ($T_{1/2}$)	Global release	
		1963* PBq (kg)	2017** PBq (kg)
^{3}H	12.33 a	1.9×10^{5}	1.1×10^{4}
^{14}C	5,730 a	2.1×10^{2}	2.1×10^{2}
^{54}Mn	312.3 d	4.0×10^{3}	~0
^{55}Fe	2.73 a	1.5×10^{3}	4.7×10^{-3}
^{89}Sr	50.53 d	1.2×10^{5}	~0
^{90}Sr	28.78 a	6.2×10^{2}	1.9×10^{2}
^{91}Y	58.51 d	1.2×10^{5}	~0
^{95}Zr	64.02 d	1.5×10^{5}	~0
^{103}Ru	39.26 d	2.5×10^{5}	~0
^{106}Ru	373.6 d	1.2×10^{4}	~0
^{125}Sb	2.76 a	7.4×10^{2}	2.6×10^{-3}
^{129}I[a]	15.7 Ma	5.3×10^{-4} (90)	5.3×10^{-4} (90)
^{131}I	8.02 d	6.8×10^{5}	0
^{137}Cs	30.07 a	9.5×10^{2}	3.0×10^{2}
^{140}Ba	12.75 d	7.6×10^{5}	0
^{141}Ce	32.50 d	2.6×10^{5}	~0
^{144}Ce	284.9 d	3.1×10^{4}	~0
^{236}U[b]	23.5 Ma	5.3×10^{-3} (900)	5.3×10^{-3} (900)
^{237}Np[c]	2.14 Ma	3.8×10^{-2} (1500)	3.8×10^{-2} (1500)
^{239}Pu	24,110 a	6.5×10^{0}	6.5×10^{0}
^{240}Pu	6,563 a	4.4×10^{0}	4.3×10^{0}
^{241}Pu	14.35 a	1.4×10^{2}	1.3×10^{1}

*Data from UNSCEAR (2000) were reported taking 1963 as the reference year.

**Data decay corrected to 2017.

[a]Mean of estimated releases (50-150 kg, refs Hou, 2004; Raisbeck and Yiou, 1999; Wagner et al., 1996).

[b]Release estimated by Sakaguchi et al., (2009).

[c]Release estimated by Beasley et al., (1998).

Table 1.2. Annual releases reported by La Hague between 2013 and 2015 (AREVA, 2015).

Radionuclide	Limit (TBq)	Activity (TBq)			% of limit in 2015
		2013	2014	2015	
^{3}H	18,500	13,400	12,700	13700	74
Iodine	2.6	1.58	1.55	1.66	63.9
^{14}C	14	8.58	8.32	8.52	60.9
^{90}Sr	11	0.29	0.47	0.22	2
^{137}Cs	8	0.58	0.86	0.57	7.1
^{134}Cs	0.5	0.03	0.043	0.033	6.7
^{106}Ru	15	1.22	1.23	1.52	10.1
^{60}Co	1.4	0.08	0.07	0.059	4.2
Other beta-gamma emitters	60	2.91	2.27	2.25	3.7
Alpha emitters	0.14	0.02	0.0214	0.023	16.2

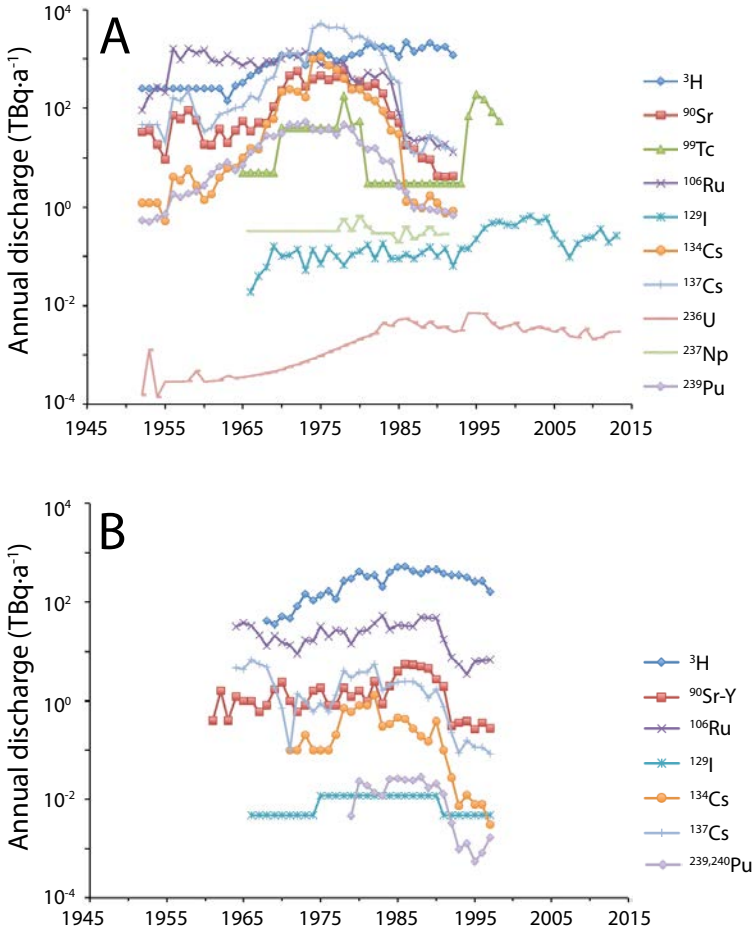

Figure 1.2. Annual liquid discharges reported from reprocessing plants of Sellafield, United Kingdom (A) and Marcoule, France (B). Releases from Sellafield were taken from Gray et al., (1995) except for: ^{99}Tc (Lindahl et al., 2003); ^{129}I and ^{236}U (Christl et al., 2015); and ^{237}Np (Beasley et al., 1998). For ^{237}Np releases we assumed a constant discharge of total releases reported for the 1966-1977 time period (Beasley et al., 1998). Releases from Marcoule were taken from Charmasson, (1998), except for ^{129}I (Hou et al., 2009).

Nuclear accidents constitute the third largest source of artificial radionuclides to the environment. Several nuclear incidents occurred after the construction of the first nuclear reactor in 1942. However, of major concern have been the nuclear accidents that occurred in Chernobyl, Fukushima Dai-ichi, Three Mile Island and the SL-1 accident in Idaho (USA). Different from global fallout, but with comparable inputs of radionuclides from the nuclear reprocessing industry, the nuclear accidents are characterized by a point-source release, well defined in time and space that needs to be constrained. This has been the recent case of the Fukushima Dai-chi nuclear accident that occurred in 2011. The loss of the cooling systems of three reactor units due to the damage of the power supply systems caused the discharge of artificial radionuclides to the Pacific Ocean, increasing the current North Pacific inventory, in the case of ^{137}Cs, by about 20% (Buesseler, 2014). After 2011,

major efforts have been done to quantify releases of artificial radionuclides to the coast off Japan, not only for those radionuclides that pose a higher radiological risk to population (e.g. ^{131}I, ^{134}Cs, etc.), but also to the radionuclides that additionally, might be used for tracer purposes in time scales from decades to centuries (^{90}Sr, ^{129}I, ^{137}Cs, etc.). *Chapter 2* covers a small part of it.

1.2. Artificial radionuclides in the oceans: distribution and application as ocean tracers

The ocean surface covering about 70% of the Earth surface is the ultimate destination of radioactive contaminants introduced directly from the atmosphere, through freshwater runoff of radionuclides deposited on land, or through direct liquid discharge from source points. Once in the marine environment, oceanic processes control the distribution and fate of artificial radionuclides. Depending on the chemical and physical properties of each nuclide, conservative radionuclides will remain in the water column and travel long distances in the open ocean transported by ocean currents (e.g. radiocaesium: Bowen et al., 1980; Livingston et al., 1984). Particle-reactive radionuclides (e.g. Pu isotopes: Baxter et al., 1995; Sholkovitz, 1983) will suffer additionally from scavenging by, and remineralization of, particulate matter. As consequence, particle-reactive radionuclides are additionally transported downward by sinking particles resulting in their removal from the water column to the sediments. The idea behind the tracer application is that artificial radionuclides can provide information (e.g. magnitude and time-scales) about the processes in which they are involved.

The full application of artificial radionuclides as tracers, however, requires a good knowledge of each source, notably the amount and timing of the release i.e. input function. One approach for quantifying the magnitude of the overall radionuclide sources in the water column or sediments is the integration of radionuclide concentrations measured at different depths. This tool also allows suggesting if there are other sources than global fallout for a given radionuclide. For example, in the water column of the Mediterranean Sea ^{236}U inventories were about 2.5 larger than expected from global fallout indicating probable inputs from the Marcoule Reprocessing Plant (Chamizo et al., 2016). The next

step is the identification of sources, which can be achieved by using radionuclide ratios. Global fallout can be distinguished from Fukushima releases using the $^{137}Cs/^{90}Sr$ activity ratio, that increased from ~1.5 before the accident (global fallout; UNSCEAR, 2000) to ~40 in spring of 2011 (Casacuberta et al., 2013). Similarly, one may use the $^{129}I/^{236}U$ atom ratio to distinguish the releases from Sellafield and La Hague reprocessing plants with mean $^{129}I/^{236}U$ ~350 from the global fallout characterized by $^{129}I/^{236}U$ atom ratios <1 (e.g. Christl et al., 2015). Once radionuclide input functions are well established, artificial radionuclides can be used as tracers of oceanic processes. This is the case of several studies that used artificial radionuclide discharges of ^{99}Tc, ^{129}I, ^{137}Cs and ^{236}U, among others, from Sellafield, La Hague or from both reprocessing plants, to investigate water transport pathways, water mixing and transit times from the northeast Atlantic to the Artic Ocean and back to the northwest Atlantic Ocean (e.g. Christl et al., 2015; Dahlgaard, 1995a; Dahlgaard et al., 1995b; Lindahl et al., 2003; Smith et al., 1998). This PhD thesis constitutes a first step towards that direction, particularly in the Mediterranean Sea.

1.3. Objectives and structure of the thesis

The aim of this PhD thesis is to understand the sources and distribution of radionuclides both in the coast off Japan (*Chapter 2*) and in the Mediterranean Sea (*Chapters 3 and 4*). This main goal was achieved by:

1) The determination of multiple radionuclide concentrations in surface and deep seawater samples and the discussion of their distributions in relation to their sources, water circulation and particle cycling.
2) The quantification of radionuclide inventories and of inventory ratios, and the comparison with radionuclide inputs from literature.
3) The characterization of the isotopic composition of water masses by considering several radionuclide relationships (e. g. $^{137}Cs/^{90}Sr$ activity ratio, $^{240}Pu/^{239}Pu$ atom ratio, etc.).

Specific objectives are addressed in *Chapters 2, 3 and 4* that cover one independent study in the coast off Fukushima and 2 studies in the Mediterranean Sea. Each of these chapters has its own particular sections covering the introduction, methodology, results, discussion and conclusion. *Chapters 2 and 3* have already been published.

The purpose of *Chapter 2* is to investigate the fate of radioactive contamination in the coast of Japan after the accident at the FDNPP, to quantify how much ^{90}Sr is still leaking from the FDNPP and to assess the change in seawater concentrations of contaminants since the nuclear accident in 2011. These are also overriding goals of the European COMET-FRAME project that aims at assessing the impact of recent releases from the Fukushima nucleaR Accident on the Marine Environment (FRAME). To this end, our group participated in a research cruise conducted in the most heavily impacted sea area comprised between 0.8 and 110 km off the FDNPP in September 2013. The distribution of the concentrations of ^{90}Sr, ^{134}Cs and ^{137}Cs are investigated in open and coastal seawater samples as well as in groundwater samples. The results for samples collected in September 2013 are further discussed in a broader time period starting before the accident in 2011 until June 2015 considering earlier studies and sea monitoring data reported by Tokyo Electric Power Company (TEPCO). This work was published in *Environmental Science and Technology* in 2016 (Castrillejo et al., 2016).

Chapter 3 presents the first zonal distributions of ^{129}I concentrations and ^{236}U/^{238}U atom ratios in the Western and Eastern Mediterranean Sea, as well as in shallow seawater samples collected from the central Black Sea. I participated in a 30-day cruise sailing across Eastern and Western Mediterranean waters in May 2013. The obtained results allow understanding the distribution of ^{129}I and ^{236}U/^{238}U in relation to water mass circulation occurring in the Mediterranean Sea. To constrain their sources, we estimated their inventories and compared measured and simulated concentrations obtained by using a relatively simple ocean circulation box model. This work has been published in *Science of the Total Environment* in 2017 (Castrillejo et al., 2017). C*hapter 4* continued the work in the Mediterranean Sea through the presentation of the first transect of ^{237}Np that will be discussed in relation to ocean circulation and other measured radionuclides (^{129}I, ^{137}Cs and ^{236}U). The addition of a substantial dataset on ^{137}Cs and Pu isotopes will also allow the general constraint of artificial radionuclide sources to the Mediterranean and will raise new

questions about the oceanic mechanisms controlling the fate of Pu isotopes in Eastern Mediterranean waters.

CHAPTER 2

Reassessment of ^{90}Sr, ^{137}Cs, and ^{134}Cs in the coast off Japan derived from the Fukushima Dai-ichi nuclear accident

This chapter is based on:

Castrillejo, M., Casacuberta, N., Breier, C., Pike, S. M., Masqué, P., Buesseler, K. O., 2016. Reassessment of ^{90}Sr, ^{137}Cs, and ^{134}Cs in the Coast off Japan Derived from the Fukushima Dai-ichi Nuclear Accident. Environmental Science and Technology, 50, 173-180.

2.1. Abstract

The years following the Fukushima Dai-ichi nuclear power plant (FDNPP) accident, the distribution of ^{90}Sr in seawater in the coast off Japan has received limited attention. Yet, ^{90}Sr is a major contaminant in waters accumulated within the nuclear facility and in the storage tanks. Seawater samples collected off the FDNPP in September 2013 showed radioactive levels significantly higher than pre-Fukushima within 6 km off the FDNPP. These samples, with 8.9 ± 0.4 Bq·m^{-3} for ^{90}Sr, 124 ± 3 Bq·m^{-3} for ^{137}Cs and 54 ± 1 Bq·m^{-3} for ^{134}Cs, appear to be influenced by ongoing releases from the FDNPP, with a characteristic ^{137}Cs/^{90}Sr activity ratio of 3.5 ± 0.2. Beach surface water and groundwater collected in Sendai Bay had ^{137}Cs concentrations of up to 43 ± 1 Bq·m^{-3}, while ^{90}Sr was within pre-Fukushima levels (1-2 Bq·m^{-3}). These samples appear to be influenced by freshwater inputs carrying a ^{137}Cs/^{90}Sr activity ratio closer to that of the FDNPP fallout deposited on land in spring 2011. Ongoing inputs of ^{90}Sr from FDNPP releases would be on the order of 2.3-8.5 GBq·d^{-1} in September 2013, likely exceeding river inputs by 2-3 orders of magnitude. These results strongly suggest that a continuous surveillance of artificial radionuclides in the Pacific Ocean is still required.

2.2. Introduction

On March 11, 2011, the Tohoku earthquake and the subsequent series of tsunamis severely damaged the Fukushima Dai-ichi nuclear power plant (FDNPP). Failure of cooling systems caused a temperature increase resulting in the production of hydrogen and other gases within the reactors. This led to explosions releasing radioactive gas and debris to the atmosphere. Additionally, cooling water was directly discharged to the sea after being in contact with the nuclear fuel. The resulting release of ^{90}Sr ($T_{1/2}$ = 28.9 yr), ^{137}Cs ($T_{1/2}$ = 30.17 yr) and ^{134}Cs ($T_{1/2}$ = 2.07 yr), among other radionuclides (e.g. ^{85}Kr, ^{129,131}I, ^{132}Te, ^{133,135}Xe), was the largest ever uncontrolled input of artificial radionuclides into the ocean (Buesseler et al., 2011; Steinhauser et al., 2014).

Before the FDNPP accident, the dominant source of ^{90}Sr and ^{137}Cs in the coast off Japan was global fallout from nuclear weapon tests. Pre-Fukushima concentrations in surface waters in the ocean were on average 1 Bq·m^{-3} for ^{90}Sr (Ikeuchi, 2003; Povinec et al., 2005) and 1 - 2 Bq·m^{-3} for ^{137}Cs (Aoyama and Hirose, 2004). Due to the short half-life of ^{134}Cs, prior sources of this isotope were no longer detectable in the coast off Japan.

Studies following the accident in 2011 focused on ^{137}Cs and ^{134}Cs, as they showed some of the highest activities and they are relatively easy to determine by gamma spectrometry, thus providing rapid information about the radioactive releases from FDNPP. Caesium is a volatile element that was released to the atmosphere and through liquid discharges in comparable amounts, with a ^{134}Cs/^{137}Cs activity ratio ~1 (e.g. Buesseler et al., 2011). Total atmospheric releases of ^{137}Cs have been estimated to range from 13 to 36 PBq (Chino et al., 2011; Morino et al., 2011; Stohl et al., 2012) from which the majority was deposited in the Pacific Ocean while about 20% were deposited on land (Chino et al., 2011; Morino et al., 2011). Most of the atmospheric releases occurred during the first week after the accident, leading to radiocaesium concentrations up to 10 Bq·m^{-3} in surface seawater as far as 1700 km off FDNPP (160 ºE and 40 ºN) in April 2011 (Aoyama et al., 2013; Honda et al., 2012). Estimates of total liquid discharges of ^{137}Cs varied from 3.5 to 27 PBq by May - July 2011 (Bailly du Bois et al., 2012; Charette et al., 2013; Rypina et al., 2013; Tsumune et al., 2013, 2012). The amount of ^{137}Cs directly discharged into the ocean was comparable to authorized releases from nuclear reprocessing plants (i.e. ~39 PBq from

1970 to 1998 from Sellafield, UK; Aarkrog, 2003) but larger than ^{137}Cs releases from Chernobyl accident (~16 PBq; IAEA, 2005). Liquid discharges to the North Pacific Ocean peaked on April 6, 2011, when concentrations of ^{137}Cs of up to 68 × 10^6 Bq·m^{-3} were recorded near the discharge channels of the FDNPP (Buesseler et al., 2011). In the same month, ^{137}Cs concentrations were 10 - 1000 times lower 30 km offshore along a transect at 141º 24′ N conducted by the Japanese Ministry of Education, Culture, Sports, Science and Technology (MEXT) (Buesseler et al., 2011). In June 2011, maximum radiocaesium concentrations were ~3.9 × 10^3 Bq·m^{-3} in waters between 30 and 600 km off FDNPP (Buesseler et al., 2012), while levels near the discharge channels at that time were still of ~33 × 10^3 Bq·m^{-3} (Buesseler et al., 2011).

At the time of the accident, the total inventory of ^{90}Sr in reactor core units 1-3 was ~500 PBq, which is about 70% of the ^{137}Cs inventory (Nishihara et al., 2012; Povinec et al., 2013). Due to the lower volatility of ^{90}Sr compared to ^{137}Cs, the majority of ^{90}Sr remained within the reactors while only a small fraction reached the atmosphere. Levels of ^{90}Sr in FDNPP fallout recorded on land were in fact up to 4 orders of magnitude lower than for ^{137}Cs (Mishra S, 2014; Povinec et al., 2012; Steinhauser et al., 2013). Most of ^{90}Sr was discharged as cooling water to the Pacific Ocean. ^{90}Sr input estimates range from 0.09 - 0.9 PBq (Casacuberta et al., 2013) to ~1 - 6.5 PBq (Povinec et al., 2012). These amounts are comparable to total authorized liquid discharges into the ocean from the nuclear reprocessing plants in Sellafield and La Hague between 1970 and 1998 (~4 PBq, decay corrected to year 2000; IAEA, 2005). Between April 2011 and February 2012, ^{90}Sr concentrations near the discharge channels and as far as 15 km off the FDNPP were up to 5 orders of magnitude higher (max. 4 × 10^5 Bq·m^{-3}) than pre-Fukushima levels, according to data made public by TEPCO (Povinec et al., 2012; TEPCO, 2015a). Beyond 15 km off the coast of Fukushima, concentrations of ^{90}Sr ranged from 0.8 to 85 Bq·m^{-3} between 30 and 600 km off FDNPP and from 1 to 31 Bq·m^{-3} further east (145 - 150 ºE and 34 - 40 ºN) in June 2011 (Casacuberta et al., 2013; Men et al., 2015). In surface waters off Miyagi, Fukushima and Ibaraki prefectures (see Figure 2.1 for location), ^{90}Sr was below 5 Bq·m^{-3} and close to pre-Fukushima levels by the end of August and mid - December 2011, respectively (Oikawa et al., 2013). More recent data for May - June 2012 shows ^{90}Sr (0.5-

3.6 $Bq \cdot m^{-3}$) close to or slightly higher than pre-Fukushima concentrations around Taiwan and off Japan between 145 – 155 ºE and 25 – 35 ºN (Men et al., 2015).

After the accident, efforts at the FDNPP attempted to reduce the amount of groundwater flowing into reactor buildings (frozen soil wall and ground water bypass), isolating highly radioactive stagnant water located in trenches (ice wall) and preventing further leakages from tanks or the nuclear facility reaching the ocean (seaside wall; TEPCO, 2015a). Despite the measures listed above, as of June 2015, ~300 $m^3 \cdot d^{-1}$ of groundwater infiltrated the reactor buildings, becoming highly enriched in radioactivity once in contact with melted nuclear fuel and/or previously contaminated water. This has resulted in ~90 $\times 10^3$ m^3 of contaminated water accumulating under the FDNPP facility in 2014 – 2015 (TEPCO, 2015a). To compensate for this, water is pumped out at a rate of ~600 $m^3 \cdot d^{-1}$ and treated in - situ with primary Cs sorbents (e.g. zeolite) to reduce radioactivity levels. Approximately half of this water is re-used for cooling the reactors down, while ~300 $m^3 \cdot d^{-1}$ are stored in tanks. Stored water (a total of 665 $\times 10^3$ m^3 by June 11, 2015; TEPCO, 2015b) is treated using additional Cs removal systems since May 2011. Additional decontamination systems such as the Multiple - Nuclide Removal System (ALPS) have been used for the partial removal of ^{90}Sr (reduction factor of 100 – 1000; TEPCO, 2014) among other radionuclides, routinely since late 2014 (TEPCO, 2015a). Despite this treatment, significant amounts of ^{90}Sr and tritium (which cannot be readily removed with current technology), remain in the stored water today.

Monitoring of ^{90}Sr is desirable for two main reasons. First, ^{90}Sr is a long-lived fission product of high radiological concern, particularly over long time periods. Chemically similar to calcium, ^{90}Sr is incorporated in bone tissue emitting highly energetic beta particles mainly during decay of its short-lived daughter ^{90}Y that can increase the chance of leukemia or bone cancer. Second, due to its conservative behavior in seawater, ^{90}Sr is also a suitable tracer of ocean circulation and can be used to identify sources with a characteristic $^{137}Cs/^{90}Sr$ activity ratio (e.g. Casacuberta et al. 2013). Nevertheless, ^{90}Sr has been much less studied than radiocaesium, either because of its laborious chemical separation or because its initial releases were not expected to be as high as for other

radionuclides during the Fukushima accident in March - April 2011. Today, ^{90}Sr is a major radioactive contaminant in reactors and storage tanks and leaks of this isotope from the FDNPP to the ocean should be monitored. Almost no ^{90}Sr data from seawater collected after 2011 and near FDNPP have been published in peer - reviewed journals, nor has the magnitude of recent releases of this isotope to the ocean been well studied.

The aim of this work is to re-evaluate the concentrations and the distribution of ^{90}Sr, as well as ^{137}Cs and ^{134}Cs, in the coast off Japan in September 2013. We also attempt to identify the current potential sources of these isotopes and estimate the magnitude of recent uncontrolled releases of ^{90}Sr from the FDNPP to the ocean. For this purpose, we present data on ^{90}Sr, ^{137}Cs and ^{134}Cs in off - shore seawater, surface beach water and groundwater collected in September 2013 and compare it with peer - reviewed literature and TEPCO's data available until June 2015.

2.3. Materials and methods

2.3.1. Study site area and sampling

Water samples for the analysis of ^{90}Sr (n = 30) and ^{134,137}Cs (n = 44) were collected in the area between 0.8 km and 110 km off the FDNPP on board the *R/V Daisan Kaiyo Maru* in September 2013 (Figure 2.1). The main transect was located in front of the FDNPP along 37.42 ºN and included surface stations and 4 shallow profiles (St.: 1, 3, 5, 7; maximum sampled depths of 10, 25, 55 and 115 m, respectively). A fifth vertical profile (St. 14, max. sampled depth of 500 m) was sampled 110 km southeast of the FDNPP. The area comprised between stations 1 to 14 is found in the confluence zone of two major western boundary currents. The warm and saline Kuroshio current penetrates from the south along the continental slope and flows off northeastward at ~35 ºN, south of FDNPP. The Oyashio penetrates from the north flowing southward and separates off Japan at ~45 ºN, north of FDNPP. Off - shelf, the confluence of the two currents results on the eastward transport of waters to the open Pacific Ocean characterized by strong and instable jet currents leading to meso - scale eddies and meanders (Rypina et al., 2013). In addition, along-shore

currents govern the coastal region near FDNPP with a predominant north to south component, although their direction and strength may change with the wind field every 3 - 4 days (Nakamura, 1991).

Collection of seawater throughout the water column was done using a conductivity – temperature - depth rosette equipped with Niskin bottles. Surface samples were collected during the occupation of each station and between stations for higher temporal and spatial resolution using the ship underway system. Additionally, beach surface water and groundwater was collected at Nagahama and Nobiru beaches, Sendai Bay, about 100 km north of FDNPP. These samples are named the northern beach samples and groundwater, hereinafter.

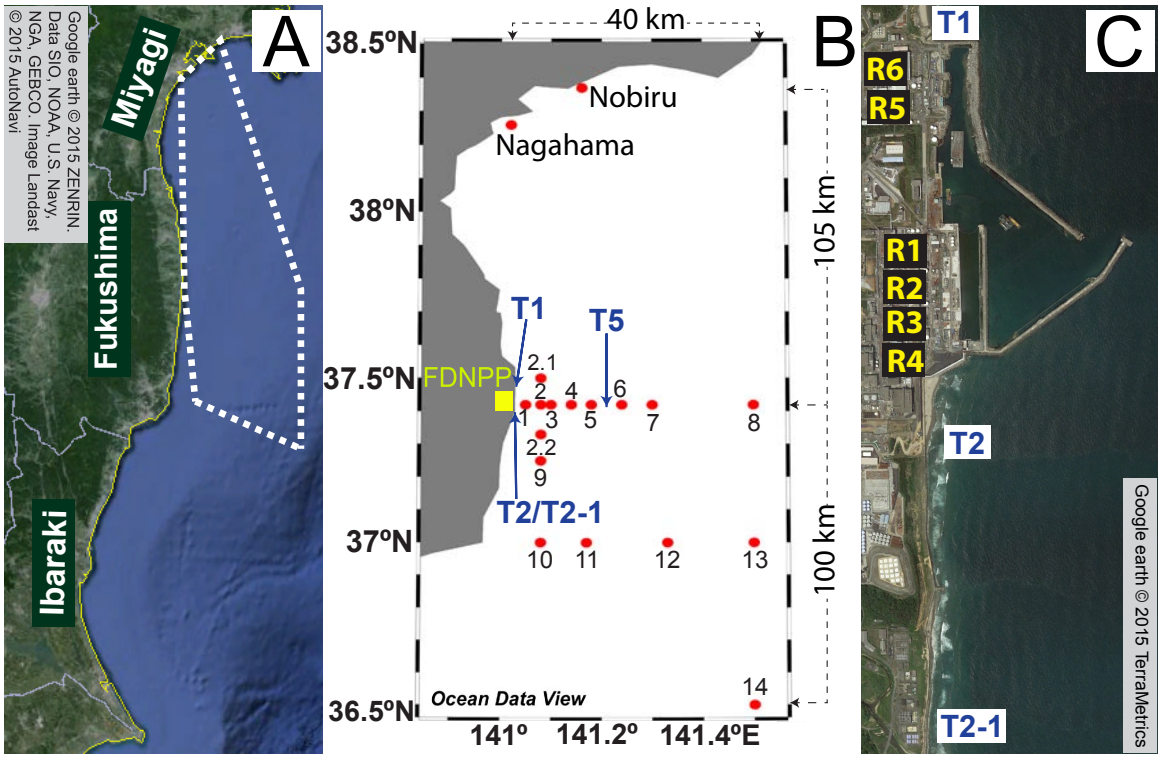

Figure 2.1. A) Prefectures of Miyagi, Fukushima and Ibaraki. Dashed line shows study area of *Daisan Kaiyo Maru* cruise in September 2013. B) Zoom of the study area showing the location of sampling sites, TEPCO's monitoring sites (T1, T2/T2-1 and T5) and FDNPP. C) FDNPP, reactor units 1 - 6 and TEPCO's monitoring sites (T1, T2 and T2-1).

2.3.2. Extraction and quantification of radionuclides

Samples of 20 L were filtered on board using a cartridge filter (GE Hytrex. 1.0 μm nominal retention), and subsequently weighed and acidified with nitric acid to pH ~1 in the shore based laboratory.

Sr-90, ^{137}Cs and ^{134}Cs were extracted from each sample. Briefly, acidified seawater was spiked with 0.7 mg and 200 mg of stable Cs and Sr, respectively. The sample was then passed through columns filled with 5 mL of KNiFC - PAN ion exchange resin (Czech Technical University, Prague) for the extraction of radiocaesium (Šebesta, 1997). The resin was dried and placed in polyethylene vials for gamma counting of ^{134,137}Cs using high - purity germanium well detectors. The minimum detectable activity (MDA) was 0.1 Bq·m^{-3} for ^{137}Cs and 0.2 Bq·m^{-3} for ^{134}Cs for typical counting times of 50 hours. Concentration uncertainties were calculated by propagation of uncertainties in the count rate and detector calibration. Stable Cs and Sr were measured by ICP mass spectrometry in aliquots taken before and after the columns to determine the extraction recovery for Cs (87 – 99 %) and to check for any losses of Sr, which averaged < 2 %.

Determination of ^{90}Sr was carried out in Cs-free samples, following a protocol (Waples and Orlandini, 2010) based on the determination of its daughter ^{90}Y ($T_{1/2}$ = 64 h), adapted for seawater (Casacuberta et al., 2013). After the addition of 10 ug of stable Y, ^{90}Y was co - precipitated with iron hydroxides and purified using anion (Bio - Rad AG1 - X8, 100 - 200 mesh) and cation (Bio - Rad AG50W - X8, 100 - 200 mesh) ion - exchange columns. ^{90}Y decay was measured using a RISØ beta counter (RISO National Lab, Roskilde Denmark). ^{90}Sr activities were corrected for recovery by determining the concentrations of stable Sr and Y from aliquots taken along the entire radiochemical process. Y recoveries ranged from 67 to 93 %. The MDA ranged from 0.02 to 0.05 Bq·m^{-3} for typical counting times of 150 hours.

Analytical methods used in this study are more sensitive and allow detecting ^{90}Sr and ^{134,137}Cs at levels 1 - 3 orders of magnitude lower than MDA's reported by TEPCO: ^{90}Sr (sites T1 - T5: average MDA for years 2011 – 2015 was >10 Bq·m^{-3}) and ^{137}Cs (sites T1 - T2/T2-1: average MDA for years 2012 – 2015 was ~1.4 × 10^{3} Bq·m^{-3}). MDA's variability may be partly explained by the smaller sample volumes and shorter counting times often

employed by TEPCO. For example, ^{134,137}Cs was initially measured in Marinelli beakers (<5 L) and counted by gamma spectrometry for 1 h, resulting in MDAs >5 × 10^3 Bq·m^{-3} in 2011. Later, they started using larger volumes (30 - 50 L), chemical separation techniques and longer counting times (~1 d) achieving MDAs >5 × 10^2 Bq·m^{-3} at sites T1 – T2/T2-1 by 2015. ^{90}Sr has been determined using a variety of extraction procedures (fuming nitric acid / ion exchange resin) and measurement techniques ('Low Background Gas Flow Counters' allowing gross beta counting, so called 'pico-beta' method or ICP-MS techniques) providing ^{90}Sr concentrations in the ~10 Bq·m^{-3} range level by 2015 (TEPCO, 2015a).

2.4. Results

The ranges of concentrations in samples collected in September 2013 were 0.6 - 8.9 Bq·m^{-3} for ^{90}Sr, 0.9 - 124 Bq·m^{-3} for ^{137}Cs and <0.2 - 54 Bq·m^{-3} for ^{134}Cs. Detailed information on the concentrations of ^{90}Sr, ^{137}Cs and ^{134}Cs (decay corrected to September 2013), ^{137}Cs/^{90}Sr activity ratio, sampling location and date, temperature and salinity are provided in the Appendix (A.1).

The highest concentrations in surface seawater were found close to FDNPP (0.8 - 6 km: stations 1 - 3), with ranges of 0.8 - 8.9, 2.3 – 124 and 0.3 - 54 Bq·m^{-3} for ^{90}Sr, ^{137}Cs and ^{134}Cs, respectively (Figure 2.2). Surface concentrations at stations located >6 km off FDNPP were 0.6 - 1.8, 1.6 - 4.7 and <0.2 - 2.6 Bq·m^{-3} for ^{90}Sr, ^{137}Cs and ^{134}Cs, respectively.

Station 1, the closest sampling site from FDNPP, showed the largest surface to bottom gradient in concentration (see Apendix A.2). At stations 3, 5, 7 and 14 (6 - 110 km off FDNPP), concentrations varied only in about 1.0 Bq·m^{-3} with depth and were usually significantly lower than at station 1. Concentrations below 2 m were lower than ~2.6 Bq·m^{-3} for ^{90}Sr and ~2.9 Bq·m^{-3} for ^{137}Cs. ^{134}C was below 0.6 Bq·m^{-3} and often undetectable (<0.2 Bq·m^{-3}) in waters between 15 and 500 m.

Concentrations in northern beach samples and groundwater in Sendai Bay were 1.0 – 1.8 Bq·m^{-3}, 9 - 43 Bq·m^{-3} and 4 - 17 Bq·m^{-3} for ^{90}Sr, ^{137}Cs and ^{134}Cs, respectively (Figure

2.2). These samples had salinities between 4 and 29, lower than that of seawater samples (salinity >33).

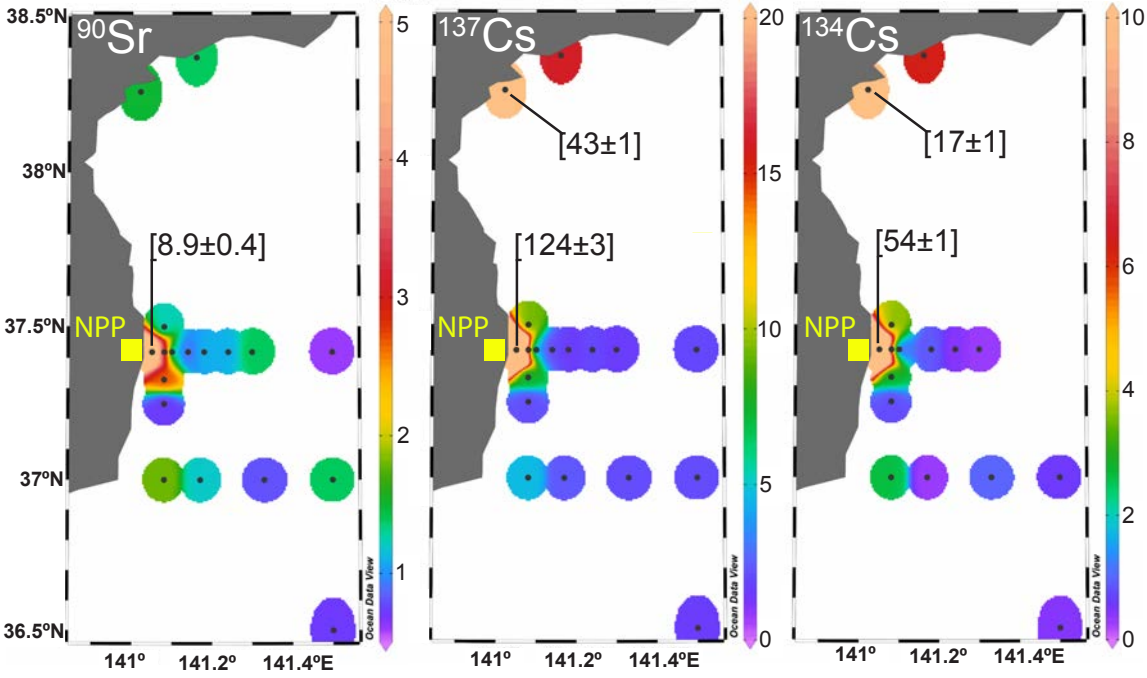

Figure 2.2. Surface concentrations of ^{90}Sr, ^{137}Cs and ^{134}Cs in September 2013 (in Bq·m^{-3}). Pre-Fukushima concentrations from literature (decay corrected to sampling) are: 0.9 - 1.1 Bq·m^{-3} for ^{90}Sr (IAEA, 2005; Povinec et al., 2012) and 1 - 2 Bq·m^{-3} for ^{137}Cs (Aoyama and Hirose, 2004).

2.5. Discussion

2.5.1. Determination of pre-Fukushima ^{90}Sr and ^{137}Cs

The pre-Fukushima levels of ^{90}Sr and ^{137}Cs in the coast off Fukushima can be calculated from our results using different approaches. One approach assumes that samples free of ^{134}Cs have not been influenced by FDNPP releases. Then, pre-Fukushima levels are calculated taking the average concentrations of ^{90}Sr and ^{137}Cs in these samples, resulting into 1.2 ± 0.7 and 1.8 ± 0.3 Bq·m^{-3}, respectively. This could be inaccurate, since decontaminated waters released from the FDNPP could be free of ^{134}Cs but still contain ^{90}Sr. Yet, only 2 samples free of ^{134}Cs have somewhat elevated ^{90}Sr concentrations (sample 13: 2.6 ± 0.2 Bq·m^{-3}; sample 26: 1.8 ± 0.1 Bq·m^{-3}). If these samples are not considered,

pre-Fukushima activities are ^{90}Sr = 0.9 ± 0.2 Bq·m^{-3} and ^{137}Cs = 1.8 ± 0.3 Bq·m^{-3} in the coast off Japan. In both cases, calculated levels are in good agreement with the literature prior to the accident (values decay corrected to September 2013): 0.9 - 1.1 Bq·m^{-3} for ^{90}Sr (IAEA, 2005; Povinec et al., 2012) and 1 - 2 Bq·m^{-3} for ^{137}Cs (Aoyama and Hirose, 2004). Pre-Fukushima levels of ^{137}Cs and ^{90}Sr will not be subtracted in this study, unless stated otherwise**.**

2.5.2. Time evolution of concentrations of ^{90}Sr and $^{134,137}Cs$ in the coast off Japan

The variation in time of ^{90}Sr (Figure 2.3A) and ^{137}Cs (Figure 2.3B) concentrations is presented for: TEPCO's sea monitoring sites (T1, T2/T2-1 and T5) near FDNPP (JAEA, 2015; JNRA, 2015; TEPCO, 2015a), published data on ^{90}Sr and ^{137}Cs between 2011 and 2015, and this study.

Compared to June 2011, concentrations had decreased one order of magnitude for ^{90}Sr and 2 - 3 orders of magnitude for $^{134,137}Cs$ by September 2013, although the sampling domain in 2013 was smaller and closer to the FDNPP (*K.O.K* cruise, 2011: 30 – 600 km; 2013: 0.8 – 110 km). In September 2013, seawater concentrations clearly above pre-Fukushima levels were recorded only near the FDNPP. Concentrations of ^{90}Sr and $^{134,137}Cs$ slightly higher than pre-Fukushima levels were also found at St. 10, south of FDNPP. These waters were probably advected southward by along-shore coastal currents. Such a pathway was observed for $^{134,137}Cs$ (Aoyama and Tsumune, 2012) as well by using surface drifters in year 2011 (Buesseler et al., 2012; Rypina et al., 2013). For example in June 2011, the radioactive plume was advected first south, then east towards the Kuroshio Current, which acted as a barrier to the southern transport of Fukushima waters. Elevated concentrations (^{90}Sr up to 30 and $^{134,137}Cs$ up to ~800 Bq·m^{-3}) were found ~600 km east off FDNPP (Yu et al., 2015) and even higher concentrations were detected associated with an eddy located 130 km southeast off FDNPP (^{90}Sr up to 85 and $^{134,137}Cs$ up to ~3800 Bq·m^{-3}; Buesseler et al., 2012; Casacuberta et al., 2013).

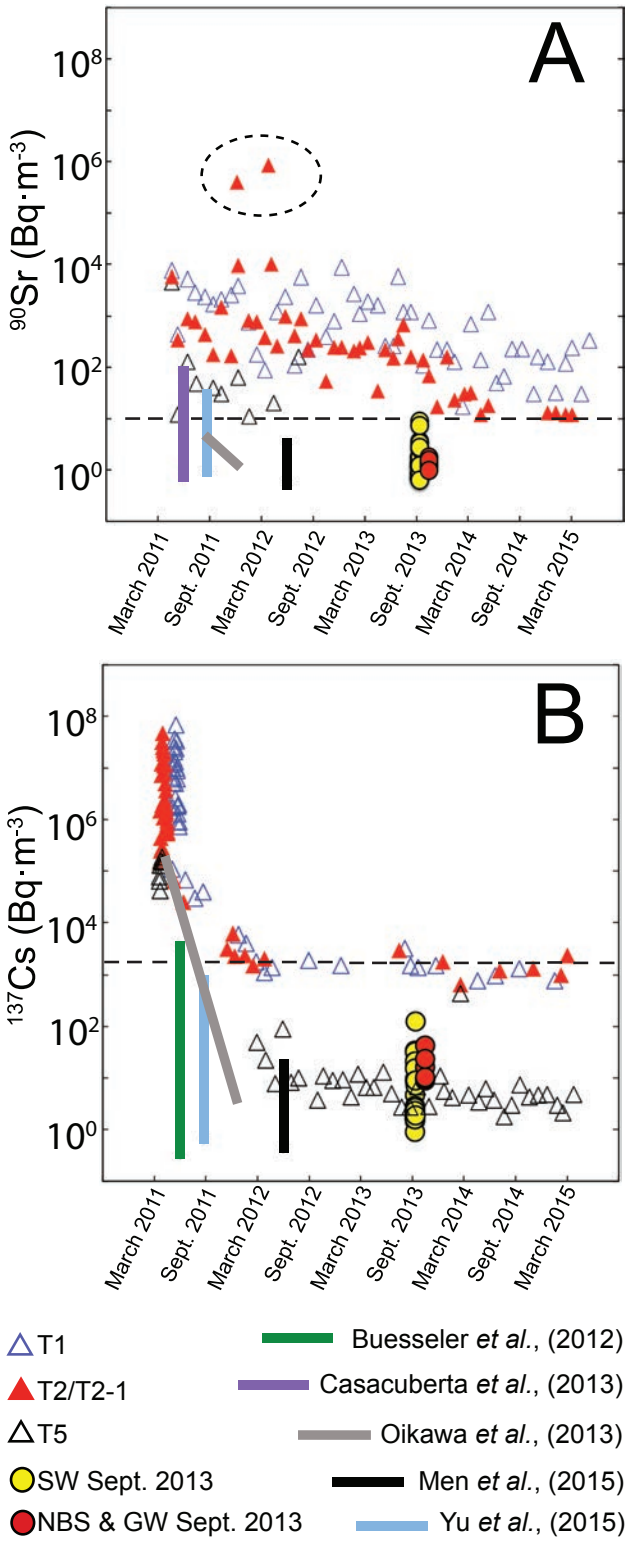

Figure 2.3. Concentrations in seawater (SW), northern beach samples (NBS) and groundwater (GW) collected in September 2013, TEPCO's sites near FDNPP (T1, T2/T2-1 and T5 surface) and in the coast off Japan (all depth) from March 2011 to July 2015 for: (A) ^{90}Sr and (B) ^{137}Cs. Major reported accidental releases (dashed black circle) and TEPCO's average MDAs for T1 and T2/T2-1 (dashed black line) are indicated.

Concentrations of ^{137}Cs in the coast off Japan in September 2013 were comparable to those measured in August - December 2011, while the ^{90}Sr maximum was about 7 Bq·m^{-3} higher in 2013 (Oikawa et al., 2013). Strontium and caesium are highly soluble in seawater and they were transported within weeks to months to the open Pacific Ocean in 2011 (Buesseler et al., 2012; Rypina et al., 2013) being diluted by advection, diffusion and meso - scale mixing (Dietze and Kriest, 2012; Min et al., 2013). These processes may explain the lower concentrations (^{90}Sr <3.57 and ^{137}Cs <18 Bq·m^{-3}) found off Japan in May – June 2012 (Men et al., 2015). Yet, concentrations in samples collected in September 2013 were higher than initially expected, since model simulations (Maderich et al., 2014a; Maderich et al., 2014b) and drifter trajectories (Buesseler et al., 2012; Rypina et al., 2013) show that very little ^{90}Sr or ^{134,137}Cs released shortly after the accident in spring 2011 should have remained in our study domain. Furthermore, the decay corrected (and pre-Fukushima levels subtracted) ^{134}Cs/^{137}Cs activity ratio recorded to September 2013 was 0.98 ± 0.01 in samples with ^{137}Cs concentrations above pre-Fukushima. This indicates continuing releases from the FDNPP.

TEPCO has been routinely monitoring the waters around FDNPP since the accident. Unfortunately, their detection limits were high (see Methods), thus much of their data are reported as below their detection limit. Also, they generally do not report the uncertainties associated with their measurements. This does not allow for a detailed reconstruction of ^{90}Sr releases and distribution in the coast off Fukushima. Nevertheless, TEPCO's data are useful to identify relevant trends of ^{90}Sr and ^{137}Cs and concentrations near the FDNPP over time (Figure 2.3). Site T1 is located ~30 m north of the discharge channel of reactor units 5 and 6 (see Figure 2.1 for site locations). T2 was initially located ~330 m south of the discharge channel of reactor units 1 - 4 and was moved 1 km further south after December 2012 (renamed T2-1). T5 is 15 km offshore, in front of FDNPP. From the peak of liquid releases on April 6, 2011, to June 2015, ^{137}Cs concentrations (Figure 2.3B) have decreased by 4-5 and 5-6 orders of magnitude near the discharge channels (T1, T2/T2-1), and 15 km offshore FDNPP (T5), respectively. By late April 2011, ^{137}Cs was about ~10^5 Bq·m^{-3} at T1 - T2/T2-1 and decreased gradually to ~10^3 Bq·m^{-3} by April 2012, remaining detectable above TEPCO's MDA (>1 × 10^3 Bq·m^{-3}) until June 2015. At T5, ^{137}Cs concentrations were lower and generally have remained within 10^1 - 10^2 Bq·m^{-3} since fall 2012.

Concentrations of ^{90}Sr (Figure 2.3A) ranged between 10 and 10^4 Bq·m^{-3} between April 2011 and February 2015, but anomalously higher concentrations had been measured at specific times, linked to accidental releases reported by TEPCO (e.g. December 5, 2011: 4 × 10^5 Bq·m^{-3}; and March 26, 2012: 8.5 × 10^5 Bq·m^{-3}). The high concentrations recorded at these sites are strong evidence of the continuous release of contaminated water to the ocean through the spring of 2015.

2.5.3. Time evolution of the sources of ^{90}Sr and ^{134,137}Cs in the coast off Japan

The sources of artificial radionuclides in the marine environment can be distinguished using the ^{134}Cs/^{137}Cs and ^{137}Cs/^{90}Sr activity ratios. The main sources of ^{90}Sr and ^{137}Cs in the coast off Japan since the accident in 2011 are two: i) global fallout from nuclear weapon tests, with a characteristic ratio of ^{137}Cs/^{90}Sr ~1.5 in the world oceans (UNSCEAR, 2000) and considered as pre-Fukushima in this study; ii) atmospheric fallout and liquid releases from the FDNPP with a ^{134}Cs/^{137}Cs activity ratio of ~1 (e.g. Buesseler et al., 2011). FDNPP fallout mainly occurred in the first two weeks after the accident, with a ^{137}Cs/^{90}Sr ratio of ~1000 (Povinec et al., 2012). Massive liquid releases of cooling water in spring 2011 resulted in seawater ^{137}Cs/^{90}Sr ratios of about 39 ± 1 in waters beyond the coast (Casacuberta et al., 2013), but the ratio of liquid releases has changed over time (Figure 2.4).

^{137}Cs/^{90}Sr activity ratios from March 2011 to July 2015 are compiled in Figure 2.4. The ^{137}Cs/^{90}Sr activity ratio shifted abruptly from the pre-Fukushima ratio (~1.5, dashed black line in Figure 2.4) due to FDNPP liquid releases and, to a minor extent, FDNPP fallout. This results in a broad range of the activity ratio, from 0.2 to 180 along the *K.O.K* study area and further east at 34 - 40 ºN in June 2011 (Casacuberta et al., 2013; Yu et al., 2015). In surface waters off the prefectures of Fukushima and neighboring Miyagi to the north and Ibaraki to the south, the ratio was (2.6 - 50) in August - December 2011 (Oikawa et al., 2013), still higher than pre–Fukushima. The ^{137}Cs/^{90}Sr activity ratio in all samples collected in September 2013 ranged from 0.6 to 28. Near FDNPP, the variability of the

$^{137}Cs/^{90}Sr$ activity ratio has been even larger (Povinec et al., 2012): at T2/T2-1, the ratio has been fluctuating between 10^{-3} and 10^{2} from April 2011 to February 2014 (last recorded data). At T1, ratios were reported until December 2014 and showed a slightly smaller range (~10^{-1} - 10^{2}). Since 2013, the ratio at T1 and T2-1 appears to be more stable, yet variations larger than 1 order of magnitude were still observable.

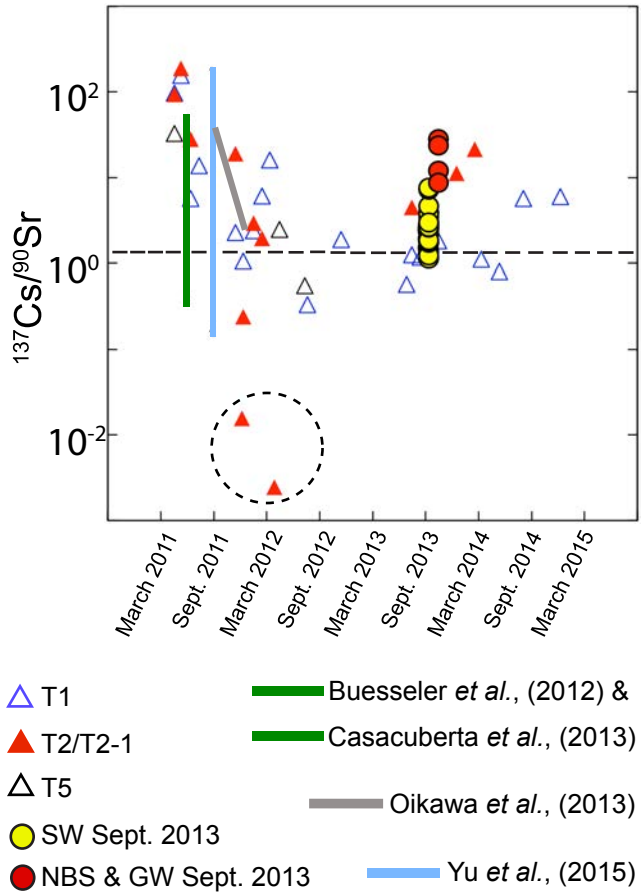

Figure 2.4. $^{137}Cs/^{90}Sr$ activity ratio in seawater (SW), northern beach samples (NBS) and groundwater (GW) collected in September 2013, in TEPCO's monitoring sites near FDNPP (T1, T2/T2-1 and T5) and other studies in the coast off Japan from March 2011 to July 2015. Accidental releases (dashed black circle) and pre-Fukushima activity ratio (dashed black line) are indicated.

After the massive releases of cooling water in spring 2011, other accidental liquid discharges have undoubtedly caused the largest variations in the ratio near FDNPP (dashed black circles, Figure 2.4). For example, ~150 L of Cs–treated water containing ~15 GBq of ^{90}Sr was discharged to the ocean in December 5, 2011, leading to a low $^{137}Cs/^{90}Sr$ activity ratio of 0.016 at T2 (Povinec et al., 2012; TEPCO, 2015a). Another ~120 tons leaked from

piping connecting a desalination unit with a concentrated water tank in March 2012 (TEPCO, 2015a). From this volume, at least 80 L reached the discharge channel T2, where the lowest ^{137}Cs/^{90}Sr activity ratio was recorded (0.002; TEPCO, 2015a). Many other leaks have been reported likely reaching the Pacific Ocean, although not all of them have been recorded in TEPCO's monitoring areas (e.g. March 11, 2015: 750 tons of contaminated rain water with maximum concentrations for total β emitters of about 8×10^6 Bq·m^{-3}; ~50% of which is commonly considered ^{90}Sr; TEPCO, 2015a). There might have been other accidental releases of which we are unaware of and whose impact in the ocean could not be identified because of low sampling frequency of the monitoring for ^{90}Sr.

In order to constrain the contributions of the distinct sources to the caesium and strontium concentrations collected in September 2013, data from this study are plotted together with the characteristic ^{137}Cs/^{90}Sr activity ratios of the known sources (Figure 2.5 A and B). Seawater samples collected in 2013, particularly those with the highest concentrations and located near surface and within 6 km from the FDNPP, were characterized by a ^{137}Cs/^{90}Sr activity ratio of 3.5 ± 0.2 (Figure 2.5B). The ratio does not differ significantly (3.4 ± 0.6) if we subtract pre-Fukushima levels of ^{90}Sr (1.2 ± 0.7 Bq·m^{-3}) and ^{137}Cs (1.8 ± 0.3 Bq·m^{-3}; see Appendix A.3). This ^{137}Cs/^{90}Sr activity ratio is about one order of magnitude lower than the liquid discharges in spring 2011 (Casacuberta et al., 2013), and consistent with the fact that any spills from the tanks or groundwater entering the ocean would be enriched in ^{90}Sr relative to releases in spring 2011, either because caesium has a higher sorption coefficient than strontium on soils (Gil-García et al., 2009), or because of active decontamination of caesium.

In some seawater samples (e.g. sample 13), the measured ^{137}Cs/^{90}Sr activity ratio was even lower than pre–Fukushima values. This can only be explained by FDNPP releases similar to those that occurred in December 2011 (Povinec et al., 2012) or February 2012 (TEPCO, 2015a) which were extremely high in ^{90}Sr. Samples collected >6 km away from the FDNPP had relatively low concentrations of ^{90}Sr and ^{137}Cs (and usually undetectable ^{134}Cs) and a ^{137}Cs/^{90}Sr activity ratio closer to pre–Fukushima (i.e. ~2). These would be waters mainly originating from the open ocean with little impact from FDNPP, as found around Taiwan and off Japan (145 - 155 ºE and 25 - 35 ºN) in May - June 2012 (Men et al., 2015).

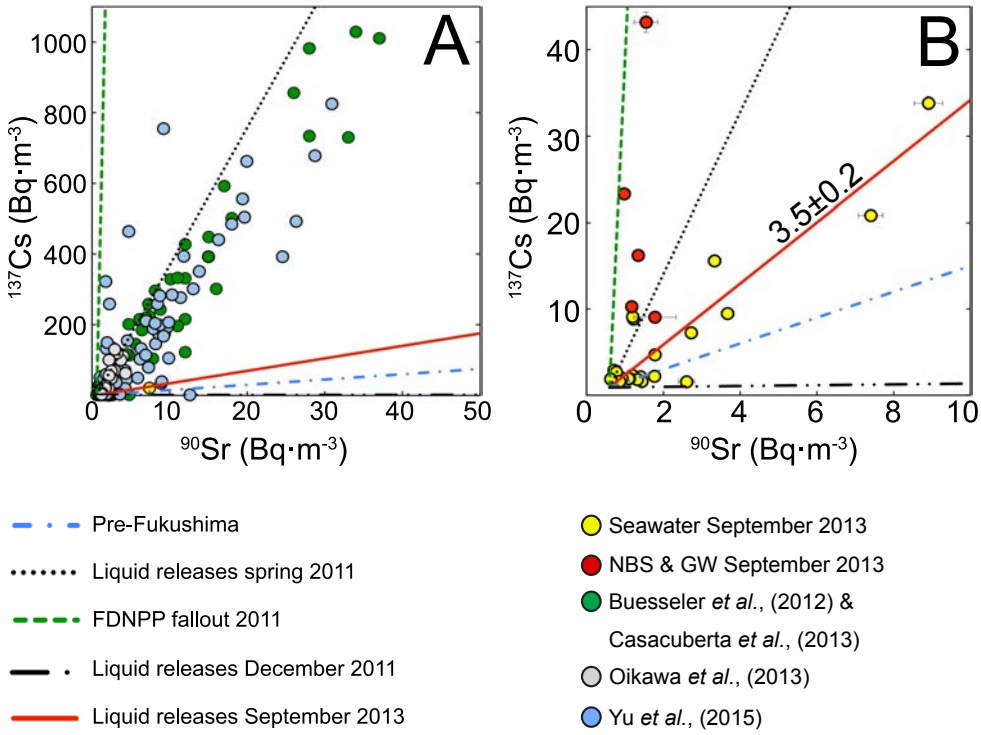

Figure 2.5. A) ^{137}Cs/^{90}Sr activity ratios in seawater (SW), northern beach samples (NBS) and groundwater (GW) collected in September 2013 together with data published elsewhere (Buesseler et al. 2012; Casacuberta et al. 2013; Oikawa et al. 2013; Yu et al. 2015). B) zoom of SW, NBS and GW samples collected in September 2013 (B). ^{137}Cs/^{90}Sr activity ratios of each end-member are included: pre-Fukushima from global fallout due to nuclear weapon tests (~ 1.5; UNSCEAR, 2000) FDNPP liquid releases in spring 2011 (i.e. ratio = 39 ± 1; Casacuberta et al. 2013), FDPP fallout in 2011 (i.e. ratio ~ 1000, Povinec et al. 2012) and FDNPP liquid releases in December 2011 (ratio = 0.016; Povinec et al. 2012; TEPCO, 2015). Also indicated, the continuing liquid releases from the FDNPP causing the highest seawater concentrations measured in samples collected within 6 km off FDNPP in September 2013 (ratio = 3.5 ± 0.2).

The northern beach samples and groundwater collected in Sendai Bay had a ^{137}Cs/^{90}Sr activity ratio (5 - 28) much higher than in seawater at that time (0.6 - 7.5). All these samples had salinities (see Appendix A.1) much lower than seawater as a result of the mixing of seawater with river runoff and/or groundwater. Considering the high ^{137}Cs/^{90}Sr activity ratio of the FDNPP fallout, the mixing with fresh water inputs tagged with the ratio from FDNPP fallout on land would result in higher ^{137}Cs/^{90}Sr activity ratios as observed in northern beach samples and groundwater.

2.5.4. Impact of the new releases in 2013

The magnitude of the continuing releases from the FDNPP, leading to the contamination observed in September 2013, can be estimated using the ^{137}Cs/^{90}Sr activity ratio of 3.5 ± 0.2 defined above together with the estimates of ongoing ^{137}Cs releases available from the literature. A continuous discharge of ^{137}Cs of 8.1 GBq·d^{-1} was estimated for summer 2012 based upon the exchange of waters between the FDNPP harbor and nearby ocean and the concentrations of ^{137}Cs in these waters (Kanda, 2013). Maderich *et al.* (2014a, 2014b) modeled the long - term dispersion and fate of radioactive contamination originating from the FDNPP. In order to match measured seawater concentrations with their model predictions, they estimated an ongoing source of 3.6 TBq·a^{-1} (or 9.9 GBq·d^{-1}) of ^{137}Cs during 2011 – 2014 (Maderich et al., 2014a). A higher release estimate of ^{137}Cs was reported for September 2013 (~30 GBq·d^{-1}; Tsumune et al., 2014), although ^{137}Cs concentrations at T1 and T2/T2-1 remained at ~1 × 10^{3} Bq·m^{-3} since 2012 suggesting no change in inputs during this time (Figure 2.3B). Considering a ^{137}Cs release range of 8.1 to 30 GBq·d^{-1} and the ^{137}Cs/^{90}Sr activity ratio of 3.5 ± 0.2 we estimate a ^{90}Sr release of 2.3 - 8.5 GBq·d^{-1} (or 71 ± 4 to 261 ± 15 GBq·month^{-1}) in September 2013. Since the ^{137}Cs/^{90}Sr activity ratio changed temporarily due to accidental releases (Figure 2.4), the calculated release rate would only be valid for that month. As a rough approximation, however, one may assume an average ^{90}Sr release rate of ~166 GBq·month^{-1}. At this rate, it would take ~45 years for the ongoing releases to equal the most conservative estimate of ^{90}Sr discharged by June 2011 (90 TBq; Casacuberta et al., 2013). By comparison, it would take ~500 years for the ongoing releases of ^{137}Cs to match some of the lowest estimates of ^{137}Cs released by the end of May 2011 (e.g. 3.5 PBq; Tsumune et al., 2012).

Freshwater inputs from land constitute another source of radionuclides to the ocean. For example, rivers transport significant amounts of particulate radiocaesium, mainly during heavy rain events, to the coast of Japan (Nagao et al., 2013; Yamashiki et al., 2014). The Abukama River basin is the largest river system affected by FDNPP-derived fallout in 2011 and its inputs of ^{137}Cs to the ocean were estimated to be of ~19 GBq·d^{-1} in 2011 – 2012 (Yamashiki et al., 2014). Unfortunately, to our knowledge, there is no information on ^{90}Sr concentrations in river water or groundwater. As a rough approximation and assuming

no modification of the FDNPP-derived fallout $^{137}Cs/^{90}Sr$ activity ratio deposited on land during river transport (i.e. ~1000; Povinec et al., 2012) river inputs of ^{90}Sr would be of ~19 $MBq \cdot d^{-1}$. The bottom line is that continuing releases of ^{90}Sr from the FDNPP probably exceed by 2 - 3 orders of magnitude those inputs from rivers.

In addition to ongoing direct releases and river runoff, about 1,500 tanks are being used by TEPCO to store more than 665×10^3 m^3 of water as of June 2015 (TEPCO, 2015b). TEPCO has reported several leaks from these storage tanks, as well as from pipes, decontamination units, etc. Major leaks include 300 tons of water with 0.28 $TBq \cdot m^{-3}$ of total β emitters in August 2013 and 100 tons with 0.23 $TBq \cdot m^{-3}$ of total β in February 2014 (TEPCO, 2015a). If these waters reach the ocean, they would add ~54 TBq of ^{90}Sr (assuming ~50 % of all β is ^{90}Sr). This is equivalent to ~6 - 60 % of the ^{90}Sr released by June 2011 (e.g. 90 to 900 TBq; Casacuberta et al., 2013) suggesting that the storage tanks are a potential large source of ^{90}Sr that needs to be carefully managed.

The decrease in the $^{137}Cs/^{90}Sr$ activity ratio from ~39 (Casacuberta et al., 2013) in spring 2011 to a ratio higher than the global fallout, suggests the ongoing release from the FDNPP to the Pacific Ocean through September 2013. This study shows the potential of using the $^{137}Cs/^{90}Sr$ activity ratio to constrain sources of artificial radionuclides in the coast off Japan, which varies widely from ~1000 on land (Povinec et al., 2012) to <1/1000 in waters stored in tanks (TEPCO, 2015a). The net result of these sources is the shift of the $^{137}Cs/^{90}Sr$ to ~3.5 in waters impacted by FDNPP in September 2013.

CHAPTER 3

Artificial ^{236}U and ^{129}I in the Mediterranean Sea: first comprehensive assessment of distribution and constraint of their sources

This chapter is based on:

Castrillejo, M., Casacuberta, N., Christl, M., Garcia-Orellana, J., Vockenhuber, C., Synal, H.–A., Masqué, P., 2017. Anthropogenic ^{236}U and ^{129}I in the Mediterranean Sea: first comprehensive distribution and constrain of their sources. Science of the Total Environment, 593-594, 745-759.

3.1. Abstract

The first basin-wide distribution of $^{236}U/^{238}U$ atom ratios and ^{129}I concentrations is presented for the Mediterranean Sea. During the GEOTRACES *GA04S-MedSeA* expedition in 2013 seawater was collected from 10 vertical profiles covering the principal sub–basins of the Mediterranean Sea. The main objective was to understand the distributions of ^{236}U and ^{129}I in relation to the water masses, and to constrain their sources in this region. The $^{236}U/^{238}U$ atom ratios and the ^{129}I concentrations ranged from $(710 \pm 40) \times 10^{-12}$ to $(2220 \pm 60) \times 10^{-12}$ and from $(4.0 \pm 0.1) \times 10^{7}$ to $(13.8 \pm 0.3) \times 10^{7}$ at·kg^{-1}, respectively. The results show that radionuclide–poor Atlantic Water is entering at the surface through the Strait of Gibraltar whereas comparably radionuclide-enriched Levantine Intermediate Water is sinking in the Eastern Basin and flowing westward at intermediate depths. Low radionuclide levels were found in the oldest water masses at about 1000 – 2000 m depth in the Eastern Basin. At greater depths, waters were relatively enriched in ^{236}U and ^{129}I due to dense water formation occurring in both, the Eastern and Western Basins. The inventories of ^{236}U and ^{129}I cannot be explained only by global fallout from atmospheric nuclear bomb testings carried out in the 1950s and 1960s. We estimate that the liquid input of ^{236}U from the nuclear reprocessing facility of Marcule (France), via the Rhône river, was of the same order of magnitude than the contribution from global fallout, whereas liquid and gaseous releases of ^{129}I from Marcoule were up to two orders of magnitude higher than global fallout. For both radionuclides, the contribution from the Chernobyl accident is found to be minor.

3.2. Introduction

The presence of ^{236}U ($T_{1/2}$=23.5 Ma) and ^{129}I ($T_{1/2}$=15.7 Ma) in the marine environment is mainly due to anthropogenic nuclear activities: the global atmospheric deposition derived from atmospheric nuclear bomb testing carried out from 1945 to the 1980s, referred to as *global fallout*; the discharge of liquid and gaseous releases from nuclear facilities such as spent fuel reprocessing plants; and nuclear accidents. The main source of ^{236}U in the environment is global fallout (~900 kg, Sakaguchi et al., 2009), and to a lesser (and more local) extent nuclear reprocessing plants, which have discharged about 100 kg into the Northeast Atlantic (Christl et al., 2015a). On the contrary, the dominant source of ^{129}I is nuclear fuel reprocessing (>6000 kg; He et al., 2013), while only a small fraction is due to global fallout (~90 kg; Hou, 2004; Raisbeck and Yiou, 1999; Wagner et al., 1996) and nuclear accidents (e.g. 1 – 6 kg Chernobyl; Aldahan et al., 2007; Paul et al., 1987). The aforementioned sources largely exceed natural amounts of ^{236}U (<0.5 kg; Steier et al., 2008) and ^{129}I (~130 kg; Snyder et al., 2010) in the world oceans. As a consequence, the upper ocean exhibits $^{236}U/^{238}U$ atom ratios (from 10^{-6} to 10^{-12}) and ^{129}I concentrations (from ~10^{6} to >10^{12} at·kg^{-1}) well above natural levels; being $^{236}U/^{238}U$ atom ratios of 10^{-14} - 10^{-13} (Christl et al., 2012; Steier et al., 2008) and ^{129}I concentrations of ~4×10^{5} at·kg^{-1} (Snyder et al., 2010).

Investigation of the distribution of ^{236}U and ^{129}I in the oceans is relevant for, at least, two main reasons. First, they have a great potential as transient tracers due to their near conservative behavior in seawater (e.g. Christl et al., 2015a; Raisbeck et al., 1995; Smith et al., 1998). For example, ^{129}I from European reprocessing plants (together with other transient tracers) was used to trace water mass transport from the Nordic Seas to the Arctic Ocean and to estimate its transit times (Smith et al., 2005, 1998). Similarly, the distribution of $^{236}U/^{238}U$ atom ratios has been used for identifying water masses and revealing their pathways in the Arctic Ocean (Casacuberta et al., 2016) and along a N-S transect in the Northwest Atlantic Ocean (Casacuberta et al., 2014; Christl et al., 2012). Recent work also investigated the combination of ^{236}U and ^{129}I in a dual tracer approach for the calculation of water mass transit times and ventilation rates in the North Atlantic and Arctic Ocean (Christl et al., 2015a). Second, ^{129}I can be a proxy for other shorter lived radionuclides that are of greater

radiological concern. For example, ^{129}I was used to study the deposition of ^{131}I released during the Chernobyl accident (Paul et al., 1987). In addition, recent developments in compact accelerator mass spectrometry (AMS) now allow measurements of ^{236}U and ^{129}I concentrations at all oceanic levels that are fast (about 1h/sample after chemical separation) and highly sensitive in small sample volumes of about 3 - 5 L and 0.3 L, respectively (Christl et al., 2015b; Vockenhuber et al., 2015). In contrast, the precise determination of other radiotracers with shorter half-life (e.g. ^{137}Cs or ^{90}Sr) using radiometric techniques requires a much larger sample volume (tens of liters) and longer counting times (>1 day, at global fallout levels).

The presence of ^{236}U and ^{129}I in the Mediterranean Sea is expected to occur due to a combination of global fallout, the Chernobyl accident and the releases derived from the surrounding nuclear industry facilities. The deposition of radionuclides from global fallout peaked in the mid-1960s and was largest in the Northern Hemisphere at mid latitudes (UNSCEAR, 2000). About 40% of the global fallout was deposited between 30º N and 60º N (Hardy et al., 1973) largely impacting the Mediterranean Sea (30º - 45º N). Based on total global fallout deposition estimates ($^{236}U \sim 10 \times 10^{12}$ at·m^{-2}, Chamizo et al., 2016); $^{129}I \sim 1 \times 10^{12}$ at·m^{-2}, Snyder et al., 2010) and a conservative approach of homogeneous mixing of waters, the concentrations of ^{236}U and ^{129}I would be of $\sim 5 \times 10^{6}$ at·kg^{-1} and $<0.1 \times 10^{7}$ at·kg^{-1}, respectively, in the Mediterranean Sea (surface area 2.51×10^{12} m^2 and a volume $\sim 4 \times 10^{15}$ m^3). The Chernobyl accident in 1986 led to the largest accidental release of artificial radionuclides to date (Steinhauser et al., 2014). The radioactive cloud spread over Europe and the former Soviet Union affecting terrestrial and marine environments such as the Mediterranean Sea and the Black Sea (Buesseler, 1987; Papucci et al., 1996). Most of the released ^{236}U, of refractory nature, was deposited near the damaged nuclear power plant (Boulyga and Heumann, 2006). Thus, Chernobyl probably had a smaller influence than global fallout on ^{236}U levels in the Mediterranean Sea (Quinto et al., 2009). In contrast, iodine is a volatile radionuclide and probably some of the atmospheric releases of ^{129}I derived from Chernobyl have entered the Mediterranean and Black Seas. Nuclear industry within the catchment area of the Mediterranean Sea includes the nuclear spent fuel reprocessing plant in Marcoule (Rhône valley, France) and several nuclear reactors located in southeast France and to a lesser extent, in Spain, Italy (these were shut down by 1990), Israel and Eslovenia. Fuel

reprocessing carried out in Marcoule reprocessing plant between 1958 and 1997 accounts for most of the radioactive effluents discharged from nuclear industry to the Mediterranean Sea (Charmasson, 1998) including about 45 kg of ^{129}I to the Rhône River and 145 kg to the atmosphere (Hou et al., 2009). Such input of ^{129}I would cause a significant increase, of about two orders of magnitude, of ^{129}I concentrations in seawater. There is no evidence of ^{236}U discharges from Marcoule, but documented ^{236}U discharges from other reprocessing plants, such as La Hague (France) and Sellafield (UK), have caused a rise in the $^{236}U/^{238}U$ atom ratios from ~10^{-9} to 10^{-6} in surface waters of the North Sea (Christl et al., 2013a).

A number of studies have characterized the input functions, distributions and concentrations of artificial radionuclides in the Mediterranean Sea and the Black Sea, mainly focusing on ^{137}Cs and Pu isotopes in water, sediments and biota (e.g. Delfanti et al., 1995; Garcia-Orellana et al., 2009; Lee et al., 2003; Miralles et al., 2004). Some of these radionuclides have been used as tracers of geochemical processes (i.e. Pu isotopes to constrain mixing and sediment accumulation rates, Garcia-Orellana et al., 2009) and/or of ventilation and transit times of waters in the Mediterranean and Black Seas (e.g. ^{90}Sr and ^{3}H; Egorov et al., 1999; Franić, 2005; Roether et al., 2013). However, a comprehensive study on the basin wide distributions of ^{236}U and ^{129}I and on their sources is still missing. Data on ^{129}I concentrations have been reported mostly for surface waters, at local or regional scale, for northern parts of the Mediterranean Sea. Elevated ^{129}I concentrations of $\geq 10^{8}$ at·kg^{-1} have been reported for the 1990s in surface seawater at the DYFAMED (Dynamics of Atmospheric Fluxes in the Mediterranean Sea) station in the Ligurian Sea (Yiou et al., 1997) and in the Aegean Sea (Zhao et al., 1998), and in 2009 in the northern Adriatic Sea (Osterc and Stibilj, 2012). One single vertical profile of ^{236}U has become recently available from the DYFAMED station (Chamizo et al., 2016). This profile showed that anthropogenic ^{236}U is present along the whole water column (2350 m) at that site, with a ^{236}U inventory of about 2.5 times larger than expected for this latitude if global fallout was the only source. These data suggest the presence of local or regional sources of contamination in addition to global fallout.

Here we present data on $^{236}U/^{238}U$ atom ratios and concentrations of ^{236}U and ^{129}I in the water column of the Mediterranean and the Black seas which are discussed in relation to the corresponding water masses. By using the radionuclide inventories and an adopted box model

(Bethoux and Gentili, 1999), the inputs of ^{236}U and ^{129}I from global fallout, the Chernobyl accident and the Marcoule reprocessing plant are assessed and discussed.

3.3. Materials and methods

3.3.1. Study area and sampling strategy

The Mediterranean Sea (average depth ~1500 m) is a marginal sea with limited and shallow exchange with the Atlantic Ocean through the Strait of Gibraltar (280 m shallowest depth) and with the Black Sea through the Strait of Bosphorus (13 m shallowest depth, ~60 m average depth). The Mediterranean Sea is divided into the Western and Eastern Basins (hereinafter WMS and EMS), connected through the Strait of Sicily (300 m maximum depth). The water mass circulation can be schematically described by three circulation cells. The shallow inter basin circulation cell is composed by the Atlantic Water (AW) entering the surface through the Strait of Gibraltar and the outflowing of the Levantine Intermediate Water (LIW) at intermediate depths. The two deep overturning cells are driven by the formation of the Western Mediterranean Deep Water (WMDW) and the Eastern Mediterranean Deep Water (EMDW) in the Western and Eastern Basins, respectively (Figure 3.1).

During the *GA04S-MedSeA* cruise in May 2013 seawater was sampled at 10 stations on board *R/V Ángeles Alvariño* (8 in the Western Basin and 2 in the Eastern Basin, Figure 3.1). A total of 76 seawater samples were collected for ^{236}U and ^{129}I from the surface down to the bottom. Water samples were collected using an oceanographic rosette equipped with conductivity, temperature and depth (CTD) sensors and 24 12 L-Niskin bottles. Samples for ^{236}U (5 - 7 L each) were collected in plastic cubitainers, while ^{129}I samples (0.5 L each) were collected in plastic bottles and stored in the dark. Cubitainers and bottles were rinsed 3 times with seawater prior to sample collection. Six additional seawater samples were collected in the central Black Sea onboard *R/V Pelagia* during the *Black Sea-Fe-Vici* cruise (64PE401) in September 2015. The water exchange occurring at the Strait of Bosphorus can be simplified in two components: at the surface (e.g. <100), fresher and predominantly shallow water from the Black Sea enters into the Mediterranean Sea; at depth, saltier Mediterranean Sea water

enters into the Black Sea (e.g. Oguz et al., 1990). In this study, only the upper 4 samples collected in the upper 100 m are used to characterize the concentrations of ^{236}U and ^{129}I in shallow waters of the Black Sea. The two cruises were part of the international GEOTRACES programme (www.bodc.ac.uk/geotraces/cruises/).

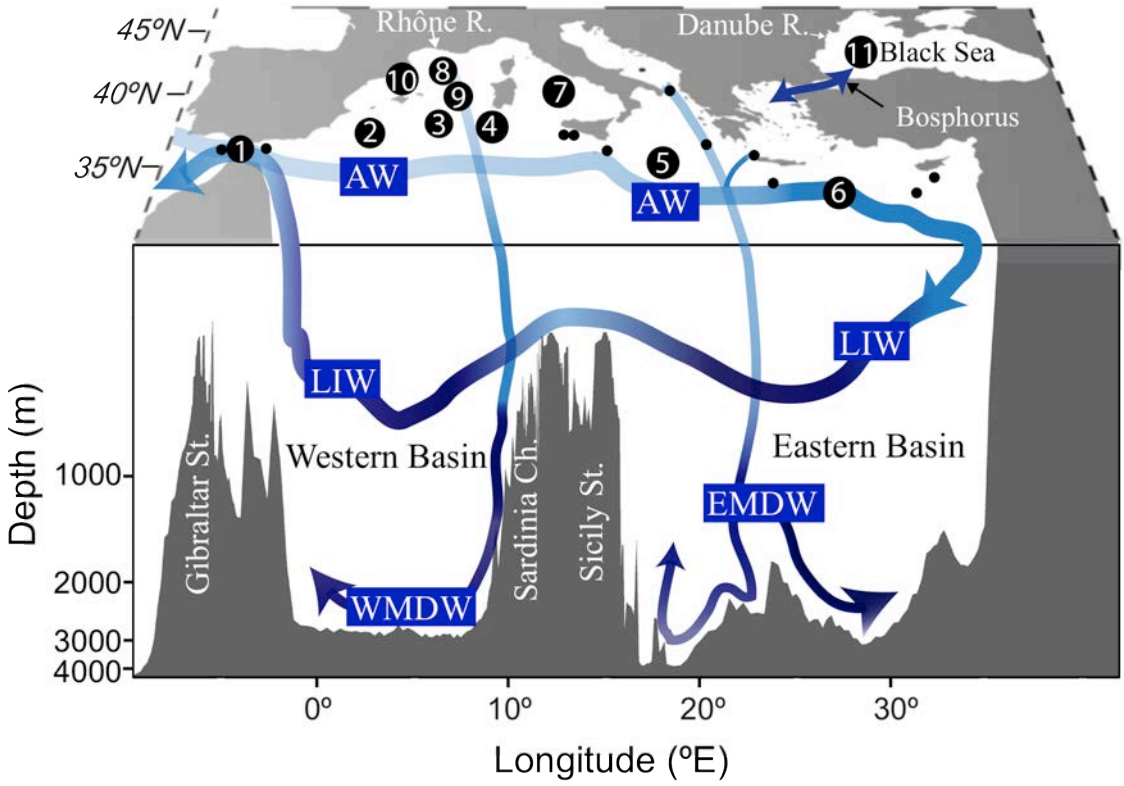

Figure 3.1. Study area of the *GA04S-MedSeA* (May 2013) and *Black Sea-Fe-Vici* (September 2015) cruises. Sampling stations for ^{236}U and ^{129}I (1 to 11) and additional hydrographic stations (black dots) are shown: 1. Gibraltar Strait (GSt); 2. Algeria (ALG); 3. Southern Alguero-Balear (SAB); 4. Sardinia Channel (SCh); 5. Ionian Sea (IS); 6. Levantine Basin (LB); 7. Tyrrhenian Sea (TS); 8. Northern Alguero-Balear (NAB); 9. Central Alguero-Balear (CAB); 10. Catalano-Balear (CB) and 11. Black Sea (BS). Blue lines represent the main patterns of water circulation: the shallow circulation cell connecting the Western and Eastern Basins and the two deep overturning cells, one in each basin (adapted from (Tsimplis et al., 2006)). Water masses are: Atlantic Water (AW), Levantine Intermediate Water (LIW), Western Mediterranean Deep Water (WMDW) and Eastern Mediterranean Deep Water (EMDW).

3.3.2. U-236 purification and AMS measurement

Seawater samples were weighed, acidified to pH <2 with concentrated nitric acid (suprapure), and spiked with ~3 pg of ^{233}U. Uranium was pre-concentrated at pH <8 by iron hydroxide co-precipitation using a U-free iron solution (200 mg of Fe^{2+} per sample) and concentrated ammonium hydroxide (suprapure). After removal of the supernatant and evaporation to dryness, iron hydroxide precipitates were redissolved in 8 M HNO_3 and passed through UTEVA (Triskem) columns. Uranium was eluted from the columns and co-precipitated again with iron hydroxides (corresponding to about 1 mg Fe). After converting the U to oxide form by heating to 650 ºC, samples were mixed with 2-3 mg of Nb (niobium) and pressed into AMS sample holders. The ^{236}U, ^{233}U and ^{238}U measurements were performed using the compact 0.5 MV Tandy AMS system at ETH-Zurich (Christl et al., 2013a). Measured $^{236}U/^{238}U$ and $^{236}U/^{233}U$ atom ratios were normalized to the ETH-Zurich in-house standard ZUTRI, with nominal values of $(4055 \pm 200) \times 10^{-12}$ and $(33170 \pm 830) \times 10^{-12}$, respectively (Christl et al., 2013a). Chemistry blanks (n=9) prepared with deionized water were treated and analyzed in the same way as the seawater samples and showed a $^{236}U/^{233}U$ atom ratio $\sim 10^{-5}$ corresponding to less than 40 ag of ^{236}U. The abundance sensitivity of the Tandy AMS system is at a level of 10^{-12} in the mass range of the actinides, leading to an instrumental $^{236}U/^{238}U$ background level at the order of $\sim 10^{-14}$.

3.3.3. I-129 purification and AMS measurement

Purification of ^{129}I was carried out following the method described in Michel et al., (2012). Briefly, ~350 mL of seawater were spiked with 1.5 – 3.0 mg of Woodward stable iodine (WWI, ^{127}I) carrier. Iodine species were oxidized to iodate with 2% $Ca(ClO)_2$ and then reduced to iodide adding $Na_2S_2O_5$ and 1M $NH_3O{\cdot}HCl$. Each sample was purified using an ion exchange column (DOWEX® 1x8). The column was rinsed with deionized water and a diluted KNO_3 solution prior to elution of iodine with a 2.25 M KNO_3 solution. The eluate was precipitated as AgI upon addition of $AgNO_3$. Iodine precipitates were mixed with 4 - 5 mg of Ag and pressed into AMS sample holders. The $^{129}I/^{127}I$ atom ratios were measured using the compact 0.5 MV Tandy AMS system at ETH–Zurich (Vockenhuber et al., 2015). ^{129}I

concentrations were calculated using the known amount of ^{127}I added to each sample. Measured $^{129}I/^{127}I$ atom ratios were normalized using the ETH-Zurich in-house standard D22 with a nominal value of $^{129}I/^{127}I = (50.35 \pm 0.16) \times 10^{-12}$ (Christl et al., 2013b). Chemistry blanks (n=9), prepared with deionized water, were treated and analyzed in the same way as the seawater samples and showed typically $^{129}I/^{127}I \sim (1.5 - 3) \times 10^{-13}$ corresponding to $(1 - 2) \times 10^{6}$ atoms of ^{129}I. This amount was substracted from the measured amount of the seawater samples. The detection limit of <0.3 fg ^{129}I depends on the measured isotopic ratio of the WWI carrier ($^{129}I/^{127}I \sim 10^{-13}$).

3.3.4. Estimation of inventories of ^{236}U and ^{129}I

Water column inventories of ^{236}U and ^{129}I were estimated using the box volumes and sizes of an existing multi box model (Sanchez-Cabeza et al., 2002) based on (Bethoux and Gentili, 1996). This model divides the Mediterranean Sea into 10 regions taking into account the topography and water mass distribution. Each region is sub-divided into up to 4 depth-layers (see Appendix A.4).

If measured ^{236}U and ^{129}I concentrations were available for a certain depth and location they were assigned to the corresponding box. If more than one data point was available, the average concentration was used. In regions where no observations were available for a given depth or box, a linear interpolation from adjacent boxes was done coherent with water mass circulation. In regions with not a single observation available and where data from the literature was not representative (e.g. earlier studies in the Adriatic and Aegean Seas, Table 3.2), average concentrations found in water masses draining from or to the given box were assigned. For example, AW and LIW are involved in the formation of Adriatic Deep Water (AdDW) that outflows over the Otranto Strait to fill the deep Ionian Sea, and to a lesser extent, the Levantine Basin (e.g. Ovchinnikov et al., 1985; Roether and Schlitzer, 1991). Thus, we used average concentrations from surface to 550 m depth and from 3000 to 3700 m depth of the Ionian Sea as representative of those of the water masses in the Adriatic Sea. In the Aegean Sea, shallow and intermediate waters (e.g. Back Sea Water, AW, LIW) precondition the formation of dense waters (e.g intermediate and deep Cretan Water, CIW and CDW,

respectively) that can outflow to the deep Levantine Basin and to a lesser extent the Ionian Sea (e.g Lascaratos et al., 1999). Thus, the average of the upper 550 m and of waters deeper than 2800 m in the Levantine Basin was taken as representative of waters in the Aegean Sea.

Radionuclide inventories (in $at \cdot m^{-2}$ and in kg) were calculated for each box using the assigned radionuclide concentrations and the corresponding box volumes and depths (see Appendix A.4). Then, boxes were summed up to calculate box inventories and total masses for each respective region.

The box model by Bethoux and Gentili (1996) was used to simulate the time evolution and spatial distribution of both ^{129}I and ^{236}U concentrations in the Mediterranean Sea. We tested several scenarios including discharges from the nuclear reprocessing plant of Marcoule as a source of ^{129}I and ^{236}U in addition to global fallout. The 20-box model of Bethoux and Gentili (1996) divides the Mediterranean Sea in 8 regions (see Appendix A.4) that are sub-divided in 3 – 4 depth layers (surface, intermediate, deep, and very deep layers for the Ionian Sea and the Levantine Basin). The model considers the physiography, the water circulation and updates previous water flux estimates (Bethoux, 1980) considering deep water exchanges in the EMS (Roether and Schlitzer, 1991), dense water formation rates in the Levantine Basin (Lascaratos et al., 1993) and measured deep water flows in the Adriatic Sea.

3.4. Results

The measured $^{236}U/^{238}U$ atom ratios and the concentrations of ^{236}U and ^{129}I are reported in Table 3.1 and represented in Figure 3.2. In the Mediterranean Sea, the $^{236}U/^{238}U$ atom ratios ranged between $(710 \pm 40) \times 10^{-12}$ and $(2220 \pm 60) \times 10^{-12}$. The ^{236}U concentrations ranged from $(6.7 \pm 0.5) \times 10^{6}$ to $(22 \pm 1) \times 10^{6}$ $at \cdot kg^{-1}$. The ^{129}I concentrations ranged from $(4.0 \pm 0.1) \times 10^{7}$ to $(13.8 \pm 0.3) \times 10^{7}$ $at \cdot kg^{-1}$. In the upper 100 m of the Black Sea, the $^{236}U/^{238}U$ atom ratios and concentrations of ^{236}U and ^{129}I averaged $(6900 \pm 1100) \times 10^{-12}$, $(39 \pm 6) \times 10^{6}$ $at \cdot kg^{-1}$ and $(12 \pm 2) \times 10^{7}$ $at \cdot kg^{-1}$, respectively. All $^{236}U/^{238}U$ atom ratios and concentrations of ^{236}U and ^{129}I measured in the Mediterranean and Black Seas were significantly above natural background levels (Table 3.2).

In both the WMS and the EMS, surface waters (0 to about 100 m) displayed a wide range of $^{236}U/^{238}U$ atom ratios and ^{129}I concentrations depending on the varying presence of AW (Fig. 3.2). Excluding the influence of surface AW, ^{236}U showed a rather homogeneous surface distribution in the whole Mediterranean Sea (Figure 3.2). Surface concentrations of ^{129}I, in contrast, were more elevated in the northwestern basin and in the Ionian Sea. Intermediate waters (~100 to ~600 m) had maxima concentrations in most stations, while deep waters (~600 to ~2000 m) displayed minima values, usually centered at about 1000 m depth. In very deep waters below 2000 m the $^{236}U/^{238}U$ atom ratios and the ^{129}I concentrations remained constant or increased slightly with depth. In the WMS, the lowest $^{236}U/^{238}U$ atom ratios and ^{129}I concentrations were recorded in surface waters at the Gibraltar Strait ($(1040 \pm 30) \times 10^{-12}$ and $(4.0 \pm 0.1) \times 10^{7}$ at·kg^{-1}, respectively) and at about 1000 m depth at most stations (~1200 $\times 10^{-12}$ and ~7.5 $\times 10^{7}$ at·kg^{-1} for the $^{236}U/^{238}U$ atom ratio and the ^{129}I concentration, respectively). The highest $^{236}U/^{238}U$ atom ratios and ^{129}I concentrations were recorded in sub-surface and intermediate waters (up to ~2200 $\times 10^{-12}$ and ~10.5 $\times 10^{7}$ at·kg^{-1}, respectively) at the southeastern stations of the WMS (2. ALG, 3. SAB and 4. SCh; Figure 3.1). The EMS displayed a broader range of $^{236}U/^{238}U$ atom ratios and ^{129}I concentrations. The lowest $^{236}U/^{238}U$ atom ratios and ^{129}I concentrations in the EMS were recorded in deep waters located between 1000 and 2000 m depth in the Ionian Sea and the Levantine Basin ($(710 \pm 40) \times 10^{-12}$ and $(4.5 \pm 0.1) \times 10^{7}$ at·kg^{-1}, respectively), while the highest values were found in sub-surface and intermediate waters of the Levantine Basin (up to about $(2220 \pm 60) \times 10^{-12}$ and about $(13.8 \pm 0.3) \times 10^{7}$ at·kg^{-1}, respectively).

Table 3.1. $^{236}U/^{238}U$ atom ratios and concentrations of ^{236}U and ^{129}I in seawater samples collected during the *GA04S-MedSeA* (in May 2013) and *Black Sea-Fe-Vici* (September 2015) cruises. Water mass acronyms are: Atlantic Water (AW), Modified Atlantic Water (MAW), Ionian Surface Water (ISW), Levantine Surface Water (LSW), Levantine Intermediate Water (LIW), Western Intermediate Water (WIW), Cretan Deep Water (CDW), Adriatic Deep Water (AdDW), Tyrrhenian Deep Water (TDW), Western Mediterranean Deep Water (WMDW), Eastern Mediterranean Deep Water (EMDW), transitional EMDW (tEMDW). Lower case n: new; o: old; mix: mixture of new and old. Uncertainties are given as one sigma deviations.

Station	ETH code	Depth m	Water Mass	Salinity	Pot. Temp. °C	Oxygen µmol·kg^{-1}	$^{236}U/^{238}U$ × 10^{-12}	^{236}U conc. × 10^{6} at·kg^{-1}	^{129}I conc. × 10^{7} at·kg^{-1}
1. Gibraltar St. (GSt)	TU0499-H140217	25	AW	36.30	15.81	222	1040 ± 30	9.4 ± 0.4	4.0 ± 0.1
35º 58.39' N	TU0500- H140218	49	AW/LIW	36.84	14.82	205	1330 ± 60	12.2 ± 0.7	5.3 ± 0.1
5º 26.03' W	TU0501- H140220	101	AW/LIW	37.74	13.88	188	1660 ± 60	15.4 ± 0.7	7.8 ± 0.2
Bottom depth: 640 m	TU0502-H140221	199	LIW	38.35	13.24	167	1920 ± 50	18.3 ± 0.6	7.8 ± 0.2
	TU0503-H140222	299	LIW/WMDW	38.44	13.20	169	1860 ± 60	17.7 ± 0.7	10.2 ± 0.2
	TU0504-H140223	496	WMDW	38.48	13.16	169	1450 ± 40	14.2 ± 0.6	8.1 ± 0.2
	TU0505-H140224	607	WMDW	38.50	13.13	171	1350 ± 50	13.1 ± 0.7	8.1 ± 0.2
2. Algeria (ALG)	TU0506-H140225	25	MAW	37.29	15.89	248	1530 ± 40	14.3 ± 0.5	7.2 ± 0.1
37º 29.22' N	TU0507-H140226	100	LIW/MAW	38.22	13.38	195	2190 ± 60	21.1 ± 0.7	10.5 ± 0.2
1º 26.82' E	TU0508-H140227	250	LIW/ WMDWo	38.48	13.29	167	1740 ± 50	17.2 ± 0.6	9.6 ± 0.2
Bottom depth: 2777 m	TU0509-H140229	500	LIW/WMDWo	38.52	13.18	171	1310 ± 40	12.9 ± 0.5	7.3 ± 0.1
	TU0510-H140230	998	WMDWo/LIW	38.47	12.94	184	1270 ± 50	12.2 ± 0.7	7.0 ± 0.1
	TU0511-H140231	1499	WMDWmix	38.46	12.90	190	1260 ± 40	12.2 ± 0.5	7.5 ± 0.1
	TU0512-H140232	1999	WMDWmix	38.46	12.90	192	1380 ± 50	13.3 ± 0.7	7.7 ± 0.1
	TU0513-H140233	2703	WMDWn	38.47	12.90	192	1400 ± 40	13.5 ± 0.5	7.8 ± 0.2
3. S. Alg.-Balear (SAB)	TU0514-H140234	25	MAW	37.62	16.24	245	1810 ± 70	16.8 ± 0.9	8.1 ± 0.2
38º 31.68' N	TU0515-H140235	100	MAW/LIW	37.95	13.70	235	1990 ± 50	18.8 ± 0.5	9.2 ± 0.2
5º 33.55' E	TU0516-H140236	250	MAW/LIW	38.40	13.38	186	1970 ± 70	18.7 ± 0.9	10.4 ± 0.2
Bottom depth: 2844 m	TU0517-H140237	500	LIW/WMDWo	38.53	13.23	166	1430 ± 70	14.5 ± 0.7	8.6 ± 0.2

Table 3.1. Continuation.

Station	ETH code	Depth m	Water Mass	Salinity	Pot. Temp. ºC	Oxygen µmol ·kg^{-1}	$^{236}U/^{238}U$ × 10^{-12}	^{236}U conc. × 10^{6} at·kg^{-1}	^{129}I conc. × 10^{7} at·kg^{-1}
	TU0518-H140238	1000	WMDWo/LIW	38.48	12.99	180	1270 ± 40	12.4 ± 0.8	7.7 ± 0.2
	TU0519-H140239	1499	WMDWo	38.46	12.89	187	1330 ± 40	13.3 ± 0.5	8.1 ± 0.2
	TU0520-H140240	1999	WMDWmix	38.46	12.90	191	1380 ± 30	13.4 ± 0.5	7.6 ± 0.1
	TU0521 H140241	2804	WMDWn	38.48	12.90	193	1380 ± 60	13.0 ± 0.7	8.0 ± 0.2
4. Sardinia Chan. (SCh)	TU0522 -H140242	25	MAW	37.97	16.09	249	2000 ± 50	19.1 ± 0.8	9.9 ± 0.2
38º 15.16' N	TU0523-H140243	101	MAW/LIW	38.24	13.50	199	2190 ± 70	21 ± 1	10.4 ± 0.2
8º 46.26' E	TU0524-H140252	250	LIW/MAW	38.57	13.57	170	1820 ± 60	18 ± 1	10.3 ± 0.2
Bottom depth: 2238 m	TU0525-H140253	500	LIW/WMDW	38.62	13.54	176	1370 ± 50	12.8 ± 0.6	7.3 ± 0.2
	TU0526-H140254	1000	WMDW/LIW	38.47	12.95	186	1260 ± 40	12.1 ± 0.6	7.0 ± 0.2
	TU0527-H140255	1499	WMDW/TDW	38.46	12.90	192	1330 ± 60	12.4 ± 0.8	7.9 ± 0.2
	TU0528-H140256	2001	WMDW/TDW	38.47	12.90	192	1370 ± 40	13.1 ± 0.6	7.7 ± 0.2
	TU0529-H140257	2202	WMDW/TDW	38.47	12.90	192	1390 ± 50	13.1 ± 0.7	7.7 ± 0.2
5. Ionian Sea (IS)	TU0530-H140258	25	MAW/ISW	38.68	17.08	236	2090 ± 80	20 ± 1	10.9 ± 0.3
35º 02.67' N	TU0531-H140261	100	MAW/ISW	38.72	15.60	234	2030 ± 60	19 ± 1	11.0 ± 0.3
18º 34.08' E	TU0532-H140262	250	ISW/LSW	38.87	15.44	220	2190 ± 60	22 ± 1	12.4 ± 0.3
Bottom depth: 3774 m	TU0533-H140263	500	LIW/CIW	38.92	14.92	209	2220 ± 60	21.2 ± 0.9	13.8 ± 0.3
	TU0534-H140264	999	AdDWo/LIW	38.78	13.77	183	1080 ± 40	10.2 ± 0.6	6.1 ± 0.2
	TU0535-H140265	2001	AdDWo/LIW	38.73	13.51	190	1020 ± 50	9.5 ± 0.7	5.5 ± 0.1
	TU0536-H140266	3001	AdDWo	38.72	13.43	192	1330 ± 40	12.5 ± 0.5	7.5 ± 0.2
	TU0537-H140267	3723	AdDWn	38.72	13.42	192	1350 ± 40	12.4 ± 0.5	7.7 ± 0.2
6. Levantine Basin (LB)	TU0538-H140268	26	MAW/LSW	38.77	20.51	222	1910 ± 70	17.7 ± 0.8	9.5 ± 0.2
33º 14.76' N	TU0539-H140270	100	MAW/LSW	38.82	16.64	226	2100 ± 80	19 ± 1	11.2 ± 0.3
28º 27.11' E	TU0540-H140271	251	LIW	39.05	15.35	201	1990 ± 60	18.5 ± 0.8	11.8 ± 0.3

Table 3.1. Continuation.

Station	ETH code	Depth m	Water Mass	Salinity	Pot. Temp. ºC	Oxygen µmol ·kg^{-1}	$^{236}U/^{238}U$ × 10^{-12}	^{236}U conc. × 10^{6} at·kg^{-1}	^{129}I conc. × 10^{7} at·kg^{-1}
Bottom depth: 2865 m	TU0541-H140272	500	LIW/AdDWo	38.84	14.02	183	1100 ± 30	10.5 ± 0.4	6.5 ± 0.2
	TU0542-H140273	999	AdDWo	38.75	13.62	181	710 ± 40	6.7 ± 0.5	5.1 ± 0.1
	TU0543-H140274	2002	CDW	38.77	13.62	185	1020 ± 40	9.4 ± 0.5	4.5 ± 0.1
	TU0544-H140275	2833	AdDWn	38.76	13.59	185	1100 ± 40	10.7 ± 0.5	8.5 ± 0.2
7. Thyrrenian Sea (TS)	-H140276	25	MAW	38.03	18.03	234			9.6 ± 0.2
39º 49.74' N	-H140277	100	MAW	38.27	13.85	225			10.7 ± 0.3
12º 30.85' E	-H140278	250	LIW	38.71	14.26	176			12.2 ± 0.3
Bottom depth: 3165 m	-H140279	504	LIW /tEMDW	38.73	14.00	170			11.8 ± 0.2
	TU0549-H140280	1000	tEMDW	38.64	13.55	173	1260 ± 100	12 ± 1	7.6 ± 0.2
	TU0550-H140281	1501	tEMDW	38.55	13.20	175	980 ± 80	9.8 ± 0.9	5.6 ± 0.1
	TU0551-H140282	1998	tEMDW/TDW	38.52	13.12	177	1070 ± 50	10.3 ± 0.6	5.4 ± 0.1
	TU0552-H140284	3154	TDW	38.48	12.98	179	1150 ± 40	11.1 ± 0.6	6.8 ± 0.2
8. N. Alg-Balear (NAB)	TU0553-H140285	25	MAW	38.31	15.42	232	1960 ± 50	18.5 ± 0.8	10.5 ± 0.2
41º 19.02' N	TU0554-H140286	100	WIW	38.41	13.26	218	1720 ± 50	16.3 ± 0.7	8.9 ± 0.2
5º 39.94' E	TU0555-	250	LIW	38.50	13.13	186	1510 ± 50	14.4 ± 0.6	
Bottom depth: 2561 m	TU0556-H140288	500	LIW/WMDWo	38.47	12.96	187	1140 ± 40	10.6 ± 0.6	8.6 ± 0.2
	TU0557- H140289	1001	WMDWo	38.47	12.92	192	1320 ± 20	12.5 ± 0.4	8.0 ± 0.2
	TU0558- H140290	1499	WMDWn	38.47	12.91	194	1150 ± 60	9.6 ± 0.8	8.3 ± 0.2
	TU0559- H140291	2502	WMDWn	38.48	12.91	196	1400 ± 190	12 ± 2	8.2 ± 0.2
9. C. Alg-Balear (CAB)	TU0560- H140293	26	MAW	37.65	16.62	236	1820 ± 70	15.3 ± 0.9	8.6 ± 0.2
40º 4.17' N	TU0561- H140294	100	MAW/WIW	37.97	13.57	238	1970 ± 30	18.1 ± 0.4	9.1 ± 0.2
5º 56.76' E	TU0562- H140295	252	WIW	38.15	13.29	229	2170 ± 30	20.6 ± 0.4	10.4 ± 0.2
Bottom depth: 2834 m	TU0563- H140296	505	LIW	38.48	13.36	178	1870 ± 50	16.9 ± 0.7	10.4 ± 0.2

Table 3.1. Continuation.

Station	ETH code	Depth m	Water Mass	Salinity	Pot. Temp. ºC	Oxygen µmol ·kg^{-1}	$^{236}U/^{238}U$ × 10^{-12}	^{236}U conc. × 10^{6} at·kg^{-1}	^{129}I conc. × 10^{7} at·kg^{-1}
	TU0564- H140297	1001	WMDWo/LIW	38.48	13.00	177	1030 ± 80	8.7 ± 0.8	7.2 ± 0.2
	TU0565- H140298	1497	WMDWmix	38.47	12.94	186	1370 ± 50	13.1 ± 0.8	8.3 ± 0.2
	TU0566- H140299	2803	WMDWn	38.48	12.91	190	1390 ± 50	12.5 ± 0.6	8.0 ± 0.2
10. Cat.-Balear (CB)	TU0567-H140300	25	MAW/WIW	38.29	16.35	246	1970 ± 50	18.3 ± 0.6	10.5 ± 0.2
40º 57.05' N	TU0568-H140302	100	MAW/WIW	38.46	13.21	206	1720 ± 30	15.7 ± 0.4	9.4 ± 0.2
3º 19.15' E	TU0569-H140303	252	LIW	38.52	13.19	184	1420 ± 30	13.2 ± 0.4	8.9 ± 0.2
Bottom depth: 2274 m	TU0570-H140304	505	LIW/WMDWn	38.50	13.06	185	1300 ± 50	12.2 ± 0.7	8.1 ± 0.2
	TU0571-H140305	1010	WMDWn	38.47	12.93	191	1320 ± 40	12.4 ± 0.5	8.3 ± 0.2
	TU0572-H140306	1499	WMDWmix	38.48	12.92	194	1390 ± 30	12.4 ± 0.3	8.9 ± 0.2
	TU0573-H140307	1800	WMDWn	38.48	12.92	195	1350 ± 70	12.2 ± 0.9	8.5 ± 0.2
	TU0574-H140308	2201	WMDWn	38.48	12.91	195	1350 ± 20	12.8 ± 0.3	8.5 ± 0.2
11. Black Sea (BS)	TU1114-TU1119	0-100	Water above	18-20	10-25	<50<500	6900 ± 1100	39 ± 6	12 ± 2
42° 53.790’ N	and		and below the						
30° 40.738’ E	H160124- H160129		picnocline						
Bottom depth: 2085 m									

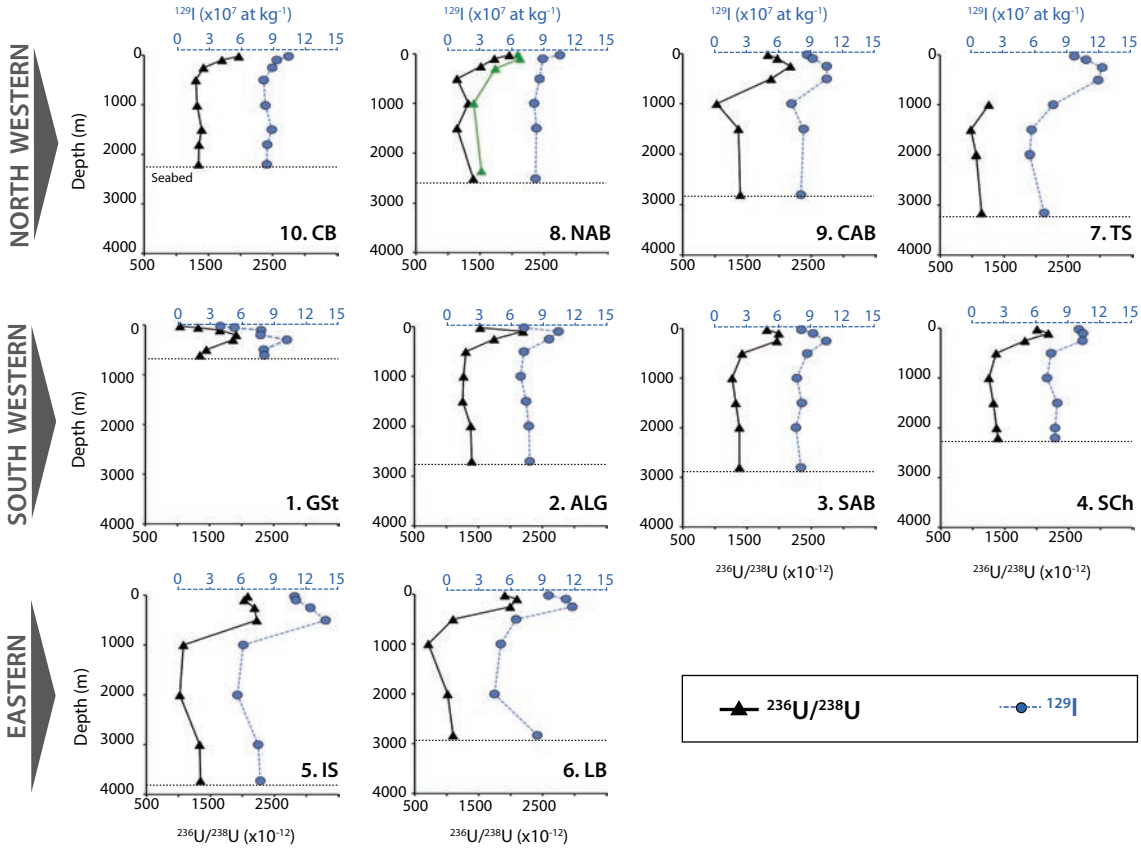

Figure 3.2. Vertical distribution of the $^{236}U/^{238}U$ atom ratios and the ^{129}I concentrations in the Mediterranean Sea in May 2013. The $^{236}U/^{238}U$ atom ratios reported at DYFAMED by Chamizo et al., (2016) are shown with green triangles. Station positions are shown in Figure 3.1. Station labels are: 1. Gibraltar Strait (GSt); 2. Algeria (ALG); 3. Southern Alguero-Balear (SAB); 4. Sardinia Channel (SCh); 5. Ionian Sea (IS); 6. Levantine Basin (LB); 7. Tyrrhenian Sea (TS); 8. Northern Alguero-Balear (NAB); 9. Central Alguero-Balear (CAB); and 10. Catalano-Balear (CB). Uncertainties are given as one sigma deviations.

The ^{129}I concentrations in the Mediterranean Sea were lower than those reported for earlier sampling time periods when Marcoule was operational (1959-1997) or had recently ceased its activity (Table 3.2). Previous studies were also limited to areas that were not covered in this study, such as the northern parts of the WMS and the EMS. The influence from Marcoule was probably larger in the Gulf of Lion, the Ligurian Sea and in the coast off the Rhône estuary, where ^{129}I concentrations in 1990's were, respectively, on average up to 2 times, 6 times and 3 orders of magnitude higher than those measured in 2013 (Yiou et al., 1997; Zhao et al., 1998). In the Aegean Sea, ^{129}I concentrations were up to 4 times higher in 1998 (Zhao et al., 1998) than those measured in 2013 in the Mediterranean Sea

and might have shown the influence from the Black Sea. In 2009, the ^{129}I concentrations in surface waters of the north Adriatic Sea were between 2 and 100 times higher than those we measured in 2013 (Osterc and Stibilj, 2012). According to the authors, such high ^{129}I concentrations could be due to atmospheric inputs from Sellafield and La Hague nuclear fuel reprocessing plants. The $^{236}U/^{238}U$ atom ratios in samples collected at the DYFAMED station in the Ligurian Sea in 2013 (Chamizo et al., 2016) had a range and a depth distribution similar (within 20%) to those we measured in the NAB at a distance of 300 km to the southwest (St. 8, Figure 3.2 and Table 3.2). The $^{236}U/^{238}U$ atom ratios and ^{236}U concentrations in the upper 100 m of the central Black Sea reported in this study were only slightly larger than those reported in surface waters collected at the Romanian coast in 2008 (Table 3.2).

Table 3.2. $^{236}U/^{238}U$ atom ratios and concentrations of ^{236}U and ^{129}I reported in this study and in the literature for the Mediterranean Sea and the Black Sea.

Location	Sampling: Depth range (m)	Sampling: Date	$^{236}U/^{238}U$ ($\times10^{-12}$)	^{236}U ($\times10^{6}$ at·kg^{-1})	^{129}I ($\times10^{7}$ at·kg^{-1})	Reference
Mediterranean Sea						
Western and Eastern Basins	25 to 3720	May-2013	710 to 2220	7 to 22	4 to 14	This study
Northern Alguero-Balear (St. 8 NAB)	25 to 2500	May-2013	1140 to 1960	10 to 19	8 to 11	This study
Ligurian Sea, DYFAMED station	10 to 2350	2013	1400 to 2130	13 to 19		Chamizo *et al.*, 2016
Gulf of Lion, excluding coast off Rhône estuary	surface	Dec-1992			15 to 25	Yiou et al., 1997
Coast off Rhône estuary	surface	Dec-1992			5400	Yiou et al., 1997
	surface	Jan-1994			400	Yiou et al., 1997
Ligurian Sea, DYFAMED station	surface to 2000	Oct-1992			8.5 (2000 m) to 60 (surface)[a]	Yiou et al., 1997
	surface	1998			30	Zhao et al., 1998
Cretan Sea, Milos Island	surface	1998			40	Zhao et al., 1998
Northern Adriatic Sea	surface	2009			23 to 980	Osterc and Stibilj, 2012
Black Sea						
Central Black Sea	0 to 100	Sept-2015	6900[b]	39[b]	12[b]	This study
Eastern Black Sea, Romanian coast	surface	May-2008	3630 (6200)[c]	~ 30		Eigl et al., 2013
Pre – nuclear or natural			~ 0.01			Steier et al., 2008
			~ 0.1			Christl et al., 2012
					~ 0.044	Snyder et al., 2010

[a]Only the $^{129}I/^{127}I$ atom ratio is reported. The ^{129}I concentrations have been calculated considering average concentration of 60 ppb for the world oceans (Broecker and Peng, 1982).

[b]Average values for the upper 100 m.

[c]Considering the reported ^{238}U concentration of ~1.9 μg·L^{-1} measured by alpha spectrometry (Eigl et al., 2013), the $^{236}U/^{238}U$ atom ratio would be about 6200 $\times10^{-12}$.

The $^{236}U/^{238}U$ atom ratios and ^{129}I concentrations in the Mediterranean Sea were compared to those values reported in the literature for the global ocean (Figure 3.3). The measured $^{236}U/^{238}U$ atom ratios (Figure 3.3A) in surface waters were on the order of 10^{-9}, which is very similar to surface waters of other oceans influenced mainly by global fallout, but several orders of magnitude lower than surface waters in the North and the Irish Seas, which receive radioactive effluents from the Sellafield and La Hague reprocessing plants (Christl et al., 2015b). Below surface waters and down to the bottom, the measured $^{236}U/^{238}U$ atom ratios remained at levels of about 10^{-9}, in contrast to most oceans where the $^{236}U/^{238}U$ atom ratios decline by 2 - 3 orders of magnitude. Thus, the Mediterranean Sea, with its shorter water mixing time scales compared to other ocean basins, exhibited the highest, deep $^{236}U/^{238}U$ atom ratios. For ^{129}I (Figure 3.3B), the concentrations measured in the whole water column of the Mediterranean Sea were at least 1 order of magnitude larger than those typical from global fallout, but lower than those in the North Sea, that receives direct inputs from european reprocessing plants (Christl et al., 2015b). The measured concentrations of ^{129}I were also relatively constant with depth and recorded concentrations about 1 - 2 orders of magnitude higher than in other deep ocean basins (Figure 3.3B).

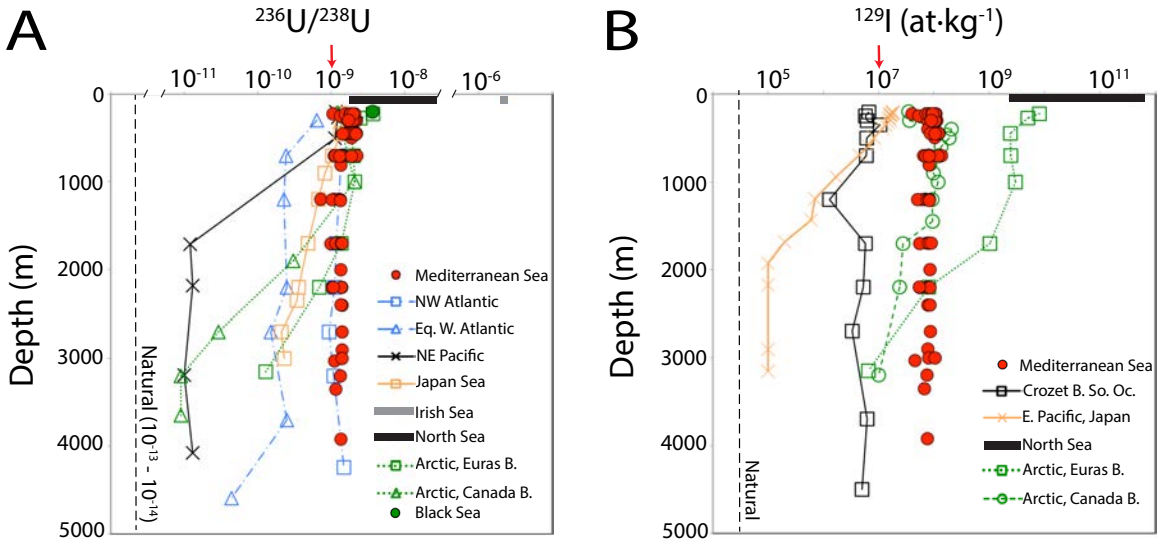

Figure 3.3. Comparison of $^{236}U/^{238}U$ atom ratios (A) and ^{129}I concentrations (B) in seawater from the Mediterranean Sea and in other oceans listed below. The $^{236}U/^{238}U$ atom ratios are shown for: the Mediterranean Sea (this study), 2 profiles in the Northwestern and Equatorial western Atlantic Ocean (Casacuberta et al., 2014), the Northeastern Pacific Ocean (Eigl et al., 2016), the Japan Sea (Sakaguchi et al.,

2012), the Irish Sea (Eigl et al., 2013), the North Sea (Christl et al., 2015b), 2 profiles in the Arctic Eurasian and Canada Basins (Casacuberta et al., 2016), and the Black Sea (Eigl et al., 2013). The ^{129}I concentrations are shown for the Mediterranean Sea (this study), the Crozet Basin in the Southern Ocean (Povinec et al., 2011), the Eastern Pacific Ocean off Japan (Suzuki et al., 2013), the North Sea (Christl et al., 2015b), one profile in the Arctic Eurasian Basin (Casacuberta et al., 2016) and one profile in the Arctic Canada Basin (Smith et al., 1998). Red arrows show the level in the upper 1000 m of the water column expected from global fallout for both the ^{236}U/^{238}U atom ratio and the ^{129}I concentrations.

The inventories of ^{236}U and ^{129}I (see Appendix A.4) were calculated to quantify the magnitude of all possible sources to the Mediterranean Sea. The inventories of ^{236}U ranged from (14.3 ± 0.2) × 10^{12} at·m^{-2} in the Adriatic Sea to (47 ± 6) × 10^{12} at·m^{-2} in the Ionian Sea and from (85 ± 4) × 10^{12} at·m^{-2} to (280 ± 37) × 10^{12} at·m^{-2} for ^{129}I, respecively. The ^{236}U inventory of the Alguero-Balear station ((35 ± 3) × 10^{12} at·m^{-2}) is comparable to that reported for the DYFAMED station ((32 ± 2) × 10^{12} at·m^{-2}; Chamizo et al., 2016). The mass inventory was: 10 ± 1 kg for ^{236}U and 33 ± 4 kg for ^{129}I in the WMS (sum of regions 1 to 5, see Appendix A.4); 21 ± 3 kg for ^{236}U and 68 ± 10 kg for ^{129}I in the EMS (sum of regions 6 to 10). In the EMS only two vertical profiles are available from the deepest locations in the Ionian Sea and the Levantinve Basin and thus the estimates of the inventories may not be as accurate as for other regions. The total inventories of ^{236}U and ^{129}I in the water column of the Mediterranean Sea would be 31 ± 4 kg and 101 ± 14 kg, respectively.

3.5. Discussion

3.5.1. Assignment of ^{236}U/^{238}U atom ratios and ^{129}I concentrations to water masses

The water masses were identified using potential temperature, salinity and dissolved oxygen concentration data from the *GA04S - MedSeA* cruise (Figures 3.4A and 3.4B), as well as from the literature (Lascaratos et al., 1999; Malanotte-Rizzoli et al., 2014; Schroeder et al., 2012; Tanhua et al., 2013; Wüst, 1961).

In the WMS (Figure 3.4 left), the surface layer with relatively fresh AW (S <37) is characterized by $^{236}U/^{238}U$ atom ratios of ~1000 × 10^{-12} and ^{129}I concentrations of ~4 × 10^{7} at·kg^{-1} (Figures 3.4C and 3.4E). AW is progressively modified (MAW) during its transport to the EMS (Figure 3.4 right), where both the $^{236}U/^{238}U$ atom ratios (up to ~2000 × 10^{-12}) and the ^{129}I concentrations (up to ~10 × 10^{7} at·kg^{-1}) become larger (Figures 3.4D and 3.4F). Salty LIW (S>39) is formed by an increase in density due to evaporation and winter cooling of surface waters in the EMS (e.g. Wüst, 1961). The LIW, which flows westward at 100–600 m depth and constitutes the lower branch of the shallow circulation cell (Figure 3.1), is characterized by the highest $^{236}U/^{238}U$ atom ratios (≥2000 × 10^{-12}) and ^{129}I concentrations (≥11 × 10^{7} at·kg^{-1}).

Below the LIW and down to about 2000 m depth, waters are charactherized by the lowest dissolved oxygen, $^{236}U/^{238}U$ atom ratios and ^{129}I concentrations, especially in the EMS (Figure 3.4 right), where the $^{236}U/^{238}U$ atom ratios and the ^{129}I concentrations were as low as ~700 × 10^{-12} and (4.5 – 6.5) × 10^{7} at·kg^{-1}, respectively. These depths correspond to the oldest waters (e.g. ~70 - 150 a for EMDW; Roether and Schlitzer, 1991; Stratford et al., 1998) in the EMS and the WMDW in the WMS.

The very deep and near bottom waters found below 2000 m (magnified $\theta - S$ diagrams, Figure 3.4) constitute the deep overturning cells in the WMS and the EMS (Figure 3.1). These waters are produced by dense water formation processes carrying relatively high $^{236}U/^{238}U$ atom ratios ((1100–1400) × 10^{-12}), ^{129}I concentrations ((7.0–8.5) × 10^{7} at·kg^{-1}) and dissolved oxygen concentrations from surface to the bottom. The magnified θ - S diagrams show the typical hook-like inversions due to the production of saltier, warmer and denser water during the Eastern Mediterranean Transient in the 1990s in the EMS (Roether et al., 1996), and the Western Mediterranean Transition in mid 2000s in the WMS (Schroeder et al., 2008).

The overall result of the circulation of the Mediterranean Sea is the conversion of relatively fresh AW into saltier Mediterranean Outflow Water (MOW), which exits the Mediterranean Sea through the Strait of Gibraltar entering intermediate depths of the Atlantic Ocean. MOW is characterized by higher $^{236}U/^{238}U$ atom ratios ((1350 - 1900) × 10^{-12}) and ^{129}I concentrations ((8 – 10) × 10^{7} at·kg^{-1}) compared to the incoming AW ($^{236}U/^{238}U$ ~1000 × 10^{-12} and ^{129}I ~4 × 10^{7} at·kg^{-1}). This increase in $^{236}U/^{238}U$ atom ratios

(~50%) and ^{129}I concentrations (>100%) during the transformation of AW into MOW cannot be explained by the ~6% increase in salinity alone.

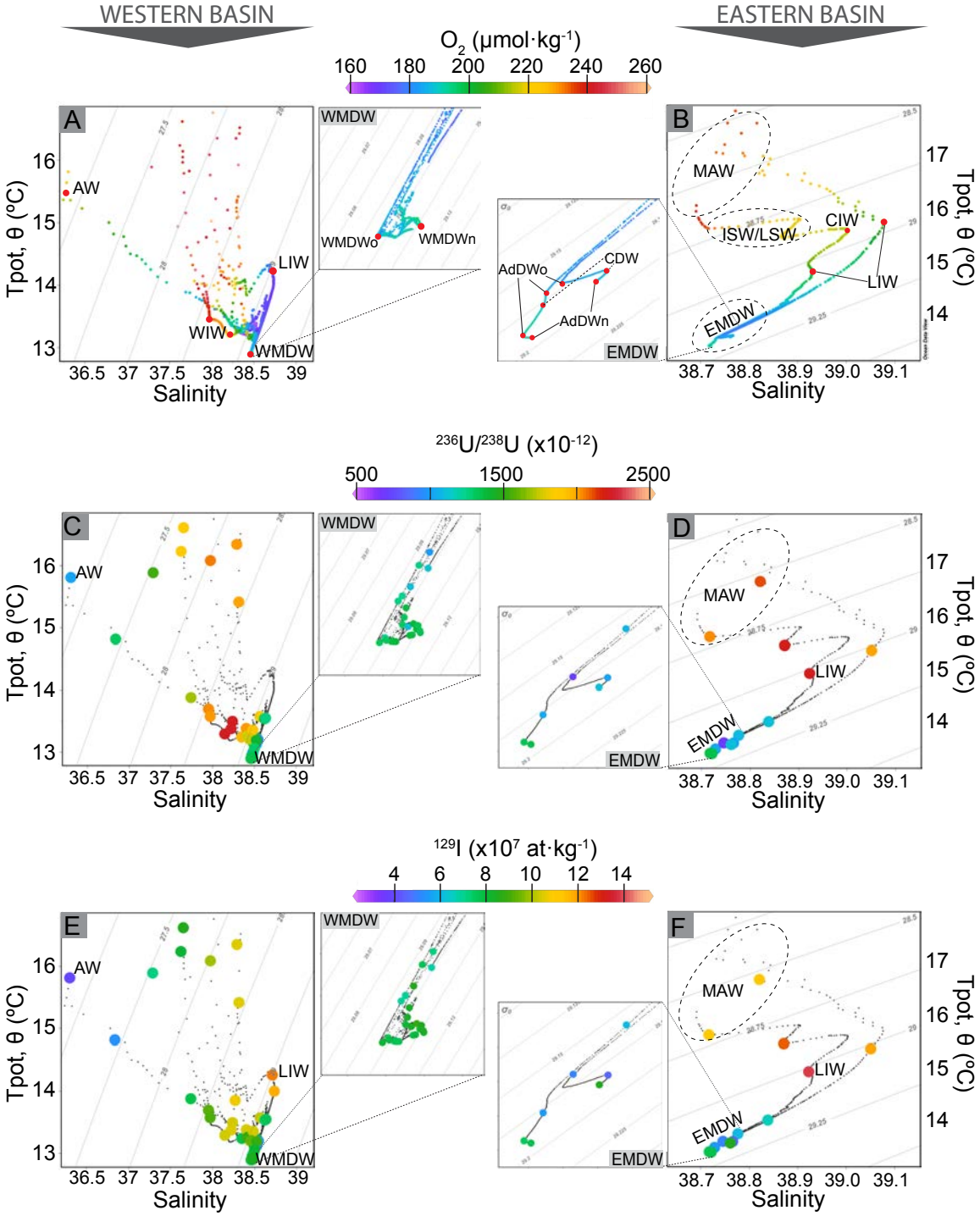

Figure 3.4. Potential temperature *(θ)* – salinity *(S)* diagrams for the Western (left) and Eastern (right) Mediterranean Sea. Z variables (coloured) are: dissolved oxygen concentrations (A, B); $^{236}U/^{238}U$ atom ratios (C, D) and ^{129}I concentrations (E, F). The WMDW and the EMDW have been magnified in the $\theta - S$ diagrams. Water mass acronyms are: Atlantic Water (AW), Modified Atlantic Water (MAW), Ionian Surface Water (ISW), Levantine Surface Water (LSW), Cretan Intermediate Water (CIW), Levantine Intermediate Water (LIW), Western Intemediate Water (WIW), Western Mediterranean Deep Water (WMDW), Eastern

Mediterranean Deep Water (EMDW) of Adriatic origin (Adriatic Deep Water, AdDW) and Cretan origin (Cretan Deep Water, CDW). Lower case n: new; o: old.

In summary, the distributions of $^{236}U/^{238}U$ atom ratios and ^{129}I concentrations along the west–east transect are coherent with the main circulation patterns in the Mediterranean Sea (Figure 3.5): i) the eastward penetration of relatively radionuclide-poor AW through the Strait of Gibraltar, ii) the formation, sinking and westward transport of radionuclide-enriched LIW, iii) dense water formation in the two basins evidenced by radionuclide-enriched very deep and bottom waters, iv) the presence of old waters associated with low $^{236}U/^{238}U$ atom ratios and ^{129}I concentrations in the EMS, and v) the exchange of these old waters between the EMS and the WMS (principally the Tyrrhenian Sea).

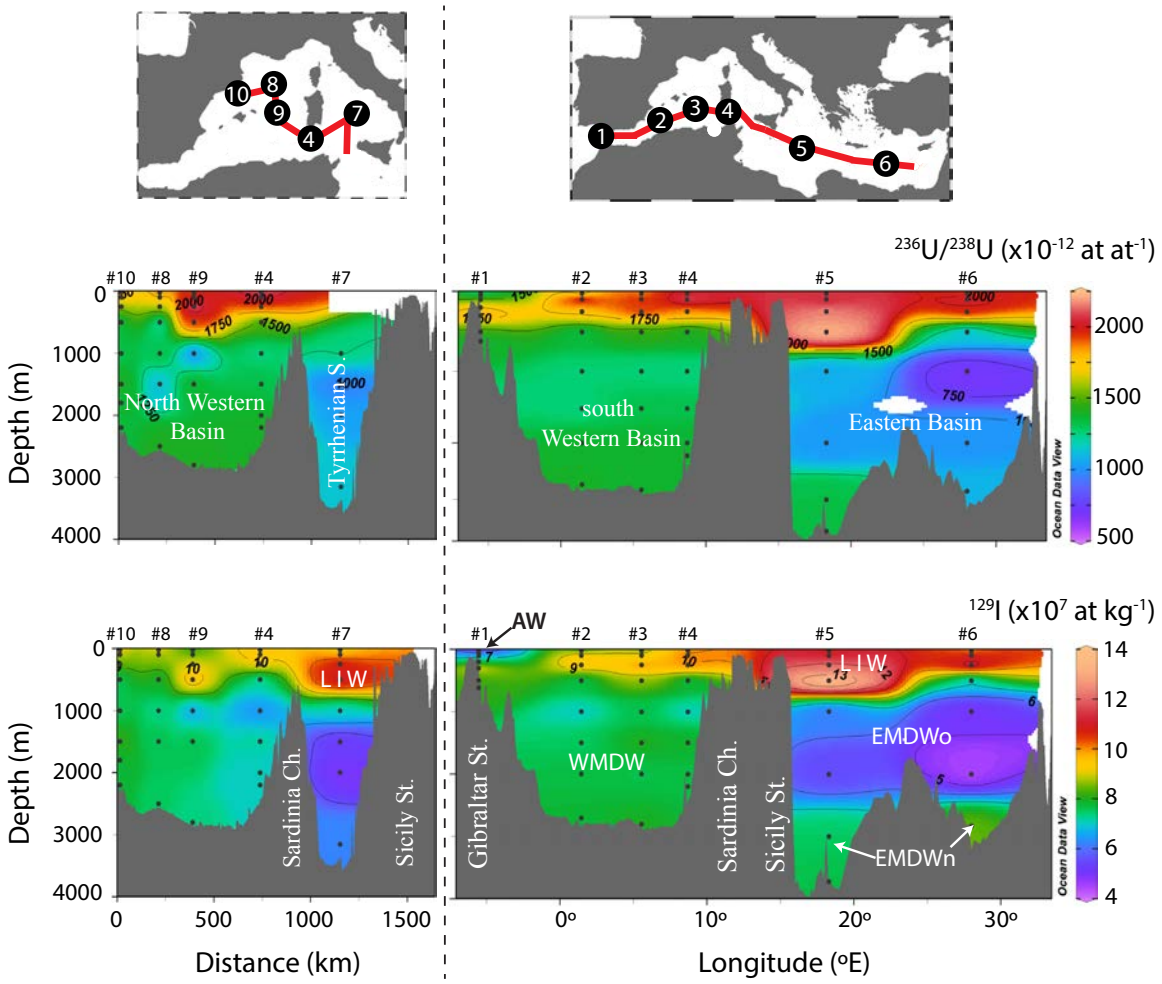

Figure 3.5. Depth distribution of the $^{236}U/^{238}U$ atom ratios (top panels) and the ^{129}I concentrations (bottom panels) along two sections of the Meditearranean Sea: 1) distance section crossing the northern Alguero-Balear region and the Tyrrhenian Sea in the WMS (left), and 2) longitudinal section crossing the Southwestern and Eastern Basins, from the Strait of Gibraltar to the Levantine Basin (right). Station numbers (#) are indicated. Main water masses are represented in bottom panels: Atlantic water (AW), Levantine

Intermediate Water (LIW), Eastern Mediterranean Deep Water (EMDW) and Western Mediterranean Deep Water (WMDW). n: new; o: old.

3.5.2. Constraining the sources of ^{236}U and ^{129}I to the Mediterranean Sea

a) Global fallout

The Mediterranean Sea has received global fallout from nuclear bomb testing through direct deposition and through secondary pathways such as river runoff, submarine groundwater discharge (SGD) and atmospheric deposition of crustal dust. Global fallout dominates the inputs of ^{236}U in the ocean, estimated in 900 to <2100 kg worldwide (Christl et al., 2012; Quinto et al., 2013; Sakaguchi et al., 2009; Winkler et al., 2012) depending on the method used (summarized in Table 1 of Quinto et al., 2013). The most recent version of the laterally averaged atmospheric box model GRACE (Elsässer et al., 2015) was run with a global ^{236}U input of 900 kg (which is the most likely input considering all oceanic ^{236}U concentrations from literature) at varying altitudes according to the explosive yield of each atmospheric bomb test (UNSCEAR, 2000). The modeled deposition of ^{236}U for the latitudinal band of the Mediterranean Sea (30 - 45 ºN, surface area of 2.51×10^{12} m^2) sums up to 11×10^{12} at·m^{-2} until 2013, or 11 kg. Similarly, the direct deposition of ^{129}I due to global fallout was modelled using a fixed ^{129}I/^{236}U ratio of 1:10 assuming a total release of 90 kg (Hou, 2004; Raisbeck and Yiou, 1999; Wagner et al., 1996), and would amount 2×10^{12} at·m^{-2}, or about 1 kg, to the Mediterranean Sea until 2013.

River runoff and SGD may transport global fallout radionuclides deposited on land to the ocean. Based on the cumulative global fallout deposition estimates until 2013 given above and considering the active drainage area (1.4×10^{12} m^2; Ludwig et al., 2009), river runoff and SGD together could potentially introduce a maximum of about 6 kg of ^{236}U and 0.6 kg of ^{129}I to the Mediterranean Sea. Separate inputs through rivers and SGD can be calculated in alternative ways. The only river with published data on concentrations of ^{236}U is the Danube River (one single measurement ($(2.5 \pm 0.7) \times 10^7$ at·L^{-1} in 2008; Eigl et al., 2013), although this value could be biased by the Chernobyl accident releases. A conservative estimate of 0.17 kg of ^{236}U is obtained by taking this figure and the annual river water flux to the Mediterranean Sea (300×10^{12} L; Ludwig et al., 2009) integrated

since the beginning of the atmospheric nuclear tests until 2013. No ^{236}U concentrations in the fresh water fraction of SGD (about 5% of the total SGD; Rodellas et al., 2015) have been documented. As a first approximation, we can take the ^{236}U concentration of the Danube River and the fresh water discharged annually as SGD ((15 - 240) × 10^{12} L; Rodellas et al., 2015), resulting in an input of less than 0.2 kg of ^{236}U since the advent of nuclear-derived emissions (1963). Therefore, rivers and SGD would have introduced only a small fraction of the 6 kg of ^{236}U deposited in the active drainage basin. We can follow a similar approach for ^{129}I. However, continental waters in Europe are largely influenced by atmospheric releases from the European reprocessing plants and thus present a very broad range of ^{129}I concentrations (e.g. (4 - 240) × 10^{7} at·kg^{-1} in rivers: Moran, 2002; Snyder and Fehn, 2004). If we assume the lowest concentration (4 × 10^{7} at·kg^{-1}) to represent waters containing only global fallout; river runoff and SGD would supply 0.15 kg and 0.01 - 0.12 kg of ^{129}I, respectively.

The Mediterranean Sea also receives significant atmospheric dust from the Sahara Desert that may carry radionuclides derived from global fallout. Chamizo et al., (2016) recently estimated a deposition of 12 × 10^{-15} kg·m^{-2} for ^{236}U for the WMS since 1963, which would translate into only 0.03 kg of ^{236}U to the whole Mediterranean Sea. The corresponding input of ^{129}I would likely be even less significant, since the total global fallout of ^{129}I was one order of magnitude smaller compared to ^{236}U.

b) Nuclear accidents

The Chernobyl accident in April 1986 led to the release of radioactivity to the lower troposphere, and thus the deposition of radionuclides was strongly dependent on regional winds and precipitation patterns, mostly affecting northeastern Europe and countries close to the nuclear power plant such as Belarus and Ukraine (IAEA, 2006). The direct deposition of ^{236}U on the Mediterranean Sea was probably small, since refractory elements such as uranium or plutonium were associated with fuel particles and deposited principally near the Chernobyl nuclear power plant. Indeed, the $^{236}U/^{238}U$ atom ratios measured in soil decreased by three orders of magnitude at a distance of 200 km from the damaged reactor (Boulyga and Heumann, 2006) and showed no influence of the accident in Italy (Quinto et

al., 2009). The minor input of ^{236}U from Chernobyl fallout is further supported by Papucci et al. (1996), who estimated that Chernobyl fallout contributed 10,000 times less than global fallout to the Mediterranean inventory of other refractory, transuranic elements such as $^{239,240}Pu$.

Larger amounts of more volatile radionuclides (e.g. ^{131}I, ^{137}Cs) were released from Chernobyl, and their deposition was particularly significant in the northern and eastern sub–basins of the Mediterranean Sea (Papucci et al., 1996). The total releases of ^{129}I have been estimated to be 1.3 – 6.0 kg based on data on ^{131}I concentrations and $^{129}I/^{131}I$ ratios measured in soils and in precipitation in western Europe and Israel (Aldahan et al., 2007; Paul et al., 1987). Considering these figures and that about 2% of total Chernobyl releases of ^{137}Cs were deposited in the Mediterranean Sea (Papucci et al., 1996; UNSCEAR, 2000), the input of ^{129}I would have been of about 0.10 kg.

The Chernobyl accident had a significant impact on the Black Sea and some rivers that discharge to the Black Sea (e.g. Dnieper and Danube). Consequently, significant amounts of radionuclides from the Chernobyl accident, in addition to global fallout, continue entering the Mediterranean Sea through the inflow of water from the Black Sea (Delfanti et al., 2014). Water influx from the Black Sea to the Mediterranean Sea occurs at a rate of 1.2×10^{12} $m^3 \cdot a^{-1}$, constrained to surface and sub-surface waters (<100 m) at the Bosphorus Strait. At these depths, the Black Sea Water concentration of ^{236}U averaged $(39 \pm 6) \times 10^6$ $at \cdot kg^{-1}$, which is close to the reported value for the Romanian coast in 2008 ($(30.0 \pm 0.5) \times 10^6$ $at \cdot kg^{-1}$; Eigl et al., 2013). Taking this concentration, due to the Chernobyl accident and the global fallout, as constant through time, about 1 kg of ^{236}U would have been introduced into the Mediterranean Sea until 2013. For ^{129}I, and taking the average concentration of $(12 \pm 2) \times 10^7$ $at \cdot kg^{-1}$, about 1.6 kg would have been added to the Mediterranean Sea from the Black Sea. These estimates, however, are subject to large uncertainties, since the lack of data precludes evaluating the variation of inputs over time, as observed for other artificial radionuclides such as ^{90}Sr and ^{137}Cs (Delfanti et al., 2014; Egorov et al., 1999).

The accident at the Fukushima Dai-ichi nuclear power plant in 2011 also released radioiodine to the atmosphere. Fukushima derived airborne ^{131}I was detected in Europe

(Masson et al., 2011), but ^{129}I was not discernable from the gaseous releases from the European reprocessing plants (Daraoui et al., 2016).

c) Nuclear industry

The presence of ^{236}U and ^{129}I in the Mediterranean Sea cannot be explained only by global fallout and the Chernobyl accident, hence significant inputs from the nuclear industry may explain the unbalance.

Most of the ^{236}U and ^{129}I produced in nuclear power plants are generally kept in irradiated fuel and stored inside the facilities (Hou et al., 2009). Thus, the release of ^{236}U and ^{129}I from nuclear power plants to the environment is considered insignificant compared to other sources such as global fallout or reprocessing plants (He et al., 2011; Hou et al., 2002; Krausová et al., 2013; Quinto et al., 2009; Rao and Fehn, 1999).

On the contrary, nuclear reprocessing plants discharge significant amounts of liquids (containing ^{129}I and ^{236}U) and gases (containing ^{129}I) to the environment (Christl et al., 2015a). In the case of Marcoule, only the discharge of ^{129}I has been reported (Hou et al., 2009 and references therein). According to this study, about 45 kg of liquid ^{129}I were released to the Rhône River at a fairly constant rate (about 1 - 2 $kg \cdot a^{-1}$) from 1967 to 1997. In addition, about 145 kg were released to the atmosphere at different rates: less than 2 $kg \cdot a^{-1}$ until 1975, up to 9 $kg \cdot a^{-1}$ between 1975 and 1990, and about 4 $kg \cdot a^{-1}$ by 1994. Taking the above values as an input function for the simple box model of the Mediterranean Sea used here, the amount of ^{129}I releases from Marcoule, as well as the partitioning between river and atmospheric inputs to the Mediterranean Sea were estimated. A description of the box model and a detailed assessment of the several model outputs can be found in the Appendix (A.5).

The box model was used for an extensive study of different input scenarios. In the following, only selected release scenarios and the main findings are discussed. First simulations were done to evaluate if the liquid input from Marcoule would suffice to explain the excess of ^{129}I in the Mediterranean Sea. When introducing 45 kg of liquid ^{129}I to surface waters of the Northern Alguero–Balear region, the simulated concentrations of ^{129}I were still about 2.5 times lower, comparing median values, than the measured

concentrations in the whole Mediterranean Sea in 2013 (Figure 3.6, black bars). In a second step, the input of gaseous ^{129}I was implemented. The geographic distribution of ^{129}I deposition into the surface boxes of the Mediterranean Sea was performed in accordance with the prevailing major wind patterns taken from an atmospheric model (http://ready.arl.noaa.gov/HYSPLIT_traj.php; see Appendix A.6).

Considering the full input of both, liquid and gaseous releases from Marcoule, the simulated ^{129}I concentrations in the Mediterranean Sea were two times (comparing median values) higher than those measured in 2013 (not shown in Figure 3.6). Consequently, we considered more realistic scenarios, including that a certain fraction of the liquid ^{129}I could have been trapped by river biota, and sediments (Hou et al., 2009 and references therein), not reaching the sea. Based on tested input scenarios, this fraction would be ≤30% of the total liquid discharge of ^{129}I. For gaseous releases of ^{129}I, it is very likely that a certain fraction was deposited locally without reaching the sea (this fraction was assumed to be about 50%; He et al., 2013), or was transported and thus deposited outside the Mediterranean Sea region (e.g. about 25% of the calculated wind trajectories ended outside the Mediterranean Sea in 2015 (information not available for 2013), see Appendix A.6). For the gaseous ^{129}I a time delay of 5 to 10 years was also tested. We considered that while most of the ^{129}I was directly deposited on the surface ocean, some might have been deposited on land and later transported by freshwater runoff. This time delay, accounting for both directly and indirectly introduced ^{129}I, is shorter than the residence times of ^{129}I reported in limited studies carried out in soils (18 - 60 years; Boone et al., 1985; Robents et al, 1989). The best match between modelled and measured concentrations in 2013, quantified by minimizing the Chi-squared value, was achieved when the inputs of ^{129}I to the Mediterranean Sea were scaled to ≥70% and 20 - 40% for liquid and gaseous (with a 5 year delay for the gaseous input) fractions, respectively (see Appendix A.5 and Figure 3.6). This represents an input of ^{129}I from Marcoule of 70 - 90 kg, almost 2 orders of magnitude larger than the global fallout. The model output shows that, from this amount, about 20 - 30 kg of ^{129}I have already been transported by water circulation to the Atlantic by 2013.

In a second set of simulations, the model was run until the 1990s and 2009 to compare simulated ^{129}I concentrations with those reported for that period of time in the literature (Table 3.2). For this purpose, a release scenario (e.g. 80% for liquid and 30% for gaseous

^{129}I input) was chosen considering previous results. Simulated ^{129}I concentrations in the Alguero-Balear surface and deep waters were $(46 \pm 5) \times 10^7$ at·kg^{-1} and $(8 \pm 1) \times 10^7$ at·kg^{-1}, respectively, in 1992, while they decreased to $(40 \pm 4) \times 10^7$ at·kg^{-1} in the surface by 1998. These concentrations agreed well with those from DYFAMED station (Table 3.2). On the contrary, simulated ^{129}I concentrations in the EMS, $(14 \pm 2) \times 10^7$ at·kg^{-1} for the Aegean Sea in 1998 and $(10 \pm 1) \times 10^7$ at·kg^{-1} for the Adriatic Sea in 2009, were significantly lower than those reported in the literature (Table 3.2). Such discrepancy could be related to the input of gaseous ^{129}I from Marcoule, which can vary significantly depending on the above assumptions and considerations (e.g. fraction of ^{129}I deposited in the vicinity of the reprocessing plant, air trajectories, the time delay for gaseous inputs and the input function itself). Also, additional atmospheric ^{129}I inputs from Sellafield and La Hague were not considered, but may not be totally ruled out, given the distance from the point-like sources, the magnitude of the releases and the air trajectories (see Appendix A.6). Finally, the model does not account for the input of radionuclides from the Black Sea, which could have elevated the concentrations of ^{129}I in Aegean surface waters according to concentrations reported in Table 3.2.

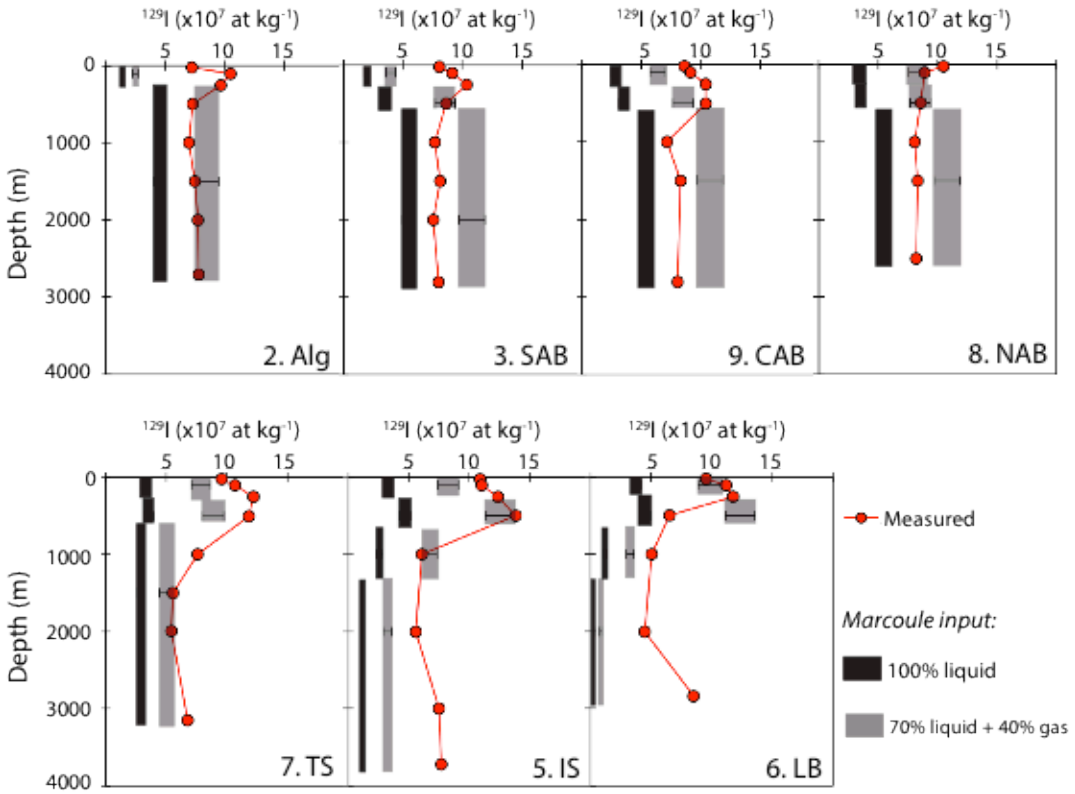

Figure 3.6. Measured and simulated concentrations of ^{129}I. Two releases scenarios are shown. The first scenario (black) considers that 100% of liquid ^{129}I discharged to the Rhône river (Hou et al., 2009) reached the Mediterranean Sea. The second scenario (grey) considers 70% of liquid ^{129}I discharged to the Rhône river and 40% of ^{129}I gaseous emissions from Marcoule reached the Mediterranean Sea. In addition, all scenarios included the global fallout, which contributed always less than 2% to the presence of ^{129}I. The input from global fallout was estimated considering a total ^{129}I release of 90 kg to the world ocean (Hou, 2004; Raisbeck and Yiou, 1999; Wagner et al., 1996) and the input function from the GRACE model (Elsässer et al., 2015). We assigned a 10% error to the simulated concentrations in order to account for the uncertainty of the box volumes and water exchange rates between boxes (not provided in Bethoux and Gentili, 1996). Station labels are: Algeria (2. ALG); Southern Alguero-Balear (3. SAB); Ionian Sea (5. IS); Levantine Basin (6. LB); Tyrrhenian Sea (7. TS); Northern Alguero-Balear (8. NAB); Central Alguero-Balear (9. CAB). The station named Algeria was close to, and has been compared to, the Alboran Sea region from Bethoux and Gentili (1996) (see Appendix A.4 for details about regions and station location).

For ^{236}U, we first considered inputs from global fallout only, assuming a global ^{236}U release of 900 kg to the world oceans (Sakaguchi et al., 2012), and using the laterally averaged depositional flux provided by the GRACE Model (Elsässer et al., 2015). With this input scenario, simulated concentrations of ^{236}U were about 2.5 times (comparing median values) lower than those measured in 2013 (Figure 3.7). A global input of more than 2000 kg would be necessary to match this difference, which is rather unlikely

(Casacuberta et al., 2014; Sakaguchi et al., 2009; Winkler et al., 2012). Several alternative scenarios were tested by adding varying liquid discharges of ^{236}U from Marcoule and the total input from global fallout (See Appendix A.5). Given the lack of data on liquid ^{236}U releases from Marcoule, and as a first approximation, a similar input function than that of liquid ^{129}I, entering the Northern Alguero-Balear surface box, was assumed. The best agreement with measured concentrations in the water column was obtained when the total global fallout ^{236}U of 900 kg (of which about 11 kg entered the Mediterranean Sea) was accompanied by an additional total input of 10-20 kg of liquid ^{236}U from Marcoule (Figure 3.7).

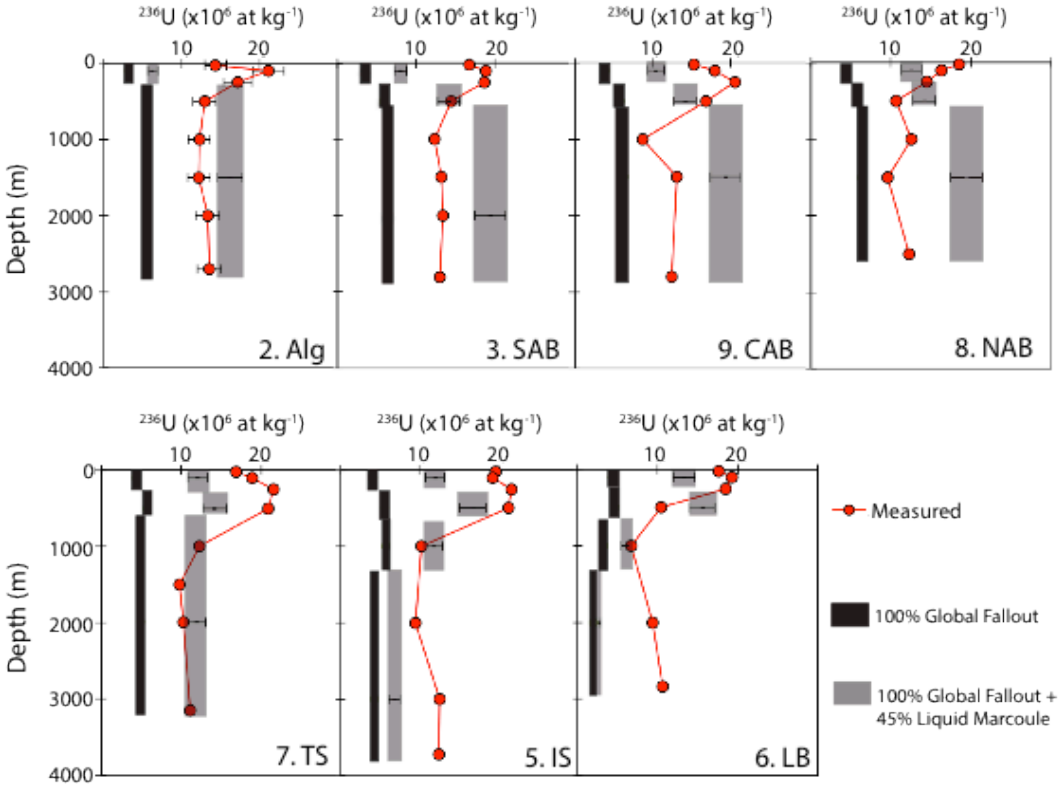

Figure 3.7. Measured and simulated concentrations of ^{236}U. Two release scenarios are shown. The first scenario (black) considers only the global fallout deposition assuming a total ^{236}U release of 900 kg to the world ocean (Sakaguchi et al., 2009). The second scenario (grey) is an example of the various tests that considered both the global fallout and the liquid release of 20 kg (45% of the mass of ^{129}I) from Marcoule (assuming a similar input function to that of liquid ^{129}I (Hou et al., 2009)). We assigned a 10% error to simulated concentrations in order to account for the uncertainty of the box volumes and water exchange rates between boxes (not provided in (Bethoux and Gentili, 1996)). The ^{236}U concentrations in the upper 500 m of the Tyrrhenian Sea have been extrapolated considering the ^{129}I/^{236}U ratio in neighbouring sub-basins at similar depths. Station labels are: Algeria (2. ALG); Southern Alguero-Balear (3. SAB); Ionian Sea (5. IS); Levantine Basin (6. LB); Tyrrhenian Sea (7. TS); Northern Alguero-Balear (8. NAB); Central Alguero-

Balear (9. CAB). The station named Algeria was close to, and has been compared to, the Alboran Sea region from Bethoux and Gentili (1996) (see Appendic A.4 for details about regions and station location).

Model outputs still show some discrepancies between measured and simulated concentrations of both ^{129}I and ^{236}U (Figure 3.6 and 3.7). In the WMS, simulated surface concentrations were systematically underestimated, while in deep waters simulated concentrations exceeded those measured in 2013. This could be due to an overestimation of the dense water formation rate which would cause an excessive radionuclide transport from surface to the ocean interior. Indeed, most dense water formation rates reported for the WMS (sumarized in Waldman et al., 2016) are lower than assumed by Bethoux and Gentili (1996) for the Alguero-Balear region (1.77 Svedrups). In the case of simulated ^{236}U concentrations, additionally, the excess in deep waters could be related to an overestimation of the liquid input through the Rhône river, suggesting that the input function of liquid ^{236}U from Marcoule probably differed from that of ^{129}I. In deep EMS waters, simulated concentrations are lower than those measured in 2013. The box model of Bethoux and Gentili (1996) used in this study did not take into account some recent changes, such as the massive dense water formation during the Eastern Mediterranean Transient (Roether et al., 1996). The discrepancy indeed points to higher renewal rates for the EMDW than those considered in the box model.

d) Summary of major sources of ^{236}U and ^{129}I

The inputs of ^{236}U and ^{129}I to the Mediterranean Sea from global fallout, the Chernobyl accident and the Marcoule reprocessing plant were investigated (Table 3.3) based on measured distributions in 2013, published data and box modeling. The results suggest that the inputs from Marcoule were the largest contributions to the total quantitites of both ^{236}U (45 - 60%) and ^{129}I (>95%) introduced into the Mediterranean Sea until 2013. The contribution from global fallout was also significant for ^{236}U (35 - 50% of the total input), but it was minor for ^{129}I (~1%). The inputs from the Chernobyl accident, through direct atmospheric deposition and the water inflow from the Black Sea, accounted for less than 5 % and 2% of the total amount of ^{236}U and ^{129}I, respectively. From all the inputs of ^{236}U and ^{129}I, about 30 - 40% has been exported as MOW into the Atlantic Ocean by 2013.

Table 3.3. Estimated inputs of ^{236}U and ^{129}I from the principal sources to the Mediterranean Sea until 2013.

	^{236}U (kg)	^{129}I (kg)
Global fallout[a]	11	1
Nuclea accidents: Chernobyl[b]	1	1 - 2
Nuclear industry: Marcoule	10 - 20	70 - 90

[a]direct deposition + post depositional transport by runoff

[b]direct deposition + input from the Black Sea

3.6. Conclusions

The first comprehensive distribution of ^{236}U and ^{129}I covering the Western and the Eastern Basins of the Mediterranean Sea is presented here. Radionuclide distributions enabled the identification of the radionuclide-poor Atlantic Water entering through the Strait of Gibraltar, the formation and transport of radionuclide-rich Levantine Intermediate Water, the exchange of water between the two basins, the dense water formation of Western and Eastern Mediterranean Deep Water and the outflow of radionuclide-rich Mediterranean Overflow Water.

All samples presented significant amounts of artificial ^{236}U and ^{129}I. The highest radionuclide concentrations were recorded at surface and intermediate depths of the EMS. This basin has a small presence of AW with relatively low ^{236}U and ^{129}I concentrations and receives more water from the Adriatic, Aegean and Black Seas, enriched in ^{236}U and ^{129}I. Measured concentrations of ^{236}U in the NAB (St. 8) were comparable to those reported at the DYFAMED station in 2013 (Chamizo et al., 2016). For ^{129}I, the concentrations measured in the Mediterranean Sea in 2013 were significantly lower than those measured earlier in the Western and Eastern Basins. In the WMS, the surface ^{129}I concentrations variation with time is likely related to the cease of nuclear reprocessing operations at Marcoule by late 1990s. In the EMS, high ^{129}I concentrations in northern Adriatic waters may have been impacted by gaseous ^{129}I inputs from distant La Hague and Sellafield reprocessing plants according to Osterc and Stibilj (2009). However, none of our samples showed such high ^{129}I concentrations.

The high radionuclide inventories and concentrations confirm the presence of regional sources of ^{236}U and ^{129}I in the Mediterranean Sea. Inventories of ^{236}U and ^{129}I would be 3 and 100 times, respectively, lower than obtained if global fallout was the only source considered. Concentrations would also be smaller ($^{236}U \sim 5 \times 10^{6}$ at·kg^{-1} and $^{129}I < 0.1 \times 10^{7}$ at·kg^{-1}) than the measured ones (on average $^{236}U \sim 15 \times 10^{6}$ at·kg^{-1} and $^{129}I \sim 10 \times 10^{7}$ at·kg^{-1}) when assuming a single global fallout source and the homogeneous mixing of Mediterranean waters. These results suggest that the excess of ^{236}U and ^{129}I is mainly related to fuel reprocessing carried out by Marcoule until the 1990s. The impact of Marcoule in the Mediterranean Sea is less evident than the impact related to Sellafield and La Hague in the Irish and North Seas. This would be explained by the deeper average depth of the Mediterranean Sea (~1500 m) compared to the Irish and North Seas, both having mean depths of about 100 m; the mixing with AW; the export of radionuclides as MOW and the dense water formation.

The excess of radionuclides was matched by the proposed discharge of ^{236}U and ^{129}I from the Marcoule reprocessing plant using a box model and considering ocean, river and atmospheric transport. The comparison between the box model and observational data shows that: i) the amount and time variation of ^{236}U discharged from Marcoule requires further studies to reduce the difference between measured and simulated ^{236}U concentrations in the WMS; ii) gaseous ^{129}I inputs from other sources, such as Sellafield and La Hague, are unlikely in the Mediterranean Sea, but, should not be dismissed in the northern sub-basins; and iii) dense water formation rates used in the model are probably overestimated in the WMS and underestimated in the EMS.

CHAPTER 4

Evolution of artificial radionuclides in the Mediterranean Sea

4.1. Abstract

Basin-wide distributions of ^{137}Cs, ^{237}Np and ^{239,240}Pu concentrations are presented for the Mediterranean Sea in May 2013. Seawater collected from 10 vertical profiles in the Western and Eastern basins was analyzed in order to relate artificial radionuclide distributions with principal water masses and biogeochemical regimes. The aim of this study was to constrain the sources of long-lived ^{237}Np, ^{239}Pu and ^{240}Pu based on their water column distributions, as well as, to discuss their basin-scale distributions (also for ^{137}Cs), in relation to particle dynamics and the Mediterranean thermohaline circulation. The concentration range of ^{137}Cs, ^{237}Np, ^{239}Pu, ^{240}Pu and ^{239,240}Pu were 0.70-2.00 Bq·m^{-3}, 0.100-0.210 mBq·m^{-3}, 1.40-13.0 mBq·m^{-3}, 1.40-9.20 mBq·m^{-3} and 3.0-22.0 mBq·m^{-3}, respectively. The results show that Marcoule reprocessing plant located in the Rhône River, France, contributed with ~7 kg of ^{237}Np, about half the amount introduced by atmospheric fallout from nuclear weapon tests. Global fallout was confirmed as the main source of plutonium because the measured median ^{240}Pu/^{239}Pu atom ratio in waters across the Mediterranean Sea was ~0.19. The first basin-scale transect of ^{237}Np in oceans followed a similar distribution as other conservative radionuclides (i.e. ^{137}Cs, ^{129}I and ^{236}U) and was coherent with Mediterranean waters masses. Distribution of ^{137}Cs between 1970s and 2013 was mainly influenced by the inputs from global fallout and the Chernobyl accident, as well as by lateral advection and dense water formation. The ^{239,240}Pu concentrations, affected additionally by particle scavenging and remineralization, suggest that this nuclide was removed faster from the water column in the Eastern Basin than in the Western Basin. We proposed two possible mechanisms: boundary scavenging of Pu onto the wider shelf sediment in the Eastern Basin, or the transport of Pu by Levantine Intermediate Waters from the Eastern to the Western Basin.

4.2. Introduction

Artificial radioactive isotopes are present in the Mediterranean Sea since the 1950s due to various sources. The largest inputs of artificial radionuclides (e.g. ^{137}Cs or plutonium) occurred as global atmospheric deposition (named *global fallout*) from atmospheric nuclear weapons tests performed during the 1950s and 1960s (Delfanti and Papucci, 2010). In April 1986, the accident in reactor 4 at the Chernobyl nuclear power plant caused the release of artificial radionuclides to the environment (UNSCEAR, 2000). Volatile elements such as ^{137}Cs travelled long distances and were deposited in remote areas such as the northern and eastern Mediterranean Sea (EMS) (Papucci et al., 1996), while refractory elements, such as plutonium, were released in smaller quantities and deposited mainly within a few hundred kilometers from the damaged power plant (Papucci et al., 1996). The inflow of water from the Black Sea with higher radionuclide concentrations than Mediterranean waters constitutes a secondary continuous pathway for Chernobyl and global fallout radionuclides into the Mediterranean Sea (e.g. for ^{137}Cs, ^{129}I and ^{236}U; Castrillejo et al., 2017; Delfanti et al., 2013; Egorov et al., 2000). The third significant source was Marcoule reprocessing plant located in southeast France. This facility is the largest contributor from the civil and military nuclear industry, having released volatile radionuclides to the atmosphere and low – level radioactive liquid effluents to the western Mediterranean Sea (WMS) through the Rhône River, from 1961 to 1997 (Charmasson, 1998; Eyrolle et al., 2004; Hou et al., 2009).

Most studies on artificial radionuclides in the Mediterranean Sea have focused on ^{137}Cs, largely due to its feasibility to provide rapid information of the general radiological impact on marine biota but also on pathways of radioactive contamination. Consequently, several studies have allowed constraining its inputs to the Mediterranean Sea, which are estimated in about 11 PBq from global fallout (reference year 1963; UNSCEAR, 2000), 2.5 PBq from Chernobyl fallout (ref. year 1986; Papucci et al., 1996) and 0.05 PBq from the nuclear industry, particularly from the Marcoule reprocessing plant (referred to 1990, Charmasson, 2003). The exchange with Black Sea waters have introduced ~0.3 PBq of ^{137}Cs since 1986 (Delfanti et al., 2013; Egorov et al., 1999), while the loss through the Mediterranean Outflow to the Atlantic Ocean is compensated by the inflow of Atlantic

waters (Gascó et al., 2002a). About 90% of the ^{137}Cs resides in the water column (Delfanti and Papucci, 2010) due to its low affinity for particles (K_d ~10^3 in open seawater; IAEA, 2004) with <1% of ^{137}Cs found in the particulate fraction in open waters (Ballestra et al., 1984). Thus in the water column, the temporal evolution of the ^{137}Cs distribution, aside from the inputs to the surface and its decay, has been driven mainly by the vertical transport by dense water formation processes occurring in the northern parts of the WMS and the EMS, and by the lateral advection of water masses (e.g. Delfanti et al., 2003; Lee et al., 2003; Papucci and Delfanti, 1999). The remaining ~10% of the ^{137}Cs inventory has been accumulated in coastal sediments, while about 1% is found in deep sediments of the Mediterranean Sea (Charmasson, 2003; Garcia-Orellana et al., 2009; Radakovitch et al., 1999). Thus, ^{137}Cs has been used as a tracer of circulation in open Mediterranean waters and of sedimentation processes mainly in coastal margins. For example, ^{137}Cs was combined with other artificial (e.g. ^{90}Sr, ^{3}H) and natural (^{210}Pb) radionuclides in the Mediterranean Sea to estimate the transport of Chernobyl contaminated waters (Delfanti et al., 2003), as well as to assess sediment mixing and accumulation rates in continental margins (e.g. Calmet and Fernandez, 1990; Miralles et al., 2004; Radakovitch et al., 1999). However, medium–lived radionuclides such as ^{137}Cs ($T_{1/2}$= 30.1 a) already reach low concentrations in the water column (<1 Bq·m^{-3}) and concentration gradients are smoothing progressively, limiting their potential as oceanic tracers. Thus, studies on conservative long-lived radionuclides (e.g. ^{236}U, ^{129}I, ^{237}Np) are necessary, in addition to learn about their distributions in the Mediterranean Sea, to use them as tracers of a variety of oceanic processes.

A long–lived artificial radionuclide that received considerable attention in the WMS due to its behavior and radiotoxicity is plutonium. Plutonium is a useful tracer of particle related processes such as scavenging and sedimentation (Lindahl et al., 2010) as a result of its strong affinity for particles (K_d~10^5; IAEA, 2004). Most frequently studied isotopes of Pu are the most abundant ^{239}Pu ($T_{1/2}$= 24,100 a), ^{240}Pu ($T_{1/2}$=6,561 a), and, to a lesser extent, ^{238}Pu ($T_{1/2}$= 87.74 a). Most Pu concentrations were reported as ^{239,240}Pu because Pu was usually measured by alpha spectrometry, which does not allow discerning between the ^{239}Pu (E_α= 5.157 MeV) and ^{240}Pu (E_α= 5.168 MeV). From measurements on soils, aerosols and rain, the mean ^{239,240}Pu deposition from global fallout has been estimated to be ~80

$Bq \cdot m^{-2}$, which translates into ~200 TBq for the whole Mediterranean Sea (e.g. Delfanti and Papucci, 2010; Hardy et al., 1973; León Vintró et al., 1999). The discharges of $^{239,240}Pu$ from Marcoule reprocessing plant have been estimated in 0.5 TBq from 1945 to 2000 (Eyrolle et al., 2004). About 30% of that amount would have been retained in sediments of the Rhone River and its delta, while the remaining ~0.35 TBq would have entered further in the Mediterranean Sea (Eyrolle et al., 2004). The Chernobyl accident released to the atmosphere ~2.5 PBq of $^{239,240}Pu$, mainly as part of solid particles that deposited in the vicinity of the nuclear power plant (UNSCEAR, 2000). Although Chernobyl fallout deposition in the Mediterranean Sea is not as well constrained as that of radiocaesium (Papucci et al., 1996), it is estimated to be about 3 orders of magnitude smaller than global fallout in the Mediterranean Sea. The inflow of Black Sea waters added ~3 and ~0.4 TBq of $^{239,240}Pu$ before and after the Chernobyl accident, respectively (Egorov et al., 1999; UNEP, 1992). Finally, a US bomber carrying 4 hydrogen bombs collided flying over Palomares, southeast Spain, in 1966. Three of the unarmed hydrogen bombs hit the ground releasing radionuclides over land, while the fourth bomb fell on the seashore. The washout of $^{239,240}Pu$ deposited on land into the ocean constituted another local source of Pu (Gascó and Antón, 1997). Plutonium sources can be tracked using the $^{238}Pu/^{239,240}Pu$ activity ratio or the $^{240}Pu/^{239}Pu$ atom ratio. To date, those ratios reported for the WMS have values around 0.03 and 0.18, respectively, confirming that global fallout is the dominating source in this basin (e.g. Bressac et al., 2017; Pham et al., 2017). Yet, those ratios may deviate significantly from the expected plutonium composition in global fallout due to local inputs like Palomares or Marcoule (e.g. Miralles et al., 2004). Full-depth water column inventories of $^{239,240}Pu$ are ~50 $Bq \cdot m^{-2}$ in the WMS (Ballestra et al., 1984; Fowler et al., 2000; Fukai et al., 1979; Garcia-Orellana, 2004; Livingston et al., 1979). Notwithstanding the error associated to these inventories, a significant fraction (>30%) of Pu introduced in the WMS has been already removed from the water column. Scavenging by sinking particles is one of the main processes responsible of the downward transport of Pu. Indeed, about ~5% of Pu in open waters is associated to particles, a value that can be higher in coastal areas (Ballestra et al., 1984; Holm et al., 1987; León Vintró et al., 1999; Mitchell et al., 1995). Plutonium can thus ultimately be incorporated onto coastal, shelf and margin sediments, where relatively large $^{239,240}Pu$ inventories have been reported (e.g. >120 $Bq \cdot m^{-}$

^{3}, Delfanti and Papucci, 1995; Gascó et al., 2002b). In open areas of the Mediterranean Sea, deep sediments contain only ~3% of the total Pu inventory, indicating that the vertical downward transport of Pu by scavenging is not as efficient as in coastal areas (Garcia-Orellana et al., 2009). Indeed, vertical profiles of Pu concentrations reported for the WMS show the influence from both particle scavenging and circulation dynamics depending on lateral advection processes and the distance from areas with significant dense water formation processes and primary production (e.g. Fowler et al., 2000; Noureddine et al., 2008). In the EMS, Pu distributions were only reported for the 1970s (Fukai et al., 1979; Livingston et al., 1979). Consequently, the constraints on Pu sources, as well as the roles of circulation and particle dynamics on the distribution of Pu, are not yet well understood in the EMS.

At present, the dataset on other long-lived conservative radionuclides in the Mediterranean Sea, such as ^{129}I, ^{236}U and ^{237}Np, is much more limited than for ^{137}Cs or plutonium. This is mainly due to two reasons. Firstly, long–lived radionuclides have lower specific activities, hence usually pose a lower radiological risk than medium-lived radionuclides such as ^{137}Cs. Secondly, their analyses are often more complicated and their measurements are more expensive compared to conventional radiometric techniques (e.g. accelerator and inductively coupled mass spectrometry; Christl et al., 2015; Kenna, 2002; Vockenhuber et al., 2015). In the Mediterranean Sea, the information on ^{129}I concentrations is sparse in space and time (Osterc and Stibilj, 2012; Yiou et al., 1997; Zhao et al., 1998), while measurements of ^{236}U and ^{237}Np were scarce until very recently (Bressac et al., 2017; Castrillejo et al., 2017; Chamizo et al., 2016). Concentrations of ^{129}I exceeded up to 3-5 orders of magnitude the levels estimated for global fallout (~10^{6} at·kg^{-1}) in the north WMS and the Adriatic Sea in 1990s and 2009, respectively, indicating the possible influence from the nuclear industry (Osterc and Stibilj, 2012; Yiou et al., 1997). Regarding ^{236}U, the first data reported for seawater, particles and atmospheric dust collected at the DYFAMED site in the north WMS confirmed that: i) most ^{236}U is soluble in the water column, ii) the contemporary ^{236}U input through the deposition of atmospheric dust is negligible, and iii) the water column inventory of ^{236}U exceeds about 2.5 times that expected from global fallout (Chamizo et al., 2016). Inventories of ^{237}Np measured at the same site (~0.34 Bq·m^{-3}) were in the same order of magnitude, but larger, than expected

from global fallout (~0.14 $Bq \cdot m^{-3}$) suggesting that Marcoule might have discharged significant ^{237}Np into the north WMS (Bressac et al., 2017). Bressac et al., (2017) further compared the concentrations of ^{237}Np, ^{137}Cs and ^{239}Pu to evaluate the relevance of particle scavenging in the upper 300 m of the water column, and of water circulation at deeper depths. In *Chapter 3* we presented a larger dataset on ^{236}U and ^{129}I for the Mediterranean Sea (Castrillejo et al., 2017), showing that these radionuclides have been transported by the thermohaline circulation in both the WMS and EMS. Further, we used data from the literature and relatively simple model simulations to constrain the inputs of ^{129}I and ^{236}U from various sources. Our results indicate that Marcoule introduced the largest amount of ^{129}I in the Mediterranean Sea, and at least as much ^{236}U as global fallout.

The aim of this study is to evaluate the sources of the long-lived radionuclides (^{237}Np, ^{239}Pu and ^{240}Pu) from their distribution in the western and eastern Mediterranean basins as well as to discuss their basin-scale distributions, also for ^{137}Cs, in relation to particle dynamics and the thermohaline circulation. The data presented here, together with that of ^{236}U and ^{129}I (Castrillejo et al., 2017) constitutes the baseline to assess future changes on the distributions of long-lived radionuclides and give a first dataset for their future use as oceanographic tracers in the Mediterranean Sea.

4.3. Materials and methods

4.3.1. Sampling strategy

The study area was described in *Chapter 3*. The sampling was designed to encompass the sub-basins so that ^{137}Cs, ^{237}Np, ^{239}Pu and ^{240}Pu could be determined in the principal water masses and biogeochemical regimes. A total of 10 stations (Figure 4.1) were visited in the WMS (n=8) and EMS (n=2) onboard R/V Ángeles Alvariño during the *GA04S–MedSeA* cruise in May 2013. Seawater sampling was conducted at 1–2 m depth using the ship intake and throughout the water column using a stainless–steel rosette equipped with CTD sensors (conductivity, temperature and depth) and 12 L Niskin bottles. Samples (n=84) of ~25 L each were collected in plastic containers rinsed with seawater three times prior to

sample loading. In the laboratory, samples were weighed, acidified with suprapure nitric acid to pH <2 and stored until analyses that were conducted about 6 months later.

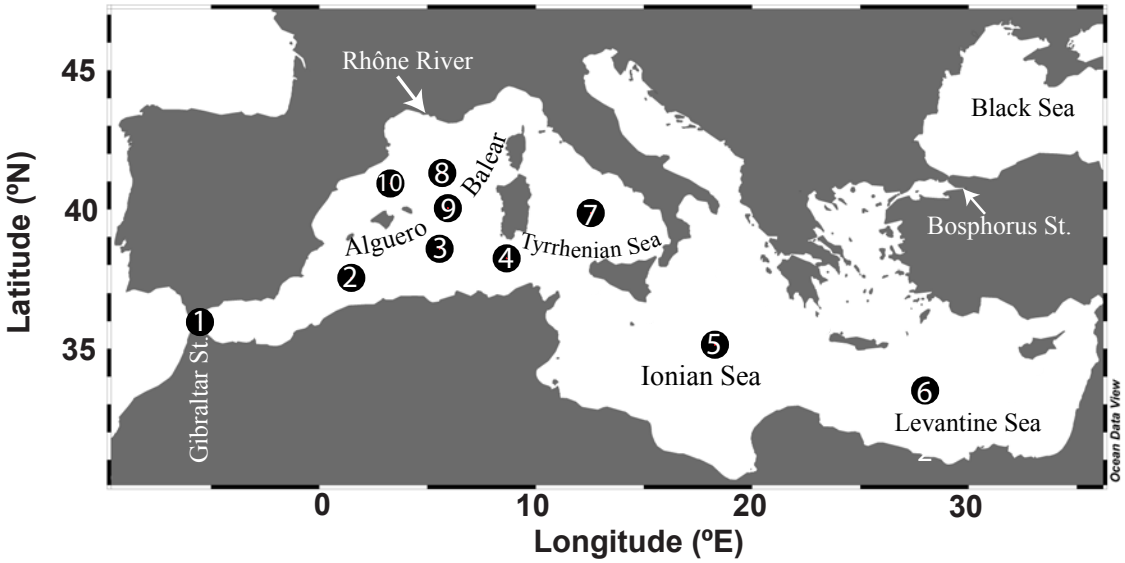

Figure 4.1. Study area of he *GA04S-MedSeA* cruise in May 2013. Sampling stations (1-10) for ^{137}Cs, ^{237}Np, ^{239}Pu and ^{240}Pu are shown: 1. Gibraltar Strait (GSt); 2. Algeria (ALG); 3. Southern Alguero-Balear (SAB); 4. Sardinia Channel (SCh); 5. Ionian Sea (IS); 6. Levantine Basin (LB); 7. Tyrrhenian Sea (TS); 8. Northern Alguero-Balear (NAB); 9. Central Alguero-Balear (CAB) and 10. Catalano-Balear (CB).

4.3.2. Sequential extraction of radionuclides

Pu isotopes and ^{237}Np, and later ^{137}Cs, were extracted sequentially from each seawater sample at the Laboratory of Environmental Radioactivity based of Universitat Autònoma de Barcelona (LRA-UAB). Briefly, standard solutions of ^{242}Pu (traceable to Lawrence Livermore National Laboratories), ^{236}Np (traceable to Los Alamos National Laboratories), and ^{134}Cs (0.25 Bq, ref. date: 15/04/2014, ^{134}Cs solution P/N 7134 from Eckert & Ziegler Isotope Products) were added to seawater samples in order to monitor Pu, Np, and Cs yields, respectively. Samples were vigorously stirred and left for >12 h to achieve homogenization between the spikes and seawater. After addition of 150 mg of Fe^{3+} (as $FeCl_3$ solution) and waiting for >1 h, Fe oxyhydroxides were precipitated by increasing the pH to 8-9 with concentrated suprapure ammonia (NH_4OH). After settling, Fe precipitates were transferred to 250 mL bottles and shipped to Lamont-Doherty Earth Observatory (LDEO, USA) for analysis of Pu and Np isotopes. The remaining supernatant was acidified

to pH<2 using reagent grade nitric acid and stored for the later extraction of Cs isotopes at LRA-UAB.

4.3.3. Purification and measurement of Np and Pu isotopes

Fe precipitates were subject to acid digestion followed by a second co-precipitation, and finally to ion exchange chromatography prior to mass spectrometry. For the following procedures, all reagents were optima grade or home-distilled and deionized 18 MΩ water was obtained from a Millipore Milli-Q system. All material was acid–cleaned and rinsed with Milli-Q water.

a) Acid digestion

The digestion procedure, adapted from Anderson et al., (2012) and Fleisher and Anderson, (1991), is designed to remove organic matter and amorphous silicon. Unless specifically noted, concentrated Optima grade acids were used. The initial coprecipitates were dissolved in concentrated nitric (HNO_3) and transferred to 60 mL PFA beakers with Milli-Q and heated at ~100°C on a hotplate until nearly dry. Additional HNO_3 and perchloric ($HClO_4$) acids were then added in proportions of 1:4, the total volume dependent on the size of the sample residue. The temperature was raised to ~210 °C, and the samples were heated until dense white $HClO_4$ fumes were visible. The beakers were then briefly removed from the hotplate and 3-5 mL of concentrated hydrofluoric (HF) acid was added to the samples, which were then heated until $HClO_4$ fumes were again visible. The HF addition step was then repeated at least 2 additional times. Once the samples returned to fuming $HClO_4$ after the final HF addition, the beaker walls were washed down with HNO_3 and the samples were heated to a viscous $HClO_4$ residue. Residues were then dissolved in hydrochloric (HCl) and Milli-Q H_2O and allowed to cool, after which, the samples were precipitated a second time by raising the pH to 8-9 with NH_4OH. The final precipitates were dissolved in HNO_3 and then taken to dryness.

b) Ion exchange column chemistry

Purification of Pu and Np was carried out using ion exchange chromatography modified after Kenna, (2002) and Maxwell et al., (2010). The first of two column separations consisted of a 20 mL reservoir and 1 mL cartridge of TEVA resin (Eichrom P/N) connected to a vacuum extraction system and conditioned by passing 25 mL of 3M HNO_3. Prior to ion exchange separation, load solutions were prepared by dissolving the residues in 10 mL 3M HNO_3 and 6 mL 2M aluminum nitrate ($Al(NO_3)_3$) directly in the Teflon jar; an additional 1.6 mL of concentrated HNO_3 was added to increase the overall HNO_3 concentration of ~2.7 M. Valence adjustment was then performed by adding 0.55 mL of 1.5 M sulfamic acid (H_3NO_3S), 0.45 mL of 0.09 M iron nitrate ($FeNO_3$) and 1.3 mL of 1.5 M ascorbic acid with at least a 3 minute wait step to reduce plutonium to Pu(III). The iron added, which is converted to Fe(II) by ascorbic acid ($C_6H_8O_6$), was added to facilitate rapid Np reduction to Np(IV). Pu was then oxidized to Pu(IV) by adding 0.9 mL of 4.2 M sodium nitrite ($NaNO_2$) to each sample solution. The load solution was then added to the pre-conditioned columns and the drip rate was adjusted to ≤1 drop per second. Once the load solution had passed, a 10 mL, 3M HNO_3 beaker rinse was added to the column. The reservoirs were then changed and 25 mL of 3M HNO_3 was added to the column to facilitate U removal, followed by 15 mL of 9M HCl to facilitate Th removal and a final 5 mL of 3M HNO_3 to remove trace HCL. Prior to eluting Pu and Np with 25 mL of 0.02 M HNO_3:0.13 M HF, a 0.5 mL cartridge of Pre-filter resin (Eichrom P/N) was added below the TEVA column to prevent any extractant bleed-through.

The second column separation consisted of a 40 mL reservoir and 1mL cartridge of TEVA resin (Eichrom P/N) connected to a vacuum extraction system and conditioned by passing 25 mL of 3M HNO_3. Prior separation, the 25 mL eluant solutions were prepared by adding 2 ml of 2M $Al(NO_3)_3$ and 7 mL of concentrated HNO_3 to increase the overall HNO_3 concentration of ~2.7 M. Valence adjustment was then performed by adding 0.8 mL of 1.5M sulfamic acid (H_3NO_3S), 0.65 mL of 0.09M iron nitrate ($FeNO_3$) and 2.1 mL of 1.5 M ascorbic acid with at least a 3 minute wait step to reduce plutonium to Pu(III). Pu was then oxidized to Pu(IV) by adding 1.7 mL of 4.2 M $NaNO_2$ to each sample solution. The load solution was then added to the pre-conditioned columns and the drip rate was

adjusted to ≤ 1 drop per second. The subsequent steps are the same as those of the first column.

After elution of Pu and Np from the second column, 0.5 mL of HNO_3 and 3 drops of $HClO_4$ was added to each of the samples, which were then dried overnight at ~100°C to a small drop of $HClO_4$ and taken up in 0.6 mL of 1% HNO_3/0.1% HF.

c) Mass spectrometry

Plutonium and Np isotope analyses were made on an Element XR+ (Thermo Scientific) sector field inductively coupled mass spectrometer (SF-ICP-MS) equipped with a single electron multiplier as well as a JET interface pump and cones. All measurements were made in ion counting mode with peak-top jumping. The mass spectrometric and data reduction procedures followed those detailed in (Kenna, 2002). Samples were introduced via an ESI Continuum and FAST auto-sampler coupled to a CETAC Aridus desolvating nebulizer system. Uncertainties of ^{237}Np, ^{239}Pu and ^{240}Pu are reported as two sigma deviations.

4.3.4. Extraction and measurement of Cs

Isotopes of caesium (^{134}Cs and ^{137}Cs) were extracted from the stored Np and Pu-free supernatant by passing the samples through columns filled with 5 mL of KNiFC-PAN ion-exchange resin obtained from the Czech Technical University, Prague (Šebesta, 1997). The resin was dried and transferred to 5 mL polyethylene vials for gamma counting of ^{134}Cs and ^{137}Cs using high-purity germanium well detectors (Canberra). The chemical recovery of ^{134}Cs averaged 80% and was quantified using the emission at 604 keV and 795 keV. The germanium detectors were calibrated in efficiency using KNiFC-PAN resin that had been spiked with known amounts of ^{134}Cs and ^{137}Cs. The minimum detectable activity was 0.15-0.40 $Bq \cdot m^{-3}$ for typical samples volumes of 25 L and counting times of 60 h. Concentration uncertainties were calculated by propagation of uncertainties of the count rates and the efficiency calibration. Concentrations and water column inventories of ^{137}Cs are always reported decay corrected to May 2013.

4.4. Results

Data on the concentrations of ^{137}Cs, ^{237}Np, ^{239}Pu and ^{240}Pu is presented in Appendix A.7. The lowest and highest ^{137}Cs concentrations (Figure 4.2) were found in the Levantine Basin: 0.70 ± 0.15 Bq·m^{-3} at 1000 m and 2.00 ± 0.10 Bq·m^{-3} at 250 m, and were within the range of the concentrations reported for the studied region between 1986 and 2013 (0.8 - 2.9 Bq·m^{-3}, see Appendix A.8). Cs-137 concentrations presented maxima at 100-500 m depths especially at stations 2, 4, 5, 6 and 9, and minima especially at ~1000 m at stations 2, 4, 5, and 6. Below 1000 m depth and down to the bottom the ^{137}Cs concentrations decreased at stations 2, 3, 4 and 5, while they increased at all other stations.

The concentration of ^{237}Np (Figure 4.2) ranged from 0.100 ± 0.002 mBq·m^{-3} at 1000 m in the Levantine Basin to 0.210 ± 0.005 mBq·m^{-3} in surface waters of the Central and Northern Alguero-Balear (stations 8 and 9, respectively). In both the WMS and EMS the highest ^{237}Np concentrations were found in the upper 600 m. In surface waters, the lowest concentrations of ^{237}Np were measured at the Strait of Gibraltar (St. 1), while the largest were found in the Northern Alguero-Balear (St. 8). All stations displayed ^{237}Np concentration maxima at intermediate depths, between ~100 and ~600 m, except in the northern Alguero-Balear (St. 8) and the Catalano-Balear (St.10). Below 600 m and down to ~2000 m, ^{237}Np reached minima concentrations at about 1000 m depth in most stations, especially in the EMS. In very deep waters below 2000 m depth, ^{237}Np concentrations increased in most stations, although they decreased at Algeria (St. 2) and the Catalano-Balear (St. 10). The measured ^{237}Np concentrations in the N. Alguero-Balear (St. 8) had the same range (0.140-0.200 mBq·m^{-3}) and a similar depth distribution than those reported at the DYFAMED station, 300 km to the northeast, in 2013 by Bressac et al., (2017).

The concentrations of Pu isotopes ranged from 1.40 ± 0.02 to 13.0 ± 0.2 mBq·m^{-3} for ^{239}Pu, from 1.40 ± 0.03 to 9.2 ± 0.1 mBq·m^{-3} for ^{240}Pu, and from 3.0 ± 0.1 to 22.0 ± 0.4 mBq·m^{-3} for combined ^{239,240}Pu (Appendix A7). The ^{239,240}Pu concentrations (3-22 mBq·m^{-3}) are in the lower end of those reported in other studies during the period from 1975 until 2013 (3-85 mBq·m^{-3}; see Appendix A.9). The ^{239,240}Pu concentrations were usually <10 mBq·m^{-3} in the upper 200 m of the water column across the Mediterranean Sea and the lowest value was measured at the Strait of Gibraltar (Figure 4.3). In the WMS, the ^{239,240}Pu

concentrations increased gradually with depth, reaching maxima levels of ≥18 mBq·m^{-3} at 500-1500 m depth. From this depth and down to the bottom, ^{239,240}Pu concentrations were of similar magnitude or decreased. In the EMS, ^{239,240}Pu concentrations increased below 200 m, with highest values averaging 14 mBq·m^{-3}, below 1000 m (lower than in the WMS ~20 mBq·m^{-3}). The ^{240}Pu/^{239}Pu atom ratios ranged from 0.180 ± 0.003 to 0.263 ±0.007 at·at^{-1}, and the median was 0.187 (see Appendix A.7). Two outliers were identified based on the ^{240}Pu/^{239}Pu atom ratios that were larger than 0.30 (Appendix A.7).

Water column inventories of radionuclides and the ratios of inventories are presented in Appendix A.10. The lowest water column inventories for all radionuclides were observed at the Strait of Gibraltar (bottom depth ~640 m) while the largest corresponded to the deepest station (3726 m) in the Ionian Sea. The ^{137}Cs inventories ranged from 0.9 ± 0.1 to 5.5 ± 0.3 kBq·m^{-2} and were within the range of post-Chernobyl inventories reported for similar water depths (800-4000 m) and regions (1-6.5 kBq·m^{-2} decay corrected to 2013; see Appendix A.8). The ^{237}Np inventories ranged from 0.100 ± 0.001 to 0.590 ± 0.005 Bq·m^{-2}. In the N. Alguero-Balear (St. 8) the inventory of ^{237}Np was 0.380 ± 0.003 Bq·m^{-2} for a water column depth of 2561 m, which is similar to that estimated at DYFAMED in 2013 (0.344 ± 0.005 Bq·m^{-2}, 2350 m), calculated using concentrations (n=5) reported in Bressac et al., (2017). The inventories of ^{239}Pu ranged from 5.90 ± 0.03 to 35.2 ± 0.1 Bq·m^{-2}, while for ^{240}Pu were between 4.10 ± 0.03 and 24.1 ± 0.1 Bq·m^{-2}. The combined ^{239,240}Pu inventories ranged from 10.1 ± 0.1 to 59.3 ± 0.2 Bq·m^{-2} and were within the range reported from 1975 until 2013 (15-81 Bq·m^{-2}; see Appendix A.9). The ^{239,240}Pu inventory calculated for the N. Alguero-Balear (43 ± 1 Bq·m^{-2}) was comparable to the that estimated for the full water column at DYFAMED site in 2013 (44 ± 1 Bq·m^{-2}, 2350 m) using data from Bressac et al., (2017).

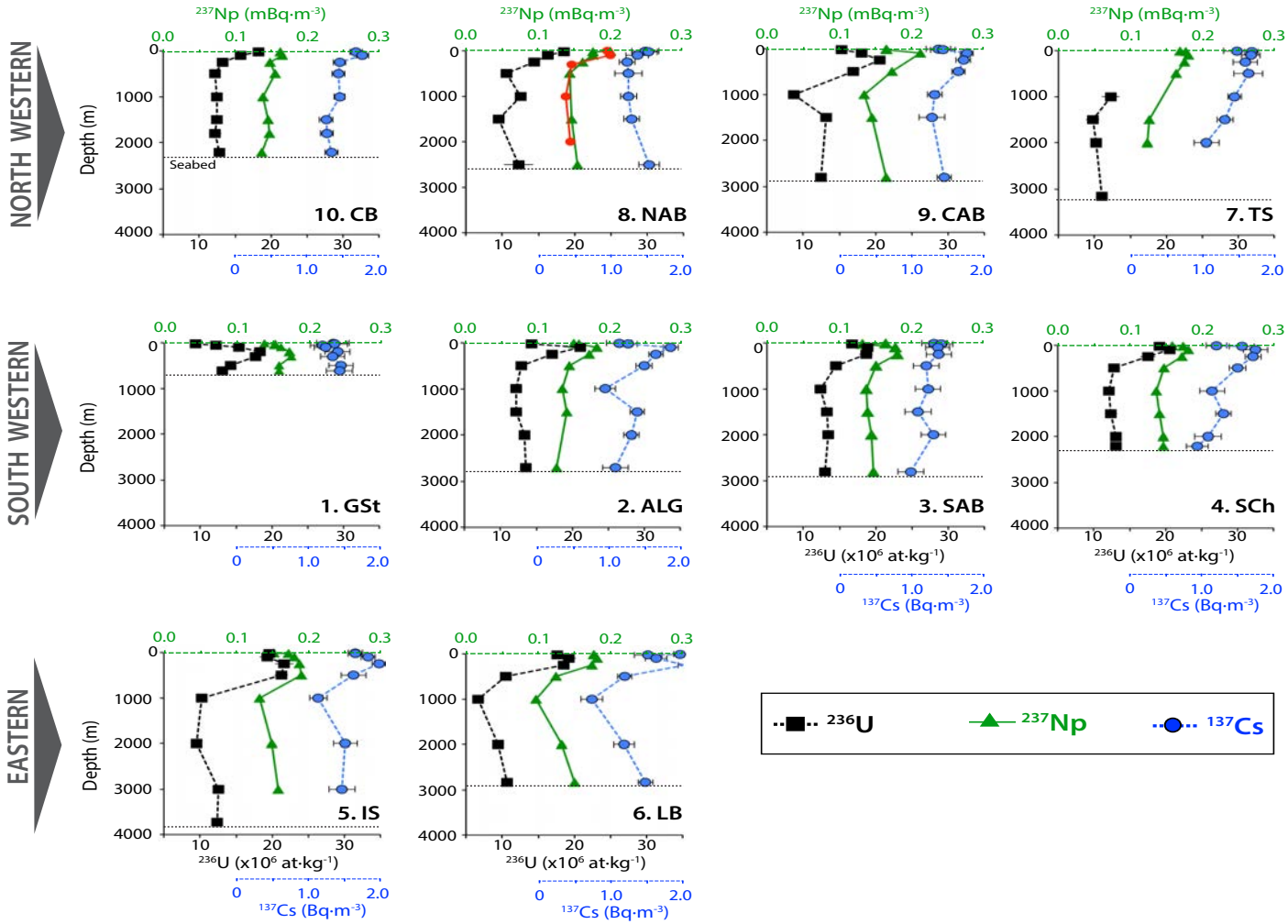

Figure 4.2. Concentration profiles of ^{137}Cs and ^{237}Np in the Mediterranean Sea in May 2013. The concentrations of ^{236}U are taken from Castrillejo et al., (2017). The ^{237}Np concentrations in 2013 reported by Bressac et al., (2017) at DYFAMED site are shown with red circles. Station positions are shown in Figure 4.1. Uncertainties of ^{137}Cs have been propagated from the counting rate and the detector calibration.

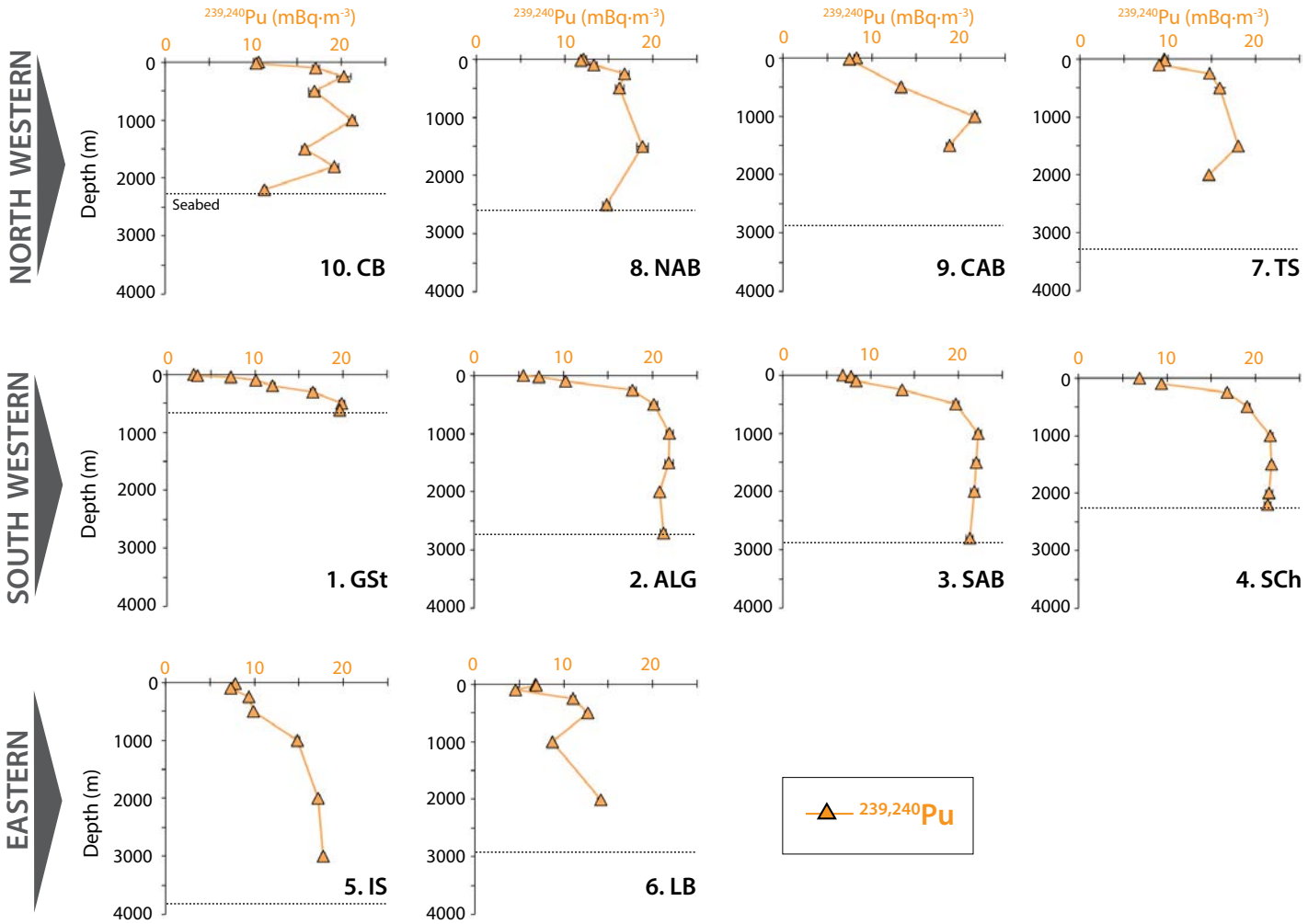

Figure 4.3. Vertical distribution of ^{239,240}Pu concentrations in the Mediterranean Sea in May 2013. Station positions are shown in Fig. 4.1. Uncertainties are given as two sigma deviations.

4.5. Discussion

4.5.1. Inputs of artificial radionuclides

a) Cs-137

Sources of ^{137}Cs have already been identified and quantified in the Mediterranean Sea. Considering the different sources of ^{137}Cs described in the introduction (section 4.1), and the water exchange with the Black Sea and Atlantic Ocean, the mean inventory of ^{137}Cs can be estimated in ~2.0 kBq·m^{-2} in 2013. Global fallout and Chernobyl accident would account for most of that inventory with ~1.4 kBq·m^{-2} (UNSCEAR, 2000) and ~0.5 kBq·m^{-2}, respectively, decay corrected to 2013 (Papucci et al., 1996). This cumulative inventory is often lower than ^{137}Cs inventories obtained in this study (0.9-5.5 kBq·m^{-2}).

b) Np-237

Water column inventories of ^{237}Np computed in 2013 ranged from 0.10 to 0.59 Bq·m^{-2} for our study area covering the entire Mediterranean Sea, except the Adriatic and Aegean Seas, and ~0.34 Bq·m^{-2} for the same year at the DYFAMED site in the northern WMS (Bressac et al., 2017).

Total global fallout release of ^{237}Np was estimated in 1500-3000 kg depending on the chosen ^{237}Np/^{239}Pu atom ratio in soil profiles and the estimates of ^{239}Pu fallout (Beasley et al., 1998; Efurd et al., 1984). ^{237}Np/^{239}Pu atomic ratios of 0.47 and 0.35 have been reported for soils sampled in the Northern and Southern Hemispheres, respectively, based on a more complete dataset (Kelley et al., 1999). Given the location of the atmospheric nuclear weapon tests and the atmospheric circulation, about 76% and 24% of the total global fallout deposited in the Northern and Southern hemispheres, respectively, and the largest deposition occurred in the latitudinal band of the Mediterranean Sea (~31% in 30-50ºN; UNSCEAR, 2000). The total global fallout of ^{239,240}Pu was ~10.9 PBq, with a ^{240}Pu/^{239}Pu atom ratio of ~0.18 (Kelley et al. 1999). Taking the above figures, the total global fallout

of ^{237}Np would be of ~1250 kg. As the Mediterranean Sea covers ~3.7% of the area in the 30-50ºN latitudinal band, a ^{237}Np input of ~14 kg (0.36 TBq, ~0.14 Bq·m^{-2}) can be estimated.

The ^{237}Np released from Chernobyl accident can be estimated in ~0.17 kg (~0.04 TBq) taking the ^{237}Np/^{239}Np atomic ratio of 1.5 in the nuclear reactor core 4 prior to the accident and the total ^{239}Np release of about 110 kg or 950 PBq to the environment (UNSCEAR, 2000). Np-237 was probably transported attached to particles and deposited mainly in the vicinity of Chernobyl, like happened to other actinides such as ^{236}U (e.g. Boulyga et al., 2002). It was estimated that only ~0.03% of the ^{239,240}Pu released to the atmosphere was transported and deposited in the Mediterranean Sea (Papucci et al., 1996). Taking the above number, the Chernobyl accident fallout deposition of ^{237}Np in the Mediterranean Sea would have been of ~5 ×10^{-5} kg (~1.5 MBq), which is 5 orders of magnitude smaller than the input from global fallout (14 kg), being thus of negligible influence.

There is no information on ^{237}Np discharges from Marcoule reprocessing plant, but there are reasons to consider this facility as a potential source of ^{237}Np to the Mediterranean Sea. Firstly, ^{237}Np is present in large amounts in spent fuel (Aarkrog, 1986) and has been reported in low level radioactive effluents discharged from other reprocessing plants (Beasley et al., 1998; Kuwabara et al., 1996). Secondly, concentrations (in at·kg^{-1}) of ^{237}Np, ^{236}U, ^{129}I and ^{137}Cs were correlated in samples collected in May 2013: ^{237}Np=(0.46 ± 0.04) * ^{236}U + (7.8 ± 0.5) × 10^{6} (R^2=0.71; n=70); ^{237}Np = (0.080 ± 0.008) * ^{129}I + (7.7 ± 0.6) × 10^{6} (R^2=0.58; n=70); and ^{237}Np=(4.4 ± 0.4) * ^{137}Cs + (6.5 ± 0.8) × 10^{6} (R^2=0.58; n=80). This suggests that ^{237}Np probably shared common origins and behavior, especially with ^{236}U. We estimated that Marcoule introduced 10-20 kg of ^{236}U, an amount that was equal or larger than the global fallout (~11 kg) (Castrillejo et al., 2017). For ^{129}I, the input from Marcoule (70-90 kg) was several times larger than the global fallout (~1 kg) (Castrillejo et al., 2017), while for ^{137}Cs the Marcoule input was ~2 orders of magnitude lower than the combined input of global fallout and Chernobyl accident.

Since concentrations of ^{237}Np and ^{137}Cs were measured in same samples in 2013, one approach for quantifying the potential ^{237}Np inputs from Marcoule is to compute the mean water column radionuclide inventories and their ratios in May 2013 (see Appendix A.10). The reasoning is that any deviation from the ^{237}Np/^{137}Cs atom ratio expected from

Chernobyl accident fallout and global fallout (~5.6) would be due to ^{237}Np inputs from Marcoule. In May 2013, the mean ^{237}Np/^{137}Cs atom ratio based on mean water column inventories was ~8.3 (see Appendix A.10). It is worth noting that this approach is valid only when: i) considering the radioactive decay of ^{137}Cs, ii) that the ^{137}Cs introduced from Marcoule was negligible compared to global fallout and Chernobyl accident (1.5×10^{-5}, Charmasson et al. 2003), and iii) assuming as a first approximation, the homogeneous distribution of different sources as a result of rapid turnover times of water in both the WMS and EMS (see *Chapter 3*). Based on this ratio and on the input of ~14 kg of ^{237}Np estimated above for global fallout in the Mediterranean Sea, the ^{237}Np input from Marcoule would be of ~7 kg. This means that Marcoule would have introduced ~30% of ^{237}Np present in the Mediterranean Sea in 2013. The ^{237}Np input would be lower than that of ^{236}U (10-20 kg) and ^{129}I (70-90 kg) confirming that Marcoule might have been a prominent source of long-lived radionuclides to this study area.

The contribution from global fallout, Chernobyl accident and Marcoule to the presence of ^{237}Np in the Mediterranean Sea in May 2013 can be distinguished by plotting concentrations of ^{237}Np against ^{236}U, ^{129}I and ^{137}Cs (Figure 4.4), together with respective end-member ratios for each source (Table 4.1). These end-member ratios have been estimated from the radionuclide inputs mentioned above or in *Chapter 3*. Some other end-members are computed taking the available data in literature (see table 4.1 for details). The ^{237}Np/^{137}Cs atom ratios in samples collected in May 2013 (Figure 4.4 A) fell between the Marcoule and the expected atom ratio if there were no inputs from Marcoule. In this case, the expected atom ratio is lower (~5.6) that for global fallout (~7.8) because the Chernobyl accident fallout added significant ^{137}Cs (2.5 PBq in 1986; Papucci et al., 1996) and negligible ^{237}Np (Table 4.1). This confirms, as calculated above, that fraction of the ^{237}Np in waters of the Mediterranean Sea could originate from Marcoule. Inputs of ^{236}U from Chernobyl accident fallout were also negligible (Table 4.1), thus the ^{237}Np/^{236}U atom ratios (Figure 4.4 B) also fell between the end–members of global fallout and Marcoule. It is worth noticing that both old Eastern and Western Mediterranean waters (EMDWo and WMDWo) and Atlantic Waters (AW) presented lower concentrations of ^{237}Np and ^{236}U, and that the ^{237}Np/^{236}U atom ratios were closer to the global fallout, consistent with the expected lower influence from Marcoule. On the contrary, MAW and younger

Mediterranean waters such as LIW were characterized by $^{237}Np/^{236}U$ ratios closer to the Marcoule end-member. Measured $^{237}Np/^{129}I$ concentration ratios (Figure 4.4 C) showed similar results supporting the hypothesis that Marcoule was a prominent source of long-lived radionuclides to the Mediterranean Sea.

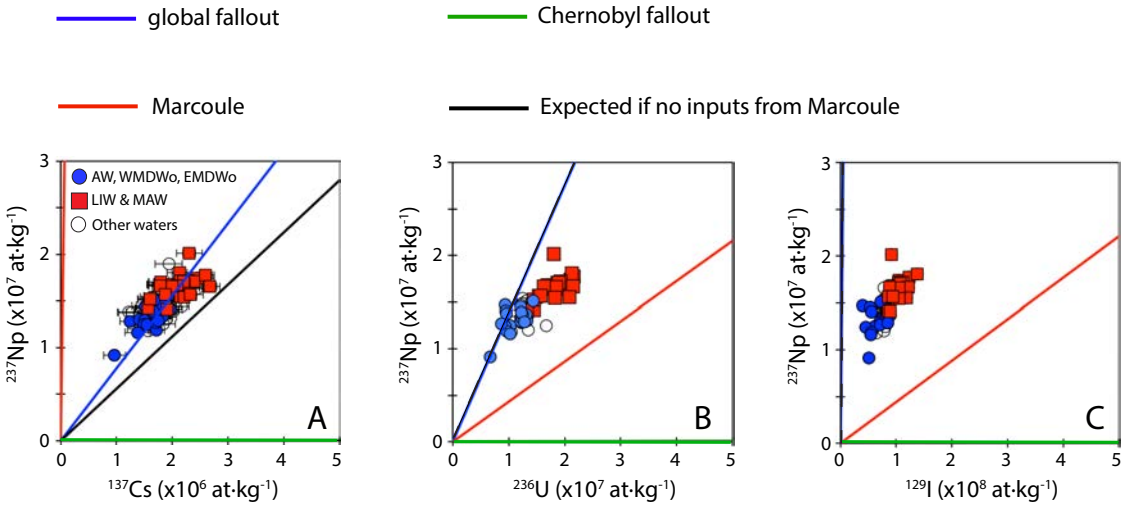

Figure 4.4. Concentrations of ^{237}Np against concentrations of ^{137}Cs (A), ^{236}U (B) and ^{129}I (C). End–member values for each radioactive source are presented in Table 4.1. The black line overlapped with that from global fallout in Figures 4.4 B and 4.4 C due to the negligible input of ^{129}I and ^{236}U from Chernobyl accident fallout (Table 4.1). Seawater acronyms are: Atlantic Water (AW), Western Mediterranean Deep Water old (WMDWo), Eastern Mediterranean Deep Water old (EMDWo), Levantine Intermediate Water (LIW) and Modified Atlantic Water (MAW).

c) Plutonium-239 and ^{240}Pu

The inventories of $^{239,240}Pu$ in the water column ranged from ~10.1 to ~59 $Bq \cdot m^{-2}$ in May 2013. These inventories are lower than expected from global fallout (~80 $Bq \cdot m^{-2}$, e.g. León Vintró et al., 1999), consistently with scavenging processes removing Pu from the water column to sediments (e.g. Fowler et al., 2000) and a net annual loss of 0.34 TBq of $^{239,240}Pu$ to the Atlantic Ocean occurring at the Strait of Gibraltar (Gascó et al., 2002a; UNEP, 1992). The influence of ocean circulation and scavenging of Pu implies that other potential sources of this element to the Mediterranean might not be recognizable only by

investigating the ^{239,240}Pu activity concentrations. One alternative is using the ^{240}Pu/^{239}Pu atom ratios, which are source dependent. The ^{240}Pu/^{239}Pu atom ratio of global fallout in the Northern Hemisphere is ~0.18 (Kelley et al., 1999), while that from Chernobyl accident is ~0.40 (Muramatsu et al., 2000). The ^{240}Pu/^{239}Pu atom ratio in effluents from Marcoule has not been well constrained. Yet, sediment cores collected in the Rhône River Delta recorded ^{240}Pu/^{239}Pu atom ratio as low as 0.133 ± 0.004 indicating that liquid effluents from Marcoule probably had ^{240}Pu/^{239}Pu atom ratios <0.14 (Miralles et al., 2004). The ^{240}Pu/^{239}Pu atom ratio in seawater samples collected in May 2013 showed a median value of ~0.19 indicating that global fallout was the predominant source of Pu in the whole Mediterranean Sea. Some samples (6 out of 60) showed ^{240}Pu/^{239}Pu atom ratio larger than 0.21 (0.22-0.26), but their distribution showed no specific pattern in the WMS and EMS. The influence from Marcoule, presumably having ^{240}Pu/^{239}Pu atom ratios lower than 0.18 was not observed in our northernmost stations in the NWS (stations 8 to 10, Figure 4.1). This was expected when considering that global fallout introduced ~500 times more ^{239,240}Pu than Marcoule and that >30% of the ^{239,240}Pu from Marcoule was retained in the Rhône Delta (Delfanti and Papucci, 2010; Eyrolle et al., 2004). In any case, the ^{240}Pu/^{239}Pu atom ratios measured in this study, except in 3 samples, were within the range reported for seawater, particles retained in sediment traps and precipitation in the Mediterranean Sea (0.18-0.23; Bressac et al., 2017; Pham et al., 2017).

d) Revised Marcoule inputs of ^{129}I and ^{236}U

Marcoule was also a significant source of ^{236}U and ^{129}I with inputs of 10-20 kg and 70-90 kg, respectively, according to simple ocean circulation model calculations *(Chapter 3)*. These inputs from Marcoule, together with those from global fallout and Chernobyl accident, after significant radionuclide loss as part of Mediterranean Overflow Waters, resulted in inventories of 13-22 kg for ^{236}U and 44-65 kg for ^{129}I in the whole Mediterranean Sea in 2013 (*Chapter 3*). The ^{236}U and ^{129}I inputs from Marcoule can alternatively be constrained by comparing the ^{236}U/^{137}Cs and ^{129}I/^{137}Cs atom ratios based on mean water column inventories obtained in May 2013 (7.8 ± 0.9 and 48 ± 4, respectively) with those expected from global fallout and Chernobyl accident fallout (4.1

and 0.8, respectively, Table 4.1). Considering that Chernobyl accident fallout was negligible for both ^{236}U and ^{129}I, and taking their global fallout inputs (11 kg for ^{236}U and ~ 1 kg for ^{129}I (Table 4.1 and *Chapter 3*), the amount of ^{236}U and ^{129}I for the whole Mediterranean Sea in 2013 can be re-calculated in ~21 kg and ~57 kg, respectively. The good agreement between inventories of ^{236}U (21 vs. 13-22 kg) and ^{129}I (57 vs. 44-65 kg) estimated by two independent approaches further supports the importance of Marcoule as a source of long-lived radionuclides.

Table 4.1. Inputs of ^{129}I, ^{137}Cs, ^{236}U and ^{237}Np into the Mediterranean Sea by 2013 as reported in the literature or estimated in this work. The atom ratios of ^{237}Np/^{137}Cs, ^{237}Np/^{236}U, ^{237}Np/^{129}I, ^{236}U/^{137}Cs and ^{129}I/^{137}Cs are reported for end – members in 2013. End – members are: global fallout (GF), Chernobyl accident fallout deposition in the Mediterranean Sea (CAF), discharge from Marcoule Reprocessing Plant (MRP) and the expected atom ratio in seawater due to the combined input from GF and CAF. All ^{137}Cs inputs were decay corrected to 2013 before computing the radionuclide atom ratios.

	^{129}I		^{137}Cs		^{236}U		^{237}Np		^{239,240}Pu	^{237}Np/^{137}Cs	^{237}Np/^{236}U	^{237}Np/^{129}I	^{236}U /^{137}Cs	^{129}I/^{137}Cs	^{240}Pu/^{239}Pu
	atoms	Bq	atoms	Bq	atoms	Bq	atoms	Bq	Bq	at·at^{-1}	at·at^{-1}	at·at^{-1}	at·at^{-1}	at·at^{-1}	at·at^{-1}
GF[a]	4.8×10^{24}	6×10^{9}	4.8×10^{24}	3.5×10^{15}	26×10^{24}	24×10^{9}	36×10^{24}	36×10^{10}	[d]2.0×10^{14}	7.8	1.4	7.5	5.7	1.0	[e]~0.18
CAF[b]	0.64×10^{24}	0.81×10^{9}	1.8×10^{24}	1.3×10^{15}	0.1×10^{24}	0.09×10^{9}	1.5×10^{20}	1.5×10^{6}	[f]17.5×10^{10}	8.1×10^{-5}	1.4×10^{-3}	2.3×10^{-4}	5.6×10^{-2}	0.35	[g]~0.4
MRP[c]	370×10^{24}	470×10^{9}	0.038×10^{24}	2.8×10^{13}	38×10^{24}	35×10^{9}	17.5×10^{24}	17.5×10^{10}	[h]0.5×10^{12}	447	0.45	4.6×10^{-2}	1×10^{3}	1×10^{4}	[i]<0.14
GF&CAF	5.4×10^{24}	6.9×10^{9}	6.4×10^{24}	4.8×10^{15}	26×10^{24}	24×10^{9}	36×10^{24}	36×10^{10}	2.0×10^{14}	5.6	1.4	6.6	4.1	0.8	~0.18
This study*										8.3 ± 0.5	1.1 ± 0.1	0.17 ± 0.01	7.8 ± 0.9	48 ± 4	0.197 ± 0.016

[a]GF deposition was estimated considering: i) 31 % of GF was deposited in 30 - 50 ºN (UNSCEAR, 2000) from which 3.7 % of the surface area is covered by the Mediterranean Sea, and ii) the following total release estimates: 90 kg of ^{129}I (Hou, 2004; Raisbeck and Yiou, 1999; Wagner et al., 1996), 291 kg of ^{137}Cs (reference year 1963; UNSCEAR, 2000), 900 kg of ^{236}U (Sakaguchi et al., 2009), 1250 kg of ^{237}Np (this study). The input of ^{237}Np was estimated based on: i) ^{237}Np/^{239}Pu atom ratios of 0.47 and 0.35 for the Northern and Southern Hemispheres (N. H and S. H, respectively) reported by (Kelley et al., 1999); ii) the latitudinal deposition of GF in N.H (0.76 %) and S.H (0.24 %) estimated from ^{90}Sr deposition (UNSCEAR, 2000), and iii) the ^{240}Pu/^{239}Pu atom ratio of 0.18 in GF (UNSCEAR 2000).

[b]Chernobyl accident fallout deposition was estimated considering that out of total releases, ~ 2.7 % of volatile radionuclides (e. g. ^{137}Cs from Papucci et al., 1996); used for ^{129}I) and ~ 0.03 % of refractory radionuclides (e. g. ^{239,240}Pu from Papucci et al., 1996); used for ^{236}U and ^{237}Np) were deposited in the Mediterranean Sea. Total releases of ^{129}I were 1.6 – 7.5 kg (this study (7.5), Aldahan et al., 2007; Paul et al., 1987). The total release of ^{129}I estimated in this study was calculated from the total release of ^{131}I the ^{129}I/^{131}I atom ratio in nuclear reactor core 4 prior to the accident (UNSCEAR, 2000). Total release of ^{137}Cs was reported for reference year 1986 by Papucci et al. (1996). Total release of ^{236}U was estimated from the ^{236}U/^{239}Pu atom ratio in nuclear reactor core 4 prior to the accident (UNSCEAR, 2000) and the total release of ^{239}Pu (UNSCEAR 2000). The total release of ^{237}Np was estimated from the ^{237}Np/^{239}Np atom ratio in the nuclear reactor core 4 prior to the accident (UNSCEAR, 2000) and the total release of ^{239}Pu (UNSCEAR 2000).

[c]Marcoule Reprocessing Plant. Total releases have been estimated for Cs (Charmasson, 2003); reported for reference year 2013), and ^{129}I and ^{236}U (mean values were taken from Castrillejo et al., 2017). The input of ^{237}Np was estimated by comparing the mean ^{237}Np/^{137}Cs atom ratio obtained in 2013 with the one expected from the summation of GF and CAF (this table).

[d]Estimated from the ^{239,240}Pu deposition of ~80 Bq·m^{-2} in the Mediterranean Sea (e.g. León-Vintró, 1999) and the Mediterranean Sea surface area of ~2.51× 10^{12} m^2.

[e]Estimated by Kelley et al. (1999).

[f]Estimated fusing the ^{239,240}Pu deposition of ~0.01 Bq·m^{-2} reported by Papucci et al. (1996) and the Mediterranean Sea surface area of ~2.51× 10^{12} m^2.

[g]Estimated by Muramatsu et al. (2000).

[h]Input estimated by Eyrolle et al (2004). According to the authors, about 30% of that amount was retained in the Rhône Delta.

[i]We assumed that ^{240}Pu/^{239}Pu atom ratio from Marcoule should be lower than 0.14 because Miralles et al. (2004) recorded ^{240}Pu/^{239}Pu atom ratios lower than 0.14 coinciding with largest ^{239,240}Pu concentrations in sediments collected in Camargue, Rhône Delta.

*Atom ratios obtained from dividing mean radionuclide inventories for the water column of the whole study area. Data reported in Appendix A.4.5.

4.5.2. Water column distribution of conservative radionuclides

a) Distribution of Cs-137

The aim of this section is to assess the temporal changes on the distribution of ^{137}Cs due to the various inputs and to recent changes in the thermohaline circulation in the Mediterranean Sea. This issue has been addressed elsewhere for certain areas and time periods (e.g. Bressac et al., 2017; Delfanti et al., 2003; Papucci and Delfanti, 1999), but here we can investigate it on the basis of a large dataset of ^{137}Cs concentrations encompassing the whole Mediterranean Sea (Figure 4.5A).

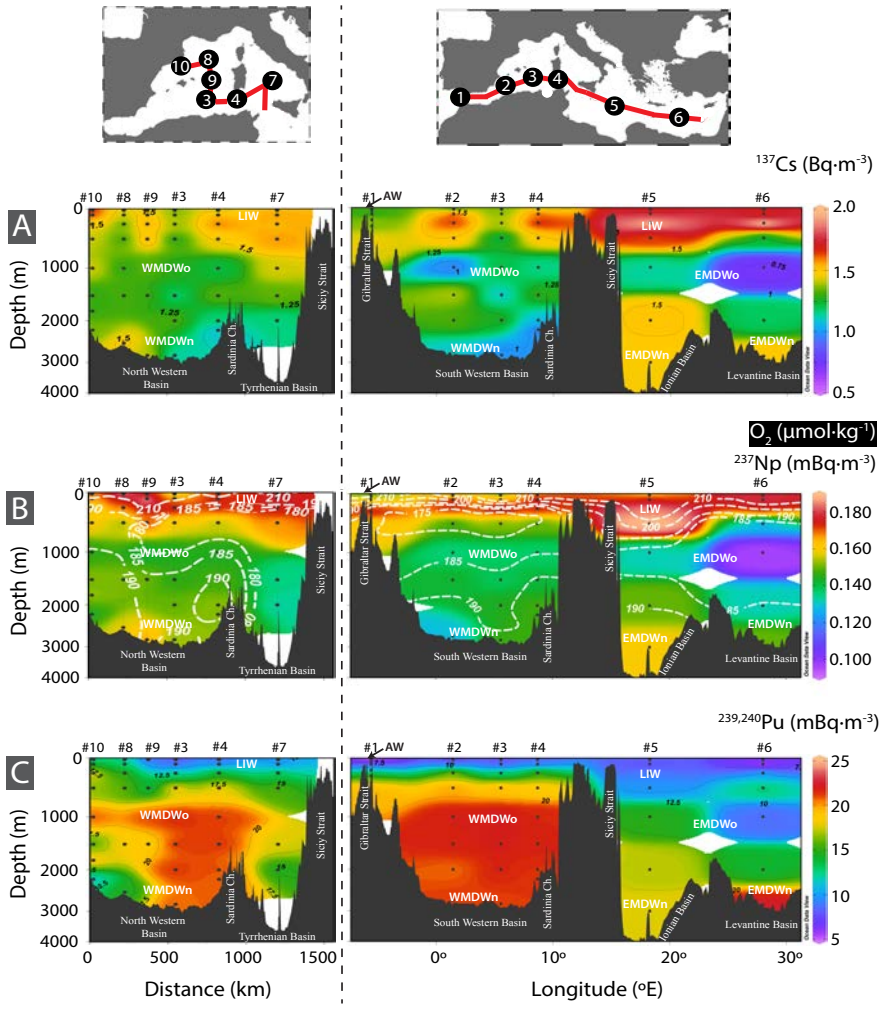

Figure 4.5. Depth distribution of radionuclide concentrations along two sections in the Mediterranean Sea: left) distance section crossing the northern Alguero-Balear region and the Tyrrhenian Sea in the WMS; right)

longitudinal section crossing the southwestern and eastern basins from the Strait of Gibraltar to the Levantine Basin. Represented radionuclides are: ^{137}Cs (A) and ^{237}Np with overlaid dissolved oxygen in white (B), and ^{239,240}Pu (C). Station numbers (#) are indicated on the top of the figures. Main water masses are represented: Atlantic water (AW), Levantine Intermediate Water (LIW), Eastern Mediterranean Deep Water (EMDW) and Western Mediterranean Deep Water (WMDW). Lower case n: new; o: old.

The temporal evolution on ^{137}Cs distributions in the water column can be associated to sources and water circulation by comparing our profiles with those reported and decay corrected to May 2013 in the literature (Figure 4.6). In the EMS, the main changes have been related to the input from the Chernobyl accident and the massive dense-water formation during the EMT in the 1990s (Delfanti et al., 2003). The Chernobyl accident caused a general increase in ^{137}Cs concentrations (Figures 4.6A and 4.6B). From the study of concentrations of ^{90}Sr and ^{137}Cs, Delfanti et al., (2003) estimated that Chernobyl-derived ^{137}Cs penetrated at all depth layers in the EMS, except in the so-called 'tracer minimum zone' layer, at that time centered at 1000-1500 m depth. This layer containing old EMDW remained relatively well isolated although it was uplifted by the intrusion of newly formed more dense EMDW of Aegean origin during the EMT (Klein et al., 1999). In 2013, no major changes in the ^{137}Cs distributions were observed compared to those measured in the 1990s, although the Adriatic Sea was restored as the main dense-water formation area in the EMS (e.g. Hainbucher et al., 2014). Concentrations of ^{137}Cs in surface and LIW continued to decrease in the Ionian and Levantine Seas (Figures 4.6 A and 4.6 B). It was postulated that the lifting of waters caused by the EMT could have forced the mixing between LIW and underlying old EMDW, characterized by low ^{137}Cs concentrations (Delfanti et al., 2003). The layer of minimum ^{137}Cs concentrations centered at ~1000 m in the EMS and continued thinning in 2013. In the Ionian Sea (Figures 4.6 A), a slight increase in ^{137}Cs concentrations of this layer was probably related to the mixing with underlying dense waters formed during and after the EMT, while in the Levantine Basin (Figures 4.6 B) ^{137}Cs concentrations decreased in the same layer, indicating less mixing than in the Ionian Sea with EMT waters.

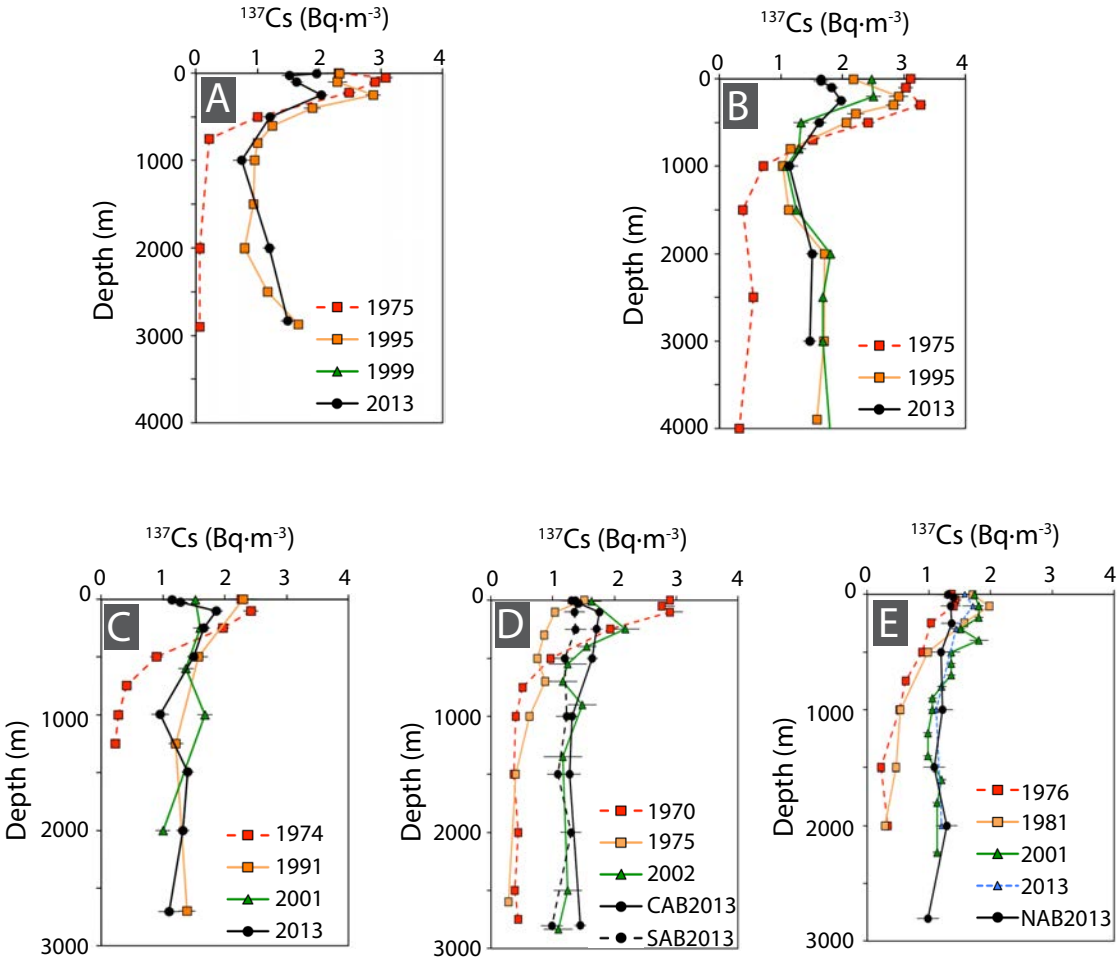

Figure 4.6. Vertical distribution of ^{137}Cs concentrations in the water column of the Mediterranean Sea. Data from the *GA04s-MedSeA* cruise in May 2013 can be compared to the literature. Ionian Sea (A): 1975 (Livingston et al., 1979), 1995 (Delfanti et al., 2003), 1999 (Delfanti et al., 2003) and 2013 (this study). Levantine Basin (B): 1975 (Livingston et al., 1979), 1995 (Delfanti et al., 2003) and 2013 (this study). Algerian Sea (C): 1974 (Kautsky, 1977), 1991 (Delfanti et al., 1994), 2001 (Noureddine et al., 2008) and 2013 (this study). Southern and Central Alguero-Balear (D): 1970 (Kautsky, 1977), 1975 (Livingston et al., 1979), 2002 (Garcia-Orellana, 2004) and 2013 (this study). Northwestern Mediterranean Sea (E): 1976 (Fukai et al., 1979), 1981 (Ballestra et al., 1984), 2001 (Lee et al., 2003), 2013 (blue triangles, Bressac et al., 2017) and 2013 (black dots, this study).

In the WMS, changes in vertical distributions of ^{137}Cs concentrations can be mainly assessed in the northern WMS for the time period spanning from the 1970s to 2013 (e.g. Bressac et al., 2017; Lee et al., 2003). In this area (Figure 4.6 C), main changes have been: i) the increase in ^{137}Cs concentrations in the upper 500 m between 1970-1980s and 2000s due to the inflow of Chernobyl-labeled LIW (e.g. Lee et al., 2003); and the general downward transport of ^{137}Cs carried out by massive dense-water formation during the WMT in the mid 2000s (e.g. Bressac et al., 2017). The vertical distributions of ^{137}Cs

concentrations in the central and southern Alguero-Balear (Figure 4.6 D), as well as in the Algerian Basin (Figure 4.6 E), suggest that mechanisms shaping the water column in the northern WMS were also important in other parts of the WMS, although the vertical homogenization of ^{137}Cs concentrations was less evident with increasing distance from dense water formation regions. For example, the maximum in ^{137}Cs concentrations at intermediate depths associated to LIW and the underlying minimum associated to old WMDW, were still evident in the Algerian Basin, while ^{137}Cs was more homogeneously distributed with depth in the central and northern Alguero-Balear.

b) Distribution of Np-137

In May 2013, ^{137}Cs concentrations were 0.7-2.0 Bq·m^{-3} with uncertainties usually larger than 10% for 20 L samples counted over 60 h (see Appendix A.7). Levels of ^{90}Sr can be even lower (e.g. Delfanti et al., 2003). One reason to shift towards longer-lived radionuclides is that they can be measured in smaller sample volumes (<0.5 L for ^{129}I, 5 L for ^{236}U) with precision better than 95 % (see Appendix A.7). To support this, herein we present the first transect of ^{237}Np for the WMS and EMS (Figure 4.5 B) and discuss its distribution in relation to water masses, dissolved oxygen and other conservative radionuclides to provide the baseline to assess future changes on the distribution of this radionuclide in relation to the thermohaline circulation in the Mediterranean Sea.

There are only few studies reporting data of ^{237}Np in the world oceans (Beasley et al., 1998; Bressac et al., 2017; Holm et al., 1987; Kenna et al., 2012; Lindahl et al., 2005). Most ^{237}Np concentrations have been reported for samples collected from the upper ~300 m, although recent work at the DYFAMED site in the NW Mediterranean Sea reported the first full-depth vertical profile of ^{237}Np down to 2230 m (Bressac et al., 2017). It is accepted that ^{237}Np is soluble in well oxygenated seawater and that it interacts very little with particulate matter present in the water column (Fisher et al., 1983). Indeed, ^{237}Np concentrations measured in 2013 were related to water masses in the Mediterranean Sea identified in *Chapter 3* according to their potential temperature and salinity during the *GA04S-MedSeA* cruise (Figure 4.7). The core of Atlantic Water (AW) in the WMS (Figure 4.7 A) was characterized by ^{237}Np concentrations of ~0.150 mBq·m^{-3} and salinities <37, and could be distinguished from the Levantine Intermediate Water (LIW) in the EMS, with

^{237}Np concentrations ≥0.180 mBq·m^{-3} and salinities >39 (Figure 4.7 B). Old Western Mediterranean Deep Water (WMDWo) and Eastern Mediterranean Deep Water (EMDWo) had, respectively, ^{237}Np concentrations as low as ~0.140 mBq·m^{-3} (Figure 4.7 C and 4.7 D) and <0.130 mBq·m^{-3} (Figure 4.7 right). Saltier and warmer waters (EMDWn and WMDWn) formed during the EMT in the 1990s (Roether et al., 1996) and the WMT in the mid 2000s (Schroeder et al., 2008) had comparably larger ^{237}Np concentrations (~0.150 mBq·m^{-3}) in both basins (Figure 4.7 C and 4.7 D).

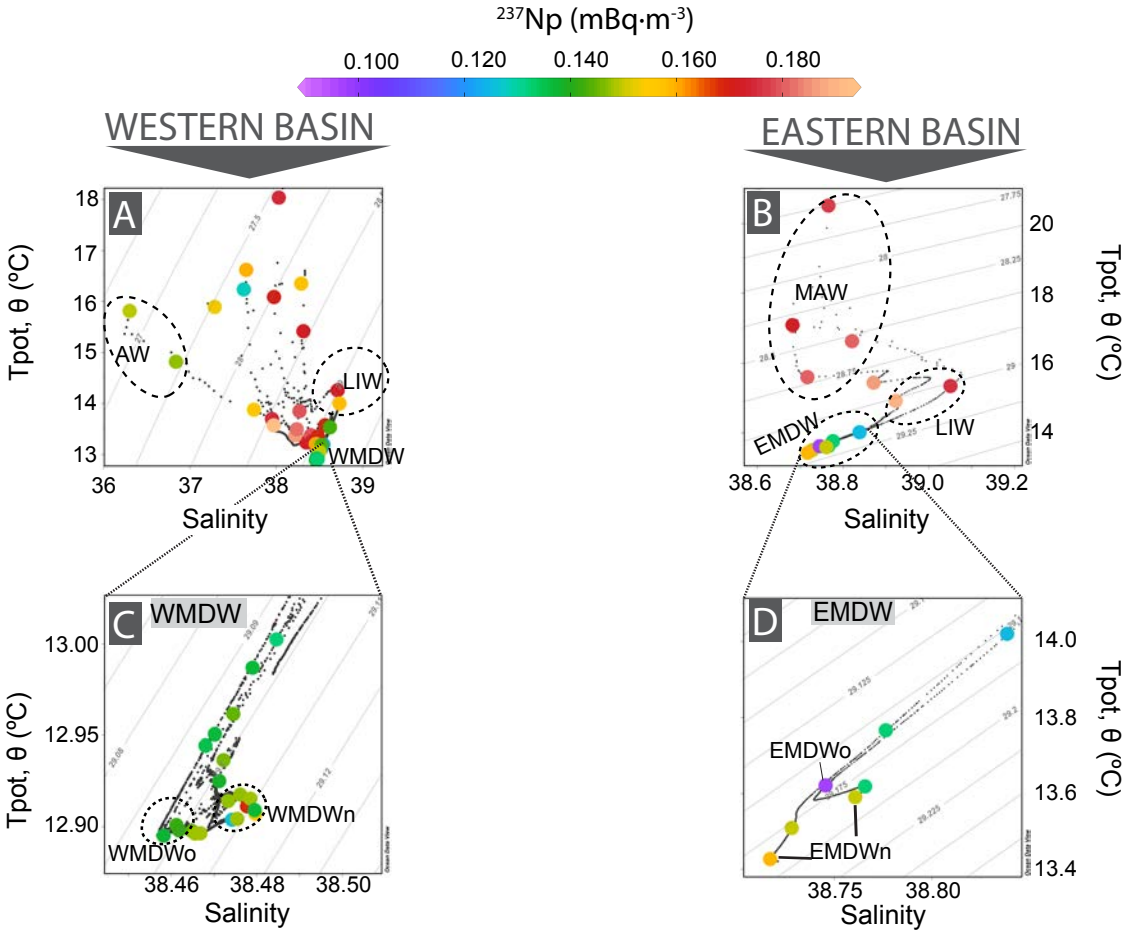

Figure 4.7. Potential temperature (Tpot, θ) – salinity diagrams for the Western and Eastern Mediterranean Sea. Concentrations of ^{237}Np are represented by the color bar. Water mass acronyms are: Atlantic Water (AW), Modified Atlantic Water (MAW), Levantine Intermediate Water (LIW),) Western Mediterranean Deep Water (WMDW) and Eastern Mediterranean Deep Water (EMDW). Lower case n: new; o: old. Water masses were identified in (Castrillejo et al., 2017).

The first transect of ^{237}Np along two zonal sections in the Mediterranean Sea (Figure 4.5B) shows that the distributions of ^{237}Np often matches that of dissolved oxygen.

Dissolved oxygen (overlay in Figure 4.5 B) is a good indicator of recent water ventilation events in regions characterized by oligotrophic conditions and rapid water turnover times typical of the Mediterranean Sea (e.g. Malanotte-Rizzoli et al., 2014). For example, the formation of LIW in the Levantine Basin, its sinking to intermediate depths in the Ionian Sea and the succeeding westward flow at 200-600 m depth (Wüst, 1961) can be traced by concentrations of ^{237}Np ≥0.180 mBq·m^{-3} and dissolved oxygen ≥200 μmol·kg^{-1}. Dense, deep waters produced during the EMT and WMT are traced by relative maxima in ^{237}Np concentrations and dissolved oxygen in waters below ~2000 m depth in both basins, while old waters having turnover times of 70-150 yr (Roether and Schlitzer, 1991; Stratford et al., 1998) are identified by ^{237}Np as low as <0.130 mBq·m^{-3} and dissolved oxygen concentrations ~180 μmol·kg^{-1} (Figure 4.5 B).

The conservative behavior of ^{237}Np is further confirmed by the similar vertical profiles compared to other conservative radionuclides such as ^{137}Cs and ^{236}U (Figure 4.2) and the correlations reported in section 4.1, although the later significant correlation is partly due to their common sources. These results are in line with earlier work showing comparable behavior of ^{237}Np, ^{99}Tc, ^{137}Cs and ^{129}I based on limited number of samples collected elsewhere (Beasley et al., 1998; Bressac et al., 2017; Keeney-Kennicutt and Morse, 1984; Lindahl et al., 2005).

4.5.3. Water column distribution of plutonium isotopes

The distribution of ^{239,240}Pu in the water column is influenced both by water mass circulation and particle cycling (Lindahl et al., 2010). As a consequence, and unlike ^{137}Cs or ^{237}Np, the ^{239,240}Pu concentrations measured in the Mediterranean Sea in May 2013 often is not related to the distribution of water masses (Figure 4.5). For instance, ^{239,240}Pu concentrations differed less than 0.5 mBq·m^{-3} between WMDW formed before and after the WMT, and they varied within a narrow range (3-7 mBq·m^{-3}) between AW and LIW (Figure 4.5 C).

Particle cycling in open Mediterranean waters is particularly relevant in the upper ~1000 m. Particles are more abundant in shallow waters because photosynthetic primary

production occurs in the euphotic zone and there is a high influence of the Saharan dust deposition on the surface ocean. Hence, plutonium scavenging occurs mainly in the upper ~200 m (e.g. Fowler et al., 2000). At these depths, ^{239,240}Pu is preferentially removed over conservative radionuclides leading to larger ^{237}Np/^{239}Pu atom ratios and ^{137}Cs/^{239,240}Pu activity ratios in the whole Mediterranean Sea (Figure 4.8). As a consequence of particle scavenging and water mass transport (discussed below), surface ^{239,240}Pu concentrations have decreased from >30 mBq·m^{-3} in the 1970s to 2-12 mBq·m^{-3} in 2013 (Figure 4.9). Plutonium exported out of the 0-200 m layer by sinking particles can be released back to the dissolved phase during particle remineralization. Remineralization caused the ^{239,240}Pu concentration maxima found at 100-400 m depth in the 1970s-1990s in both the WMS and EMS (e.g. Fowler et al., 2000; Fukai et al., 1982), but that feature faded away leading to a gradual increase of ^{239,240}Pu concentrations until ~1000 m by the 2000s-2013 (Figure 4.9).

Thermohaline circulation also shapes the water column distribution of ^{239,240}Pu in the Mediterranean Sea. For example, the decrease of ^{239,240}Pu concentrations in the upper ~500 m can be attributed, in addition to scavenging, to the inflow of Atlantic Water with ^{239,240}Pu concentrations <5 mBq·m^{-3} and the outflow of Mediterranean Water with ^{239,240}Pu concentrations >16 mBq·m^{-3} (see ^{239,240}Pu profile at Gibraltar Strait in Figure 4.3). The lateral advection of Tyrrhenian Deep Waters carrying ^{239,240}Pu concentrations 5-7 mBq·m^{-3} was also suggested to explain the ^{239,240}Pu minimum found at 900-1400 m depth in the central Alguero-Balear in 2001 (Figure 4.9) by Garcia-Orellana (2004). Finally, DWF can carry plutonium from the surface to the abyss and vertically mix the water column. DWF would be responsible of ^{239,240}Pu concentration increase from about 14 to 21 mBq·m^{-3} below ~1000 m in the WMS between the 1970s and 2013 (Figure 4.9). The homogenization of ^{239,240}Pu profiles from 2001-2002 to 2013 in the WMS, and from the 1970s to 2001-2013 in the EMS, could also be explained by DWF through the intense vertical mixing occurring in the mid 2000s and the late 1990s (Roether et al., 1996; Schroeder et al., 2008), respectively, during the WMT and EMT (Figure 4.9). The general downward transport of ^{239,240}Pu by circulation and particle sinking was also accompanied by the decrease in ^{239,240}Pu inventories (Table 4.2) in the 0-1000 m depth layer and the subsequent increase in >1000 m from the 1970s until early 2000s in the WMS, and until

the 1990s in the EMS. From early 2000s until 2013, ^{239,240}Pu inventories seemed to be more vertically mixed, as stated above, probably due to the WMT and the EMT (Table 4.2).

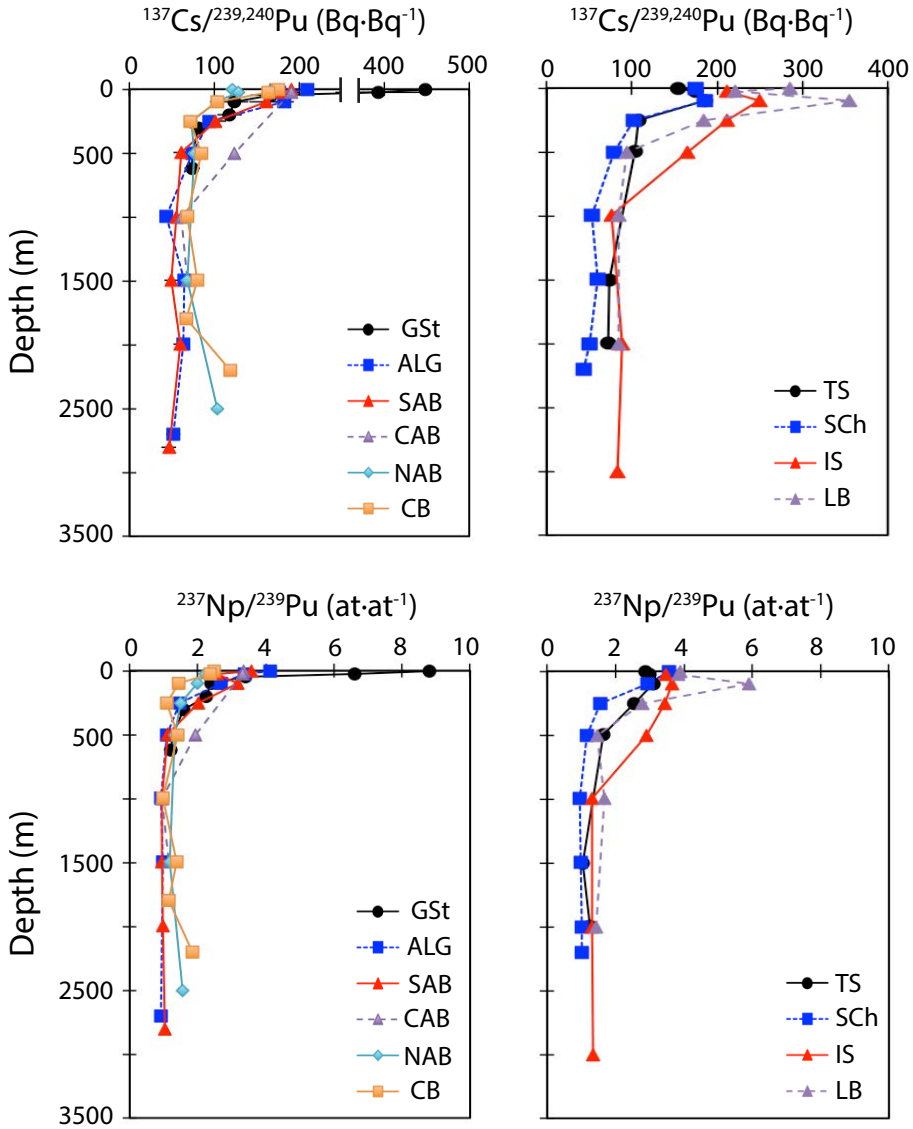

Figure 4.8. ^{137}Cs/^{239,240}Pu activity ratio and ^{237}Np/^{239}Pu atom ratio in samples collected during the *GA04S-MedSeA* cruise in May 2013.

The spatial distribution of ^{239,240}Pu in the Mediterranean Sea (Figure 4.5 C) also provides information on the behavior of this radionuclide in the water although the evolution of plutonium was not available for both the WMS and EMS simultaneously since the 1970s. One remarkable difference in May 2013 (Figure 4.5 C) was the difference on the distribution and the magnitude of ^{239,240}Pu concentrations between the two basins. While ^{239,240}Pu concentrations increased gradually from concentrations <10 mBq·m^{-3} in the

surface to 20-22 mBq·m^{-3} in waters below 1000 m in the WMS, the ^{239,240}Pu distribution in the EMS was more complex and its concentrations in waters below ~200 m were all lower (<18 mBq·m^{-3}) than in the WMS. The difference between the WMS and the EMS was also observable from the ^{239,240}Pu inventories (Table 4.2). In the WMS the full-depth inventories of ^{239,240}Pu remained at 51 ± 7 Bq·m^{-2} between 1975 and 2013. Despite the limited data in the EMS, a decrease can be observed from 81 ± 4 to 60 ± 4 Bq·m^{-2} in the Ionian Sea and from 55 ± 5 to 35 ± 1 Bq·m^{-2} in the Levantine Basin for the same time period. Considering that global fallout was the main source of ^{239,240}Pu (section 4.1) and its deposition was distributed evenly on the surface of both the WMS and EMS, the relevance of water mass circulation and scavenging should have been different in the two basins.

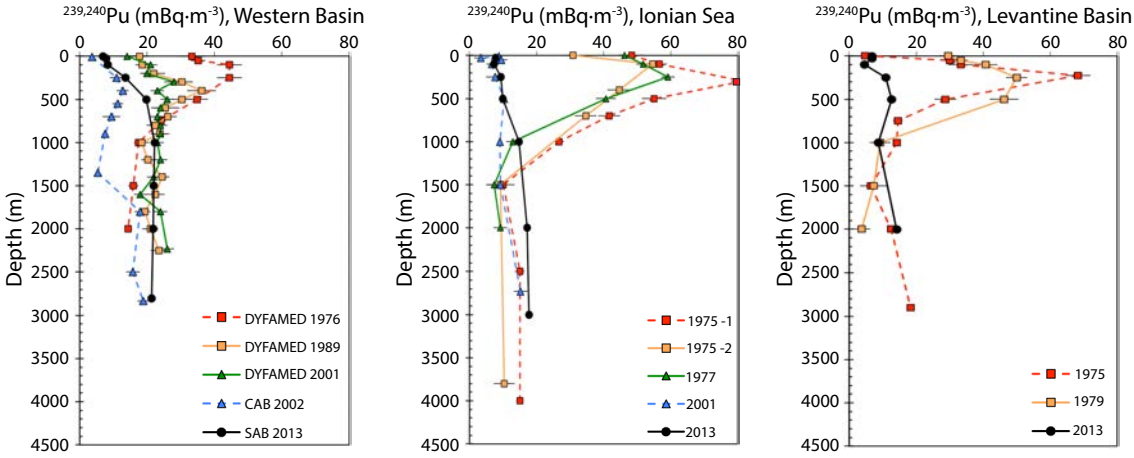

Figure 4.9. Vertical profiles of ^{239,240}Pu concentrations from the 1970s to 2013. In the Western Basin ^{239,240}Pu concentrations are reported for the DYFAMED site in the Ligurian Sea for 1976 (Fukai et al., 1979), 1989 (Fowler et al., 2000) and 2001 (Lee et al., 2003), the Central Alguero-Balear (CAB) in 2002 (Garcia-Orellana, 2004) and the Southern Alguero-Balear (SAB) in 2013 (this study). In the Ionian Sea ^{239,240}Pu concentrations are reported for two profiles in 1975 (Livingston et al., 1979), 1977 (Fukai et al., 1982), 2001 (Garcia-Orellana pers. comm.) and 2013 (this study). In the Levantine Basin ^{239,240}Pu concentrations are reported for 1975 (Livingston et al., 1979), 1979 (Fukai et al., 1982) and 2013 (this study).

Hypotheses can be postulated based on the importance of various processes and the differences between the two basins. The intensity of scavenging depends mainly on particle abundance. This is higher in coastal areas than in the open ocean because of particle supply from the coast and shallow sediments. In coastal seawater, ~10% of ^{239,240}Pu can be found in the particulate fraction (Mitchell et al., 1995) and because of

relatively shallow depths, ^{239,240}Pu is efficiently trapped into sediments instead of being remineralized in the water column. Consequently, ^{239,240}Pu inventories range between 1 and ~110 Bq·m^{-2} in sediments affected by continental margins (Ballestra et al., 1984; Gascó et al., 2002b; Gascó and Antón, 1997; Merino, 1997). In open Mediterranean waters, particulate ^{239,240}Pu is less than 5 % of the total in the water column (Ballestra et al., 1984; Holm et al., 1987; León Vintró et al., 1999), and most that ^{239,240}Pu remineralizes along the water column. Consequently, ^{239,240}Pu inventories in deep sediments of the Mediterranean Sea are ~3 Bq·m^{-2} (Delfanti and Papucci, 1995; Garcia-Orellana et al., 2009) and account for less than 5% of the mean global fallout inventory (~80 Bq·m^{-2}, e.g. León Vintró et al., 1999). The other factor affecting ^{239,240}Pu scavenging, that becomes more relevant in the open ocean, is particle composition. Biogenic particles are the responsible of the export of most ^{239,240}Pu out of the surface layer (e.g. Fowler et al., 2000).

Considering the above, one possibility to explain the larger ^{239,240}Pu loss from the water column in the EMS than in the WMS is boundary scavenging occurring near shelf sediments. Indeed, the shelf is wider and shallower in the Aegean, Adriatic and southwestern Ionian Sea than in the WMS. In the Gulf of Taranto, located in the Ionian Sea, sediments located at 150-2000 m depth recorded ^{239,240}Pu inventories between 45 and >160 Bq·m^{-2}, that were generally larger than in the WMS (Delfanti et al., 1995). However, a larger dataset would be necessary to test this hypothesis. A biology driven export of ^{239,240}Pu is discarded in the ultra-oligotrophic EMS, since primary production is larger in the WMS, particularly in its northern regions (e.g. Malanotte-Rizzoli et al., 2014). A second hypothesis is that given the ultra-oligotrophic nature of EMS waters, ^{239,240}Pu was less scavenged than in the WMS. Consequently, most ^{239,240}Pu would have remained in the upper water column. This would allow the transport of ^{239,240}Pu residing above ~500 m by LIW to the WMS. That would translate in lower ^{239,240}Pu concentrations recorded in the deep waters of the EMS compared to the WMS (Figure 4.3 and 4.5 C) and in reduced water column inventories of ^{239,240}Pu in the EMS. But, it would not explain the constancy of deep sediment ^{239,240}Pu inventories in the two basins (~3 Bq·m^{-2}, Garcia-Orellana et al., 2009). Thus it is probable that the first hypothesis about boundary scavenging was the main reason for the observed difference in ^{239,240}Pu distributions between the WMS and the EMS.

Table 4.2. Inventories of ^{239,240}Pu for different depth intervals in the Western and Eastern Mediterranean Sea. Inventories were computed using data from samples collected in May 2013. Data from the literature are taken from: 1) Livingston *et al.* (1979), 2) Fukai *et al.* (1979), 3) Ballestra *et al.* (1984), 4-6) Fowler *et al.* (2000), 7) Lee *et al.* (2003), 8) Garcia-Orellana (2004), 9-13) this study, 14-15) Livingston *et al.,* (1979), 16) Garcia-Orellana (unpub), 17) this study, 18) Livingston *et al.* (1979), 19) Fukai *et al.* (1982), and 20) this study.

Location	Sampling year	No. Sampled Depths	Max. Sampled Depth (m)	Bottom Depth (m)	Inventory In Bq·m^{-2} and in (%)						Ref.
					0 -200 m	0 – 1000 m	1000 – 2000 m	0 – 2000 m	> 2000 m	Total	
Western Basin											
C. Alguero – Balear (41º 12.4' N, 5º 52.3' E)	1975	8	2600	2612	3.4 ± 0.7 (8)	22 ± 2 (53)	19.5 ± 3.8 (47)	42 ± 3 (100)	12.2 ± 6.0 (23*)	54 ± 5	(1)
DYFAMED (43º 32' N, 7º 32' E)	1976	9	2000	2000	8.4 ± 0.4 (21)	26 ± 1 (65)	14.4 ± 1.6 (35)	41 ± 1 (100)	–	41 ± 1	(2)
C. Alguero – Balear (41º 0' N, 6º 45' E)	1981	7	2000	2600	8.5 ± 0.7 (21)	26 ± 2 (65)	14.0 ± 2.9 (35)	40 ± 3 (100)	8.4 ± 4.3 (18*)	48 ± 4	(3)
DYFAMED (43º 32' N, 7º 32' E)	1989	17	2230	2260	5.5 ± 0.3 (11)	22 ± 1 (41)	31 ± 5 (59)	53 ± 5 (100)	8.3 ± 8.3 (14*)	61 ± 7	(4)
DYFAMED (43º 32' N, 7º 32' E)	1989	17	2250	2260	4.4 ± 0.3 (10)	23 ± 1 (50)	23 ± 3 (50)	46 ± 2 (100)	6.1 ± 3.9 (12*)	53 ± 3	(5)
N. WMS (41º 57' N, 5º 56' E)	1990	19	2470	2475	5.8 ± 0.3 (13)	23 ± 1 (50)	23 ± 2 (50)	46 ± 1 (100)	10.8 ± 2.4 (19*)	57 ± 2	(6)
DYFAMED (43º 32' N, 7º 32' E)	2001	16	2230	2260	4.2 ± 0.2 (9)	22 ± 1 (46)	26 ± 2 (54)	49 ± 2 (100)	6.8 ± 3.3 (12*)	55 ± 3	(7)
C. Alguero – Balear (39º 28.3' N, 6º0.4' E)	2002	10	2836	2850	1.3 ± 0.2 (5)	8.7 ± 0.5 (32)	18.1 ± 1.4 (68)	27 ± 1 (100)	16.1 ± 3.0 (37*)	43 ± 3	(8)
Algeria (37º 29.2' N, 1º 26.8' E)	2013	9	2703	2777	2.3 ± 0.1 (6)	18.8 ± 0.1 (47)	21.3 ± 0.1 (53)	40.1 ± 0.2 (100)	16.4 ± 0.1 (29*)	57 ± 1	(9)
S. Alguero -Balear (38º 31.7' N, 5º 33.6' E)	2013	9	2804	2844	1.9 ± 0.1 (5)	18.0 ± 0.1 (45)	21.9 ± 0.1 (55)	39.9 ± 0.2 (100)	18.0 ± 0.1 (31*)	58 ± 1	(10)
Catalano - Balear (40º 57.1' N, 3º 19.2' E)	2013	9	2201	2274	3.1 ± 0.1 (9)	18.6 ± 0.2 (53)	16.7 ± 0.1 (47)	35.3 ± 0.2 (100)	3.1 ± 0.1 (8*)	38 ± 1	(11)
Tyrrhenian Sea (39º 49.7' N, 12º 30.9' E)	2013	7	3154	3165	2.1 ± 0.1 (7)	15.1 ± 0.6 (48)	16.4 ± 0.1 (52)	31.5 ± 0.6 (100)	17.1 ± 0.1 (35*)	49 ± 1	(12)
Sardinia Channel (38º 15.2' N, 8º 46.3' E)	2013	8	2202	2238	2.2 ± 0.1 (5)	18.2 ± 0.1 (46)	21.6 ± 0.0 (54)	39.8 ± 0.2 (100)	5.1 ± 0.1 (11*)	45 ± 1	(13)
Eastern Basin											
Ionian Sea (35º 35.9' N, 17º 55,8' E)	1975	9	4000	4000	12.2 ± 0.7 (24)	37 ± 1 (73)	13.8 ± 2.5 (27)	51 ± 2 (100)	30 ± 1 (37*)	81 ± 4	(14)
Ionian Sea 36º 0' N, 18º 0' E)	1975	6	3800	3800	9.7 ± 0.6 (23)	33 ± 1 (78)	9.3 ± 2.3 (22)	42 ± 2 (100)	18.6 ± 4.4 (31*)	60 ± 4	(15)
Ionian Sea (34º 52.4' N, 20º 48.9' E)	2001	9	2730	2760	1.5 ± 0.2 (7)	9.1 ± 0.9 (41)	13.0 ± 1.9 (59)	22.1 ± 1.7 (100)	11.6 ± 3.1 (34*)	34 ± 3	(16)
Ionian Sea (35º 2.7' N, 18º 34,1' E)	2013	7	3726	3774	1.5 ± 0.1 (5)	11.2 ± 0.1 (40)	16.6 ± 0.1 (60)	28 ± 1 (100)	31± 1 (53*)	59 ± 1	(17)
Lev. Basin (34º 1.3' N, 28º 59.8' E)	1975	10	2900	2900	8.9 ± 0.3 (23)	22 ± 1 (59)	15.7 ± 2.6 (41)	39 ± 2 (100)	16.5 ± 5.5 (30*)	55 ± 5	(18)
Lev. Basin (32º 0' N, 28º 0' E)	1979	8	2000	2000	8.4 ± 0.5 (28)	27 ± 1 (88)	3.7 ± 2.0 (12)	30 ± 1 (100)	-	30 ± 1 (100)	(19)
Lev. Basin (33º 14.8' N, 28º 27.1' E)	2013	7	2833	2865	1.4 ± 0.1 (6)	9.9 ± 0.1 (44)	12.8 ± 0.1 (56)	23 ± 1 (100)	12.2 ± 0.1 (35*)	35 ± 1	(20)

*Percentage calculated with respect to total inventory of ^{239,240}Pu

4.6. Conclusions

Distribution of ^{137}Cs, ^{237}Np and ^{239,240}Pu concentrations were presented for samples collected in the WMS and EMS in May 2013. Firstly, their sources in the Mediterranean Sea were constrained based on radionuclide concentrations and water column inventories. Like for ^{129}I and ^{236}U (*Chapter 3*), low-level radioactive releases from Marcoule reprocessing plant can explain the ~50 % excess of ^{237}Np estimated from our radionuclide inventory ratios. Radionuclide inventory ratios also indicated that Marcoule releases of ^{129}I and ^{236}U were probably in the higher end of the estimated in *Chapter 3* (~90 kg of ^{129}I and ~20 kg of ^{236}U). This demonstrates that the study of several radionuclides having similar chemical behavior help constraining their sources in the oceans. Median ^{240}Pu/^{239}Pu atom ratios of ~0.19 confirmed that the main source of plutonium in Mediterranean waters is global fallout. Secondly, the radionuclide distributions were discussed in relation to sources, ocean circulation and particle cycling. This study presented the first oceanic transect of ^{237}Np in world oceans. From its distribution and relationship with water masses and with other conservative radionuclides, it was evident that ^{237}Np behaved like a conservative element. Thus, its distribution was related to that of water masses. Temporal changes on water column distribution of ^{137}Cs between 1970s and 2013 were related to inputs and lateral and vertical transport of waters indicating profound effects from events such as the WMT and the EMT. The distribution of ^{239,240}Pu presented for both the WMS and EMS showed the additional influence from particle scavenging and remineralization along the water column. Concentrations and inventories of ^{239,240}Pu in waters below ~200 m were lower in the EMS than in the WMS. Two hypotheses were postulated to explain the apparently larger loss of Pu in the EMS. More Pu could have been exported by boundary scavenging into shelf sediments, which cover a larger surface area in the EMS than in the WMS. Or, given the lower primary production in the EMS than in the WMS, the low Pu vertical export associated sinking particles would allow a larger lateral transport of Pu by LIW in the EMS than in the WMS. Refusal or approval of these hypotheses would require a more complete dataset on Pu concentrations and inventories in sediment traps and shelf sediments in the EMS.

CHAPTER 5

Conclusions

This PhD dissertation aimed to contribute to the understanding of sources and distributions of a diverse set of artificial radionuclides (^{90}Sr, ^{129}I, ^{134}Cs, ^{137}Cs, ^{236}U, ^{237}Np, ^{239}Pu and ^{240}Pu) in two contrasting regions. On the one hand, the Pacific Ocean close to Japan, largely impacted by the accident that occurred at the Fukushima Dai-ichi Nuclear Power Plant (FDNPP) in 2011, which led to the release of radioactive contaminants to the environment immediately following the accident and during the following years. On the other hand, the semi-enclosed Mediterranean Sea, impacted by various sources since the mid-twentieth century: i) on a global scale by atmospheric nuclear weapon tests carried during the 1950s-1960s and the Chernobyl nuclear accident in 1986; ii) at a regional level, by the low level radioactive discharges from the Marcoule nuclear reprocessing plant between 1958 and 1997; iii) and locally by the Palomares accident in 1966.

In *Chapter 2* we assessed the impact of radioactive releases from the FDNPP. We focused on ^{90}Sr, which was largely understudied despite being of major concern due to its large presence in cooling waters stored in tanks in the nuclear facility since 2011. To evaluate the levels of ^{90}Sr and radiocaesium in the area we collected seawater, groundwater and surface beach water samples between 0.8 and ~100 km off FDNPP in September 2011, two and a half years after the accident. In this work we also evaluated the temporal evolution of ^{134}Cs, ^{137}Cs and ^{90}Sr concentrations, highlighting the relative importance of various sources in the coast off Japan over time. Most importantly, we confirmed and quantified for the first time the ongoing ^{90}Sr releases from the nuclear facility to the Pacific Ocean of 2.3-8.5 GB·d^{-1} in September 2013, exceeding in 2 to 3 orders of magnitude the ^{90}Sr inputs through rivers, although substantially lower than the rates estimated to have occurred soon after the accident. Considering that releases from FDNPP continued through time and that leaks from the facility could potentially be much larger, our study evidenced the importance of continuous surveillance of artificial radionuclides in the Pacific Ocean. A further reason to do so is that long-lived radionuclides released from the FDNPP can serve as tracers of the thermohaline circulation and particle cycling in the Pacific Ocean.

The two studies in the Mediterranean Sea (*Chapters 3 and 4*) allowed us to provide with a global view on the sources and distribution of artificial radioactivity in 2013. The main sources of artificial radionuclides to the Mediterranean Sea had been already identified and, to some extent, quantified in earlier studies, notably for ^{137}Cs and, less so,

for plutonium: global fallout, the Chernobyl accident and the emissions from the Marcoule site. However, knowledge on their respective contributions to the presence of ^{129}I, ^{236}U, ^{237}Np and Pu isotopes in the Mediterranean Sea was limited or completely unknown. Our data on ^{129}I and ^{236}U (*Chapter 3*) showed that their distributions are governed by the thermohaline circulation, and highlighted the importance of constraining each radionuclide source. In particular, we estimate that the contamination derived from the Marcoule nuclear reprocessing plant is comparable to that from global fallout for ^{236}U and about 2 orders of magnitude larger for ^{129}I. In *Chapter 4* we discuss the data on ^{137}Cs, ^{237}Np and Pu isotopes, with the novelty of reporting for the first time a comprehensive dataset of ^{237}Np. The distributions of both ^{237}Np and ^{137}Cs are driven by the circulation of the water masses, as expected for conservative radionuclides. The principal sources of ^{237}Np were found to be global fallout and Marcoule, the later probably contributing to about 30% of the ^{237}Np present in the Mediterranean Sea in 2013. The distribution of ^{137}Cs showed the influence of inputs and recent changes in water circulation, such as the Eastern Mediterranean Transient in 1990s and the Western Mediterranean Transition in the 2000s. The main source of Pu was confirmed to be global fallout, as shown by the $^{240}Pu/^{239}Pu$ atom ratios of about 0.18 throughout the Mediterranean Sea. The distribution of $^{239,240}Pu$ was affected by, in addition to circulation, particle scavenging and remineralization. A notable result of this study was the lower levels of $^{239,240}Pu$ in the water column of the Eastern Basin than in the Western Basin. The question remains open on whether this feature is due to boundary scavenging in the continental margins, or it was caused by the combined effect of limited scavenging by particles in open waters and enhanced westward transport by Levantine Intermediate Waters. Despite the intended comprehensiveness of this study in the Mediterranean Sea, future work should also cover the Adriatic Sea, the main source of deep waters in the Eastern Mediterranean Sea (EMS). Also, the Aegean Sea should be studied in more detail, as it is the entry pathway of waters from the Black Sea, affected by both global fallout and, particularly, the Chernobyl accident. Furthermore, attention to other compartments (e.g. shelf sediments in the EMS and particles collected using sediment traps) would allow explaining the distinct distribution of plutonium in the EMS.

Three main tools have been used to understand the distribution and sources of radionuclides, both in the coast off Fukushima and in the Mediterranean Se,: i) concentrations of radionuclides in a space-scale distribution (*Chapters 2, 3 and 4*); ii) water column or box inventories (*Chapters 3 and 4*) and, iii) activity/atom ratios between either isotopes of the same element ($^{240}Pu/^{239}Pu$, $^{137}Cs/^{134}Cs$) or of different elements (*Chapters 2 and 4*).

The data on concentrations of the various isotopes studied here provided essential information about their distributions in the Mediterranean Sea and the oceanic processes governing their fate in the water column (*Chapters 3 and 4*). After their introduction in surface waters, ^{129}I, ^{236}U and ^{237}Np were transported laterally and vertically, by dense water formation, showing similar distributions to^{137}Cs in the Mediterranean Sea (*Chapters 3 and 4*). Pu isotopes are particle-reactive, and their concentrations increased from relatively low levels in the surface due to Pu scavenging to larger concentrations in deeper waters due to both particle remineralization and vertical water transport. The radionuclide concentrations measured in both the Pacific and Mediterranean waters evidenced the impact of other sources than global fallout. This was clear in the coast off Japan (*Chapter 2*), were concentrations in seawater were up to 8.9 ± 0.4 $Bq \cdot m^{-3}$ for ^{90}Sr, 124 ± 3 $Bq \cdot m^{-3}$ for ^{137}Cs and 54 ± 1 $Bq \cdot m^{-3}$ for ^{134}Cs in 2013, while their typical concentrations prior to the 2011 accident due to the nuclear tests conducted in the past were ~1 $Bq \cdot m^{-3}$, 1-2 $Bq \cdot m^{-3}$ and neglible, respectively. In Mediterranean waters sampled in 2013 (*Chapters 3 and 4*), the average concentrations of ^{129}I, ^{236}U and ^{237}Np were respectively, about 3, 100 and 1.5 times larger than their expected values from global fallout, which would be $<1 \times 10^6$ $at \cdot kg^{-1}$, $\sim 5 \times 10^6$ $at \cdot kg^{-1}$, and ~0.100 $mBq \cdot m^{-3}$, respectively. The comparison of measured concentrations in Mediterranean waters with those simulated using a box model allowed the quantification of the inputs from the Marcoule complex, that were estimated in 70-90 kg of ^{129}I and 10-20 kg of ^{236}U.

The radionuclide inventories in the Western and Eastern Mediterranean Basins in 2013 were also estimated. The inventories of ^{129}I and ^{236}U were (85-280) $\times 10^{12}$ and (19-47) $\times 10^{12}$ $at \cdot m^{-2}$, respectively, while the water column inventories of ^{237}Np were 0.1-0.6 $Bq \cdot m^{-2}$. In all cases, we obtained larger inventories than those expected from global fallout (~2 $\times 10^{12}$ $at \cdot m^{-2}$ for ^{129}I, ~11 $\times 10^{12}$ $at \cdot m^{-2}$ for ^{236}U and ~0.14 $Bq \cdot m^{-2}$ for ^{237}Np), confirming the

significant inputs of these radionuclides from the Marcoule reprocessing plant. The impact of the Chernobyl accident was either minor or negligible for these radionuclides in the Mediterranean Sea. The total mass of ^{129}I and ^{236}U was estimated in 101 ± 14 kg and 31 ± 14 kg, from which only ~1 kg of ^{129}I and ~11 kg of ^{236}U were introduced by global fallout. In the case of ^{239,240}Pu, water column inventories in May 2013 (~10-59 Bq·m^{-2}) were lower than those expected from global fallout (~80 Bq·m^{-2}). If no other relevant sources were to be considered (see later conclusions on radionuclide ratios), this result would point to scavenging occurring in coastal waters. One weakness of the inventory approach is that its magnitude depends not only on the measured radionuclide concentration, but also on the vertical sampling resolution and the water column depth. The sampling during May 2013 in the Mediterranean Sea was carried out in the deepest areas of each sub-basin in order to characterize the radionuclide concentrations in the main water masses, and thus shallow coastal areas were missed (except for the Strait of Gibraltar and the Sardinia Channel).

Concentration and inventory ratios were instrumental to constrain the sources of radioactive contamination. In the coast off Japan (*Chapter 2*), two activity ratios were used: ^{134}Cs/^{137}Cs and ^{137}Cs/^{90}Sr. The ^{134}Cs/^{137}Cs activity ratio of ~1 (decay corrected to April 2011) was an unequivocal indication of FDNPP derived radiocaesium. However, the short half-life of ^{134}Cs (2.06 years) limits the use of the ^{134}Cs/^{137}Cs activity ratio to trace Fukushima derived contamination to the most contaminated areas. Indeed, about 90% of the ^{134}Cs released from the FDNPP in 2011 have decayed by 2017. Therefore we used the ^{137}Cs/^{90}Sr activity ratio to identify FDNPP discharges enriched in ^{90}Sr relative to ^{137}Cs from 2011 to 2015. The decrease in the ^{137}Cs/^{90}Sr activity ratio from ~40 in spring 2011 to ~3.5 in September 2013 (higher than the global fallout, ~1.5), indicated the ongoing releases from the FDNPP to the Pacific Ocean, that we were able to quantify.

In the Mediterranean Sea, several atom ratios were estimated for global fallout, the Chernobyl accident and Marcoule (*Chapter 4*) and used as end-members against to which we could compare the data obtained from the water column to identify the significance of the releases from Marcoule. We used the ^{237}Np/^{137}Cs atom ratio to estimate the Marcoule ^{237}Np input of ~7 kg. The ^{129}I/^{137}Cs and ^{236}U/^{137}Cs atom ratios helped to confirm the validity of ^{129}I and ^{236}U inputs proposed in *Chapter 3*. Results of ^{240}Pu/^{239}Pu atom ratios also showed that most of the Pu present in Mediterranean seawater was from global fallout

(*Chapter 4*). Finally, radionuclide ratios also helped distinguishing between processes governing the distribution of artificial radionuclides in the Mediterranean water column (*Chapter 4*). The $^{137}Cs/^{239,240}Pu$ activity ratios and the $^{237}Np/^{239}Pu$ atom ratios deviated in the upper water column due to faster removal of Pu compared to conservative radionuclides, while below ~1000 m these ratios were rather uniform. Such deviations in the upper ~200 m are attributed as in previous studies, to Pu scavenging by sinking particles, while water mass circulation is the most relevant process affecting the distribution of both conservative and particle-reactive radionuclides below 1000 m depth.

The radionuclides studied in this thesis have distinct characteristics that should be considered in future studies. The short-lived ^{134}Cs and medium-lived ^{137}Cs and ^{90}Sr are useful to provide information on the magnitude and the transport pathways of radioactive contamination from recent sources, such as the FDNPP. These radionuclides can be measured using conventional radiometric techniques, that have a relatively reduced cost compared to Inductively Coupled and Accelerator mass spectrometry techniques (ICP-MS and AMS, respectively). Further, in the case of radiocaesium, the straightforward radiochemistry and measurement allows a rapid assessment of a potential impact in the event of a nuclear accident. However, ^{137}Cs and ^{90}Sr can reach very low concentrations in seawater a few decades after their introduction to the oceans (and ^{134}Cs would not be detectable well before), due to radioactive decay and mixing with waters carrying only the global fallout signal. This is specially the case of the Mediterranean Sea characterized by rapid water turnover times of water. There, ^{137}Cs presented mean concentrations lower than 1.5 $Bq \cdot m^{-3}$ in 2013, even with the additional input from Chernobyl accident. Uncertainties associated to these concentration levels of ^{137}Cs were typically larger than 10% for samples of 25 L and counting times of ~60 h per sample. An alternative for using radionuclides as tracers in the marine environment is the transition to longer-lived radionuclides, which can be measured in lower sample volumes with greater precision due to the significant improvements in ICP-MS and AMS techniques. For example, ^{129}I and ^{236}U (*Chapter 3*) were measured in seawater samples of less than 0.5 L and 7 L respectively in the Mediterranean Sea and with high precision using AMS facilities at ETH-Zürich, while the uncertainty was less than 3% for ^{237}Np and Pu isotopes measured in samples of 25L using ICP-MS techniques at Lamont-Doherty Earth Observatory. The

major disadvantage of these long-lived radionuclides (except for Pu) is the limited information on their input functions and on their distributions since the advent of the nuclear era. Indeed, here we provided with the first estimates of the amounts of ^{129}I, ^{236}U and ^{237}Np released from the Marcoule site, which were in the same order of magnitude as global fallout, or even greater (i.e. for ^{129}I). However, the temporal evolution of discharges from Marcoule are unknown for many of these isotopes, limiting their potential as tracers of water circulation in the Mediterranean Sea. A potential solution would be studying the historical inputs from Marcoule using environmental archives. In the case of ^{236}U, we know that it may accumulate in certain bivalves and in corals. In future studies and particularly in the event of a new accidental release, one should consider the measurement of multiple long-lived radionuclides together with those that pose a major radiological risk (e.g. ^{131}I, ^{134}Cs, ^{137}Cs, ^{90}Sr). In this way, we could achieve both to assess the impact of a new source and use them as tracers of oceanic processes.

References

Aarkrog, A., 1986. Proc. of Co - ordinated Research Programme on Behavior of Long - lived Radionuclides Associated with Deep- Sea Disposal of Radioactive Wastes, International Atmoic Energy Agency. IAEA TEDOC-368. Vienna.

Aarkrog, A., 2003. Input of anthropogenic radionuclides into the World Ocean. Deep Sea Res. Part II Top. Stud. Oceanogr. 50, 2597–2606. doi:10.1016/S0967-0645(03)00137-1

Aldahan, A., Alfimov, V., Possnert, G., 2007. ^{129}I anthropogenic budget: Major sources and sinks. Appl. Geochemistry 22, 606–618. doi:10.1016/j.apgeochem.2006.12.006

Anderson, R.F., Fleisher, M.Q., Robinson, L.F., Lawrence-Edwards, R., Hoff, J.A., Moran, B., Rutgers van der Loeff, M., Thomas, A.L., Roy-Barman, M., Francois, R., 2012. GEOTRACES intercalibration of ^{230}Th, ^{232}Th, ^{231}Pa, and prospects for ^{10}Be. Limnol. Oceanogr. Methods 10, 179–213. doi:10.4319/lom.2012.10.179

Aoyama, M., Hirose, K., 2004. Artificial radionuclides database in the Pacific Ocean: HAM database. Scientific World Journal. 4, 200–215. doi:10.1100/tsw.2004.15

Aoyama, M., Tsumune, D., 2012. Temporal variation of ^{l34}Cs and ^{l37}Cs activities in surface water at stations along the coastline near the Fukushima Dai-ichi Nuclear Power Plant accident site,. Geochem. J. 46, 321–325.

Aoyama, M., Tsumune, D., Hamajima, Y., 2013. Distribution of ^{137}Cs and ^{134}Cs in the North Pacific Ocean: Impacts of the TEPCO Fukushima-Daiichi NPP accident. J. Radioanal. Nucl. Chem. 296, 535–539. doi:10.1007/s10967-012-2033-2

AREVA, 2015. AREVA la Hague site information report.

Bailly du Bois, P., Laguionie, P., Boust, D., Korsakissok, I., Didier, D., Fiévet, B., 2012. Estimation of marine source-term following Fukushima Dai-ichi accident. J. Environ. Radioact. 114, 2–9. doi:10.1016/j.jenvrad.2011.11.015

Ballestra, S., Bojanowski, R., Fukai, R., Vas, D., 1984. Behavior of selected radionuclides in the Northwestern Mediterranean basin influenced by river discharge. A. Cigna C. Myttenaere [eds.], Int. Symp. Behav. long-lived radionuclides Mar. Environ. Comm. Eur. Communities. 215–232.

Baxter, M.S., Fowler, S.W., Povinec, P., 1995. Observations on plutonium in the oceans. Appl. Radiat. Isot. 46, 1213–1223.

Beasley, T., Cooper, L.W., Grebmeier, J.M., Aagaard, K., Kelley, J.M., Kilius, L.R., 1998. ^{237}Np/^{129}I Atom Ratios in the Arctic Ocean: Has ^{237}Np from Western European and Russian Fuel Reprocessing Facilities Entered the Arctic Ocean ? J. Environ. Radioact. 39, 255–277.

Beasley, T.M., Kelley, J.M., Maiti, T.C., Bond, L.A., 1998. ^{237}Np/^{239}Pu atom ratios in Integrated Global Fallout: a Reassessment of the Production of ^{237}Np. J. Environ. Radioact. 38, 133–146.

Benmansour, M., Laissaoui, A., Benbrahim, S., Ibn Majah, M., Chafik, A., Povinec, P.P., 2006. Radionuclides in the Environment - Int. Conf. On Isotopes in Env. Studies, Radioactivity in the Environment, Radioactivity in the Environment. Elsevier. doi:10.1016/S1569-4860(05)08009-5

Bethoux, J.P., 1980. Mean water fluxes across sections in the Mediterranean Sea, evaluated on the basis of water and salt budgets and of observed salinities. Oceanol. Acta, 3, 79-88.

Bethoux, J.P., Gentili, B., 1996. The Mediterranean Sea, coastal and deep-sea signatures of climatic and environmental changes. J. Mar. Syst. 7, 383–394. doi:10.1016/0924-7963(95)00008-9

Boone, F. W., Kantelo, M. V., Mayer, P. G., Palms, J. M., 1985. Residence half-times of ^{129}I in undisturbed surface soils based on measured soil concentration profiles. Health Phys. 48, 401-13.

Boulyga, S.F., Heumann, K.G., 2006. Determination of extremely low ^{236}U/^{238}U isotope ratios in environmental samples by sector-field inductively coupled plasma mass spectrometry using high-efficiency sample introduction. J. Environ. Radioact. 88, 1–10. doi:10.1016/j.jenvrad.2005.12.007

Boulyga, S.F., Matusevich, J.L., Mironov, V.P., Kudrjashov, V.P., Halicz, L., Segal, I., McLean, J.A., Montaser, A., Sabine Becker, J., 2002. Determination of ^{236}U/^{238}U isotope ratio in contaminated environmental samples using different ICP-MS instruments. J. Anal. At. Spectrom. 17, 958–964. doi:10.1039/b201803a

Bowen, V.T., Noshkin, V.E., Livingston, H.D., Volchok, H.L., 1980. Fallout radionuclides in the Pacific Ocean: Vertical and horizontal distributions, largely from GEOSECS stations. Earth Planet. Sci. Lett. 49, 411–434. doi:10.1016/0012-821X(80)90083-7

Bressac, M., Levy, I., Chamizo, E., La Rosa, J.J., Povinec, P.P., Gastaud, J., Oregioni, B., 2017. Temporal evolution of ^{137}Cs, ^{237}Np, and $^{239+240}$Pu and estimated vertical $^{239+240}$Pu export in the northwestern Mediterranean Sea. Sci. Total Environ. 595, 178–190. doi:10.1016/j.scitotenv.2017.03.137

Broecker, W.S., Peng, T.H., 1982. Tracers in the Sea. Eldigio, New York.

Buesseler, K.O., 1987. Chernobyl: Oceanographic Studies in the Black Sea. Oceanus 30.

Buesseler, K., Aoyama, M., Fukasawa, M., 2011. Impacts of the Fukushima nuclear power plants on marine radioactivity. Environ. Sci. Technol. 45, 9931–9935. doi:10.1021/es202816c

Buesseler, K.O., Jayne, S.R., Fisher, N.S., 2012. Fukushima-derived radionuclides in the ocean and biota off Japan. Proc. Natl. Acad. Sci. 109, 5984–5988.

Buesseler, K.O., 2014. Fukushima and ocean radioactivity. Oceanography 27, 92–105.

Calmet, D., Fernandez, J., 1990. Ceasium distribution in northwestern Mediterranean seawater, suspended particles and sediments. Cont. Shelf Res. 10, 895–913.

Casacuberta, N., Masqué, P., Garcia-Orellana, J., Garcia-Tenorio, R., Buesseler, K.O., 2013. ^{90}Sr and ^{89}Sr in seawater off Japan as a consequence of the Fukushima Dai-ichi nuclear accident. Biogeosciences 10, 3649–3659. doi:10.5194/bg-10-3649-2013

Casacuberta, N., Christl, M., Lachner, J., Rutgers van der Loeff, M., Masqué, P., Synal, H.-A., 2014. A first transect of ^{236}U in the north atlantic ocean. Geochim. Cosmochim. Acta 133, 34–46. doi:10.1016/j.gca.2014.02.012

Casacuberta, N., Masqué, P., Henderson, G., Rutgers van-der-Loeff, M., Bauch, D., Vockenhuber, C., Daraoui, a., Walther, C., Synal, H. -a., Christl, M., 2016. First ^{236}U data from the Arctic Ocean and use of ^{236}U/^{238}U and ^{129}I/^{236}U as a new dual tracer. Earth Planet. Sci. Lett. 440, 127–134. doi:10.1016/j.epsl.2016.02.020

Castrillejo, M., Casacuberta, N., Christl, M., Garcia - Orellana, J., Vockenhuber, C., Synal, H.-A., Masqué, P., 2017. Anthropogenic ^{236}U and ^{129}I in the Mediterranean Sea: First comprehensive distribution and constrain of their sources. Sci. Total Environ. 593–594, 745–759. doi:10.1016/j.scitotenv.2017.03.201

Castrillejo, M., Casacuberta, N., Breier, C.F., Pike, S.M., Masqué, P., Buesseler, K.O., 2016. Reassessment

of ^{90}Sr, ^{137}Cs, and ^{134}Cs in the Coast off Japan Derived from the Fukushima Dai - ichi Nuclear Accident. Environ. Sci. Technol. 50, 173–180. doi:10.1021/acs.est.5b03903

Chamizo, E., López-Lora, M., Bressac, M., Levy, I., Pham, M.K., 2016. Excess of ^{236}U in the northwest Mediterranean Sea. Sci. Total Environ. 565, 767–776. doi:10.1016/j.scitotenv.2016.04.142

Charette, M. a., Breier, C.F., Henderson, P.B., Pike, S.M., Rypina, I.I., Jayne, S.R., Buesseler, K.O., 2013. Radium-based estimates of cesium isotope transport and total direct ocean discharges from the Fukushima Nuclear Power Plant accident. Biogeosciences 10, 2159–2167. doi:10.5194/bg-10-2159-2013

Charmasson, S., 1998. Cycle tu combustible nucléaire et milieu marin - Devenir des effluents rhodaniens en Méditerranée et des déchets immergés en Atlantique Nord-est. Thèse Etat, Report CEA-R65826, CEA/Saclay 91191 Gif/yvette Cedex, France. ISSN 0429-3460

Charmasson, S., 2003. Cs inventory in sediment near the Rhone mouth : role played by different sources Inventaires de ^{137}Cs dans les sédiments à l ' embouchure du Rhône : contribution des différentes sources 26, 435–441. doi:10.1016/S0399-1784(03)00036-7

Chino, M., Nakayama, H., Nagai, H., Terada, H., Katata, G., Yamazawa, H., 2011. Cs Accidentally Discharged from the Fukushima Daiichi Nuclear Power Plant into the Atmosphere. J. Nucl. Sci. Technol. 48, 1129–1134. doi:10.1080/18811248.2011.9711799

Christl, M., Casacuberta, N., Vockenhuber, C., Elsässer, C., Bailly du Bois, P., Herrmann, J. jürgen, Synal, H.-A., 2015a. Reconstruction of the ^{236}U input function for the Northeast Atlantic Ocean: Implications for ^{129}I/^{236}U and ^{236}U/^{238}U-based tracer ages. J. Geophys. Res. Ocean. 1–16. doi:10.1002/2014JC010472.Received

Christl, M., Casacuberta, N., Lachner, J., Maxeiner, S., Vockenhuber, C., Synal, H.A., Goroncy, I., Herrmann, J., Daraoui, A., Walther, C., Michel, R., 2015b. Status of ^{236}U analyses at ETH Zurich and the distribution of ^{236}U and ^{129}I in the North Sea in 2009. Nucl. Instruments Methods Phys. Res. Sect. B Beam Interact. with Mater. Atoms 361, 510–516. doi:10.1016/j.nimb.2015.01.005

Christl, M., Lachner, J., Vockenhuber, C., Goroncy, I., Herrmann, J., Synal, H.A., 2013a. First data of Uranium-236 in the North Sea. Nucl. Instruments Methods Phys. Res. Sect. B Beam Interact. with Mater. Atoms 294, 530–536. doi:10.1016/j.nimb.2012.07.043

Christl, M., Lachner, J., Vockenhuber, C., Lechtenfeld, O., Stimac, I., van der Loeff, M.R., Synal, H.-A., 2012. A depth profile of uranium-236 in the Atlantic Ocean. Geochim. Cosmochim. Acta 77, 98–107. doi:10.1016/j.gca.2011.11.009

Christl, M., Vockenhuber, C., Kubik, P.W., Wacker, L., Lachner, J., Alfimov, V., Synal, H., 2013b. Nuclear Instruments and Methods in Physics Research B The ETH Zurich AMS facilities : Performance parameters and reference materials. Nucl. Inst. Methods Phys. Res. B 294, 29–38. doi:10.1016/j.nimb.2012.03.004

Dahlgaard, H., 1995. Transfer of European Coastal Pollution to the Arctic : Radioactive Tracers. Mar. Pollut. Bull. 31, 3–7.

Dahlgaard, H., Chen, Q., Herrmann, J., Nies, H., Ibbett, R.D., Kershaw, P.J., 1995. On the background level of 99Tc, 90Sr and 137Cs in the North Atlantic. J. Mar. Syst. 6, 571–578. doi:10.1016/0924-7963(95)00025-K

Daraoui, A., Riebe, B., Walther, C., Wershofen, H., Schlosser, C., Vockenhuber, C., Synal, H., 2016. Concentrations of iodine isotopes (^{129}I and ^{127}I) and their isotopic ratios in aerosol samples from Northern Germany. J. Environ. Radioact. 154, 101–108. doi:10.1016/j.jenvrad.2016.01.021

Delfanti, R., Papucci, C., 2010. Mediterranean Sea: Radionuclides, in: Encyclopedia of Inorganic and Bioinorganic Chemistry. doi:10.1002/9781119951438.eibc0444

Delfanti, R., Klein, B., Papucci, C., 2003. Distribution of ^{137}Cs and other radioactive tracers in the eastern Mediterranean: Relationship to the deepwater transient. J. Geophys. Res. 108, 1–10. doi:10.1029/2002JC001371

Delfanti, R., Desideri, D., Martinotti, W., Assunta Meli, M., Papucci, C., Queirazza, G., Test, C., Triulzi, C., 1995. Plutonium concentration in sediment cores collected in the Mediterranean Sea. Sci. Total Environ. 173/174, 187–193.

Delfanti, R., Papucci, C., 1995. Inventories of ^{239,240}Pu in slope and deep-sea sediments from the Ionian Sea and the Algerian Basin, in: Rappo. Comm. Int. Mer Médit.

Delfanti, R., Papucci, C., Alboni, M., Lorenzillo, R., S., S., 1995. Cs-137 inventories in the water column and in sediments of the western Mediterranean Sea, in: Rapports Commission Internationale Pour L'exploration Scientifique de La Mer Méditerranée. p. 226.

Delfanti, R., Papucci, C., Vives i Batlle, J., Downes, A.B., Mitchell, P.I., 1994. Distribution of ^{137}Cs and transuranics elements in seawater of the western Mediterranean Sea, in: The Radiological Exposure of the Population of the European Community in the Mediterranean Sea (Marina Project). EUR 15564.

Delfanti, R., Özsoy, E., Kaberi, H., Schirone, A., Salvi, S., Conte, F., Tsabaris, C., Papucci, C., 2014. Evolution and fluxes of ^{137}Cs in the Black Sea/Turkish Straits System/North Aegean Sea. J. Mar. Syst. doi:10.1016/j.jmarsys.2013.01.006

Dietze, H., Kriest, I., 2012. ^{137}Cs off Fukushima Dai-ichi, Japan – Model based estimates of dilution and fate. Ocean Sci. 8, 319–332. doi:10.5194/os-8-319-2012

Efurd, D.W., Knobeloch, G.W., Perrin, R.E., Barr, D.W., 1984. An estimate of the ^{237}Np produced during atmospheric testing. Helath Phys. 47, 786–787.

Egorov, V.N., Polikarpov, G.G., Stokozov, N.A., Mirzoyeva, N.Y., 2000. Estimation and prediction of ^{90}Sr and ^{137}Cs radioactive pollution of the Mediterrnean Basin from the Black Sea after the Chernobyl NPP accident.

Egorov, V.N., Povinec, P.P., Polikarpov, G.G., Stokozov, N.A., Gulin, S.B., Kulebakina, L.G., Osvath, I., 1999. ^{90}Sr and ^{137}Cs in the Black Sea after the Chernobyl NPP accident: Inventories, balance and tracer applications. J. Environ. Radioact. 43, 137–155. doi:10.1016/S0265-931X(98)00088-5

Eigl, R., Srncik, M., Steier, P., Wallner, G., 2013. ^{236}U/^{238}U and ^{240}Pu/^{239}Pu isotopic ratios in small (2 L) sea and river water samples. J. Environ. Radioact. 116, 54–58. doi:10.1016/j.jenvrad.2012.09.013

Eigl, R., Steier, P., Winkler, S.R., Sakata, K., Sakaguchi, A., 2016. First study on ^{236}U in the Northeast Pacific Ocean using a new target preparation procedure for AMS measurements. J. Environ. Radioact. 162–163, 244–250. doi:10.1016/j.jenvrad.2016.05.025

Elsässer, C., Wagenbach, D., Levin, I., Stanzick, A., Christl, M., Wallner, A., Kipfstuhl, S., Seierstad, I.K., Wershofen, H., Dibb, J., 2015. Simulating ice core ^{10}Be on the glacial-interglacial timescale. Clim. Past 11, 115–133. doi:10.5194/cp-11-115-2015

European Community to Radioactivity in the Mediterranean Sea (Marina Project). EUR 15564. pp. 427–439.

Eyrolle, F., Charmasson, S., Louvat, D., 2004. Plutonium isotopes in the lower reaches of the River Rhône over the period 1945-2000: Fluxes towards the Mediterranean Sea and sedimentary inventories. J. Environ. Radioact. 74, 127–138. doi:10.1016/j.jenvrad.2004.01.017

Fisher, N.S., Bjerregard, P., Fowler, S.W., 1983. Biokinetics of neptunium, plutonium, americium, and californium in phytoplankton. Limnol. Ocean. 28, 432–447.

Fleisher, M.Q., Anderson, R., 1991. Particulate matter digestion (from mg to 10's of g) and radionuclide blanks, in: Hurd, D.C., Spencer, D.W. (Eds.), Marine Particles: Analysis and Characterization. American Geophysical Union, Washington DC, pp. 221–222.

Fowler, S.W., Ballestra, S., Villeneuve, J.-P., 1990. Flux of transuranium nuclides and chlorinated hydrocarbons in the northwestern Mediterranean. Cont. Shelf Res. 10, 1005–1023.

Fowler, S.W., Noshkin, V.E., Rosa, J. La, Gastaud, J., 2000. Temporal variations in plutonium and americium inventories and their relation to vertical transport in the northwestern Mediterranean Sea. Limnol. Oceanogr. 45, 446–458.

Franić, Z., 2005. Estimation of the Adriatic Sea water turnover time using fallout ^{90}Sr as a radioactive tracer. J. Mar. Syst. 57, 1–12. doi:10.1016/j.jmarsys.2004.11.005

Fukai, R., Ballestra, S., Vas, D., 1982. Characteristics of the vertical transport of transuranic elements through the Mediterranean water column. VIes journées ëtud. Pollutions, Cannes, C. I. E. S. M 95–101.

Fukai, R., Holm, E., Ballestra, S., 1979. A note on vertical distribution of plutonium and americium in the Mediterranean Sea. Oceanol. Acta 2, 129–132.

Garcia-Orellana, J., 2004. Distribució i transferència de ^{137}Cs, ^{239,240}Pu i ^{210}Pb al mar Mediterrani: la conca Alguero - Balear. Universitat Autònoma de Barcelona.

Garcia-Orellana, J., Pates, J.M., Masqué, P., Bruach, J.M., Sanchez-Cabeza, J.A., 2009. Distribution of artificial radionuclides in deep sediments of the Mediterranean Sea. Sci. Total Environ. 407, 887–98. doi:10.1016/j.scitotenv.2008.09.018

Gascó, C., Antón, M.P., Delfanti, R., González, A.M., Meral, J., Papucci, C., 2002a. Variation of the activity concentrations and fluxes of natural (^{210}Po, ^{210}Pb) and anthropogenic (^{239,240}Pu, ^{137}Cs) radionuclides in the Strait of Gibraltar (Spain). J. Environ. Radioact. 62, 241–262. doi:10.1016/S0265-931X(01)00167-9

Gascó, C., Antón, M.P., Pozuelo, M., Meral, J., González, A.M., Papucci, C., Delfanti, R., 2002b. Distributions of Pu, Am and Cs in margin sediments from the western Mediterranean (Spanish coast). J. Environ. Radioact. 59, 75–89. doi:10.1016/S0265-931X(01)00037-6

Gascó, C., Antón, P., 1997. Influence of the Submarine Orography on the Distribution of Long-Lived Radionuclides in the Palomares Marine Ecosystem. J. Environ. Radioact. 34.

Gil-García, C., Rigol, a., Vidal, M., 2009. New best estimates for radionuclide solid-liquid distribution coefficients in soils, Part 1: Radiostrontium and radiocaesium. J. Environ. Radioact. 100, 690–696. doi:10.1016/j.jenvrad.2008.10.003

Gray, J., Jones, S.R., Smith, A.D., 1995. Discharges to the environment from the Sellafield site, 1951-1952. J. Radiol. Prot. 15, 99–131.

Hainbucher, D., Rubino, a., Cardin, V., Tanhua, T., Schroeder, K., Bensi, M., 2014. Hydrographic situation during cruise M84/3 and P414 (spring 2011) in the Mediterranean Sea. Ocean Sci. 10, 669–682.

doi:10.5194/os-10-669-2014

Hardy, E.P., Krey, P.W., Volchok, H.L., 1973. Global inventory and distribution of fallout plutonium. Nature 241, 444.

He, C., Hou, X., Zhao, Y., Wang, Z., Li, H., Chen, N., Liu, Q., 2011. Nuclear Instruments and Methods in Physics Research A. ^{129}I level in seawater near a nuclear power plant determined by accelerator mass spectrometer. Nucl. Inst. Methods Phys. Res. A 632, 152–156. doi:10.1016/j.nima.2010.12.182

He, P., Hou, X., Aldahan, A., Possnert, G., Yi, P., 2013. Iodine isotopes species fingerprinting environmental conditions in surface water along the northeastern Atlantic Ocean. Sci. Rep. 3, 2685.

Holm, E., Aarkrog, A., Ballestra, S., 1987. Determination of ^{237}Np in large volume samples of seawater by radiochemical procedure. J. Radioanal. Nucl. Chem. 115, 5–11. doi:10.1038/srep02685

Honda, M.C., Aono, T., Aoyama, M., Hamajima, Y., Kawakami, H., Kitamura, M., Masumoto, Y., Miyazawa, Y., Takigawa, M., Saino, T., 2012. Dispersion of artificial caesium-134 and -137 in the western North Pacific one month after the Fukushima accident. Geochem. J. 46, 1–9.

Hou, X., 2004. Application of ^{129}I as an environmental tracer 262, 67–75.

Hou, X., Hansen, V., Aldahan, A., Possnert, G., Christian, O., Lujaniene, G., 2009. A review on speciation of iodine-129 in the environmental and biological samples. Anal. Chim. Acta 632, 181–196. doi:10.1016/j.aca.2008.11.013

Hou, X.L., Dahlgaard, H., Nielsen, S.P., Kucera, J., 2002. Level and origin of Iodine-129 in the Baltic 61, 331–343.

Ikeuchi, Y., 2003. Temporal variations of ^{90}Sr and ^{137}Cs concentrations in Japanese coastal surface seawater and sediments from 1974 to 1998. Deep. Res. Part II Top. Stud. Oceanogr. 50, 2713–2726. doi:10.1016/S0967-0645(03)00143-7

International Atmomic Energy Agency (IAEA), 2006. Chernobyl's Legacy: Health, Environmental and Socio-Economic Impacts and Recommendations to the Governments of Belarus, the Russian Federation and Ukraine. Second Revis. version 54, 258.

International Atmomic Energy Agency (IAEA), 2005. Worldwide marine radioactivity studies (WOMARS): Radionuclide levels in oceans and seas. 197.

International Atmomic Energy Agency (IAEA), 2004. Sediment Distribution Coefficients and Concentration Factors for Biota in the Marine Environment. In technical report 422. Vienna.

JAEA, 2015. Japan Atomic Energy Agency: Database for Radioactive Substance Monitoring Data [WWW Document]. URL emdb.jaea.go.jp (accessed 5.15.15).

JNRA, 2015. Japan Nuclear Regulation Authority: Monitoring information of environmental radioactivity level. URL radioactivity.nsr.go.jp (accessed 6.15.15).

Kanda, J., 2013. Continuing ^{137}Cs release to the sea from the fukushima dai-ichi nuclear power plant through 2012. Biogeosciences 10, 6107–6113. doi:10.5194/bg-10-6107-2013

Kautsky, H., 1977. Die Vertikalverteilung radioaktiver Falloutprodukte im westlichen Mittelmeer in den Jahren 1970 und 1974. Dtsch. Hydrogr. Zeitschrift 30, 175–184.

Keeney-Kennicutt, W.L., Morse, J.W., 1984. The interaction of $Np(V)O^{2+}$ with common mineral surfaces in

dilute aqueous solutions and seawater. Mar. Chem. 15, 133–150.

Kelley, J.M., Bond, L.A., Beasley, T.M., 1999. Global distribution of Pu isotopes and Np-237. Sci. Total Environ. 237/238, 483–500.

Kenna, T.C., 2002. Determination of plutonium isotopes and neptunium-237 in environmental samples by inductively coupled plasma mass spectrometry with total sample dissolution. J. Anal. At. Spectrom. doi:10.1039/b205001c

Kenna, T.C., Masqué, P., Mas, J.L., Camara-Mor, P., Chamizo, E., Scholten, J., Eriksson, M., Sanchez-Cabeza, J.-A., Gastaud, J., Levy, I., 2012. Intercalibration of selected anthropogenic radionuclides for the GEOTRACES Program. Limnol. Oceanogr. Methods 10, 590–607. doi:10.4319/lom.2012.10.590

Klein, B., Roether, W., Manca, B.B., Bregant, D., Beitzel, V., Kovacevic, V., Luchetta, A., 1999. The large deep water transient in the Eastern Mediterranean. Deep. Res. Part I Oceanogr. Res. Pap. 46, 371–414. doi:10.1016/S0967-0637(98)00075-2

Krausová, I., Kucera, J., Svetlik, I., 2013. Determination of ^{129}I in biomonitors collected in the vicinity of a nuclear power plant by neutron activation analysis 295, 2043–2048. doi:10.1007/s10967-012-2200-5

Kuwabara, J., Yamamoto, M., Assinder, D.J., Komura, K., Ueno, K., 1996. Sediment profiles of ^{237}Np in the Irish Sea: estimation of the total amount of ^{237}Np from Sellafield. Radiochim. Acta 73, 73–81.

Lascaratos, A., Roether, W., Nittis, K., Klein, B., 1999. Recent changes in deep water formation and spreading in the eastern Mediterranean Sea: a review. Prog. Oceanogr. 44, 5–36. doi:10.1016/S0079-6611(99)00019-1

Lascaratos, A., Williams, R. G., Tragou, E., 1993. A mixed-layer study of the formation of Levantine intermediate water. J. Geophys. Res. Ocean. 98, 14739-14749. doi: 10.1029/93JC00912

Lee, S.-H., Mantoura, F.R., Povinec, P.P., Sanchez-Cabeza, J.A., Pontis, J.-L., Mahjoub, A., Noureddine, A., Boulahdid, M., Chouba, L., Samaali, M., Reguigui, N., 2006. Distribution of anthropogenic radionuclides in the water column of the South-western Mediterranean Sea, in: Radioactivity in the Environment. pp. 137–147.

Lee, S.H., La Rosa, J.J., Levy-Palomo, I., Oregioni, B., Pham, M.K., Povinec, P.P., Wyse, E., 2003. Recent inputs and budgets of ^{90}Sr, ^{137}Cs, ^{239,240}Pu and ^{241}Am in the northwest Mediterranean Sea. Deep. Res. Part II Top. Stud. Oceanogr. 50, 2817–2834. doi:10.1016/S0967-0645(03)00144-9

León Vintró, L., Mitchell, P.I., Condren, O.M., Downes, A.B., Papucci, C., Delfanti, R., 1999. Vertical and horizontal fluxes of plutonium and americium in the western Mediterranean and the Strait of Gibraltar. Sci. Total Environ. 237/238, 77–91.

Lindahl, P., Lee, S.-H., Worsfold, P., Keith-Roach, M., 2010. Plutonium isotopes as tracers for ocean processes: A review. Mar. Environ. Res. 69, 73–84. doi:10.1016/j.marenvres.2009.08.002

Lindahl, P., Roos, P., Holm, E., Dahlgaard, H., 2005. Studies of Np and Pu in the marine environment of Swedish e Danish waters and the North Atlantic Ocean. J. Environ. Radioact. 82, 285–301. doi:10.1016/j.jenvrad.2005.01.011

Lindahl, P., Ellmark, C., Gävert, T., Mattsson, S., Roos, P., Holm, E., Erlandsson, B., 2003. Long-term study of ^{99}Tc in the marine environment on the Swedish west coast. J. Environ. Radioact. 67, 145–156. doi:10.1016/S0265-931X(02)00176-5

Livingston, H.D., Kupferman, S.L., Bowen, V.T., Moore, R.M., 1984. Vertical profile of artificial radionuclides concentrations in the Central Arctic Ocean. Geochim. Cosmochim. Acta 48, 2195–2203.

Livingston, H.D., Casso, S.A., Bowen, V.T., Burke, J.C., 1979. Soluble and particle-associated fallout radionuclides in Mediterranean water and sediments. Rapp. Comm. Internat. Explor. Sci. Mer Médit 25/26, 71–76.

Ludwig, W., Dumont, E., Meybeck, M., Heussner, S., 2009. River discharges of water and nutrients to the Mediterranean and Black Sea: Major drivers for ecosystem changes during past and future decades? Prog. Oceanogr. 80, 199–217. doi:10.1016/j.pocean.2009.02.001

Maderich, V., Bezhenar, R., Heling, R., de With, G., Jung, K.T., Myoung, J.G., Cho, Y.K., Qiao, F., Robertson, L., 2014a. Regional long-term model of radioactivity dispersion and fate in the Northwestern Pacific and adjacent seas: Application to the Fukushima Dai-ichi accident. J. Environ. Radioact. 131, 4–18. doi:10.1016/j.jenvrad.2013.09.009

Maderich, V., Jung, K.T., Bezhenar, R., de With, G., Qiao, F., Casacuberta, N., Masque, P., Kim, Y.H., 2014b. Dispersion and fate of ^{90}Sr in the Northwestern Pacific and adjacent seas: global fallout and the Fukushima Dai-ichi accident. Sci. Total Environ. 494–495, 261–71. doi:10.1016/j.scitotenv.2014.06.136

Malanotte-Rizzoli et al., G., 2014. Physical forcing and physical/biochemical variability of the Mediterranean Sea: a review of unresolved issues and directions for future research. Ocean Sci. 10, 281–322. doi:10.5194/os-10-281-2014

Masson, O. et al., 2011. Tracking of Airborne Radionuclides from the Damaged Fukushima Dai-Ichi Nuclear Reactors by European Networks. Environ. Sci. Technol. 45, 7670–7677. doi:10.1021/es2017158

Maxwell, S.L., Culligan, B.A., Jones, V.D., Nichols, S.T., Noyes, G.W., 2010. Rapid determination of 237 Np and Pu isotopes in water by inductively-coupled plasma mass spectrometry and alpha spectrometry. J. Radioanal. Nucl. Chem. doi:10.1007/s10967-010-0825-9

Men, W., He, J., Wang, F., Wen, Y., Li, Y., Huang, J., Yu, X., 2015. Radioactive status of seawater in the northwest Pacific more than one year after the Fukushima nuclear accident. Sci. Rep. 5, 7757. doi:10.1038/srep07757ç

Merino, J., 1997. Estudios sobre el ciclo del plutonio en ecosistemas acuáticos. PhD Thesis. Universitat Autònoma de Barcelona.

Michel, R., Daraoui, a., Gorny, M., Jakob, D., Sachse, R., Tosch, L., Nies, H., Goroncy, I., Herrmann, J., Synal, H. a., Stocker, M., Alfimov, V., 2012. Iodine-129 and iodine-127 in European seawaters and in precipitation from Northern Germany. Sci. Total Environ. 419, 151–169. doi:10.1016/j.scitotenv.2012.01.009

Min, B. Il, Periáñez, R., Kim, I.G., Suh, K.S., 2013. Marine dispersion assessment of 137Cs released from the Fukushima nuclear accident. Mar. Pollut. Bull. 72, 22–33. doi:10.1016/j.marpolbul.2013.05.008

Miralles, J., Radakovitch, O., Cochran, J.K., Véron, a., Masqué, P., 2004. Multitracer study of anthropogenic contamination records in the Camargue, Southern France. Sci. Total Environ. 320, 63–72. doi:10.1016/S0048-9697(03)00443-1

Mishra S, et al., 2014. Activity Ratio of Caesium, Strontium and Uranium with Site Specific Distribution Coefficients in Contaminated Soil near Vicinity of Fukushima Daiichi Nuclear Power Plant. J. Chromatogr. Sep. Tech. 5, 250. doi:10.4172/2157-7064.1000250

Mitchell, P.I., Vives i Batlle, J., Downes, A.B., Condren, O.M., León Vintró, L., Sánchez-Cabeza, J.A., 1995. Recent Observations on the Physico-chemical Speciation of Plutonium in the Irish Sea and the Western Mediterranean. Appl. Radiat. Isot. 46, 1175–1190.

Molero, J., Sánchez-Cabeza, J.A., Merino, J., Pujol, L., Mitchell, P.I., Vidal-Quadras, A., 1995. Vertical Distribution of Radiocaesium , Plutonium and Americium in the Catalan Sea (Northwestern Mediterranean). J. Environ. Radioact. 26, 205–216.

Moran, J.E., 2002. Sources of iodine and iodine-129 in rivers. Water Resour. Res. 38, 1–10. doi:10.1029/2001WR000622

Morino, Y., Ohara, T., Nishizawa, M., 2011. Atmospheric behavior, deposition, and budget of radioactive materials from the Fukushima Daiichi nuclear power plant in March 2011. Geophys. Res. Lett. 38, 1–7. doi:10.1029/2011GL048689

Muramatsu, Y., Rühm, W., Yoshida, S., Tagami, K., Uchida, S., Wirth, E., 2000. Concentrations of ^{239}Pu and ^{240}Pu and their isotopic ratios determined by ICP-MS in soils collected from the Chernobyl 30-km zone. Environ. Sci. Technol. 34, 2913–2917.

Nagao, S., Kanamori, M., Ochiai, S., Tomihara, S., Fukushi, K., Yamamoto, M., 2013. Export of ^{134}Cs and ^{137}Cs in the Fukushima river systems at heavy rains by typhoon roke in september 2011. Biogeosciences 10, 6215–6223. doi:10.5194/bg-10-6215-2013

Nakamura, Y., 1991. Studies on the fishing ground formation of Sakhalin surf clam and the hydraulic environment in coastal region. Fukushima suisan shikenjo Res. Rep. 1–118.

Nishihara, L., Iwamoto, H., Suyama, K., 2012. Estimation of Fuel Compositions in Fukushima-Daiichi Nuclear Power Plant. Japan At. Energy Agency. doi:JAEA-Data/Code 2012-018

Noureddine, A., Benkrid, M., Maoui, R., Menacer, M., Boudjenoun, R., Kadi-hanifi, M., Lee, S.-H., Povinec, P.P., 2008. Radionuclide tracing of water masses and processes in the water column and sediment in the Algerian Basin. J. Environ. Radioact. 99, 1224–32. doi:10.1016/j.jenvrad.2008.02.007

Oguz T., Özsoy, E., Latif, M.A., Sur, H.I., Ünlüata, Ü., 1990. Modeling of hydraulically controlled exchange flow in the Bosphorus Strait, J. Phys. Oceanogr., 20, 945-965.

Oikawa, S., Takata, H., Watabe, T., Misonoo, J., Kusakabe, M., 2013. Distribution of the Fukushima-derived radionuclides in seawater in the Pacific off the coast of Miyagi, Fukushima, and Ibaraki Prefectures, Japan. Biogeosciences 10, 5031–5047. doi:10.5194/bg-10-5031-2013

Osterc, A., Stibilj, V., 2012. Influence of releases of I-129 from reprocessing plants on the marine environment of the North Adriatic Sea. Chemosphere 86, 1020–1027. doi:10.1016/j.chemosphere.2011.11.044

Ovchinnikov, I.M., Zats, V.I., Krivosheya, V.G, Udodov, A.I., 1985. Formation of the Eastern Mediterranean waters in the Adriatic Sea. Oceanology 25, 704-707.

Papucci, C., Delfanti, R., 1999. ^{137}Caesium distribution in the eastern Mediterranean Sea: recent changes and future trends. Sci. Total Environ. 237–238, 67–75. doi:10.1016/S0048-9697(99)00125-4

Papucci, S., Charmasson, S., Delfanti, R., Gascó, C., Mitchell, P., Sánchez - Cabeza, J.A., 1996. Time evolution and levels of manmade radioactivity in the Mediterranean Sea, in: Radionuclides in the Oceans. Les Ulis, p. 177.

Paul, M., Fink, D., Hollos, G., Kaufman, A., Kutschera, W., Magaritz, M., 1987. Measurement of ^{129}I concentrations in the environment after the Chernobyl reactor accident. Nucl. Instruments Methods Phys. Res. Sect. B Beam Interact. with Mater. Atoms 29, 341–345. doi:10.1016/0168-583X(87)90262-X

Pham, M.K., Chamizo, E., Mas-Malbuena, J.L., Miquel, J.-C., Martín, J., Osvath, I., Povinec, P.P., 2017. Impact of Saharan dust events on radionuclide levels in Monaco air and in the water column of the northwest Mediterranean Sea 166, 2–9. doi:10.1016/j.jenvrad.2016.04.014

Povinec, P.P., Aarkrog, A., Buesseler, K.O., Delfanti, R., Hirose, K., Hong, G.H., Ito, T., Livingston, H.D., Nies, H., Noshkin, V.E., Shima, S., Togawa, O., 2005. ^{90}Sr, ^{137}Cs and ^{239,240}Pu concentration surface water time series in the Pacific and Indian Oceans - WOMARS results. J. Environ. Radioact. 81, 63–87. doi:10.1016/j.jenvrad.2004.12.003

Povinec, P.P., Breier, R., Coppola, L., Groening, M., Jeandel, C., Jull, A.J.T., Kieser, W.E., Lee, S.-H., Liong Wee Kwong, L., Morgenstern, U., Park, Y.-H., 2011. Tracing of water masses using a multi isotope approach in the southern Indian Ocean. Earth Planet. Sci. Lett. 302, 14–26. doi:10.1016/j.epsl.2010.11.026

Povinec, P.P., Hirose, K., Aoyama, M., 2012. Radiostrontium in the western North Pacific: Characteristics, behavior, and the Fukushima impact. Environ. Sci. Technol. 46, 10356–10363. doi:10.1021/es301997c

Povinec, P.P., Hirose, K., Aoyama, M., 2013. Fukushima dai-ichi nuclear power plant, in: Fukushima Accident: Radioactivity Impact on the Environment. Elsevier, p. 365. doi:10.1016/B978-0-12-408132-1.00002-4

Quinto, F., Hrnecek, E., Krachler, M., Shotyk, W., Steier, P., Winkler, S.R., 2013. Measurements of ^{236}U in ancient and modern peat samples and implications for postdepositional migration of fallout radionuclides. Environ. Sci. Technol. 47, 5243–5250. doi:10.1021/es400026m

Quinto, F., Steier, P., Wallner, G., Wallner, A., Srncik, M., Bichler, M., Kutschera, W., Terrasi, F., Petraglia, A., Sabbarese, C., 2009. The first use of ^{236}U in the general environment and near a shutdown nuclear power plant. Appl. Radiat. Isot. 67, 1775–1780. doi:10.1016/j.apradiso.2009.05.007

Radakovitch, O., Charmasson, S., Arnaud, M., Bouisset, P., 1999. Pb-210 and caesium accumulation in the Rhone delta sediments. Estuar. Coast. Shelf Sci. 48, 77–92. doi:10.1006/ecss.1998.0405

Raisbeck, G.M., Yiou, F., 1999. ^{129}I in the oceans: origins and applications. Sci. Total Environ. 237–238, 31–41. doi:10.1016/S0048-9697(99)00122-9

Raisbeck, G.M., Yiou, F., Zhou, Z.Q., Kilius, L.R., 1995. ^{129}I from nuclear fuel reprocessing facilities at Sellafield (U.K.) and La Hague (France); potential as an oceanographie tracer. J. Mar. Syst. 6, 561–570. doi:10.1016/0924-7963(95)00024-J

Rao, U., Fehn, U., 1999. Sources and Reservoirs of Anthropogenic Iodine-129 in Western New York 63, 1927–1938.

Robens, E., Hauschild, J., Aumann, D. C., 1989. Iodine-129 in the Environment of a Nuclear Fuel reprocessing Plant: IV. ^{129}I and ^{127}I Undisturbed surface Soils. J. Environ. Radioactivity 9, 17-29.

Rodellas, V., Garcia-Orellana, J., Masqué, P., Feldman, M., Weinstein, Y., 2015. Submarine groundwater discharge as a major source of nutrients to the Mediterranean Sea. Proc. Natl. Acad. Sci. 112,

201419049. doi:10.1073/pnas.1419049112

Roether, W., Jean-Baptiste, P., Fourré, E., Sültenfuß, J., 2013. The transient distributions of nuclear weapon-generated tritium and its decay product ^{3}He in the mediterranean sea, 1952-2011, and their oceanographic potential. Ocean Sci. 9, 837–854. doi:10.5194/os-9-837-2013

Roether, W., Manca, B.B., Klein, B., Bregant, D., Georgopoulos, D., Beitzel, V., Kovacevic, V., Luchetta, A., 1996. Recent Changes in Eastern Mediterranean Deep Waters. Science (80-.). 271, 333–335. doi:10.1126/science.271.5247.333

Roether, W., Schlitzer, R., 1991. Eastern Mediterranean deep water renewal on the basis of chlorofluoromethane and tritium data. Dyn. Atmos. Ocean. 15, 333–354. doi:10.1016/0377-0265(91)90025-B

Rypina, I.I., Jayne, S.R., Yoshida, S., Macdonald, a. M., Douglass, E., Buesseler, K., 2013. Short-term dispersal of Fukushima-derived radionuclides off Japan: modeling efforts and model-data intercomparison. Biogeosciences 10, 4973–4990. doi:10.5194/bg-10-4973-2013

Sakaguchi, A., Kadokura, A., Steier, P., Takahashi, Y., Shizuma, K., Hoshi, M., Nakakuki, T., Yamamoto, M., 2012. Uranium-236 as a new oceanic tracer: A first depth profile in the Japan Sea and comparison with caesium-137. Earth Planet. Sci. Lett. 333–334, 165–170. doi:10.1016/j.epsl.2012.04.004

Sakaguchi, A., Kawai, K., Steier, P., Quinto, F., Mino, K., Tomita, J., Hoshi, M., Whitehead, N., Yamamoto, M., 2009. First results on ^{236}U levels in global fallout. Sci. Total Environ. 407, 4238–42. doi:10.1016/j.scitotenv.2009.01.058

Sanchez-Cabeza, J.A., Ortega, M., Merino, J., Masqué, P., 2002. Long-term box modelling of Cs-137 in the Mediterranean Sea. J. Mar. Syst. 33–34, 457–472.

Schroeder, K., et al., 2012. Circulation of the mediterranean sea and its variability, The Climate of the Mediterranean Region. doi:10.1016/B978-0-12-416042-2.00003-3

Schroeder, K., Ribotti, a., Borghini, M., Sorgente, R., Perilli, a., Gasparini, G.P., 2008. An extensive western Mediterranean deep water renewal between 2004 and 2006. Geophys. Res. Lett. 35, 1–7. doi:10.1029/2008GL035146

Šebesta, F., 1997. Composite sorbents of inorganic ion-exchangers and polyacrylonitrile binding matrix. J. Radioanal. Nucl. Chem. 220, 77–88. doi:10.1007/BF02035352

Sholkovitz, E.R., 1983. The geochemistry of plutonium in fresh and marine water environments. Earth-Science Rev. 19, 95–161.

Smith, J.N., Jones, E.P., Moran, S.B., Jr, W.M.S., Kieser, W.E., 2005. Iodine-129/CFC-11 transit times for Denmark Strait Overflow Water in the Labrador and Irminger Seas 110, 1–16. doi:10.1029/2004JC002516

Smith, J.N., Ellis, K.M., Kilius, L.R., 1998. ^{129}I and ^{137}Cs tracer measurements in the Arctic Ocean. Deep. Res. Part I Oceanogr. Res. Pap. 45, 959–984. doi:10.1016/S0967-0637(97)00107-6

Snyder, G., Aldahan, A., Possnert, G., 2010. Global distribution and long-term fate of anthropogenic I-129 in marine and surface water reservoirs. Geochemistry Geophys. Geosystems 11. doi:10.1029/2009GC002910

Snyder, G., Fehn, U., 2004. Global distribution of ^{129}I in rivers and lakes: Implications for iodine cycling in

surface reservoirs. Nucl. Instruments Methods Phys. Res. Sect. B Beam Interact. with Mater. Atoms 223–224, 579–586. doi:10.1016/j.nimb.2004.04.107

Steier, P., Bichler, M., Keith Fifield, L., Golser, R., Kutschera, W., Priller, A., Quinto, F., Richter, S., Srncik, M., Terrasi, P., Wacker, L., Wallner, A., Wallner, G., Wilcken, K.M., Maria Wild, E., 2008. Natural and anthropogenic ^{236}U in environmental samples. Nucl. Instruments Methods Phys. Res. Sect. B Beam Interact. with Mater. Atoms 266, 2246–2250. doi:10.1016/j.nimb.2008.03.002

Steinhauser, G., Brandl, A., Johnson, T.E., 2014. Comparison of the Chernobyl and Fukushima nuclear accidents: A review of the environmental impacts. Sci. Total Environ. 470–471, 800–817. doi:10.1016/j.scitotenv.2013.10.029

Steinhauser, G., Schauer, V., Shozugawa, K., 2013. Concentration of strontium-90 at selected hot spots in Japan. PLoS One 8, 1–5. doi:10.1371/journal.pone.0057760

Stohl, a., Seibert, P., Wotawa, G., Arnold, D., Burkhart, J.F., Eckhardt, S., Tapia, C., Vargas, a., Yasunari, T.J., 2012. Xenon-133 and caesium-137 releases into the atmosphere from the Fukushima Dai-ichi nuclear power plant: Determination of the source term, atmospheric dispersion, and deposition. Atmos. Chem. Phys. 12, 2313–2343. doi:10.5194/acp-12-2313-2012

Stratford, K., Williams, R.G., Drakopoulos, P.G., 1998. Estimating climatological age from a model-derived oxygen-age relationship in the Mediterranean. J. Mar. Syst. 18, 215–226. doi:10.1016/S0924-7963(98)00013-X

Suzuki, T., Otosaka, S., Kuwabara, J., Kawamura, H., Kobayashi, T., 2013. Iodine-129 concentration in seawater near Fukushima before and after the accident at the Fukushima Daiichi Nuclear Power. Clim. Biogeosciences 3839–3847. doi:10.5194/bg-10-3839-2013

Tanhua, T., Hainbucher, D., Schroeder, K., Cardin, V., Álvarez, M., Civitarese, G., 2013. The Mediterranean Sea system: a review and an introduction to the special issue. Ocean Sci. 9, 789–803. doi:10.5194/os-9-789-2013

TEPCO, 2014. Tepco Electric Power Company: Towards reducing the risk of contaminated water in tanks [WWW Document]. URL http://www.tepco.co.jp/en/nu/fukushima-np/handouts/2014/images/handouts_141016_04-e.pdf (accessed 6.15.15).

TEPCO, 2015a. Tokyo Electric Power Company [WWW Document]. URL www.tepco.co.jp (accessed 6.15.15).

TEPCO, 2015b. Situation of Storage and Treatment of Accumulated Water including Highly Concentrated Radioactive Materials at Fukushima Daiichi Nuclear Power Station (115 4, 1–5.

Tsimplis, M.N., Zervakis, V., Josey, S.A., Peneva, E.L., Struglia, M. V., Stanev, E. V., Theocaris, A., Lionello, P., Malanotte-Rizzoli, P., Artale, V., E. Tragou, Oguz, T., 2006. Changes in the oceanography of the Mediterranean Sea and their link to climate variability, in: Mediterranean Climate Variability. Lionello, P., Malanotte-Rizzoli, P., Boscolo, R. (Ed.), . Elsevier B.V., Amsterdam, p. 227.

UNEP, 1992. Assessment of the State of Pollution of the Mediterranean Sea by Radioactive Substances. Athens.

United Nations Scientific Committee on the Effects of Atomic Radiation (UNSCEAR), 2000. Sources and Effects of Ionizing Radiation, Annexes: Exposures to the public from man-made sources of radiation. doi:10.1158/0008-5472.CAN-10-0276

Tsumune, D., Aoyama, M., Tsubono, T., Tateda, Y., Misumi, K., Hayami, H., Toyoda, Y., Maeda, Y., Yoshida, Y., Uematsu, M., 2014. Reconstruction of ^{137}Cs activity in the ocean following the Fukushima Daiichi Nuclear Power Plant Accident. Geophys. Res. Lett. Abstr. 16, 9566.

Tsumune, D., Tsubono, T., Aoyama, M., Hirose, K., 2012. Distribution of oceanic ^{137}Cs from the Fukushima Dai-ichi Nuclear Power Plant simulated numerically by a regional ocean model. J. Environ. Radioact. 111, 100–108. doi:10.1016/j.jenvrad.2011.10.007

Tsumune, D., Tsubono, T., Aoyama, M., Uematsu, M., Misumi, K., Maeda, Y., Yoshida, Y., Hayami, H., 2013. One-year, regional-scale simulation of ^{137}Cs radioactivity in the ocean following the Fukushima Dai-ichi Nuclear Power Plant accident. Biogeosciences 10, 5601–5617. doi:10.5194/bg-10-5601-2013

Vockenhuber, C., Casacuberta, N., Christl, M., Synal, H.A., 2015. Accelerator Mass Spectrometry of ^{129}I towards its lower limits. Nucl. Instruments Methods Phys. Res. Sect. B Beam Interact. with Mater. Atoms 361, 445–449. doi:10.1016/j.nimb.2015.01.061

Wagner, M.J.M., Dittrich-Hannen, B., Synal, H.A., Suter, M., Schotterer, U., 1996. Increase of ^{129}I in the environment. Nucl.Instrum.Meth.B 113, 490–494. doi:10.1016/0168-583X(95)01348-2

Waldman, R., Somot, S., Herrmann, M., Testor, P., Estournel, C., Sevault, F., Prieur, L., Mortier, L., Coppola, L., Taillandier, V., Conan, P., Dausse, D., 2016. Estimating dense water volume and its evolution for the year 2012-2013 in the Northwestern Mediterranean Sea: An observing system simulation experiment approach. J. Geophys. Rs. Oceans 121. Doi: 10.1002/2016JC011694

Waples, J., Orlandini, K. a., 2010. A method for the sequential measurement of yttrium-90 and thorium-234 and their application to the study of rapid particle dynamics in aquatic systems. Limnol. Oceanogr. Methods 8, 661–677. doi:10.4319/lom.2010.8.661

Winkler, S.R., Steier, P., Carilli, J., 2012. Bomb fall-out ^{236}U as a global oceanic tracer using an annually resolved coral core. Earth Planet. Sci. Lett. 359–360, 124–130. doi:10.1016/j.epsl.2012.10.004

Wüst, G., 1961. On the vertical circulation of the Mediterranean Sea. J. Geophys. Res. 66, 3261. doi:10.1029/JZ066i010p03261

Yamashiki, Y., Onda, Y., Smith, H.G., Blake, W.H., Wakahara, T., Igarashi, Y., Matsuura, Y., Yoshimura, K., 2014. Initial flux of sediment-associated radiocesium to the ocean from the largest river impacted by Fukushima Daiichi Nuclear Power Plant. Sci. Rep. 4, 3714. doi:10.1038/srep03714

Yiou, F., Raisbeck, G.M., Zhou, Z.Q., Kilius, L.R., 1997. I-129 in the Mediterranean Sea. Radioprot. - Colloq. 32.

Yu, W., He, J., Lin, W., Li, Y., Men, W., Wang, F., Huang, J., 2015. Distribution and risk assessment of radionuclides released by Fukushima nuclear accident at the northwest Pacific. J. Environ. Radioact. 142, 54–61. doi:10.1016/j.jenvrad.2015.01.005

Zhao, X.-L., Kieser, W.E., Litherland, A.E., 1998. The AMS Analysis of I-129 and Cs-135: Development of tools for ocenographic tracind and pollution source identification.

Appendix

A.1. Concentrations of ^{90}Sr, ^{137}Cs and ^{134}Cs, ^{137}Cs/^{90}Sr activity ratios during *Daisan Kaiyo Maru* cruise, September 2013.

Table A1. Concentrations of ^{90}Sr, ^{137}Cs and ^{134}Cs, ^{137}Cs/^{90}Sr activity ratios, sampling dates and location, salinity and temperature in seawater samples collected in the coast off Japan during the *Daisan Kaiyo Maru* cruise, September 2013. All activities are decay corrected to sampling date. Samples that were not available for the determination of ^{90}Sr are shown as '-'. Northern beach samples (NBS), samples 40 and 44, were collected from the sea surface.

Station ID, Lat, Long, Bottom Depth	Sample ID	Sampling Date	Depth (m)	Temp. (ºC)	Salinity	^{90}Sr (Bq·m^{-3})	^{137}Cs (Bq·m^{-3})	^{134}Cs (Bq·m^{-3})	^{137}Cs/^{90}Sr
St. 1 (NP0)	1	10-Sep-13 22:00	2		32.31	8.9 ± 0.4	34 ± 1	15.4 ± 0.4	3.8 ± 0.2
37.42 ºN	2	10-Sep-13 22:15	2			-	32 ± 1	13.5 ± 0.4	
141.05 ºE	3	10-Sep-13 22:30	2	23.18	31.40	7.4 ± 0.3	21 ± 1	8.9 ± 0.3	2.8 ± 0.1
15 m	4	10-Sep-13 22:30	5	23.24	32.99	3.3 ± 0.2	15.6 ± 0.4	6.4 ± 0.3	4.7 ± 0.3
	5	10-Sep-13 22:30	10	22.66	33.39	1.2 ± 0.1	8.8 ± 0.3	3.2 ± 0.2	7.2 ± 0.5
	6	11-Sep-13 02:30	2		32.10	-	124 ± 3	54 ± 1	
St. 2 (RA6)	7	10-Sep-13 21:50	2		33.24	3.7 ± 0.2	9.5 ± 0.3	4.0 ± 0.2	2.6 ± 0.1
37.42 ºN									
141.08 ºE									
St. 2.1 (NPE1)	8	11-Sep-13 05:00	2		33.31	2.7 ± 0.1	7.3 ± 0.2	2.7 ± 0.2	2.7 ± 0.2
37.33 ºN									
141.08 ºE									
St. 2.2 (NPE2)	9	11-Sep-13 11:45	2		30.58	1.2 ± 0.1	9.1 ± 0.3	3.6 ± 0.2	7.5 ± 0.5
37.50 ºN									
141.08 ºE									
St. 3 (NP2)	10	10-Sep-13 14:30	2		33.44	0.78 ± 0.07	2.7 ± 0.1	0.42 ± 0.10	3.4 ± 0.3
37.42 ºN	11	10-Sep-13 14:45	2			-	2.3 ± 0.1	0.33 ± 0.06	
141.10 ºE	12	10-Sep-13 15:00	5	23.46	33.44	-	1.7 ± 0.1	0.48 ± 0.16	
30 m	13	10-Sep-13 15:00	15	23.06	33.51	2.6 ± 0.2	1.6 ± 0.1	< 0.2	0.6 ± 0.1
	14	10-Sep-13 15:00	25	22.56	33.56	0.86 ± 0.06	1.6 1.20.1	< 0.2	1.9 ± 0.2
St. 4 (RA5)	15	10-Sep-13 13:45	2		33.48	0.92 ± 0.08	2,0 ± 0.1	< 0.2	2.1 ± 0.2
37.42 ºN									
141.14 ºE									
St. 5 (NP1)	16	10-Sep-13 09:30	2		33.40	1.1 ± 0.1	1.9 ± 0.1	0.88 ± 0.17	1.7 ± 0.2
37.42 ºN	17	10-Sep-13 09:35	2			-	1.6 ± 0.1	< 0.2	
141.18 ºE	18	10-Sep-13 09:45	20	21.69	33.67	-	2.0 ± 0.1	< 0.2	
60 m	19	10-Sep-13 09:45	40	21.26	33.74	0.79 ± 0.06	1.9 ± 0.1	< 0.2	2.4 ± 0.2
	20	10-Sep-13 09:45	55	20.74	33.72	0.72 ± 0.07	2.9 ± 0.2	0.65 ± 0.12	4.0 ± 0.4
St. 6 (RA4)	21	10-Sep-13 08:00	2		33.50	1.1 ± 0.1	1.9 ± 0.1	0.36 ± 0.11	1.7 ± 0.2
37.42 ºN									
141.24 ºE									
St. 7 (NP3)	22	10-Sep-13 03:00	2		33.52	1.4 ± 0.1	1.6 ± 0.1	< 0.2	1.1 ± 0.1
37.42 ºN	23	10-Sep-13 03:15	20	22.66	33.55	-	1.9 ± 0.1	< 0.2	
141.30 ºE	24	10-Sep-13 03:15	50	19.01	33.89	1.3 ± 0.1	1.8 ± 0.1	< 0.2	1.4 ± 0.1
120 m	25	10-Sep-13 03:15	80	17.50	33.92	-	1.8 ± 0.1	< 0.2	
	26	10-Sep-13 03:15	115	11.01	33.69	1.8 ± 0.1	2.2 ± 0.1	< 0.2	1.2 ± 0.1
	27	10-Sep-13 03:20	2			-	1.7 ± 0.1	0.34 ± 0.13	
St. 8 (N01)	28	11-Sep-13 20:00	2		33.51	0.63 ± 0.05	1.9 ± 0.1	< 0.2	3.0 ± 0.3
37.42 ºN									
141.50 ºE									
St. 9 (RA3b)	29	10-Sep-13 00:14	2		33.47	0.71 ± 0.07	2.1± 0.1	0.84 ± 0.20	3.0 ± 0.3
37.25 ºN									
141.08 ºE									
St. 10 (RA3)	30	9-Sep-13 22:30	2		33.47	1.8 ± 0.1	4.7 ± 0.2	2.6 ± 0.2	2.6 ± 0.2
37.00 ºN									
141.08 ºE									
St. 11 (RA2)	31	9-Sep-13 21:40	2		33.54	1.2 ± 0.1	2.3 ± 0.2	0.35 ± 0.16	1.9 ± 0.2
37.00 ºN									
141.17 ºE									

Table A1. Continuation.

Station ID, Lat, Long, Bottom Depth	Sample ID	Sampling Date	Depth (m)	Temp. (ºC)	Salinity	^{90}Sr ($Bq \cdot m^{-3}$)	^{137}Cs ($Bq \cdot m^{-3}$)	^{134}Cs ($Bq \cdot m^{-3}$)	$^{137}Cs/^{90}Sr$
St. 12 (RA1) 37.00 ºN 141.33 ºE	32	9-Sep-13 20:20	2		33.52	0.83 ± 0.07	2.0 ± 0.1	1.00 ± 0.16	2.4 ± 0.3
St. 13 (N02) 37.00 ºN 141.50 ºE	33	9-Sep-13 16:30	2		33.52	1.4 ± 0.1	2.1 ± 0.1	0.58 ± 0.23	1.5 ± 0.1
St. 14 (F1)	34	9-Sep-13 04:15	2		33.54	0.72 ± 0.05	1.7 ± 0.1	< 0.2	2.4 ± 0.2
36.50 ºN	35	9-Sep-13 04:30	50	14.74	33.39	-	1.9 ± 0.1	0.42 ± 0.15	
141.50 ºE	36	9-Sep-13 04:30	100	10.27	33.73	-	1.8 ± 0.1	< 0.2	
1250 m	37	9-Sep-13 04:30	200	6.70	33.80	-	1.9 ± 0.1	< 0.2	
	38	9-Sep-13 04:30	300	3.30	33.57	-	1.4 ± 0.1	< 0.2	
	39	9-Sep-13 04:30	500	3.28	33.89	-	0.91 ± 0.05	< 0.2	
Nobiru 38.3650 ºN 141.1607 ºE	40	14-Sep-13 01:45	NBS		18.54	1.8 ± 0.5	9.0 ± 0.2	3.6 ± 0.1	5.1 ± 1.5
Nobiru	41	14-Sep-13 01:55	GW		18.55	1.4 ± 0.1	16.2 ± 0.5	6.4 ± 0.3	12.0 ± 0.9
38.3650 ºN	42	14-Sep-13 03:13	GW		4.31	-	9.8 ± 0.3	4.9 ± 0.3	
141.1607 ºE									
Nagahama 38.2610 ºN 141.0198 ºE	43	14-Sep-13 06:42	GW		29.00	1.2 ± 0.1	10.3 ± 0.3	4.7 ± 0.2	8.7 ± 0.7
Nagahama	44	14-Sep-13 06:45	NBS		28.51	1.5 ± 0.3	43± 1	17± 1	28 ± 6
38.2610 ºN	45	14-Sep-13 07:30	GW		25.28	0.99 ± 0.08	23.3 ± 0.5	10.1 ± 0.3	24 ± 2
141.0198 ºE									

A.2. Vertical distribution of ^{90}Sr, ^{137}Cs and ^{134}Cs concentrations at stations 1, 3, 5, 7 and 14.

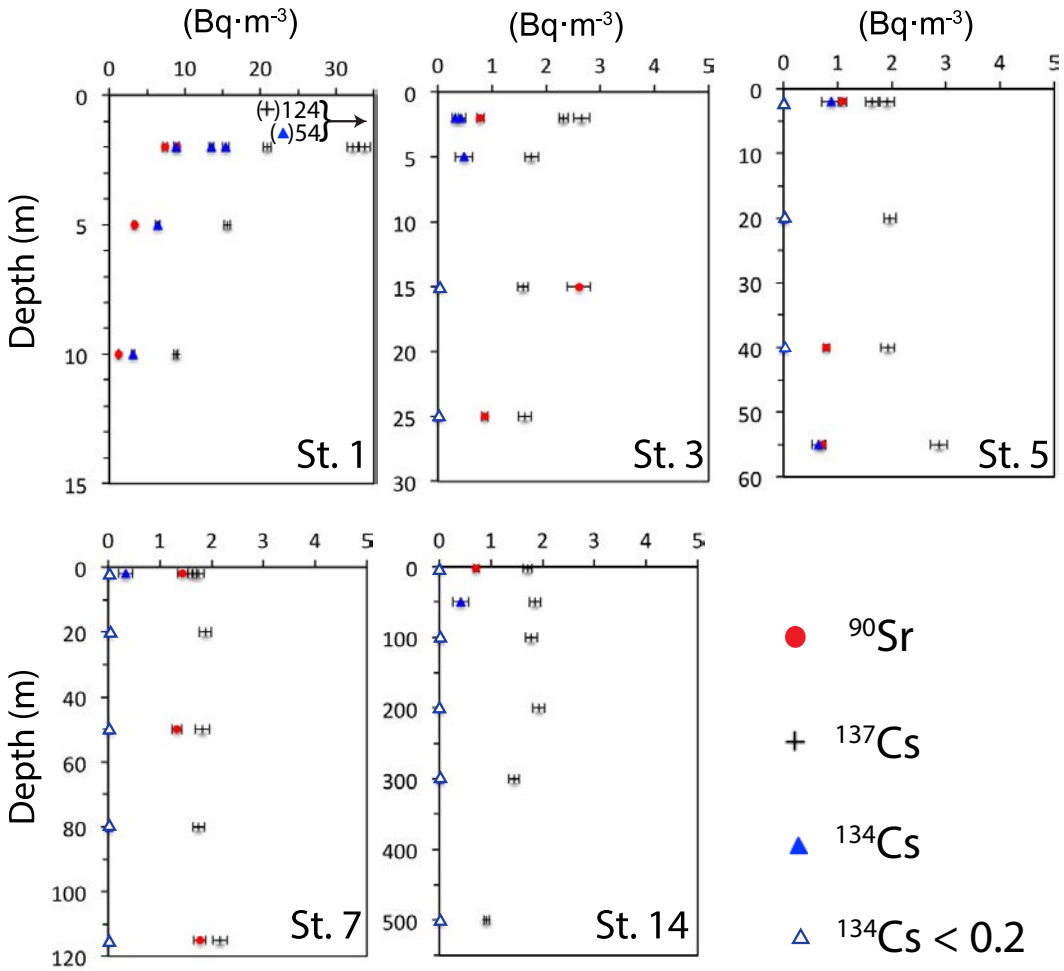

Figure A.1. Vertical distribution of ^{90}Sr, ^{137}Cs and ^{134}Cs concentrations at stations 1, 3, 5, 7 and 14.

A.3. $^{137}Cs/^{90}Sr$ activity ratio calculated in seawater samples with measurable ^{134}Cs collected in September 2013.

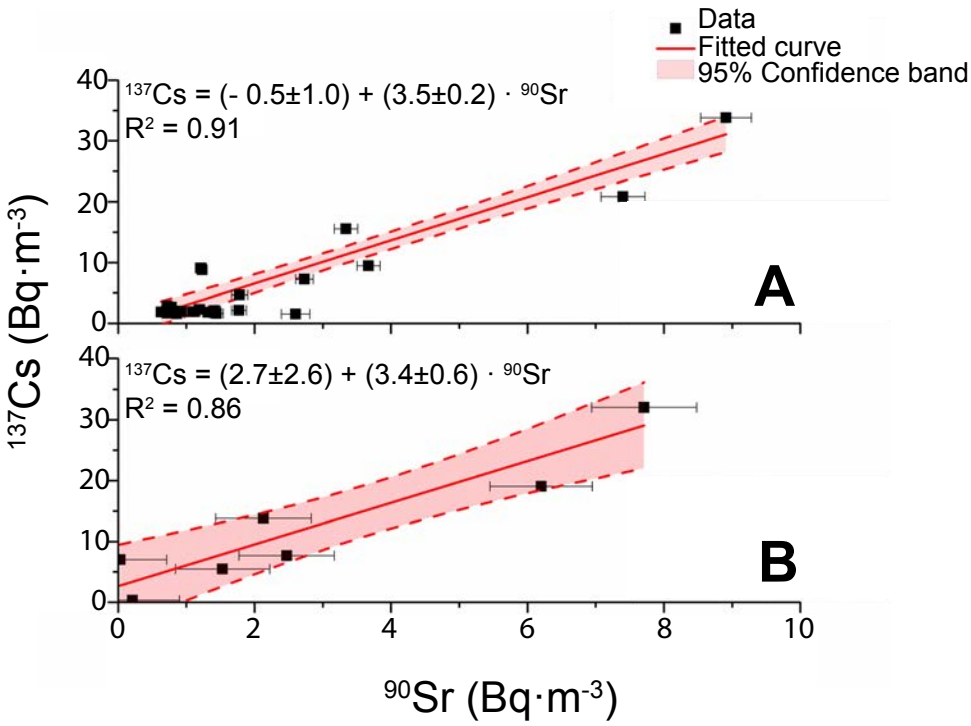

Figure A.2. $^{137}Cs/^{90}Sr$ activity ratio calculated in seawater samples with measurable ^{134}Cs collected in September 2013. Regression using data (A) with pre-Fukushima concentrations; and (B) without pre-Fukushima concentrations. For the calculation in (B), the pre-Fukushima concentrations are considered as the average of ^{137}Cs (1.8 ± 0.3 Bq·m^{-3}) and ^{90}Sr (1.2 ± 0.7 Bq·m^{-3}) in samples without ^{134}Cs. Regressions were performed weighting both 'x' and 'y' errors.

A.4. Inventories of ^{236}U and ^{129}I in the Mediterranean Sea

The inventories were calculated for 10 different regions dividing the Mediterranean as shown in Figure A.3 and (Sanchez-Cabeza et al., 2002). The calculated inventories ($at \cdot m^{-2}$) and total masses (kg) of ^{236}U and ^{129}I for each region are listed in Table A.2.

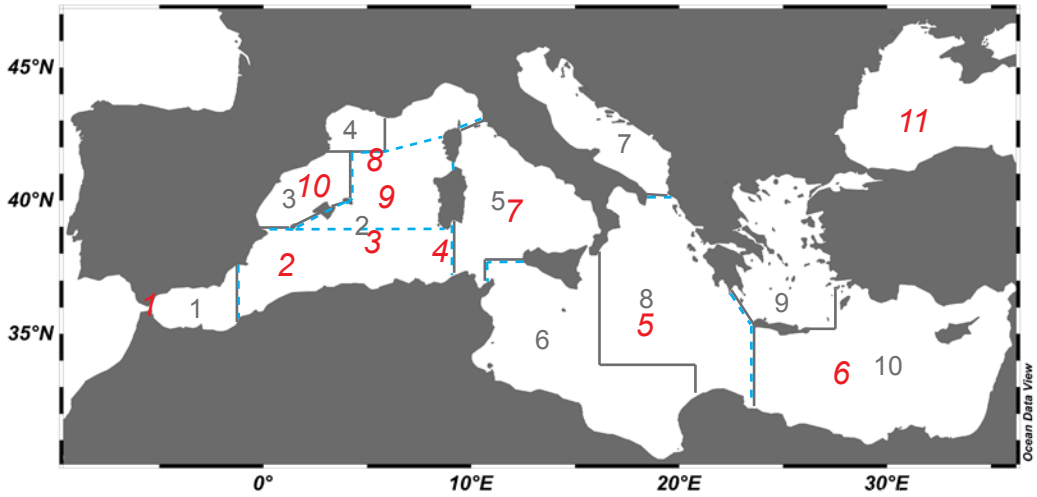

Figure A.3. The 10 regions considered for the calculation of radionuclide inventories in grey (adapted from (Sanchez-Cabeza et al., 2002)): 1. Alboran Sea, 2. Central-Occidental Basin, 3. Catalan Sea, 4. Gulf of Lions, 5. Tyrrhenian Sea, 6. Lybian Sea, 7. Adriatic Sea, 8. Ionian Sea, 9. Aegean Sea and 10. Levantine Basin. In discontinuous blue line, the model of Bethoux and Gentili (1996) divides the Alguero-Balear (regions 2 to 4 in Sanchez Cabeza et al., (2002)) in Northern (Catalan Sea, Gulf of Lions and Ligurian Sea), Central and Southern components (discontinuos line in blue). For ease, we will name these regions as Northern, Central and Southern Alguero-Balear. Bethoux and Gentili (1996) also consider the Ionian Sea as a single region resulting from the sum of regions 6 and 8 of Sanchez Cabeza et al., (2002). Red numbers (1-11) show stations sampled during *GA04S-MedSeA* (May 2013) and *Black Sea-Fe-Vici* (September 2015) cruises.

Table A.2. Calculated inventories and total masses of ^{236}U and ^{129}I in the Mediterranean Sea in May 2013.

Region	^{236}U Inventory		^{129}I Inventory	
	$x10^{12}$ at·m^{-2}	kg	$x10^{12}$ at·m^{-2}	kg
1. Alboran Sea	23 ± 1	0.82 ± 0.16	132 ± 8	2.1 ± 0.5
2. Alguero-Balear	35 ± 3	6.2 ± 0.8	212 ± 18	20 ± 2
3. Catalan Sea	15.1 ± 0.3	0.34 ± 0.02	99 ± 2	1.2 ± 0.1
4. Gulf of Lions	25 ± 2	0.51 ± 0.05	166 ± 4	1.9 ± 0.1
5. Tyrrhenian Sea	33 ± 2	2.2 ± 0.2	193 ± 21	7.2 ± 0.9
6. Lybian Sea	19.1 ± 0.5	3.0 ± 0.2	113 ± 4	9.6 ± 0.6
7. Adriatic Sea	14.3 ± 0.2	0.58 ± 0.03	85 ± 4	1.9 ± 0.1
8. Ionian Sea	47 ± 6	12 ± 2	280 ± 37	40 ± 6
9. Aegean Sea	27 ± 4	0.76 ± 0.11	161 ± 21	2.5 ± 0.3
10. Levantine Basin	22 ± 3	4.0 ± 0.6	149 ± 27	15 ± 3
Total mass (kg):				
WMS		10 ± 1		33 ± 4
EMS		21 ± 3		68 ± 10
Mediterranean Sea		31 ± 4		101 ± 14

A.5. Estimates of the inputs of ^{236}U and ^{129}I to the Mediterranean Sea from the global fallout and the Marcoule spent nuclear fuel reprocessing plant.

We used the box model of Bethoux and Gentili (1996) to estimate the radionuclide concentrations in the water column of the Mediterranean Sea assuming different radionuclide sources and release scenarios. The model divides the Mediterranean Sea in 8 regions (the Alguero-Provençal Basin, named Alguero–Balear in this study; the Alboran, the Tyrrhenian, the Adriatic, the Ionian and the Aegean Seas, and the Levantine Basin) that are sub-divided in 3–4 depth layers (surface, intermediate, deep and also, a very deep layer for the Ionian Sea and the Levantine Basin), as shown in Figure A.3. Box volumes and water exchange rates were obtained based on circulation studies, topography and geographical features (Bethoux and Gentili, 1996).

The quality of the model output is assessed by calculating the squared distance between the estimated and the measured concentrations (Table A.3.1 for ^{129}I and Table A.3.2 for ^{236}U). For ^{129}I, several scenarios were tested including varying inputs of liquid and gaseous ^{129}I scaled from the input functions provided in (Hou et al., 2009). In the Western Basin, the best fits were achieved when liquid releases were larger than 50%. This result agrees with our assumption that most of the liquid releases should have arrived to the sea. In the Eastern Basin, the fitting inproved significantly when increasing the atmospheric input (independently of the liquid release), which is expected when considering the distance from the reprocessing plant and the limited water exchange between the Western and the Eastern Basins. Following the assumption of (He et al., 2013), we consider that about 50% of the gaseous ^{129}I was likely deposited near Marcoule. From the reminaing 50%, about 75% of the air trajectories from the reprocessing plant arrive to the Mediterranean Sea (Supplemental A.3). Thus, we consider that the input of gaseous releases should be less than 40% (and probably more than 20%) of the total gaseous ^{129}I input of 145 kg reported in (Hou et al., 2009). All these scenarios included inputs from global fallout, liquid ^{129}I inputs from Marcoule and a 5-year delayed input of gaseous ^{129}I from Marcoule. A longer time delay of 10-year was also tested (not shown in Table A.3.1.) for the gaseous releases and for several scenarios, obtaining worse results.

Table A.3.1. Model output assessed by the least square distance between measured and simulated concentrations of ^{129}I. Eastern Basin (blue), the Western Basin (green) and the whole Mediterranean Sea (red).

Liquid ^{129}I from Marcoule: percentage out of 45 kg (Hou et al., 2009)	Gaseous ^{129}I from Marcoule: percentage out of 145 kg (Hou et al., 2009)								
	0%	10%	20%	30%	40%	50%	60%	80%	100%
0%	1,48		1,13		0,85		0,63	0,98	0,35
	1,22		0,55		0,39		0,73	1,59	2,96
	2,70		1,68		1,24		1,36	2,57	3,31
20%	1,42		1,08		1,20		0,59	0,44	0,34
	0,95		0,44		0,47		0,94	1,96	3,48
	2,36		1,52		1,67		1,53	2,39	3,82
40%	1,36		1,03		0,77		0,56	0,42	0,33
	0,73		0,64		0,53		1,20	2,37	4,05
	2,08		1,67		1,30		1,76	2,79	4,38
50%	1,33	1,16	1,01	0,87	0,75	0,64			
	0,64	0,44	0,36	0,42	0,60	0,91			
	1,96	1,60	1,37	1,29	1,35	1,55			
60%	1,30	1,13	0,98	0,85	0,73	0,61	0,54	0,40	0,32
	0,56	0,40	0,36	0,46	0,68	1,16	1,50	2,83	4,68
	1,85	1,53	1,35	1,31	1,41	1,77	2,04	3,23	5,00
70%	1,27	1,11	0,96	0,83	0,71	0,61			
	0,49	0,37	0,37	0,51	0,77	1,16			
	1,76	1,48	1,34	1,34	1,48	1,77			
80%	1,24	1,08	0,94	0,81	0,69	1,08	0,51	0,38	0,31
	0,44	0,35	0,40	0,57	0,87	1,30	1,86	3,35	5,35
	1,68	1,44	1,34	1,38	1,57	2,38	2,36	3,73	5,67
90%	1,21	1,06	0,91	0,79	0,68	0,58			
	0,56	0,55	0,66	0,89	0,99	1,46			
	1,77	1,61	1,57	1,68	1,67	2,04			
100%	1,19	1,03	0,89	0,77	0,66	0,56	0,48	0,37	0,31
	0,36	0,36	0,49	0,74	1,12	1,63	2,26	3,91	6,07
	1,55	1,39	1,38	1,51	1,78	2,19	2,74	4,28	6,38

The level of agreement between the simulated and measured concentrations of ^{236}U is shown for the Eastern Basin (blue), Western Basin (green) and the whole Mediterranean Sea (red) in Table A.3.2. Several release scenarios led to reasonable good fittings between simulated and measured concentrations of ^{236}U: 1) when the liquid input from Marcoule was low (<15%) and the global fallout 2.5 times higher than expected; 2) when the liquid input from Marcoule was larger (about 45% of 45 kg) and the global fallout was 900 kg, that is the estimate of (Sakaguchi et al., (2009)); or 3) when both inputs from global fallout and Marcoule were in the mid range (global fallout 1.5 to 2 times, that is 1350-1800 kg); Marcoule ~30% (13.5 kg)). Considering the concentrations of ^{236}U reported in seawater and the atmospheric models, the most probable estimate for the total global fallout release is of about 900 kg. Thus, we conclude that under these circumstances ((1 to 1.5) × 900 kg for global fallout), Marcoule would have added about 10-20 kg or 30-45% liquid ^{236}U (out of the total of 45 kg suggested for liquid ^{129}I by (Hou et al., 2009)).

Table A.3.2. Model output assessed by the least square distance between measured and simulated concentrations of ^{236}U. Eastern Basin (blue), the Western Basin (green) and the whole Mediterranean Sea (red).

		^{236}U from global fallout: assuming X times the total release to the ocean of 900 kg (Sakaguchi et al., 2009)			
		x1	x1,5	x2	x2,5
Liquid ^{236}U from Marcoule: percentage out of 45 kg, similar to 129I (Hou et al., 2009)	0%	4,67	3,15	2,02	1,27
		3,24	2,09	1,32	0,93
		7,91	5,24	3,33	2,20
	15%	2,93	1,82	1,09	0,74
		2,04	1,32	0,99	1,04
		4,97	3,14	2,07	1,78
	30%	1,68	0,97	0,64	0,69
		1,36	1,08	1,18	1,66
		3,04	2,04	1,82	2,36
	45%	0,92	0,61	0,68	1,13
		1,19	1,34	1,88	2,81
		2,11	1,95	2,56	3,94
	60%	0,65	0,74	1,21	2,06
		1,53	2,13	3,10	4,46
		2,18	2,86	4,31	6,52

A.6. Air mass trajectories from Marcoule and other European reprocessing plants

We computed the archived air mass trajectories using the NOAA Air Resources Laboratory Hybrid Single-Particle Lagrangian Integrated Trajectory (HYSPLIT) model ((Draxler and Hess, 1998; Stein et al., 2015); http://ready.arl.noaa.gov/HYSPLIT_traj.php) in order to check if gaseous releases from Marcoule, and more distant Sellafield and La Hague reprocessing plants, could have contributed to the inventory of ^{129}I in the Mediterranean sea. The GDAS (1 degree, global) meteorology and the normal form of the model were used to obtain weekly air mass trajectories throughout year 2015 (2013 was not available). We assigned point-like sources for the three European reprocessing plants: Marcoule (44.1ºN, 4.7ºE), La Hague (49.7ºN, 1.9ºW) and Sellafield (54.4ºN, 3.5ºW). Sources were set at 50 m high and trajectories were run for 1 week (168 h), which is less time than the residence time of ^{129}I in the troposphere (2 to 4 weeks (Aldahan et al., 2007)). The air mass trajectories (Figure A.3) showed that 75% of the trajectories from Marcoule reached the Mediterranean Sea in the following proportions: Northern Alguero-Balear (36.2%), Central Alguero-Balear (12.1%), Southern Alguero-Balear (4.4%), Tyrrhenian Sea (15.4%), Adriatic Sea (13.2 %), Ionian Sea (12.1 %), Aegean Sea (2.2 %) and Levantine Basin (4.4%). The air trajectories from Sellafield and La Hague only arrived 4% and 24% of the times, respectively, making their input to the Mediterranean Sea less significant than that from Marcoule: for example, the ^{129}I input from La Hague would probably be less than 10% of that from Marcoule if 1) we take the above air trajectories; 2) consider a total gaseous ^{129}I release about 2 times smaller than that of Marcoule (Hou et al., 2009); and 3) we assume that most of the ^{129}I (e.g. 50%) is deposited near the reprocessing plant or further removed from the atmosphere by precipitation and aerosols during the >4 days transport (on average) to reach the Mediterranean Sea (we assumed the loss of ^{129}I to be at least 50%, which is a conservative figure considering the assumption of He et al., (2013) that 50% is already deposited in the vicinity of the source). Thus, the inputs from La Hague or Sellafield are not included in the model box model of (Bethoux and Gentili, 1996).

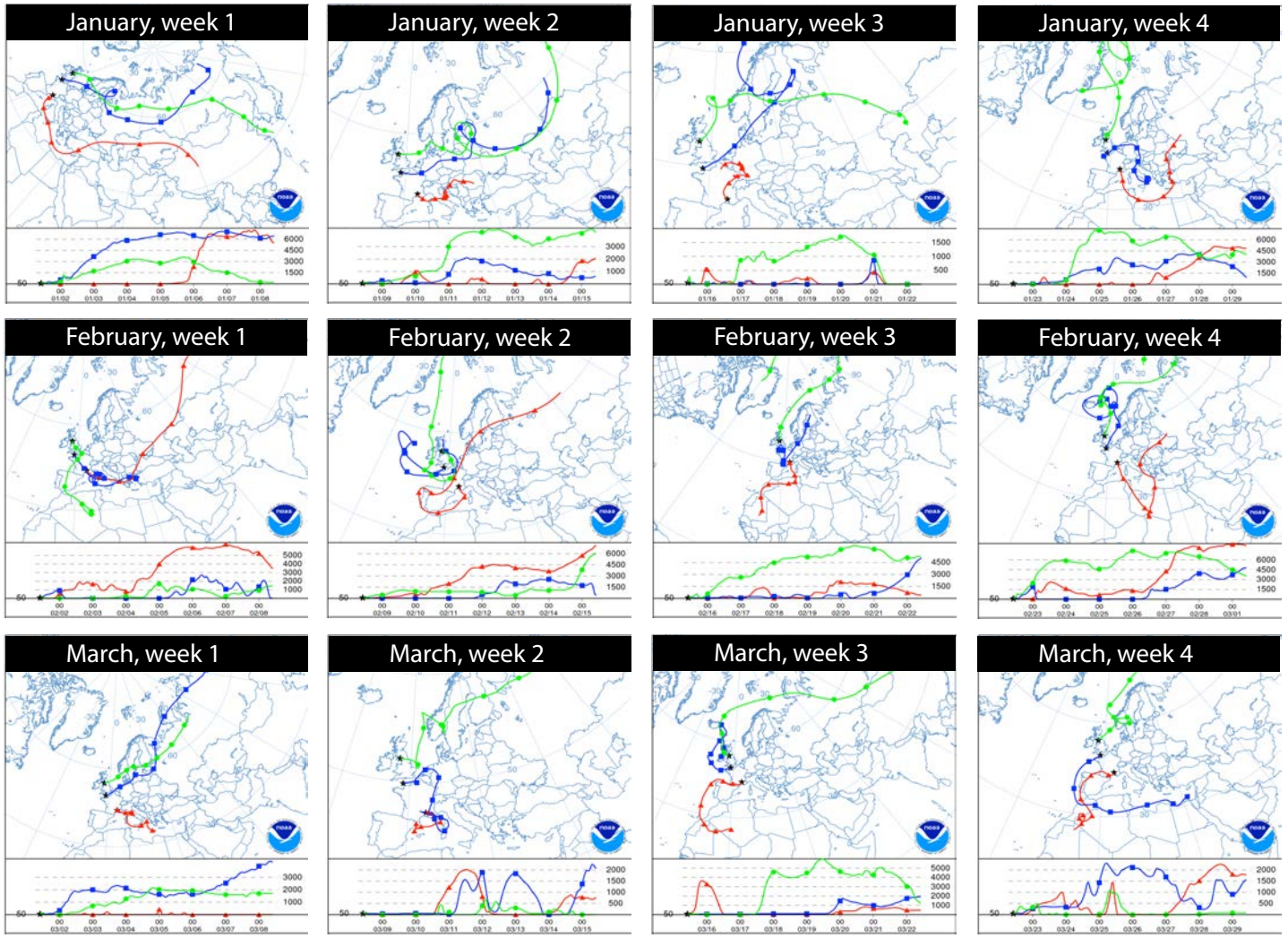

Figure A.4. Air mass trajectories from Marcoule (red), La Hague (blue) and Sellafield (green). 24 h intervals are indicated by symbols.

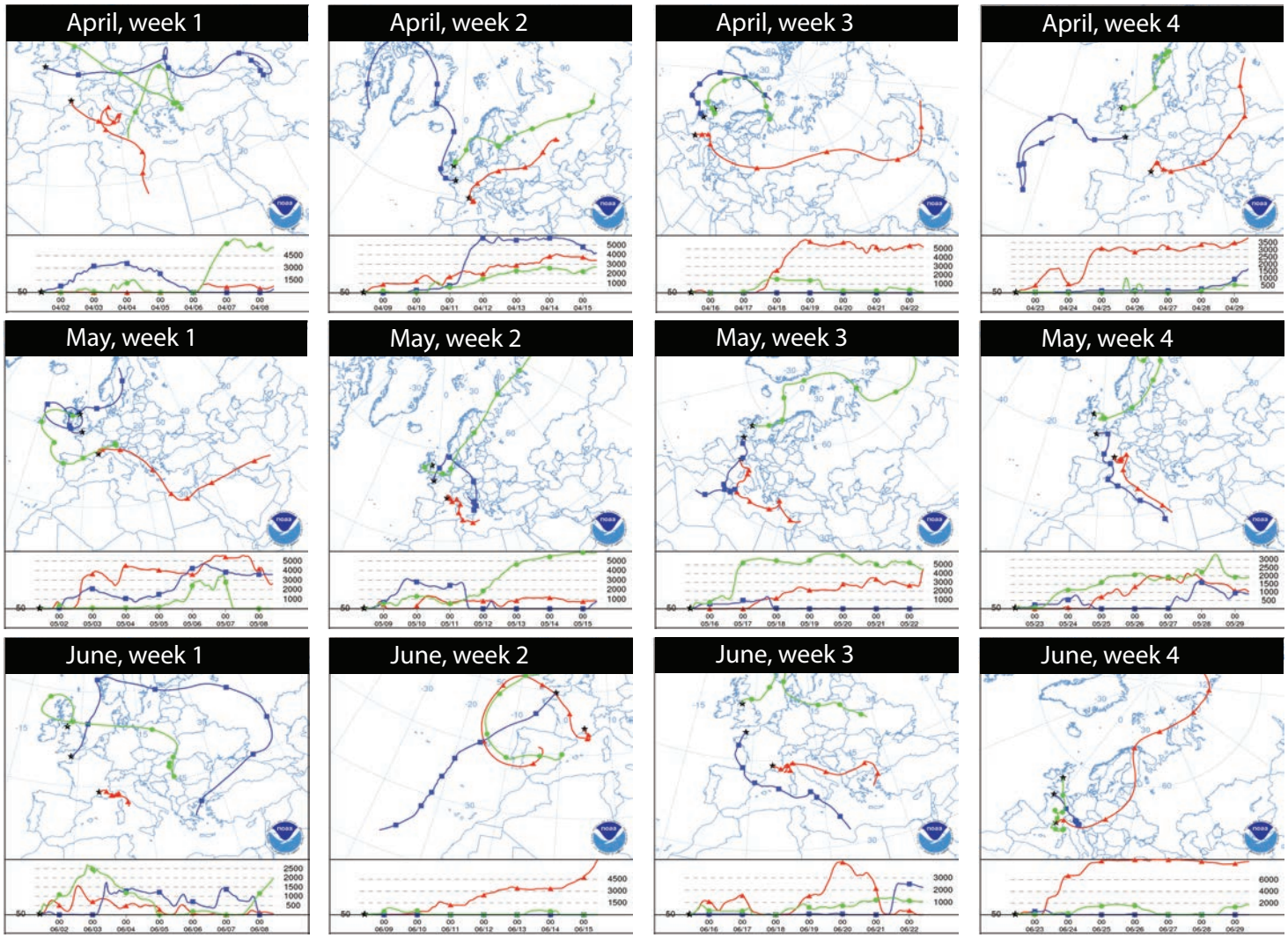

Figure A.4. Continuation

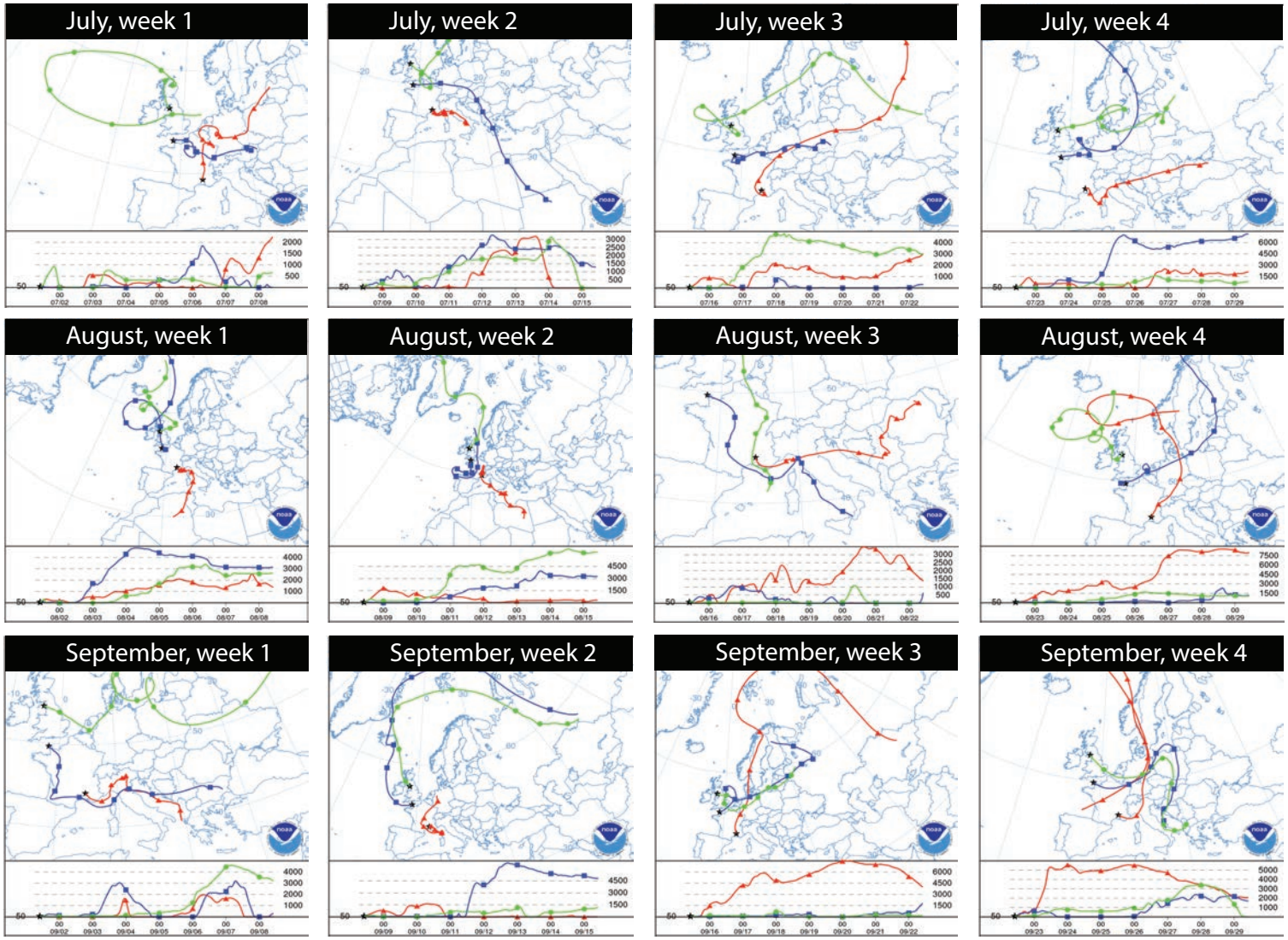

Figure A.4. Continuation

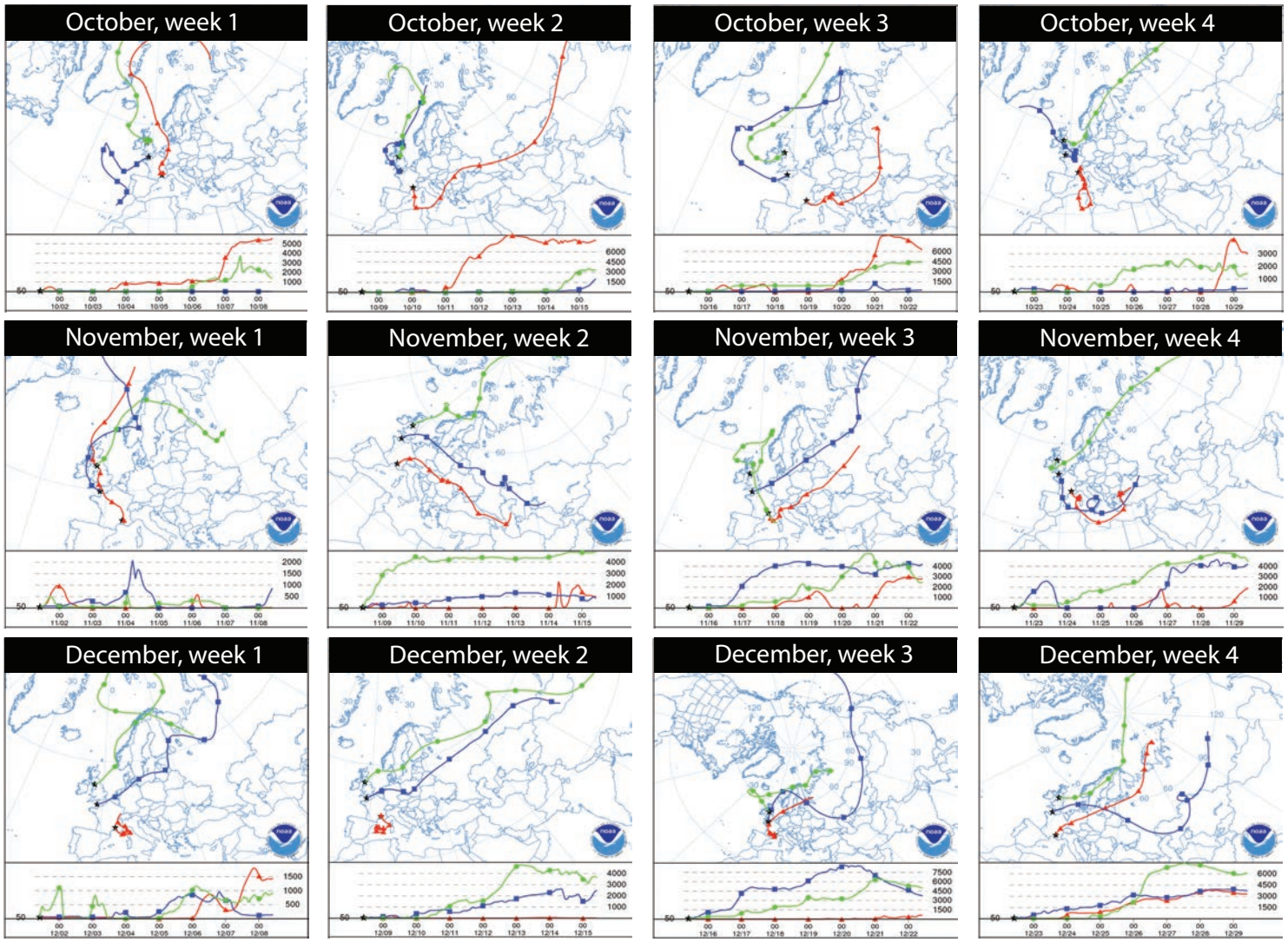

Figure A.4. Continuation

A.7. Concentrations of ^{137}Cs, ^{237}Np, ^{239}Pu and ^{240}Pu in seawater samples collected during *GA04s-MedSeA* cruise in May 2013.

Table A.4. Concentrations of ^{137}Cs, ^{237}Np, ^{239}Pu and ^{240}Pu in seawater samples collected during *GA04s-MedSeA* cruise in May 2013. Concentration uncertainties of ^{137}Cs were calculated by the propagation of uncertainties in the chemical recovery, count rate and the detector calibration. Concentration uncertainties of ^{237}Np, ^{239}Pu, ^{240}Pu and ^{239,240}Pu are reported as 2 sigma deviations. Water mass acronyms are: Atlantic Water (AW), Modified Atlantic Water (MAW), Ionian Surface Water (ISW), Levantine Surface Water (LSW), Levantine Intermediate Water (LIW), Western Intermediate Water (WIW), Cretan Deep Water (CDW), Adriatic Deep Water (AdDW), Tyrrhenian Deep Water (TDW), Western Mediterranean Deep Water (WMDW), Eastern Mediterranean Deep Water (EMDW), transitional EMDW (tEMDW). Lower case n: new; o: old; mix: mixture of new and old. *Probable outliers.

Station	Depth	Water mass	Salinity	Pot. temp.	Pot. Dens.	Oxygen	^{137}Cs conc.	^{237}Np conc.	^{239}Pu conc.	^{240}Pu conc.	^{240}Pu/^{239}Pu
	m			°C	kg·m^{-3}	µmol·kg^{-1}	Bq·m^{-3}	mBq·m^{-3}	mBq·m^{-3}	mBq·m^{-3}	at·at^{-1}
1. Gibraltar St (GSt)	5	AW	36,26	16,89	1026,5	235	1,35 ± 0,23	0,140 ± 0,002	1,41 ± 0,02	1,61 ± 0,05	*0,309 ± 0,012
35° 58.39′ N	25	AW	36,30	15,81	1026,8	222	1,38 ± 0,17	0,155 ± 0,003	2,08 ± 0,03	1,42 ± 0,03	0,186 ± 0,005
5° 26.03′ W	49	AW/LIW	36,84	14,82	1027,4	205	1,21 ± 0,17	0,153 ± 0,001	3,99 ± 0,06	3,26 ± 0,05	0,222 ± 0,005
Bottom depth: 640 m	101	AW/LIW	37,74	13,88	1028,3	188	1,25 ± 0,17	0,162 ± 0,002	6,02 ± 0,05	4,10 ± 0,04	0,185 ± 0,002
	199	LIW	38,35	13,24	1028,9	167	1,42 ± 0,17	0,175 ± 0,003	6,94 ± 0,07	5,08 ± 0,11	0,199 ± 0,005
	299	LIW/WMDW	38,44	13,20	1029,0	169	1,35 ± 0,17	0,177 ± 0,003	9,90 ± 0,12	6,70 ± 0,08	0,184 ± 0,003
	496	WMDW	38,48	13,16	1029,1	169	1,46 ± 0,17	0,160 ± 0,003	11,29 ± 0,09	8,58 ± 0,12	0,207 ± 0,003
	613	WMDW	38,50	13,13	1029,1	171	1,44 ± 0,18	0,160 ± 0,003	11,77 ± 0,11	7,85 ± 0,09	0,182 ± 0,003
2. Algeria (ALG)	5	AW/MAW	37,00	17,80	1026,9	235	1,15 ± 0,18	0,152 ± 0,004	3,27 ± 0,03	2,21 ± 0,03	0,184 ± 0,003
37° 29.22′ N	25	MAW	37,29	15,89	1027,5	248	1,28 ± 0,12	0,159 ± 0,003	4,20 ± 0,04	3,05 ± 0,04	0,198 ± 0,003
1° 26.82′ E	100	LIW/MAW	38,22	13,38	1028,8	195	1,87 ± 0,10	0,184 ± 0,003	6,11 ± 0,11	4,12 ± 0,06	0,184 ± 0,004
Bottom depth: 2777 m	250	LIW/WMDWo	38,48	13,29	1029,0	167	1,66 ± 0,10	0,173 ± 0,003	10,46 ± 0,11	7,31 ± 0,15	0,190 ± 0,004
	500	LIW/WMDWo	38,52	13,18	1029,1	171	1,50 ± 0,11	0,146 ± 0,002	11,90 ± 0,16	8,22 ± 0,14	0,188 ± 0,004
	998	WMDWo/LIW	38,47	12,94	1029,1	184	0,96 ± 0,14	0,136 ± 0,002	13,13 ± 0,14	8,80 ± 0,14	0,182 ± 0,003
	1499	WMDWmix	38,46	12,90	1029,1	190	1,40 ± 0,10	0,142 ± 0,004	13,00 ± 0,23	8,85 ± 0,12	0,185 ± 0,004
	1999	WMDWmix	38,46	12,90	1029,1	192	1,32 ± 0,11	±	12,44 ± 0,06	8,37 ± 0,05	0,183 ± 0,001
	2703	WMDWn	38,47	12,90	1029,1	192	1,10 ± 0,18	0,128 ± 0,004	12,60 ± 0,15	8,60 ± 0,09	0,186 ± 0,003
3. S. Alg.-Balear (SAB)	5	MAW	37,65	16,99	1027,6	238	1,31 ± 0,17	0,164 ± 0,003	4,06 ± 0,05	2,79 ± 0,05	0,187 ± 0,004
38° 31.68′ N	25	MAW	37,62	16,24	1027,7	245	1,40 ± 0,17	0,132 ± 0,003	4,57 ± 0,06	3,22 ± 0,06	0,192 ± 0,004
5° 33.55′ E	100	MAW/LIW	37,95	13,70	1028,5	235	1,35 ± 0,17	0,177 ± 0,003	4,97 ± 0,05	3,41 ± 0,04	0,187 ± 0,003
Bottom depth: 2844 m	251	MAW/LIW	38,40	13,38	1029,0	186	1,37 ± 0,17	0,180 ± 0,002	7,96 ± 0,04	5,61 ± 0,07	0,192 ± 0,003
	500	LIW/WMDWo	38,53	13,23	1029,1	166	1,20 ± 0,18	0,150 ± 0,002	11,78 ± 0,18	7,95 ± 0,07	0,184 ± 0,003
	1000	WMDWo/LIW	38,48	12,99	1029,1	180	1,22 ± 0,17	0,137 ± 0,003	13,06 ± 0,12	9,18 ± 0,13	0,191 ± 0,003
	1499	WMDWo	38,46	12,90	1029,1	187	1,09 ± 0,18	0,138 ± 0,003	13,16 ± 0,18	8,88 ± 0,07	0,184 ± 0,003
	1999	WMDWmix	38,46	12,90	1029,1	191	1,29 ± 0,17	0,144 ± 0,002	13,05 ± 0,18	8,76 ± 0,12	0,183 ± 0,004
	2804	WMDWn	38,48	12,90	1029,1	193	0,99 ± 0,18	0,147 ± 0,002	12,60 ± 0,08	8,68 ± 0,14	0,188 ± 0,003
4. Sardinia Chan. (SCh)	5	MAW	37,77	17,50	1027,5	244	1,21 ± 0,15	0,160 ± 0,004	3,99 ± 0,04	2,90 ± 0,05	0,198 ± 0,004
38° 15.16′ N	25	MAW	37,97	16,09	1028,0	249	1,56 ± 0,17	0,174 ± 0,004			
8° 46.26′ E	101	MAW/LIW	38,24	13,50	1028,8	199	1,75 ± 0,17	0,181 ± 0,003	5,48 ± 0,05	3,91 ± 0,07	0,194 ± 0,004
Bottom depth: 2238 m	250	LIW/MAW	38,57	13,57	1029,0	170	1,71 ± 0,11	0,173 ± 0,003	9,98 ± 0,06	6,82 ± 0,08	0,186 ± 0,003

Table A.4. Continuation.

Station	Depth	Water mass	Salinity	Pot. temp.	Pot. Dens.	Oxygen	^{137}Cs conc.	^{237}Np conc.	^{239}Pu conc.	^{240}Pu conc.	^{240}Pu/^{239}Pu
	m			°C	kg·m^{-3}	µmol·kg^{-1}	Bq·m^{-3}	mBq·m^{-3}	mBq·m^{-3}	mBq·m^{-3}	at·at^{-1}
	500	LIW/WMDW	38,62	13,54	1029,1	176	1,50 ± 0,12	0,148 ± 0,002	11,31 ± 0,09	7,77 ± 0,11	0,187 ± 0,003
	1000	WMDW/LIW	38,47	12,95	1029,1	186	1,15 ± 0,17	0,137 ± 0,002	12,94 ± 0,09	8,75 ± 0,10	0,184 ± 0,003
	1499	WMDW/TDW	38,46	12,90	1029,1	192	1,30 ± 0,11	0,141 ± 0,002	12,93 ± 0,08	8,88 ± 0,08	0,187 ± 0,002
	2001	WMDW/TDW	38,47	12,90	1029,1	192	1,09 ± 0,19	0,147 ± 0,003	12,79 ± 0,09	8,73 ± 0,15	0,186 ± 0,003
	2202	WMDW/TDW	38,47	12,90	1029,1	192	0,94 ± 0,15	0,147 ± 0,002	12,71 ± 0,10	8,66 ± 0,12	0,185 ± 0,003
5. Ionian Sea (IS)	5	MAW/ISW	38,64	19,53	1027,7	218	1,65 ± 0,10	0,152 ± 0,005			
35° 02.67′ N	25	MAW/ISW	38,68	17,08	1028,3	236	1,65 ± 0,10	0,172 ± 0,003	4,41 ± 0,04	3,40 ± 0,06	0,210 ± 0,004
18° 34.08′ E	100	MAW/ISW	38,72	15,60	1028,7	234	1,83 ± 0,10	0,180 ± 0,002	4,38 ± 0,04	2,96 ± 0,03	0,184 ± 0,003
Bottom depth: 3774 m	250	ISW/LSW	38,87	15,44	1028,9	220	1,98 ± 0,09	0,187 ± 0,003	4,84 ± 0,05	4,52 ± 0,09	0,254 ± 0,006
	500	LIW/CIW	38,92	14,92	1029,0	209	1,63 ± 0,17	0,190 ± 0,002	5,86 ± 0,05	4,03 ± 0,06	0,187 ± 0,003
	999	AdDWo/LIW	38,78	13,77	1029,2	183	1,14 ± 0,12	0,132 ± 0,002	8,91 ± 0,09	5,91 ± 0,09	0,181 ± 0,003
	2001	AdDWo/LIW	38,73	13,51	1029,2	190	1,51 ± 0,16	0,150 ± 0,001	10,07 ± 0,09	7,11 ± 0,05	0,192 ± 0,002
	3001	AdDWo	38,72	13,43	1029,2	192	1,47 ± 0,18	0,159 ± 0,002	10,60 ± 0,07	7,14 ± 0,06	0,183 ± 0,002
	3726	AdDWn	38,72	13,42	1029,2	192					
6. Lev. Basin (LB)	5	MAW/LSQ		20,60	1024,6		1,96 ± 0,09	0,177 ± 0,003	4,03 ± 0,04	2,83 ± 0,06	0,191 ± 0,004
33° 14.76′ N	26	MAW/LSQ	38,77	20,51	1027,5	222	1,52 ± 0,19	0,177 ± 0,003	4,11 ± 0,03	2,78 ± 0,05	0,184 ± 0,004
28° 27.11′ E	100	MAW/LSQ	38,82	16,64	1028,5	226	1,63 ± 0,15	0,181 ± 0,002	2,73 ± 0,03	1,87 ± 0,05	0,187 ± 0,005
Bottom depth: 2865 m	251	LIW	39,05	15,35	1029,0	201	2,04 ± 0,10	0,175 ± 0,003	5,60 ± 0,07	5,43 ± 0,12	0,263 ± 0,007
	500	LIW/AdDWo	38,84	14,02	1029,2	183	1,20 ± 0,10	0,125 ± 0,002	7,53 ± 0,04	5,19 ± 0,14	0,188 ± 0,005
	999	AdDWo	38,75	13,62	1029,2	181	0,74 ± 0,15	0,097 ± 0,002	5,14 ± 0,05	3,59 ± 0,06	0,190 ± 0,004
	2002	CDW	38,77	13,62	1029,2	185	1,19 ± 0,14	0,132 ± 0,004	8,12 ± 0,12	6,02 ± 0,11	0,202 ± 0,005
	2833	AdDWn	38,76	13,59	1029,2	185	1,49 ± 0,10	0,150 ± 0,002			
7. Tyrrhenian Sea (TS)	5	MAW	37,98	18,60	1027,4	227	1,48 ± 0,18	0,169 ± 0,003	5,20 ± 0,10	4,40 ± 0,10	0,230 ± 0,007
39° 49.74′ N	25	MAW	38,03	18,03	1027,6	234	1,68 ± 0,09	0,177 ± 0,002	5,24 ± 0,06	4,43 ± 0,07	0,230 ± 0,004
12° 30.85′ E	100	MAW/LIW	38,27	13,85	1028,8	225	1,67 ± 0,13	0,180 ± 0,004	5,16 ± 0,08	3,83 ± 0,09	0,202 ± 0,006
Bottom depth: 3165 m	250	LIW	38,71	14,26	1029,0	176	1,59 ± 0,17	0,175 ± 0,007	6,12 ± 0,13	8,63 ± 0,18	*0,384 ± 0,012
	500	LIW/tEMDW	38,73	14,00	1029,1	170	1,64 ± 0,20	0,164 ± 0,005	8,93 ± 0,23	7,01 ± 0,24	0,214 ± 0,009
	1000	tEMDW	38,64	13,55	1029,1	173	1,45 ± 0,09				
	1501	tEMDW	38,55	13,20	1029,1	175	1,32 ± 0,11	0,126 ± 0,002	10,83 ± 0,10	7,20 ± 0,09	0,181 ± 0,003
	1998	tEMDW/TDW	38,52	13,12	1029,1	177	1,06 ± 0,18	0,124 ± 0,002	8,79 ± 0,14	5,92 ± 0,12	0,183 ± 0,005
	3154	TDW	38,48	12,98	1029,1	179					
8. N. Alg.-Balear (NAB)	5	MAW		15,52	1026,6	229	1,47 ± 0,19	0,199 ± 0,003	7,23 ± 0,09	4,94 ± 0,11	0,186 ± 0,005
41° 19.02′ N	25	MAW	38,31	15,42	1028,4	232	1,52 ± 0,12	0,175 ± 0,004	7,05 ± 0,09	4,81 ± 0,09	0,186 ± 0,004
5° 39.94′ E	100	WIW	38,41	13,26	1029,0	218	1,36 ± 0,16	0,176 ± 0,004	7,86 ± 0,10	5,42 ± 0,15	0,187 ± 0,006
Bottom depth: 2561 m	250	LIW	38,50	13,13	1029,1	186	1,22 ± 0,11	0,161 ± 0,004	9,62 ± 0,15	7,18 ± 0,19	0,203 ± 0,006
	500	LIW/WMDWo	38,47	12,96	1029,1	187	1,24 ± 0,19	0,144 ± 0,004	9,57 ± 0,19	6,67 ± 0,15	0,190 ± 0,006
	1001	WMDWo	38,47	12,92	1029,1	192	1,24 ± 0,11				
	1499	WMDWn	38,47	12,91	1029,1	194	1,28 ± 0,11	0,146 ± 0,004	10,95 ± 0,17	7,87 ± 0,25	0,196 ± 0,007
	2502	WMDWn	38,48	12,91	1029,1	196	1,52 ± 0,14	0,154 ± 0,001	8,73 ± 0,09	6,00 ± 0,15	0,187 ± 0,005
9. C. Alg.-Balear (CAB)	5	MAW		16,79	1023,5	226	1,37 ± 0,17	0,164 ± 0,004	4,36 ± 0,03	3,89 ± 0,13	0,243 ± 0,009
40° 4.17′ N	26	MAW	37,65	16,62	1027,6	236	1,43 ± 0,17	0,165 ± 0,003	4,42 ± 0,04	3,07 ± 0,04	0,189 ± 0,003
5° 56.76′ E	100	MAW/WIW	37,97	13,57	1028,6	238	1,76 ± 0,09	0,212 ± 0,005			
Bottom depth: 2834 m	250	WIW	38,15	13,29	1028,8	229	1,71 ± 0,10				
	500	LIW	38,48	13,36	1029,0	178	1,64 ± 0,09	0,173 ± 0,001	7,99 ± 0,07	5,29 ± 0,07	0,180 ± 0,003

Table A.4. Continuation.

Station	Depth	Water mass	Salinity	Pot. temp.	Pot. Dens.	Oxygen	^{137}Cs conc.	^{237}Np conc.	^{239}Pu conc.	^{240}Pu conc.	^{240}Pu/^{239}Pu
	m			°C	kg·m^{-3}	µmol·kg^{-1}	Bq·m^{-3}	mBq·m^{-3}	mBq·m^{-3}	mBq·m^{-3}	at·at^{-1}
	1001	WMDWo/LIW	38,48	13,00	1029,1	177	1,32 ± 0,10	0,134 ± 0,002	12,79 ± 0,16	8,79 ± 0,08	0,187 ± 0,003
	1498	WMDWmix	38,47	12,94	1029,1	186	1,28 ± 0,18	0,145 ± 0,002	11,11 ± 0,09	7,66 ± 0,15	0,188 ± 0,004
	2803	WMDWn	38,48	12,91	1029,1	190	1,45 ± 0,10	0,164 ± 0,003			
10. Cat.-Balear (CB)	5	MAW	38,33	16,81	1028,1	217	1,86 ± 0,08	0,172 ± 0,002	6,19 ± 0,09	4,42 ± 0,08	0,194 ± 0,005
40° 57.05′ N	25	MAW/WIW	38,29	16,35	1028,2	246	1,68 ± 0,09	0,163 ± 0,002	6,15 ± 0,07	4,14 ± 0,03	0,183 ± 0,002
3° 19.15′ E	100	MAW/WIW	38,46	13,21	1029,0	206	1,77 ± 0,09	0,165 ± 0,004	10,16 ± 0,14	6,96 ± 0,13	0,186 ± 0,004
Bottom depth: 2274 m	250	LIW	38,52	13,19	1029,1	184	1,45 ± 0,08	0,149 ± 0,004	11,98 ± 0,16	8,31 ± 0,32	0,189 ± 0,008
	500	LIW/WMDWn	38,50	13,06	1029,1	185	1,44 ± 0,09	0,156 ± 0,004	9,87 ± 0,25	7,05 ± 0,18	0,194 ± 0,007
	1000	WMDWn	38,47	12,93	1029,1	191	1,45 ± 0,07	0,139 ± 0,003	12,64 ± 0,09	8,56 ± 0,14	0,184 ± 0,003
	1499	WMDWmix	38,48	12,92	1029,1	194	1,26 ± 0,10	0,146 ± 0,003	9,29 ± 0,10	6,54 ± 0,13	0,191 ± 0,004
	1800	WMDWn	38,48	12,92	1029,1	195	1,27 ± 0,09	0,147 ± 0,003	11,47 ± 0,10	7,75 ± 0,17	0,184 ± 0,004
	2201	WMDWn	38,48	12,91	1029,1	195	1,34 ± 0,09	0,137 ± 0,003	6,65 ± 0,10	4,62 ± 0,08	0,189 ± 0,004

A.8. Concentration range and total water column inventories of ^{137}Cs reported for depth profiles in the literature.

Table A.5. Concentration range and total water column inventories of ^{137}Cs reported for depth profiles in the literature. All radionuclide inventories were estimated by trapezoidal depth integration of radionuclide concentrations. Acronyms are: ALG (Algeria), SAB and CAB (Southern and Central Alguero-Balear), IS (Ionian Sea), LB (Levantine Basin), WMS (Western Mediterranean Sea), CB (Catalano-Balear) and GibSt (Gibraltar Strait).

Sampling Year	Location	Max. sampled Depth (m)	Bottom Depth (m)	^{137}Cs concentrations (Bq·m^{-3}) at sampling	in May 2013	^{137}Cs inventory in May 2013 (kBq·m^{-2})	Reference
Before Chernobyl accident in April 1986							
1970	Alboran (36º 0’ N, 4º 40’ W)	1000	1095	0.81-10.00	0.30-3.73	1.4±0.1	Kautsky, 1977
1970	ALG (37º 2’ N, 0º 1,3’ W)	2500	2655	1.56-21.48	0.58-8.01	5.3±0.1	Kautsky, 1977
1970	SAB (39º 0’ N, 6º 40’ E)	2750	2800	1.00-7.78	0.37-2.90	1.9±0.1	Kautsky, 1977
1970	CAB (40º 48’ N, 6º 51’ E)	2750	2755	1.15-8.52	0.43-3.18	1.9±0.1	Kautsky, 1977
1974	SAB (36º 0’ N, 4º 0’ W)	1250	1300	0.74-6.30	0.30-2.58	1.1±0.1	Kautsky, 1977
1974	Alboran (36º 16’ N, 2º 1’ W)	1250	1850	0.70-5.56	0.29-2.27	1.2±0.1	Kautsky, 1977
1974	ALG (37º 0’ N, 0º 1’ E)	1250	2660	0.67-6.67	0.27-2.73	1.6±0.1	Kautsky, 1977
1974	ALG (37º 30’ N, 2º 0’ E)	1250	2700	0.56-12.59	0.23-5.51	1.4±0.1	Kautsky, 1977
1975	CAB (41º 12.4’ N, 5º 52.3’ E)	2600	2612	0.67-3.62	0.28-1.51	1.4±0.1	Livingston et al., 1979
1975	IS (35º 56.4’ N, 17º 55.8’ E)	4000	4000*	0.77-7.80	0.32-3.26	3.3±0.1	Livingston et al., 1979
1975	IS (36º 0’ N, 18º 0’ E)	3800	3800*	0.70-5.43	0.29-2.27	2.4±0.1	Livingston et al., 1979
1975	LB (34º 1.3’ N, 28º 59.8’ E)	2900	2900*	0.15-7.35	0.06-3.08	1.2±0.1	Livingston et al., 1979
1976	DYFAMED (43º 32’ N, 7º 32’ E)	2000	2260	0.52-3.33	0.22-1.43	1.1±0.1	Fukai et al., 1979
1981	DYFAMED (43º 32’ N, 7º 32’ E)	1300	2260	1.66-3.55	0.80-1.71	2.0±0.1	Ballestra et al., 1984
1981	NWMS (41º 0’ N, 6º 45’ E)	2000	2600	0.60-4.13	0.29-1.98	1.6±0.1	Ballestra et al., 1984
1981	NWMS (42º 57’ N, 5º 15’ E)	1000	1300	1.17-3.62	0.56-1.74	1.0±0.1	Ballestra et al., 1984
1981	NWMS (42º 40’ N, 4º 42’ E)	1000	1010	1.22-4.85	0.59-2.33	0.8±0.1	Ballestra et al., 1984
After Chernobyl Accident in April 1986							
1991	ALG (37º 49’ N, 2º 32’ E)	2700	2700*	2.00-3.80	1.21-2.30	**	Delfanti et al., 1994
1991	CS (~40º N, ~2º E)	1000	1000*	1.80-4.40	1.09-2.66	1.7±0.1	Molero et al., 1995
1992	CB (42º 0’ N, 3º 40’ E)	900	900*	1.80-3.20	1.11-1.98	1.2±0.1	Delfanti et al., 1994
1993	CB (no coordinates reported)	1160	1165	1.90-4.50	1.20-2.85	2.0±0.1	Merino, 1997
1995	IS (35º 34.9’ N, 17º 15.1’ E)	3900	3953	1.56-4.42	1.03-2.91	6.5±0.2	Delfanti et al., 2003
1995	LB (32º 59.9’ N, 28º 29.9’ E)	2872	2980	1.20-4.36	0.79-2.88	3.9±0.1	Delfanti et al., 2003
1998	Adriatic (41º 59.1’ N, 18º 4.9’ E)	1150	1199	2.60-3.26	1.87-2.34	2.5±0.1	Delfanti et al., 2003
1999	IS (35º 35.1’ N, 17º 15.1’ E)	4012	4030	1.51-3.48	1.09-2.50	6.5±0.2	Delfanti et al., 2003
1999	Crete (35º 20.1’ N, 23º 16.1’ E)	3152	3162	1.35-3.40	0.97-2.45	5.6±0.2	Delfanti et al., 2003
1999	IS (35º 44.6’ N, 20º 31.8’ E)	3144	3152	1.35-3.23	0.97-2.32	5.4±0.2	Delfanti et al., 2003
1999	IS (36º 30.0’ N, 15º 50.0’ E)	3300	3309	1.50-3.34	1.08-2.40	5.2±0.2	Delfanti et al., 2003
1999	GibSt (35º 47’ N, 4º 48’ W)	900	900*	2.29-2.50	1.68-1.84	1.6±0.1	Benmansour et al., 2006
2001	DYFAMED (43º 32’ N, 7º 32’ E)	2230	2260	1.30-2.40	0.98-1.81	2.8±0.1	Lee et al., 2003
2001	ALG (36º 54.1’ N, 3º 20.5’ E)	1200	1220	2.21-2.33	1.69-1.78	2.1±0.1	Noureddine et al., 2008
2001	ALG (36º 44.7’ N, 1º 38.5’ E)	2000	2000*	1.31-2.20	1.00-1.68	2.8±0.1	Noureddine et al., 2008

Table A.5. Continuation.

Sampling Year	Location	Max. sampled Depth (m)	Bottom Depth (m)	^{137}Cs concentrations (Bq·m^{-3}) at sampling	in May 2013	^{137}Cs inventory in May 2013 (kBq·m^{-2})	Reference
After Chernobyl Accident in April 1986							
2002	CAB (39º 28.3' N, 6º 0.4' E)	2836	2850	1.40-2.80	1.09-2.18	3.6±0.3	Garcia-Orellana, 2004
2004	Sicily Ch. (37º 36' N, 11º 28' E)	650	1200	1.50-2.60	1.22-2.12	**	Lee et al., 2006
2004	Sardinia Ch (38º 9' N, 9º 7' E)	1483	1483*	1.32-2.40	1.08-1.96	2.1±0.1	Lee et al., 2006
2013	DYFAMED (43º 32' N, 7º 32' E)	2000	2350	1.10-1.69	1.11-1.71	2.9±0.1	Bressac et al., 2017

*Bottom depth not reported and assumed in this study to be equal to maximum sampled depth.

**Inventory was not calculated due to low vertical resolution (n≤4 in water column >2000 m).

A.9. Concentration range and total water column inventories of ^{239,240}Pu reported in the literature.

Table A.6. Concentration range and total water column inventories of ^{239,240}Pu reported in the literature. All radionuclide inventories were estimated by trapezoidal depth integration of radionuclide concentrations. *Bottom depth not reported and assumed in this study to be equal to maximum sampled depth.

Sampling Year	Location	Max. sampled Depth (m)	Bottom Depth (m)	^{239,240}Pu concentrations (mBq·m^{-3})	^{239,240}Pu inventory (Bq·m^{-2})	Reference
1975	C. Alguero-Balear (41º 12.4' N, 5º 52.3' E)	2600	2612	8.3-43.3	54±5	Livingston et al., 1979
1975	Ionian Sea (35º 56.4' N, 17º 55.8' E)	4000	4000*	10.0-81.7	81±4	Livingston et al., 1979
1975	Ionian Sea (36º 0' N, 18º 0' E)	3800	3800*	9.2-54.7	60±4	Livingston et al., 1979
1975	Levantine Basin (34º 1.3' N, 28º 59.8' E)	2900	2900*	4.8-68.3	55±5	Livingston et al., 1979
1976	DYFAMED (43º 32' N, 7º 32' E)	2000	2260	14.4-44.4	41±1	Fukai et al., 1979
1977	Ionian Sea (~37º 0' N, ~19º 0' E)	2000	2000*	7.4-59.3	38±2	Fukai et al., 1982
1977	E. Levantine Basin (~33º 0' N, ~32º 0' E)	1500	1700	7.4-51.9	33±2	Fukai et al., 1982
1979	Levantine Basin (~32º 0' N, ~28º 0' E)	2000	2000*	3.7-50.0	30±1	Fukai et al., 1982
1981	Off Rhône Stuary (~42º 30' N, ~4º 45' E)	1000	1700	25.6-40.7	31±2 (up to 1000 m)	Fukai et al., 1982
1981	Off Rhône Stuary (~42º 0' N, ~4º 45' E)	1000	2250	18.1-44.4	27±2 (up to 1000 m)	Fukai et al., 1982
1981	Catalano-Balear (~40º 0' N, ~2º 0' E)	1000	1700	29.6-51.9	35±2 (up to 1000 m)	Fukai et al., 1982
1981	Alboran Sea (~36º 10' N, ~4º 30' E)	1000	1100	18.5-48.1	32±2	Fukai et al., 1982
1981	DYFAMED (43º 32' N, 7º 32' E)	1300	2260	26.0-40.0	41±6 (up to 1300 m)	Ballestra et al., 1984
1981	NWMS (41º 0' N, 6º 45' E)	2000	2600	14.0-54.0	40±3 (up to 2000 m)	Ballestra et al., 1984
1981	NWMS (42º 57' N, 5º 15' E)	1000	1300	21.0-35.0	32±2	Ballestra et al., 1984
1981	NWMS (42º 40' N, 4º 42' E)	1000	1010	19.0-37.0	28±1	Ballestra et al., 1984
1986	Gulf of Lions (42º 25' N, 3º 30' E)	610	610*	19.6-27.0	15±1	Fowler et al., 1990
1986	Gulf of Lions (42º 50' N, 4º 38' E)	1100	1100*	13.3-26.3	19±1	Fowler et al., 1990
1989	DYFAMED (43º 32' N, 7º 32' E)	2230	2260	18.1-34.9	61±7	Fowler et al., 2000
1989	DYFAMED (43º 32' N, 7º 32' E)	2250	2260	17.8-36.2	53±3	Fowler et al., 2000
1990	EROS-2000 'RETRO' (41º 57' N, 5º 56' E)	2470	2475	16.9-31.9	57±2	Fowler et al., 2000
1991	ALG (37º 49' N, 2º 32' E)	2700	2700*	11.0-28.0	60±7	Delfanti et al., 1994
1991	Catalan Sea (~40º N, ~2º E)	1000	1000*	13.9-26.0	23±2	Molero et al., 1995
1991/2	Alboran Sea (37º 49' N, 2º 32' E)	2745	2770	12.6-29.1	64±2	Mitchell et al., 1995
1991/2	Catalano-Balear (42º 0' N, 3º 40' E)	911	931	14.8-33.4	24±1	Mitchell et al., 1995
1994	Alboran Sea (36º 20' N, 2º 59.9' E)	977	1000	11.1-24.5	20±1	León Vintró et al., 1999
1994	Alboran Sea (35º 56' N, 4º 30' E)	1200	1280	8.5-23.5	23±1	León Vintró et al., 1999
1994	Algerian Basin (37º 30' N, 4º 30' E)	2500	2733	8.1-20.7	47±1	León Vintró et al., 1999
1999	Gibraltar Strait (35º 47' N, 4º 48' W)	900	900*	8.3-33.0	23±1	Benmansour et al., 2006
2001	DYFAMED (43º 32' N, 7º 32' E)	2230	2260	14.0-28.0	55±3	Lee et al., 2003
2001	Algerian Sea (36º 44.7' N, 1º 38.5' E)	2000	2000*	8.2-25.5	42±4	Noureddine et al., 2008
2001	Ionian Sea (34º 52.4' N, 20º 48.9' E)	2730	2760	3.4-15.2	34±3	Garcia-Orellana (unpub.)
2002	C. Alguero-Balear (39º 28.3' N, 6º 0.4' E)	2836	2850	3.6-18.9	43±3	Garcia-Orellana, 2004
2004	Sicily Ch. (37º 36' N, 11º 28' E)	650	1200	6.5-22.0	24±1	Lee et al., 2006
2004	Sardinia Ch (38º 9' N, 9º 7' E)	1483	1483*	6.9-22.0	18±1	Lee et al., 2006
2013	DYFAMED (43º 32' N, 7º 32' E)	2000	2350	7.3-20.3	44±1	Bressac et al., 2017

A.10. Water column inventories of ^{137}Cs, ^{237}Np, and ^{239,240}Pu obtained from measured concentrations during *GA04s-MedSeA* cruise in May 2013.

Table A.7. Water column inventories of ^{137}Cs, ^{237}Np, and ^{239,240}Pu obtained from measured concentrations during *GA04s-MedSeA* cruise in May 2013. Inventories of ^{129}I and ^{236}U were calculated using data from Castrillejo *et al*. (2017). All radionuclide inventories were estimated by trapezoidal depth integration of radionuclide concentrations.

Station	Bottom depth m	^{129}I × 10^{12} at·m^{-2}			^{137}Cs kBq·m^{-2}			^{236}U × 10^{12} at·m^{-2}			^{237}Np Bq·m^{-2}			^{239,240}Pu Bq·m^{-2}		
1. Gibraltar St (GSt)	640	54	±	0	0,9	±	0,0	9,9	±	0,2	0,10	±	0,00	10,1	±	0,1
2. Algeria (ALG)	2777	222	±	2	3,6	±	0,2	39	±	1	0,39	±	0,01	56,6	±	0,3
3. S. Alguero-Balear (SAB)	2844	239	±	2	3,3	±	0,2	41	±	1	0,41	±	0,00	57,9	±	0,3
4. Sardinia Channel (SCh)	2238	184	±	2	2,8	±	0,1	31	±	1	0,33	±	0,00	44,9	±	0,2
5. Ionian Sea (IS)	3774	305	±	3	5,5	±	0,3	51	±	1	0,59	±	0,00	59,3	±	0,2
6. Levantine Basin (LB)	2865	204	±	2	3,6	±	0,2	31	±	1	0,383	±	0,003	34,9	±	0,3
7. Tyrrhenian Sea (TS)	3165	238	±	2	4,0	±	0,2	41	±	1	0,43	±	0,01	48,6	±	0,7
8. N. Alguero-Balear (NAB)	2561	221	±	2	3,4	±	0,2	31	±	2	0,38	±	0,00	42,3	±	0,8
9. C. Alguero-Balear (CAB)	2834	248	±	3	4,0	±	0,2	39	±	1	0,45	±	0,01	49,7	±	0,8
10. Catalano-Balear (CB)	2274	202	±	2	3,1	±	0,1	30	±	1	0,33	±	0,00	38,4	±	0,2
Mean radionuclide inventory:																
Western Basin		201	±	63	3,1	±	1,0	33	±	10	0,35	±	0,11	44	±	15
Eastern Basin		255	±	71	4,6	±	1,4	41	±	14	0,49	±	0,15	47	±	17
Whole Mediterranean Sea		212	±	65	3,4	±	1,2	34	±	11	0,38	±	0,12	44	±	15

A.11. Radionuclide half-lives, atomic masses and specific activities used to convert units of mass to units of activities.

A.4.6. Radionuclide half-lives, atomic masses and specific activities used to convert units of mass to units of activities. Ratios between radionuclide inventories. Information taken from https://www-nds.iaea.org/relnsd/vcharthtml/VChartHTML.html and http://www.iem-inc.com.

Radionuclide	$T_{1/2}$	Atomic mass	Specific Activity		
	years	g·mol^{-1}	Curie·g^{-1}	Bq·g^{-1}	Bq·at^{-1}
^{90}Sr	2,89 ×10^{1}	89,9	1,5 ×10^{2}	5,6×10^{12}	8,3 ×10^{-10}
^{129}I	1,57 ×10^{7}	128,9	1,6 ×10^{-4}	5,9 ×10^{6}	1,3 ×10^{-15}
^{131}I	2,20 ×10^{-2}	130,9	1,2 ×10^{5}	4,4 ×10^{15}	9,7 ×10^{-7}
^{134}Cs	2,06	133,9	1,2 ×10^{3}	4,4 ×10^{13}	9,9 ×10^{-9}
^{137}Cs	3,02 ×10^{1}	136,9	8,8 ×10^{1}	3,3 ×10^{12}	7,4 ×10^{-10}
^{236}U	2,34 ×10^{7}	236,0	6,3 ×10^{-5}	2,3 ×10^{6}	9,1 ×10^{-16}
^{237}Np	2,14 ×10^{6}	237,0	6,9 ×10^{-4}	2,6 ×10^{7}	1,0 ×10^{-14}
^{239}Np	6,45 ×10^{-3}	239,1	2,3 ×10^{5}	8,5 ×10^{15}	3,4 ×10^{-6}
^{238}Pu	8,77 ×10^{1}	238,0	1,7 ×10^{1}	6,3 ×10^{11}	2,5 ×10^{-10}
^{239}Pu	2,41 ×10^{4}	239,1	6,2 ×10^{-2}	2,3 ×10^{9}	9,1 ×10^{-13}

... i continuarem obrint pas!